The regulatory design of glycogen metabolism in mammalian skeletal muscle

by

Daniel Christiaan Palm

Dissertation presented for the degree of Doctor of Philosophy (Biochemistry) in the Faculty of Science at Stellenbosch University

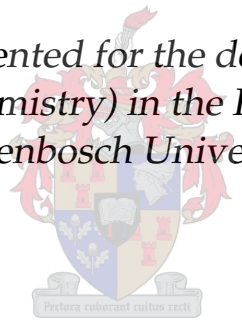

Department of Biochemistry
University of Stellenbosch
Private Bag X1, 7602 Matieland, South Africa

Promoters:

Prof. J.-H.S. Hofmeyr (promoter) Prof. J.M. Rohwer (co-promoter)

March 2013

Declaration

By submitting this dissertation electronically, I declare that the entirety of the work contained therein is my own, original work, that I am the sole author thereof (save to the extent explicitly otherwise stated), that reproduction and publication thereof by Stellenbosch University will not infringe any third party rights and that I have not previously in its entirety or in part submitted it for obtaining any qualification.

Signature: .....
D.C. Palm

Date: 27 March 2013 .....

Summary

It is widely accepted that insufficient insulin-stimulated activation of muscle glycogen synthesis is one of the major components of non-insulin-dependent (type 2) diabetes mellitus. Glycogen synthase, a key enzyme in glycogen synthesis, is extensively regulated, both allosterically (by glucose-6-phosphate, ATP, and other ligands) and covalently (by phosphorylation). Although glycogen synthase has been a topic of intense study for more than 50 years, its kinetic characterization has been confounded by its large number of phosphorylation states. Questions remain regarding the function of glycogen synthase regulation and the relative importance of allosteric and covalent modification in fulfilling this function. The regulation of glycogen synthase and glycogen phosphorylase, the enzyme that catalyses the degradation of glycogen chains, are reciprocal in many respects.

In the present research, using mathematical modelling, we aim to establish the function of the allosteric and covalent regulation of glycogen synthase and glycogen phosphorylase in muscle and, in the case of glycogen synthase, the relative importance of these two mechanisms in performing this function. In order to realize these aims it is essential that a detailed kinetic model of glycogen metabolism is constructed.

We begin with a thorough review of the kinetics and regulation of glycogen synthase in which we propose that both allosteric and covalent modification of glycogen synthase can be described by a Monod-Wyman-Changeux model in terms of apparent changes to L_0, the equilibrium constant between the T and R conformers. We then proceed to develop a rate equation according to the proposed Monod-Wyman-Changeux model and determine values for its kinetic parameters from published experimental data using non-linear least-squares regression. We show that the application of the Monod-Wyman-Changeux model to glycogen synthase kinetics also has important implications for the rate equations of enzymes that catalyse the phosphorylation and dephosphorylation of glycogen synthase. We formalize these impli-

cations for a generic protein that follows Monod-Wyman-Changeux-type conformational change and then also show how the findings apply to glycogen synthase. Taking into account the kinetic model of glycogen synthase and how it also influences the covalent regulation of the enzyme, we proceed to construct a detailed mathematical model of glycogen synthesis that includes the glycogen synthase phosphorylation cascade. A variation of this model in which glycogen synthase phosphorylation is described with a single parameter is also provided. We reuse an existing model of muscle glycogenolysis and also combine these models in an overall model of glycogen metabolism. Finally, we employ the theoretical frameworks of metabolic control analysis, supply-demand analysis, and co-response analysis to investigate the function of glycogen synthase and glycogen phosphorylase regulation. We show that the function of glycogen synthase regulation is not flux control, as assumed in the textbook view, but rather the maintenance of glucose-6-phosphate within a narrow range far from equilibrium. Similarly, we show that regulation of glycogen phosphorylase functions to minimize variation in cellular energy charge in the face of highly variable energy demand. We conclude with an appeal for a renewed interest in the enzyme kinetics of muscle glycogen metabolism.

Opsomming

Daar word wyd aanvaar dat onvoldoende insulien-gestimuleerde aktivering van spierglikogeensintese een van die hoofkomponente van insulien-onafhanklike (tipe 2) diabetes mellitus is. Glikogeensintase, 'n sleutelensiem in glikogeensintese is onderworpe aan breedvoerige regulering, beide allosteries (deur glukose-6-fosfaat, ATP, en ander ligande) en kovalent (deur fosforilering). Alhoewel glikogeensintase reeds vir meer as 50 jaar deeglik bestudeer word, word die kinetiese karakterisering daarvan bemoeilik deur die groot aantal fosforilasiestate waarin die ensiem voorkom. Daar is steeds vrae betreffende die funksie van die regulering van glikogeensintase en die relatiewe bydrae van allosteriese en kovalente regulering in die vervulling van hierdie funksie. Die regulering van glikogeensintase en glikogeenfosforilase, die ensiem wat die afbraak van glikogeenkettings kataliseer, is in baie opsigte resiprook.

In hierdie studie beoog ons om met die hulp van wiskundige modellering vas te stel watter funksie die regulering van glikogeensintase en glikogeenfosforilase vervul en, in die geval van glikogeensintase, wat die relatiewe belang is van allosteriese en kovalente regulering in die vervulling van hierdie funksie. Om hierdie oogmerke te verwesentlik is dit nodig dat 'n kinetiese model van glikogeenmetabolisme ontwikkel word.

Ons begin met 'n omvattende oorsig van die kinetika en regulering van glikogeensintase waarin ons voorstel dat beide die allosteriese en kovalente regulering van glikogeensintase beskryf kan word met die Monod-Wyman-Changeux model in terme van oënskynlike veranderings aan L_0, die ekwilibriumkonstante tussen die T en R konformasies. Ons gaan dan voort om 'n snelheidsvergelyking te ontwikkel volgens die voorgestelde Monod-Wyman-Changuex-model en bepaal ook die waardes van hierdie vergelyking se parameters vanaf gepubliseerde eksperimentele data deur middel van nie-lineêre kleinste-vierkantsregressie. Ons wys dat die toepassing van die Monod-Wyman-Changuex-model op glikogeensintase-kinetika

belangrike gevolge het vir die snelheidsvergelykings van die ensieme wat die fosforilering en defosforilering van glikogeensintase kataliseer. Ons formaliseer hierdie gevolge vir 'n generiese Monod-Wyman-Changeux-tipe proteïen en wys dan ook hoe die bevindings op glikogeensintase van toepassing is. Met inagneming van die kinetiese model vir glikogeensintase en hoe dit die kovalente regulering van die ensiem beïnvloed, gaan ons voort om 'n gedetaileerde wiskundige model van glikogeensintese, wat ook die glikogeensintase-fosforileringskaskade insluit, te ontwikkel. 'n Variasie op hierdie model waarin die fosforilering van glikogeensintase deur 'n enkele parameter beskryf word, word ook voorsien. Ons herbruik 'n bestaande model van spierglikogenolise en kombineer ook hierdie modelle in 'n oorkoepelende model van glikogeenmetabolisme. Uiteindelik span ons die teoretiese raamwerke van metaboliese kontrole-analise, vraag-aanbod-analise, en ko-responsanalise in om die funksie van die regulering van glikogeensintase en glikogeenfosforilase te ondersoek. Ons wys dat die funksie van die regulering van glikogeensintase nie fluksiekontrole, soos algemeen in handboeke aangeneem word, is nie, maar liewer dat dit glukose-6-fosfaat handhaaf binne 'n noue band ver vanaf ekwilibrium. Insgelyks wys ons dat die regulering van glikogeenfosforilase funksioneer om variasie in sellulêre energielading te beperk ten spyte van hoogs wisselende vlakke van energie-aanvraag. Ons sluit af met 'n pleidooi vir hernieude belangstelling in die ensiemkinetika van glikogeenmetabolisme in die spier.

Für Ronell

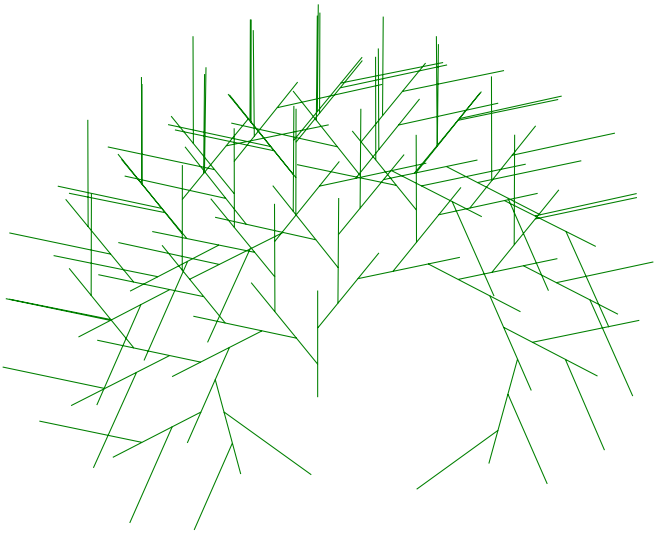

$$R \rightarrow F[+R]F[-R]F$$

Acknowledgements

I would like to express my sincerest gratitude to:

Prof Jannie Hofmeyr whose enthusiasm for molecular cell physiology is both contagious and inspiring. His work is original and rigorous. One can only watch and learn.

Prof Johann Rohwer for simplifying my life with a seemingly endless supply of command-line shortcuts and for his keen eye for mistakes. He sparked the idea that would eventually let everything fall into place.

Marnette Coetzee for asking all the questions I thought I had answers to.

Triple J-Group, especially Jálene, for company, discussion, coffee breaks, and laughs.

Illuminati for good food and red wine-infused philosophy. What a rare privilege to be surrounded by so many exceptionally bright people.

The Open-Source Community for free software.

National Research Foundation for funding.

My parents for believing in me.

Ronell for endless love, encouragement, and support.

God for miracles.

Contents

List of Figures

List of Tables

Chapter 1

Introduction

Glycogen, a branched polymer of glucose, is used by numerous organisms as a glucose store when glucose is abundant or as a source of glucose under conditions of metabolic depletion [1]. The structure of glycogen has been optimized to store a large amount of glucose that is readily available without affecting cellular osmolarity [2]. In mammals, skeletal muscle is the major site of glucose disposal [3, 4], storing significantly more glycogen than the liver [5]. Although skeletal muscle insulin resistance is not a sufficient causative agent in non-insulin-dependent (type 2) diabetes mellitus, it is considered a primary defect in this disease [6]. Jensen *et al.* [7] suggest that, in muscle with a high glycogen content, insulin resistance is not necessarily manifested as decreased glucose uptake, but rather as impaired muscle glycogen synthase (GS) activity. GS, the enzyme that incorporates glucose from UDP-glucose (UDPG) into glycogen, is extensively regulated by both allosteric and covalent modification. Glucose-6-phosphate (G6P), acting as an activator, and ATP, acting as an inhibitor, as well as many other ligands, compete for an allosteric site on GS. In addition, GS is phosphorylated at nine serine residues, resulting in marked inhibition.

The extensive regulation of GS activity, and its relatively low activity, has led to the view that it is the "rate-limiting" enzyme of glycogen synthesis [8]. Accordingly, phosphorylation and activation by G6P are traditionally considered mechanisms that control the flux of glycogen synthesis. This view has been called into question by several *in vivo* NMR studies, as reviewed by Shulman *et al.* [8], in which it was found that, in general, there is no correlation between the glycogen synthetic flux and the degree of GS phosphorylation, as measured by the fractional velocity. Instead, the glycogen synthetic flux was found to be proportional to the glucose im-

port activity. These findings led Shulman *et al.* [8] to suggest that the regulation of GS activity is not involved in controlling the flux of glycogen synthesis, but rather serves to maintain G6P homeostasis [9]. In this view phosphorylation functions to maintain the sensitivity of GS to its feedforward activator, G6P.

The theoretical framework of metabolic control analysis (MCA) [10, 11] has been applied to the model proposed by Shulman *et al.* [8] in a number of studies [9, 12, 13], confirming that the glycogen synthetic flux is controlled by glucose uptake, and suggesting a role for phosphorylation in the coordinate activation of glucose transporter 4 (GLUT4) and GS by insulin as a mechanism of G6P homeostasis. Other metabolic control analytic (MCA) studies, however, found that control of the glycogen synthetic flux is shared almost equally between the glucose uptake and glycogen synthesis activities [14]. Recently, Roach *et al.* [1] argued for a more neutral view in which both glucose uptake and GS potentially control the flux, depending on cellular conditions.

The notion that the regulation of GS activity by phosphorylation can be a mechanism that maintains metabolite homeostasis [9] is in good agreement with the findings of Hofmeyr & Cornish-Bowden [15] that allosteric regulation in feedback inhibition loops does not function to control the flux through the regulated enzyme, but rather to maintain the concentration of the regulatory metabolite within a narrow range far from equilibrium. If a similar function is assumed for feedforward loops, as in the activation of GS by G6P, the allosteric and covalent regulation of GS activity would appear to be involved in the homeostatic maintenance of G6P. However, Hofmeyr *et al.* [16] argue that, unlike the situation in feedback inhibition, the type of activation—whether by increasing the k_{cat} or decreasing K_{m} of the regulated enzyme—has important consequences for the effectiveness of the mechanism in maintaining the concentration of the regulatory metabolite homeostatically, predicting that an increase in k_{cat} is to be expected rather than a decrease in K_{m}.

The presence of allosteric *and* covalent regulation of GS activity, and the fact that various stimuli such as insulin signalling make use of both these mechanisms to affect GS activity, raise questions regarding the relative importance of these two mechanisms in the regulation of GS activity. Recent studies using mutant mice in which glycogen synthase kinase 3 (GSK3), a kinase that phosphorylates GS at various sites, was rendered constitutively active [17] or in which GS was rendered insensitive to activation by G6P [18] suggest that, in response to insulin, the activation of GS is predominantly mediated through allosteric and not covalent regulation.

At present no detailed kinetic treatment exists that is able to account for both the allosteric and covalent regulation of GS. The development of such a model is severely complicated by the numerous phosphorylation states in which the enzyme can exist. It is thus no surprise that GS phosphorylation is almost always discussed in terms of a two-state model, as the reciprocal of glycogen phosphorylase (GP) phosphorylation.

Similar questions arise when glycogen degradation is considered. In many respects, the regulation of GP, the enzyme that catalyses the phosphorolysis of non-reducing glucose residues from glycogen chains to produce glucose-1-phosphate (G1P), is reciprocal to that of GS. Phosphorylation inhibits GS, but activates GP. G6P activates GS but inhibits GP. GP is furthermore activated by AMP and inhibited by ATP. Using a mathematical model of glycogenolysis, Lambeth & Kushmerick [19] found that the glycogen degradation flux is controlled by the demand for ATP. This finding raises questions regarding the function, if not flux control, of the covalent and allosteric regulation of GP.

In this dissertation, using mathematical modelling, we aim to establish 1) the function of the allosteric and covalent regulation of GS and GP in muscle and 2) in the case of GS, the relative importance of these two mechanisms in performing this function. In order to realize these aims it is essential that a detailed kinetic model of glycogen metabolism, with emphasis on the kinetics of GS, is constructed.

We begin with a comprehensive review of the allosteric and covalent regulation of GS and suggest that the kinetics of GS is indicative of the classic Monod-Wyman-Changeux (MWC) model. In Chapter 3 we develop a rate equation for GS based on the kinetics as reviewed in Chapter 2, and obtain kinetic parameter values for this equation using non-linear regression of published experimental data. In Chapter 4 we show that the kinetic model identified as providing the best description of GS kinetics has important implications for the kinetics of any enzymes that covalently modify GS and other proteins that exhibit MWC-type conformational change. Taking these implications into account, we proceed to construct various detailed mathematical models of glycogen metabolism (Chapter 5). The model of Lambeth & Kushmerick [19] is incorporated as a description of glycogen degradation. Finally, in Chapter 6, we make use of analytical frameworks such as MCA and co-response analysis to investigate the regulatory design of glycogen synthesis and breakdown. We also discuss several aspects that must be taken into consideration in the construction of an overall model of glycogen synthesis and degradation. We conclude

in Chapter 7 with a general discussion of our main findings and suggest directions for future research.

Chapter 2

Allosteric and covalent regulation of glycogen synthase activity[1]

2.1 Introduction

In this chapter we provide a comprehensive review of the kinetics and regulation of glycogen synthase (GS). We discuss both the earlier kinetic studies and the more recent site-directed mutagenesis and crystal structure studies and show how the results from these studies can form the basis of a unifying view of the covalent and allosteric regulation of GS that largely overcomes the combinatorial explosion resulting from the numerous phosphorylation states of the enzyme. We begin with a detailed general discussion of the kinetics, structure, and regulation of GS. We then proceed to formulate these aspects in terms of a phenomenological kinetic rate equation for the purpose of discussing the effects of covalent and allosteric regulation on the kinetic properties of GS. Finally, we propose a variation on the classic Monod-Wyman-Changeux (MWC) model that succinctly accounts for all the apparent modifications to GS kinetic properties.

This review is not intended as a comprehensive survey of glycogen metabolism in general, but specifically concerns the regulation of mammalian skeletal muscle GS from a kinetic perspective. For a comprehensive general review of developments in glycogen metabolism research over the last decade, the reader is referred to the recent publication by Roach *et al.* [1]. The present review follows what could be considered a "bottom-up" approach, as we avoid discussing higher level regulatory phenomena such as insulin signalling, but rather focus on the mechanisms under-

[1] An abridged version of this chapter has been published in *FEBS Journal* [20].

pinning GS regulation. For a discussion of the effects of exercise, adrenaline and insulin stimulation on GS, the reader is referred to the recent "top-down" review by Jensen & Lai [5]. Where no mammalian muscle data were available we also considered, with due care, results from research conducted on other mammalian tissues, other eukaryotes, or even prokaryotes. Unless stated otherwise, or where the context indicates otherwise, "GS" refers to the muscle enzyme.

2.2 Glycogen synthase and its kinetics

Reaction and thermodynamics

Glycogen chains are readily elongated by glycogen phosphorylase (GP) operating in the reverse direction using glucose-1-phosphate (G1P) as substrate. However, Leloir and co-workers showed—first in liver [21] and then in muscle [22]—that the physiologically relevant synthetic pathway uses UDP-glucose (UDPG) as substrate, leading to the discovery of GS. GS catalyses the bi-bi reaction in which the glucosyl (Glc) moiety from UDPG is incorporated into a glycogen molecule comprising n glucose residues by means of an $\alpha(1 \rightarrow 4)$ glycosidic bond to produce UDP and a glycogen molecule comprising $n + 1$ glucose residues [22, 23] according to the equation

$$\text{UDPG} + \text{Glc}_n \rightleftharpoons \text{UDP} + \text{Glc}_{n+1} \tag{2.1}$$

GS requires an oligosaccharide primer as a glucose acceptor and is therefore not capable of *de novo* glycogen synthesis. Glucose, maltose, and other short oligosaccharides are either unsuitable or only weak primers [22, 24]. Instead, *de novo* glycogen synthesis is initialized in two phases by the homodimer glycogenin (EC 2.4.1.186). In the first phase, a tyrosyl residue of one subunit (Tyr194 in rabbit muscle) [25, 26] is glycosylated in an intersubunit reaction by its partner [27, 28]. In the second phase, a further seven glucosyl residues are added successively in an intrasubunit reaction [26], producing a suitable primer for GS. Like GS, glycogenin uses UDPG as substrate, but has an additional divalent cation (Mn^{2+} or Mg^{2+}) requirement [29]. GS is initially complexed with glycogenin and it is believed that this association is necessary for proper initiation of glycogen synthesis [30]. Branches are initiated by branching enzyme (EC 2.4.1.18), which cleaves $\alpha(1 \rightarrow 4)$ bonds to reintroduce them as $\alpha(1 \rightarrow 6)$ bonds [31], thus creating new chains that can serve as primers for elon-

gation by GS. On average, each glycogen chain branches twice and is 12–14 glucose residues long [2]. The terminal glucosyl residues of glycogen chains are referred to as *non-reducing ends*.

The equilibrium constant of the GS reaction is expressed as

$$K_{\text{eq}} = \frac{[\text{UDP}]_{\text{eq}}[\text{Glc}_{\text{n+1}}]_{\text{eq}}}{[\text{UDPG}]_{\text{eq}}[\text{Glc}_{\text{n}}]_{\text{eq}}} \tag{2.2}$$

While Glc_n and Glc_{n+1} typically denote entire glycogen molecules, it is really only the non-reducing ends of a glycogen molecule that can partake in the elongation reaction. We may thus define $[\text{Glc}_n]$ and $[\text{Glc}_{n+1}]$ as the total concentrations of all non-reducing ends that can serve as substrates and products. The majority of non-reducing ends can, however, serve as both substrates and products. For sufficiently large glycogen molecules, the difference between the equilibrium values of $[\text{Glc}_{\text{n}}]$ and $[\text{Glc}_{\text{n+1}}]$ therefore becomes negligible, so that Eq. 2.2 simplifies to

$$K_{\text{eq}} = \frac{[\text{UDP}]_{\text{eq}}}{[\text{UDPG}]_{\text{eq}}} \tag{2.3}$$

Kornfeld & Brown [32] reported the formation of 0.0018 μmoles UDPG from 7 μmoles UDP in the presence of GS and 5 mg glycogen (pH 7.5, 30°C), from which a K_{eq} of 3900 can be calculated using Eq. 2.3. Assuming that all $\alpha(1 \rightarrow 4)$ glycosidic bonds in the glycogen molecule are equivalent, an assumption supported by Goldberg *et al.* [33], the K_{eq} can also be calculated from the free energy changes of the component half-reactions. Gold [34] estimated a value of 400 at pH 7.0 and 25°C. A value of 230 (pH 7.0, 25°C) is estimated for the reaction with maltopentaose as glucose acceptor using the group contribution method developed by Jankowski *et al.* [35] as implemented by the online service *eQuilibrator* [36]. Adjusted for pH (7.15) and ionic strength (0.2 mM), this value increases to about 1000. Kashiwaya *et al.* [37] report a much lower value of 37.7 (corrected for physiological pH and Mg^{2+} in rat heart).

The difference of more than two orders of magnitude in reported K_{eq} values is a testament to the dependence of this value on experimental conditions. The value increases both with ionic strength and pH [36]. The temperature dependence of the K_{eq} is not clear. The large value calculated from the results of Kornfeld & Brown [32] can probably be ascribed both to the high pH and to difficulties in accurately measuring the reactant concentrations. In comparison, the equilibrium ratio of ADP to ADP-glucose for the *E. coli* enzyme has been reported as ranging from 55.5 to 151

as the pH ranges from 5.27 to 6.82 at 37°C [38]. Considering the similarity of the ADP-glucose and UDPG phosphoester bonds and the muscle pH of 6.8–7.15 [39], the physiologically relevant K_{eq} for GS in muscle is probably in the order of 10^2. Regardless of the precise value, it is clear that the reaction will not operate in the reverse direction under physiological conditions.

Kinetic mechanism

The determination of the GS kinetic mechanism is complicated by glycogen's dual function as both substrate and product. In addition to the usual substrate binding terms, initial velocity equations are required to include product binding terms for glycogen [40]. Moreover, if the glycogen concentration is varied, it will always vary in both its capacity as substrate and product [34]. As a result, the interpretation of Lineweaver-Burk and other reciprocal plots, in which each substrate is varied while keeping the other constant, changes significantly. For instance, Brown & Larner [41] suggested a ping-pong mechanism on the basis of parallel Lineweaver-Burk plots, whereas due to the presence of glycogen it can be shown that a ping-pong mechanism should in fact result in intersecting plots [40]. Others [24, 42] have obtained reciprocal plots indicative of either rapid equilibrium random or ordered sequential mechanisms, while Plesner *et al.* [40] would accept only the rapid equilibrium random mechanism. In order to overcome the pitfalls associated with reciprocal plots, Gold [34] studied the mechanism of the rabbit muscle enzyme by determining the equilibrium isotope exchange rates between UDPG and glycogen, and UDPG and UDP. Gold [34] concluded that the mechanism is rapid equilibrium random, but conceded that it cannot be distinguished from a rapid equilibrium ordered mechanism with dead-end binary complexes by any of the methods he employed. Although the majority of research seems to favour the random order mechanism, an ordered sequential mechanism cannot be ruled out at this point.

The rapid equilibrium random bi-bi mechanism is seemingly incompatible with the observation [34, 43, 44] that glycogen forms stable complexes (lasting 3 min on average) with glycogen synthase [34]. However, the kinetic mechanism only describes the rapid exchange of individual non-reducing ends and does not preclude additional interaction of the glycogen molecule as a whole with GS. Considering the lifetime of the glycogen-GS complex and the kinetic mechanism, Gold [34] makes the conservative estimate that up to 550 chains are visited by GS. It has also been suggested that GS is able to add several glucosyl residues successively to the same chain

of a glycogen molecule, i.e., that elongation is processive [34, 45, 46]. The number of successively added residues is known as the *action pattern*. Action patterns of 1.4–1.7 [45] and 9 (estimated by [34] from [46]) have been reported. These action patterns are however incompatible with a rapid equilibrium random mechanism, which predicts that exactly one glucose residue is successively incorporated in the same chain (distributive elongation) [34]. Parodi *et al.* [46] observed higher action patterns for liver GS as the molecular weight of glycogen increased. They ascribed the increase to the possibility that GS penetrates glycogen molecules of higher molecular weight and thus loses mobility, increasing the likelihood that the same chain will be glycosylated repetitively. More recently, Baskaran *et al.* [47] found that yeast GS exhibited a distributive pattern of catalysis with maltooctaose as glucose acceptor. If similar behaviour is exhibited by the muscle enzyme, deviation from distributive elongation is then not necessarily linked to a change in the kinetic mechanism, but rather the result of limited access to chains. At any rate, if glycogen saturation is assumed—a reasonable assumption given the tight association of GS with glycogen—the kinetic mechanism is of little import to initial velocity kinetic treatments, as all the bi-substrate mechanisms suggested simplify to the simple uni-reactant case in which only UDPG is considered a substrate [42].

Tertiary and quaternary structure

Glycogen synthases are members of the GT-B superfamily of glycosyltransferases [48]. The tertiary structure of members of this family, which also includes GP, is characterized by a duo of N-terminal and C-terminal Rossmann fold domains separated by an interdomain cleft that houses the active site. The C-terminus typically folds back onto the N-terminal Rossmann fold domain so that the two domains are linked by a two-stranded hinge [49]. Significant rotation around this narrow hinge is possible and GT-B members differ widely with regard to the size of the interdomain cleft. Glycogen synthases have a particularly deep fissure between the N- en C-domains [50] and it has been suggested that an interdomain closure is required to bring glycogen (binding along the N-domain) and the nucleotide sugar (binding to the C-domain) together for catalysis [49]. Glycogen synthases can be further classified into the ADP-glucose-utilizing non-regulated GT-3 family—including the bacterial and archaeal enzymes—and the UDPG-utilizing regulated GT-5 family—including the mammalian and yeast enzymes [49]. The most significant structural differences between the GT-3 (comprising $\sim$50 kDa protomers) and GT-5 (compris-

ing ∼80 kDa protomers) families are the presence of two N-terminal inserts (β2–β5 and β7–α10), and a C-terminal insert (β11–α17) of which the most prominent secondary structures is a coiled-coil formed by helices α15 and α16 in GT-5 members. Another unique feature of eukaryotic GS is the presence of a conserved arginine-rich cluster (Arg580/581/583/587/589/592 in yeast) on the regulatory R helix (helix α22), believed to be involved in allosteric and covalent regulation.

The only available GS crystal structures are those of the bacteria *Agrobacterium tumefaciens* (AtGS) [49] and *E. coli* (EcGS) [50], the archaeon *Pyrococcus abyssi* (PaGS) [52], and only recently the yeast—and first eukaryote—*S. cerevisiae* (ScGS) [51]. The oligomerization of the known structures range from monomeric to tetrameric and the secondary structures involved in intersubunit interactions differ widely. AtGS was solved as an asymmetric dimer [49] in which a 10-residue C-domain insert (407–416) facilitates the primary intersubunit contacts [52]. PaGS, the smallest known GS, lacks the AtGS dimerization insert, but terminates in an 11-residue hydrophobic tail (427–437) not present in bacteria [52]. The C-terminal hydrophobic tail (folded back onto the N-domain) associates with a hydrophobic pocket (53–55, 105–115, 141–142) on the N-domain of a neighbouring subunit, resulting in a trimeric quaternary structure with a three-fold symmetry in which the three N-domains are tightly associated. ScGS contains both the AtGS dimerization insert and the PaGS hydrophobic tail involved in trimerization, but neither sequence is conserved and they appear not to be involved in oligomerization [51]. Instead, ScGS [51, 53] is a two-fold symmetric dimer of a two-fold symmetric dimer pair, in which the subunits can be numbered (following Baskaran *et al.* [51]) from A to D (Fig. 2.1). The intersubunit contacts in the A/D (and B/C) interface involve the reciprocal association of helix α16 (located in the eukaryote-specific C-terminal insert) of one subunit with the region between helix α2 and sheet β4 (located in the first of the unique N-terminal inserts) of the partner subunit. In the interface between dimer pairs (AD/BC), the main contacts comprise a reciprocal association of helix α15 from one subunit to the region between α15 and β10, so that the α15/16 helix pairs of subunits A and C associate, and those of subunits B and D associate. The A/B and C/D interfaces house the allosteric sites, whereas the A/D and B/C interfaces house the active sites. Intriguingly, in AtGS and the activated form of ScGS the movement of the N-domains are unrestricted; whereas in PaGS the N-domains are involved in the trimerization permitting only C-domain movement. It appears that GS oligomerization evolved independently in bacteria, archaea, and eukaryotes.

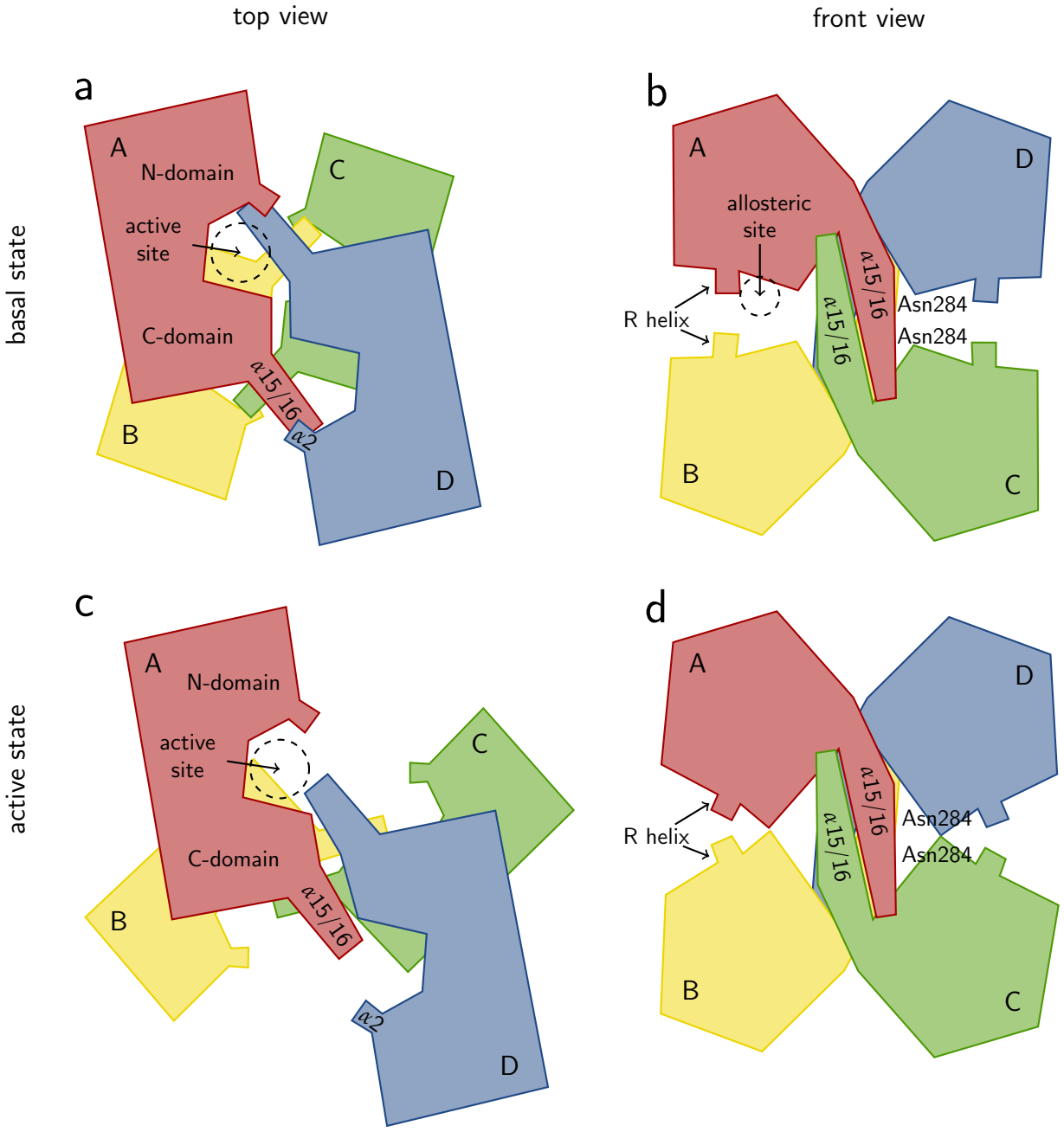

Figure 2.1: Cartoon of the tetrameric structure of yeast GS. Due to the high overall similarity between mammalian and yeast GS, it is expected that the mammalian muscle GS assumes a similar quaternary structure and undergoes a comparable conformational transition upon activation. In the basal state (a, b) closure of the interdomain cleft that houses the active site is impeded by interaction across the A/D and B/C interfaces of α15/16 and α2. In the active state (c, d), which is induced by glucose-6-phosphate, interaction across the A/C and B/D interfaces is established and the impediment on interdomain closure is abrogated. Adapted from [51].

The oligomerization state of the muscle GS isozyme (∼84 kDa) has been reported by various workers as dimeric [54, 55], trimeric [41, 54, 56], or tetrameric [44, 54, 57–61]. It is unlikely that the dimeric forms reflect the *in vivo* state, as they were either shown to contain a proteolytic fragment [54] or were obtained at very low concentrations, with the authors [55] suggesting the formation of a tetramer at higher *in vivo* concentrations. Horcajada *et al.* [52] point out that in many of these earlier investigations the oligomerization state was determined based on the sedimentation coefficient, a measure which assumes a strictly globular protein shape. Based on the presence in muscle GS of an insert analogous to the PaGS hydrophobic tail, and on the findings of Brown & Larner [41] using sedimentation equilibrium ultracentrifugation, a technique not influenced by the protein shape, Horcajada *et al.* [52] favour a trimeric state for muscle GS. Other workers [59], however, also using sedimentation equilibrium ultracentrifugation, observed results indicative of a tetramer. The structure of eukaryotic GS is highly conserved, with only the phosphorylation sites and loops between conserved secondary structures differing [51]. Considering this high degree of conservation, and, in particular, the presence in muscle GS of the secondary structures corresponding to the yeast α15–16 helices, the quaternary structure of muscle GS is probably, as for the yeast enzyme, tetrameric. It has, however, been reported that glycogen, the degree of phosphorylation [62], glucose-6-phosphate (G6P), and ATP [55] influence the degree of GS oligomerization; higher or lower degrees of oligomerization can therefore not be ruled out.

Regulatory arginine cluster

Following the assumption that the allosteric and covalent regulation of eukaryotic GS is brought about by the interaction of the negatively charged phosphorylated residues and G6P with basic amino acid residues, Pederson *et al.* [63] identified several arginine and lysine residues that are conserved in eukaryotes. They proceeded to generate 23 yeast GS mutants in which these residues were systematically replaced with alanine residues, with up to three mutations per mutant enzyme. Two of the mutants, R579A/R580A/R582A (human muscle numbering used for comparison; initial methionine included) and R586A/R588A/R591A, were completely insensitive to activation by G6P, while still exhibiting significant activity in the absence of G6P. Upon phosphorylation the V_{max} for GS of mutant R579A/R580A/R582A, which was already very low, did not decrease much further, whereas GS of the mutant R586A/R588A/R591A, which displayed normal activity in the dephosphory-

Figure 2.2: Sequence alignment of the regulatory arginine cluster from mammalian and yeast glycogen synthases. The arginine residues (blue) are conserved across eukaryotes. Sequences were obtained from the NCBI RefSeq database [65].

lated state, was significantly inactivated. Hanashiro & Roach [64], working with the rabbit muscle enzyme, obtained essentially the same overall results, with the important difference that in their work the R579A/R580A/R582A mutant's activity was decreased four-fold upon phosphorylation, whereas the R586A/R588A/R591A mutant was unaffected. The six arginine residues in these mutants constitute what is now referred to as the regulatory arginine cluster and are located on the R helix (Fig. 2.2).

Noting that the mutations introduced by Hanashiro & Roach [64] not only abolished G6P sensitivity, but also altered the enzyme's activity in the absence of G6P, Bouskila *et al.* [18], also working with the muscle enzyme, mutated the six arginine residues singly or in pairs and found that the single point mutations R582A and R586A had no effect on GS activity, but were sufficient to abrogate G6P sensitivity. Both mutants were, however, still activated by dephosphorylation. These findings suggest that Arg582 and Arg586 mediate regulation by G6P, a view that is supported by the crystal structure data of the yeast enzyme, which position these residues in the G6P binding pocket [51]. Baskaran *et al.* [51] found that the R579A/R580A double mutant exhibited activity comparable to the wildtype enzyme, but was significantly inhibited by phosphorylation. In contrast, the R588A/R591A double mutant was significantly inactivated compared to the wildtype, but could be activated to wildtype levels by addition of G6P. Note the differences between the yeast triple mutant R579A/R580A/R582A and double mutant R579A/R580A. The basal activity of the triple mutant is much lower than that of the double mutant; the triple mutant is also unresponsive to phosphorylation, whereas the double mutant is further inhibited. Similar disagreement is observed between the R586A/R588A/R591A and R588A/R591A mutants in yeast. In both cases the yeast double mutants appear to be in closer agreement with the muscle triple mutants from Hanashiro & Roach [64]. To

Table 2.1: Response of arginine cluster mutants to G6P and phosphorylation compared to wildtype GS [18, 51, 64]. Amino acids are numbered according to the muscle enzyme [18]. [a]Inactivation occurs to a lesser extent than in wildtype. [b]Dephosphorylation activates the enzyme. [c]Only slight additional inactivation is observed.

Enzyme	Inactivated by mutation	Inactivated by phosphorylation	Reactivated by G6P
wildtype	N/A	Yes	Yes
R579A, R580A	No	Yes[a]	Yes
R582A, R586A	No	Yes[b]	No
R588A, R591A	Yes	No[c]	Yes

our knowledge the R579A/R580A and R588A/R591A double mutants have not been investigated for muscle. Considering the sequence similarity between the yeast and muscle enzymes, however, we speculate that the individual functions of the six arginine residues are similar in yeast and muscle. In summary (Table 2.1), Baskaran *et al.* [51] suggest that Arg579 and Arg580 interact with phosphorylated serine residues, thereby stabilizing an inactive conformation; whereas Arg582 and Arg586 interact with the phosphate group of G6P, thereby stabilizing an active conformation. Finally, Arg588 and Arg591 stabilize the dephosphorylated, non-activated enzyme; phosphorylation or replacement by alanine residues neutralize the charge of these residues, leading to inactivation.

Kinetics

As noted earlier, UDPG and UDP are believed to bind in the interdomain cleft to the C-terminal Rossmann fold. As Rossmann fold domains are associated with nucleoside binding capability [66], the enzyme-ligand interaction probably mostly involves the UDP moiety. In agreement with this position, UDP has been found to be a competitive inhibitor with regard to UDPG. There is no reason to believe that either UDPG or UDP binds to additional sites on the GS subunit. In the majority of kinetic studies UDPG exhibits hyperbolic saturation curves [24, 40–42, 58, 67–70], with only a few accounts [69, 71–73] reporting deviations from Michaelian kinetics, mostly in the form of negative cooperativity [74]. Sølling [42] argues that the observed negative cooperativity is an artefact that disappears if appropriate measures are taken to minimize UDP product inhibition. In support of the argument of Sølling [42], Roach *et al.* [72] observed that hyperbolic kinetics is restored in the presence of G6P. In at

least one account, G6P has been shown to counter UDP inhibition [75].

The formation of tight enzyme-glycogen complexes [34, 43] indicates that, apart from the N-domain binding site in the catalytic cleft, glycogen likely interacts with GS at several additional sites. Díaz *et al.* [76] identified a non-catalytic glycogen binding site on the surface of the N-domain of PaGS. Four glucose moieties of maltohexaose were found to bind at this site by curling around Tyr174. Mutation of Tyr174 to alanine decreased the acceptor affinity and specific activity with glycogen as substrate, but had no effect on specific activity with maltohexaose as acceptor. In cosedimentation experiments, the native enzyme was found in the pellet fraction, whereas the mutant (which still had an intact catalytic glycogen binding site) was located in the supernatant, suggesting that the non-catalytic site has a much higher affinity for glycogen than the catalytic site. Díaz *et al.* [76] continued to identify Tyr239 as the human muscle GS counterpart to Tyr174. Mutation of Tyr239 and the nearby Tyr242 decreased both the affinity for glycogen and the specific activity, whereas specific activities were essentially unchanged with maltohexaose as acceptor. Baskaran *et al.* [47] identified four maltodextran binding sites, in addition to the catalytic site, on ScGS. One of these sites (site 1) corresponds roughly to the site identified for PaGS, but involves unique eukaryotic structures and interestingly does not include the residue corresponding to Tyr174. The remaining three sites are located on the C-domain, with site 4 located in the catalytic cleft near the catalytic glycogen binding site. For all four sites, mutation of key residues decreased the V_{max} and affinity for glycogen. Only mutation of site 4 affected the activity with maltooctaose as acceptor, leading the authors to suggest that this site is involved in positioning the acceptor in the catalytic site.

The enhanced glycogen affinity brought about by the non-catalytic glycogen binding sites essentially dictates that glycogen binding occurs in a positively cooperative fashion. As these additional sites have little or no effect on the affinity for oligosaccharides such as maltohexaose, this cooperativity is not expected to be the result of any conformational change, but rather an increase in the apparent concentration of chains (from the same glycogen molecule) in the vicinity of unoccupied sites on the same and, possibly, neighbouring subunits. It is therefore surprising that kinetic studies report non-cooperative glycogen binding [24, 40, 41] or even negative cooperativity [74]. We speculate that this apparent contradiction could be resolved if complex formation, which likely proceeds by positive cooperative binding, positions the tetramer such that only a single catalytic site is accessible to a glycogen chain. In

such a situation, glycogen binding can be considered infinitely negatively cooperative. Infinitely negative cooperativity is kinetically equivalent to Michaelian kinetics. Deviation from this strict infinite negative cooperativity—such as if rotation of the enzyme allows an additional catalytic site to become available, albeit with a reduced affinity for glycogen—would be observed as classic negative cooperativity.

Before we discuss the effects of modifiers on GS activity, a brief note on nomenclature is warranted. Following Cornish-Bowden [77], we use the term *specific* to refer to any modification that results in an altered substrate affinity; and the term *catalytic* to refer to modification that results in an altered maximal velocity. We adopt these terms because the more familiar terms (*competitive* and *non-competitive*) do not apply to the case of enzyme activation. The term *competitive* is still used to indicate that ligands physically compete for the same site, as opposed to affecting each other's binding affinity by another mechanism.

GS is allosterically regulated by G6P, ATP, and several other ligands. G6P is a potent activator of GS [22] and is generally recognized as the most important allosteric modifier of GS. Several workers have reported that G6P activates GS by increasing the substrate affinity, catalytic rate, or both. We will discuss the nature of G6P activation in detail in Section 2.4. ATP, on the other hand, inhibits GS [39, 42, 67, 78, 79]. This inhibition is brought about by decreasing the enzyme's affinity for UDPG [39, 42]. To the best of our knowledge, there is no evidence that ATP also inhibits GS catalytically, but this possibility cannot be ruled out. Regrettably, ATP inhibition is often neglected in GS kinetic studies. Kinetic studies that include both G6P and ATP indicate a competitive binding pattern [42, 67, 78]. However, contrary to what is expected for pure competition, it has been noted in a few cases that G6P saturation is unable to reverse ATP inhibition completely [42, 67]. Two explanations have been offered in this regard. First, G6P and ATP bind to different allosteric sites, but binding of either ligand significantly decreases the affinity for the other ligand [67]. Alternatively, both ligands compete for the same allosteric site, but ATP also competes with UDPG at the catalytic site [42]. In support of the latter explanation, it has been observed that the rat muscle enzyme is able to use ADP-glucose as a glucose donor at half the rate of UDPG [80], showing that the adenosine moiety is able to bind to the active site. Moreover, ScGS crystal structure data show that in the G6P binding pocket only the amino acid residues that bind the phosphate moiety are ordered, with the remaining residues only assuming an ordered conformation upon ligand binding [51]. The phosphate moiety is therefore likely a major determinant

of ligand specificity at the allosteric site. This provides a basis on which G6P and ATP—though structurally disparate, apart from the phosphate moiety—could both bind to the same site. Activation and inhibition curves of G6P and ATP have been found by different workers to be either hyperbolic or sigmoidal. Cooperative G6P binding has mostly been observed for the phosphorylated enzyme [67, 69, 72, 81], but the dephosphorylated form has also been found to exhibit mild cooperativity [42]. ATP cooperativity has been observed for the dephosphorylated enzyme [67]. There is also strong evidence for positive heterotropic cooperativity between G6P and ATP binding [42, 67, 69]. ATP and ADP are probably equally important GS inhibitors [39, 79], but detailed kinetic data for the latter ligand are very limited. AMP has also been reported as a weak inhibitor of GS at high concentrations [39, 79], but considering the low AMP concentration in muscle it is unlikely that AMP is a significant effector of GS *in vivo*. In the remainder of this review ATP serves as a model GS inhibitor.

The kinetics of GS is influenced by several additional effectors, many of which do not clearly exhibit either activation or inhibition. Several G6P analogues such as galactose-6-phosphate and glucosamine-6-phosphate activate GS, but to a lesser extent than G6P [22, 78]. Therefore, despite activating GS, these analogues inhibit activation by G6P. UTP is a competitive inhibitor with respect to UDPG [67] and possibly G6P [69]. ADP and AMP bind to the allosteric site and inhibit GS in a similar way as ATP [42, 79]. Sølling [42] suggests that these nucleotide inhibitors will all probably bind both to the catalytic site—by virtue of being nucleotides—and to the allosteric site—by possessing phosphate moieties. Sulphate and inorganic phosphate have been reported as either activators [42] or inhibitors [82], depending on phosphorylation state. Others found inorganic phosphate to be inhibitory regardless of GS phosphorylation [39, 79].

Mg^{2+} activates GS, but becomes inhibitory in the absence of inhibitors [42]. Although direct interaction with GS cannot be ruled out, the ambiguous effect of Mg^{2+} is probably not the result of interaction with GS; instead, Mg^{2+} forms chelate complexes with the various GS activators and inhibitors, thereby mitigating their effects [42, 82]. Mg^{2+} activation is strongest with respect to allosteric site inhibitors such as ATP [42]. The contention that a phosphate (or anionic) moiety is required for binding at the allosteric site is supported by this observation, as the effect of Mg^{2+} is to neutralize the phosphate moiety. Activation by G6P, which also binds to the allosteric site, is not noticeably influenced by Mg^{2+} [42, 82], presumably because the associa-

tion constant of Mg-G6P ($K_a = 70\,M^{-1}$, 30°C; calculated from [83]) is three orders of magnitude lower than that of Mg-ATP ($K_a = 73 \times 10^3\,M^{-1}$, 30°C [84]). Activation by pyrophosphate, which readily complexes with Mg^{2+}, is however completely abolished by Mg^{2+} [42]. The phosphate moiety is probably less important for binding at the catalytic site, as UDP inhibition is not markedly influenced by Mg^{2+} even though UDP readily complexes with Mg^{2+} ($K_a = 4 \times 10^3\,M^{-1}$) [42]. Based on these observed effects of Mg^{2+}, we speculate that at high concentrations of Mg^{2+}, ATP inhibition could shift away from the allosteric site to the catalytic site.

Finally, GS is phosphorylated *in vivo* at at least nine serine residues [85, 86]. Overall, phosphorylation has a potent inhibitory effect, but not all phosphorylation sites affect the enzyme's activity. We will discuss the regulation of GS by phosphorylation in detail in Section 2.3. Briefly, inhibition by phosphorylation is the result of an altered affinity of GS for its reactants and modifiers and possibly a decrease in the turnover number (k_{cat}).

Phenomenological rate equation

Up to this point, we have reviewed the general properties and kinetics of GS. We now proceed to develop a detailed formal treatment of GS kinetics that will serve as the setting within which we will discuss the allosteric and covalent regulation of GS. The kinetics of most enzymes is adequately described with only the familiar concepts of maximal velocity and half-saturation concentrations parametrized by the V_{max} and Michaelis constants. In addition to these concepts, a formal treatment of GS kinetics must also describe cooperativity, and catalytic and specific modification. To describe these concepts, we will here adopt the Hill formalism as generalized by Hofmeyr & Cornish-Bowden [87], and Westermark *et al.* [88]. It is often considered a weakness of the Hill equation that it does not have a mechanistic interpretation; that is, it is largely independent of the kinetic mechanism and the mechanism of cooperativity, at least for non-integer values of the Hill coefficient. However, we consider this a strength when, as for GS, there is little agreement regarding these mechanisms in the first place. Moreover, while not all the Hill equation's parameters have mechanistic interpretations, they have clear operational definitions. Nevertheless, it should be mentioned that the Hill equation is unable to describe heterotropic cooperativity such as is observed for GS between G6P and ATP. This shortcoming does not alter the meaning of any parameter, but requires us to consider ATP as constant when G6P is varied and the other way around.

Based on the properties and kinetics of GS discussed up to this point, we make the following simplifying assumptions:

- glycogen is saturating and binds equally well as substrate and product to GS and is therefore left out
- product inhibition by UDP is significant, but binding at the allosteric site is negligible
- G6P could be both a catalytic and specific activator
- ATP is only a specific inhibitor
- ATP binds to both the catalytic and allosteric site
- all other effectors are constant and their effects are absorbed in the explicit parameters

Eq. 2.4 then describes the velocity of the GS reaction as in Eq. 2.1 for a particular GS phosphorylation state at constant G6P and ATP concentrations [87]:

$$v = \frac{\mu_{\text{cat}} V_{\text{max}} \sigma(\sigma+\pi)^{h-1}}{\mu_{\text{spec}} + (\sigma+\pi)^{h}} \times \left(1 - \frac{\Gamma}{K_{\text{eq}}}\right) \tag{2.4}$$

where $V_{\text{max}} = k_{\text{cat}} \cdot [\text{E}]_{\text{tot}}$; k_{cat} is the catalytic constant; $[\text{E}]_{\text{tot}}$ is the total GS concentration; $\sigma = [\text{UDPG}]/\text{UDPG}_{0.5}$; $\pi = [\text{UDP}]/\text{UDP}_{0.5}$; $\text{UDPG}_{0.5}$ and $\text{UDP}_{0.5}$ are the UDPG and UDP half-saturation concentrations in the absence of other ligands; h is the degree of reactant (UDPG and UDP) binding cooperativity; Γ is the mass-action ratio; K_{eq} is the equilibrium constant; and μ_{cat} and μ_{spec} describe catalytic and specific modification. Note that when $\mu_{\text{cat}} = 1$ and $\mu_{\text{spec}} = 1$, then Eq. 2.4 simplifies to the standard reversible Hill equation without modifier effects [87].

From the derivation by Westermark *et al.* [88] and considering our assumptions, the expression for μ_{cat} is given by

$$\mu_{\text{cat}} = \frac{1 + \gamma_{\text{G6P}} \cdot \alpha_{\text{G6P}} \cdot \xi_{\text{G6P}}^{h_{\text{G6P}}} + \alpha_{\text{ATP}} \cdot \xi_{\text{ATP}}^{h_{\text{ATP}}}}{1 + \alpha_{\text{G6P}} \cdot \xi_{\text{G6P}}^{h_{\text{G6P}}} + \alpha_{\text{ATP}} \cdot \xi_{\text{ATP}}^{h_{\text{ATP}}}} \tag{2.5}$$

where $\xi_{\text{G6P}} = [\text{G6P}]/\text{G6P}_{0.5}$; $\xi_{\text{ATP}} = [\text{ATP}]/\text{ATP}_{0.5}$; $\text{G6P}_{0.5}$ and $\text{ATP}_{0.5}$ are the G6P and allosteric site ATP half-saturation concentrations in the absence of other ligands; $\gamma_{\text{G6P}} \geq 1$ is the factor by which saturating G6P multiplies k_{cat} (values larger than unity indicate activation); $\alpha_{\text{G6P}} \geq 1$ and $\alpha_{\text{ATP}} < 1$ are the factors by which saturating

G6P and ATP divide the reactant half-saturation concentrations; h_{G6P} is the degree of G6P binding cooperativity; and h_{ATP} is the degree of ATP binding cooperativity at the allosteric site. Although we assume that ATP is not a catalytic inhibitor, it does reverse catalytic activation by G6P and must therefore appear in μ_{cat}. In the absence of G6P or if ATP is saturating, $\mu_{cat} = 1$, thus reflecting our assumption that ATP does not affect the enzyme's catalytic capacity. In the absence of ATP, on the other hand, μ_{cat} increases from unity to γ_{G6P} as the G6P concentration changes in the range from zero to saturation. At saturating G6P concentrations, the maximal velocity of GS is thus multiplied by a factor γ_{G6P}.

Specific activation by G6P and ATP at the catalytic and allosteric sites is described by μ_{spec} [87]:

$$\mu_{spec} = \left(1 + \xi_{ATP'}^{h_{ATP'}}\right)\left(\frac{1 + \xi_{G6P}^{h_{G6P}} + \xi_{ATP}^{h_{ATP}}}{1 + \alpha_{G6P} \cdot \xi_{G6P}^{h_{G6P}} + \alpha_{ATP} \cdot \xi_{ATP}^{h_{ATP}}}\right) \tag{2.6}$$

where $\xi_{ATP'} = [ATP]/ATP'_{0.5}$; $ATP'_{0.5}$ is the catalytic site ATP half-saturation concentration in the absence of other ligands; and $h_{ATP'}$ is the degree of ATP binding cooperativity at the catalytic site. If $[G6P] \gg G6P_{0.5}$, Eq. 2.6 simplifies to

$$\mu_{spec} = \frac{1}{\alpha_{G6P}}\left(1 + \xi_{ATP'}^{h_{ATP'}}\right) \tag{2.7}$$

showing that, although G6P completely overcomes ATP inhibition at the allosteric site, ATP inhibition at the catalytic site would only be abolished for a large value of α_{G6P}. Saturation by ATP, on the other hand, causes $\mu_{spec} \to \infty$; that is, reactant binding is completely inhibited.

The non-mathematically minded may safely ignore these equations, but should keep the operational definitions of the parameters in mind, as they form the basis for further discussion.

Measures of activity

The complex allosteric and covalent regulation of GS has led to the adoption of measures such as activity ratio and fractional velocity to quantify the effects of phosphorylation and the enzyme's sensitivity to G6P. It was initially thought that GS—like GP—is phosphorylated at only one site and that the phosphorylated form is entirely dependent on G6P for activity. This led Villar-Palasi & Larner [89] to introduce the activity ratio as the ratio of enzyme activity in the absence of G6P (representative

of I form activity) to that at saturating (typically 7.2 or 10 mM) G6P concentrations (representative of the total enzyme activity):

$$AR = \frac{v_{\text{G6P}=0}}{v_{\text{G6P}\gg\text{G6P}_{0.5}}} = \frac{I}{I+D} \tag{2.8}$$

The activity ratio, which is often alternatively known as the -G6P/+G6P ratio or expressed as a percentage ($\%I$), can thus be interpreted as the fraction of total enzyme that is present in the I form. However, as more phosphorylation sites were discovered, it became clear that—although it provided a good measure of the effect of phosphorylation on GS kinetics—the activity ratio could no longer be considered a mole fraction. Guinovart *et al.* [90] offered an interpretation at the hand of the Michaelis-Menten equation, assuming that G6P has no catalytic effect and increases the UDPG affinity to the point of saturation for even the most phosphorylated states:

$$AR = \frac{v}{V_{\text{max}}} = \frac{\sigma}{1+\sigma} \tag{2.9}$$

where $\sigma = [\text{UDPG}]/K_{\text{UDPG}}$. It is clear from Eq. 2.9 that the activity ratio is independent of the affinity of GS for G6P [90]. With Eq. 2.4 we are now in a position to provide a more general expression for the activity ratio, accounting for both catalytic and specific activation. Setting $[\text{UDP}] = 0$ and $[\text{ATP}] = 0$, and substituting Eq. 2.4 in Eq. 2.8, we obtain:

$$AR = \frac{1+\alpha_{\text{G6P}}\cdot\sigma}{\gamma_{\text{G6P}}\cdot\alpha_{\text{G6P}}(1+\sigma)} \tag{2.10}$$

As in Eq. 2.9 the enzyme's affinity for G6P does not influence the activity ratio, however, the degree to which saturating G6P activates GS catalytically (quantified by γ_{G6P}) and specifically (quantified by α_{G6P}) is reflected in this value. In the limit where $\alpha_{\text{G6P}} \to \infty$, i.e., supposing that saturating G6P will also enhance UDPG binding to the point of saturation, and if $\gamma_{\text{G6P}} = 1$, i.e., G6P results in no catalytic activation, Eq. 2.10 simplifies to Eq. 2.9. On the other hand, strong catalytic activation (very large γ_{G6P}) will generally result in low activity ratios. In the context of phosphorylation, the activity ratio is then a measure of the effect of phosphorylation on UDPG binding affinity, and specific and catalytic activation by G6P. But it cannot be determined from the activity ratio alone whether phosphorylation affects the k_{cat} or $\text{G6P}_{0.5}$. Moreover, Guinovart *et al.* [90] point out that the activity ratio is only sensitive to changes in phosphorylation if $\sigma \approx 1$, necessitating the use of high, impractical UDPG concentrations for extensively phosphorylated enzyme states.

Fractional velocity has been proposed as a more sensitive measure of the effects of phosphorylation [90]. It is defined as the ratio of enzyme activity in the presence of low physiological G6P concentrations to that in the presence of saturating G6P:

$$FV_x = \frac{v_{\mathrm{G6P}=x}}{v_{\mathrm{G6P}\gg\mathrm{G6P}_{0.5}}} \tag{2.11}$$

where x is a physiological G6P concentration. Substituting Eq. 2.4 into Eq. 2.11 yields

$$FV_x = \frac{(1+\alpha_{\mathrm{G6P}}\cdot\sigma)\left(\frac{1+\gamma_{\mathrm{G6P}}\cdot\alpha_{\mathrm{G6P}}\cdot\xi_{\mathrm{G6P}}^{h_{\mathrm{G6P}}}}{1+\alpha_{\mathrm{G6P}}\cdot\xi_{\mathrm{G6P}}^{h_{\mathrm{G6P}}}}\right)}{\gamma_{\mathrm{G6P}}\cdot\alpha_{\mathrm{G6P}}\left(\frac{1+\xi_{\mathrm{G6P}}^{h_{\mathrm{G6P}}}}{1+\alpha_{\mathrm{G6P}}\cdot\xi_{\mathrm{G6P}}^{h_{\mathrm{G6P}}}}+\sigma\right)} \tag{2.12}$$

Since G6P increases the affinity of GS for UDPG, the fractional velocity reflects changes in the degree of phosphorylation even if UDPG is not near its half-saturation concentration [90]. Furthermore, it also reflects the effects of phosphorylation on G6P affinity.

Due to the complex kinetics of GS, even recent studies on the allosteric and covalent regulation of GS often only report the activity ratio or fractional velocity. It is in principle possible to determine kinetic parameter values from these ratios, provided they were determined under differing conditions. In the sections to come, however, we will use the activity ratio and fractional velocity—keeping in mind their interpretations in terms of Eq. 2.4—only to examine *trends* in parameter values.

2.3 Regulation by phosphorylation

Rosell-Perez *et al.* [71] showed that GS can be isolated as two kinetically distinct forms: the active G6P-independent (I) form and the less active G6P-dependent (D) form. Their work was prompted by the observation that pre-incubation with insulin or G6P increased the enzyme's activity in the absence of G6P. This activation was the first indication of the covalent modification now known to be reversible phosphorylation. To date more than 15 phosphorylation sites have been discovered, but only nine sites have so far been confirmed as *in vivo* targets [85]. GS was the first enzyme in which hierarchical multisite phosphorylation was discovered and serves as a paradigm for this, now recognized as common, phenomenon [86, 91].

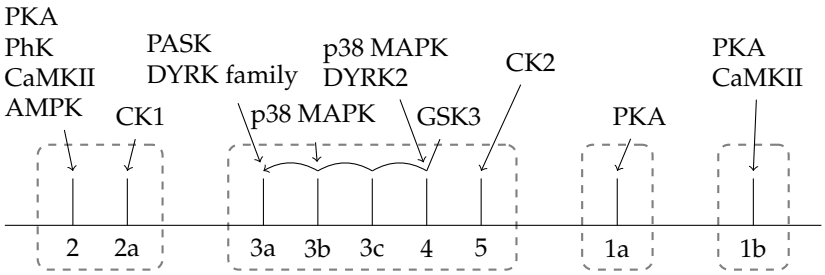

Figure 2.3: *In vivo* phosphorylation sites in mammalian GS [85, 86, 91–94]. Dashed boxes indicate phosphorylation clusters. The listed kinases are known to phosphorylate the indicated sites *in vitro*.

Phosphorylation sites and clusters

GS is phosphorylated *in vivo* by a variety of kinases at at least nine phosphorylation sites (Table 2.2). The confirmed *in vivo* phosphorylation sites are grouped into four phosphorylation clusters [86, 91] (Fig. 2.3). Phosphorylation sites in a cluster are equally spaced and are phosphorylated in a hierarchical, sequential manner. Each cluster has a primary phosphorylation site that must be phosphorylated before sequential phosphorylation of the secondary sites can proceed. Phosphorylation of the primary site by the primary kinase creates the recognition motif for the secondary kinase at the second site. Phosphorylation of the secondary sites recursively creates the recognition motif of the secondary kinase as long as free sites remain in the cluster. Primary and secondary phosphorylation is generally catalysed by different enzymes; otherwise, since the primary kinase has no requirement for prior phosphorylation, the process would not occur sequentially. However, amino acids such as Glu and Asp mimic the chemistry of phosphate groups and can thus serve as recognition motifs for secondary kinases, eliminating the need for a primary kinase [91].

Sites 2 and 2a form a cluster in the N-terminal region (Ser7 to Ser10). Site 2 is phosphorylated by a number of kinases, including cAMP-dependent protein kinase (PKA), phosphorylase kinase (PhK), calmodulin-dependent protein kinase II (CaMKII), and AMP-activated protein kinase (AMPK). Casein kinase 1 (CK1), with a recognition motif of S(P)-X-X-S, catalyses the secondary phosphorylation at site 2a [100, 106, 107]. Although phosphorylation at site 2 significantly enhances phosphorylation at site 2a, the latter can proceed in the absence of phosphorylation at site 2. Sites 5, 4, 3c, 3b, and 3a form a cluster near the C-terminus. Site 5 is the primary site and is phosphorylated by casein kinase 2 (CK2). Phosphorylation of site 5 creates

Table 2.2: *In vivo* phosphorylation sites in mammalian GS. Amino acids are numbered according to the rabbit muscle enzyme.

Residue	Name	Kinase	References
Ser7	2	PKA	[95]
		PhK	[96, 97]
		CaMKII	[98]
		AMPK	[99]
Ser10	2a	CK1	[100]
Ser656	5	CK2	[101]
Ser652	4	GSK3	[102]
		p38 MAPK	[94]
		DYRK2	[92]
Ser648	3c	GSK3	[103]
Ser644	3b	GSK3	[103]
		p38 MAPK	[94]
Ser640	3a	GSK3	[103]
		PASK	[93]
		DYRK family	[92]
Ser697	1a	PKA	[104]
Ser710	1b	PKA	[104]
		CaMKII	[105]

the glycogen synthase kinase 3 (GSK3) recognition motif S-X-X-X-S(P) and is an absolute prerequisite for secondary phosphorylation by GSK3 [102, 108]. Proceeding in the N-terminal direction, GSK3 sequentially phosphorylates sites 4, 3c, 3b, and 3a.

Sites 1a (Ser697) and 1b (Ser710) can technically not be considered phosphorylation clusters. However, both are located in motifs that resemble the amino acid sequence surrounding site 2. In particular, both are phosphorylated *in vivo* by PKA and are located three residues N-terminal to a serine or threonine residue [86]. Phosphorylation of these downstream residues by CK1 has been demonstrated with synthetic peptides, but the *in vivo* significance of these sites is unknown [86]. As such, sites 1a and 1b can be considered primary sites of vestigial (or emerging!) clusters that are in theory capable of hierarchical phosphorylation. Site 1b is also phosphorylated by CaMKII [105].

GS dephosphorylation is catalysed by protein phosphatase 1 (PP1), which is targeted to glycogen by several regulatory subunits [5, 31]. It is not known whether

dephosphorylation follows a sequential pattern. There is some indication that dephosphorylation of sites 2 and 2a proceeds sequentially and in the opposite direction to phosphorylation: a phosphate at site 2a inhibits dephosphorylation of site 2 [109]. At least one case has been reported where a protein phosphorylated sequentially by CK2 and GSK3 undergoes sequential dephosphorylation in the reverse direction [110]. However, it is not known whether the GS sites phosphorylated by these enzymes are also dephosphorylated sequentially.

Despite the cluster organization of phosphorylation sites, phosphorylation does not always proceed hierarchically. Members of the dual specificity tyrosine phosphorylation regulated protein kinase (DYRK) family [92], PAS kinase (PASK) [93], and mitogen-activated protein kinase (p38 MAPK) [94] do not require prior phosphorylation (their recognition motifs do not include a phosphorylated serine residue) and are thus able to circumvent hierarchical phosphorylation. DYRK1A, DYRK1B, DYRK2, and PASK directly phosphorylate site 3a. DYRK2 possibly phosphorylates site 4 [92], acting as a primary kinase by creating the recognition motif of GSK3 that would allow secondary phosphorylation by this kinase without prior phosphorylation by CK2 at site 5. Likewise p38 MAPK phosphorylates sites 4 and 3b. p38 MAPK also phosphorylates three other sites—Thr713, Thr718, and Ser724—*in vitro*, but it is not known whether these sites are phosphorylated *in vivo*. Thr173 is the "secondary" site of site 1b.

The obligate sequential phosphorylation of GS by GSK3 begs the question whether the phosphorylation is processive (several sites are phosphorylated before the kinases dissociates from its substrate) or distributive (at most one site is phosphorylated before the kinase dissociates). Working with synthetic peptides, Fiol *et al.* [111] observed intermediate phosphorylation states, suggesting that phosphorylation is distributive. However, they also noted that some intermediate states accumulated to a lesser extent than others, indicating that phosphorylation at these sites is also processive to some degree.

Kinetic effects of phosphorylation

The majority of kinetic studies on GS have been done within the paradigm of the two-state I/D model of phosphorylation. However, as the exact phosphorylation state of many of the isolated I or D forms is unknown, kinetic parameters reported in these studies are highly variable. The difficulty in isolating completely dephosphorylated GS is well-known to experimentalists and has led to the adoption of

bacterial expression systems [107]. It is also unlikely that the D forms isolated by various workers were phosphorylated to the same extent or at the same sites. Moreover, supraphysiological kinase concentrations were often used, resulting in non-specific phosphorylation and phosphorylation at sites that would not occur *in vivo* [86]. Nevertheless, a comparison of the reported I and D kinetics provides useful information regarding the general effect of phosphorylation. In this section we will explore the general effects of phosphorylation—which is believed to be mediated by the interaction of phosphorylated serine residues with the basic residues in the arginine cluster—on the kinetic parameters of GS as defined by Eq. 2.4, and the contribution of individual phosphorylation sites towards these effects.

Modification of kinetic parameters

It is not clear whether phosphorylation affects the k_{cat} of GS. Due to the low activity of phosphorylated GS, the specific activity is often determined at saturating G6P. However, by comparing these specific activities, one can only draw conclusions about the effect of phosphorylation on the apparent k_{cat}, which is defined as $k_{cat,app} = k_{cat} \cdot \gamma_{G6P}$ at saturating G6P. Interestingly, $k_{cat,app}$ appears to be unaffected by phosphorylation, since phosphorylated and dephosphorylated forms have similar maximal activities in the presence of G6P [71, 72, 112, 113]. This could either be interpreted to mean that phosphorylation does not alter k_{cat}, or that both k_{cat} and γ_{G6P} are altered such that their product remains constant. In cases where the specific activity has been determined for various phosphorylation states of GS in the absence of G6P [114, 115], a decline in this value cannot be attributed exclusively to a decline in k_{cat}, as in the absence of G6P the UDPG concentration (4.4 mM) used in the assays is not necessarily saturating. Roach *et al.* [72] observed essentially the same V_{max} for a number of phosphorylation states; assuming similar enzyme concentrations, this suggests that phosphorylation does not affect the k_{cat}.

As will be discussed in Section 2.3, particular phosphorylation sites target GS to specific subcellular locations. Phosphorylation at these sites does not affect the activity of GS *per se*, but by targeting GS to glycogen-rich pools could increase the apparent local total GS concentration $[E]_{tot}$, and thus the maximal velocity.

The most pronounced effect of phosphorylation is a marked decrease in UDPG affinity, i.e., phosphorylation increases $UDPG_{0.5}$. Rosell-Perez and co-workers observed a four-fold higher $UDPG_{0.5}$ in rat muscle [71], a 1.5-fold higher $UDPG_{0.5}$ in rabbit muscle [116], and a five-fold higher $UDPG_{0.5}$ in dog muscle [117] for the D

form than for the I form. The fold increase was much smaller in all three cases in the presence of G6P. These and other data have been interpreted to mean that at saturating G6P the apparent $UDPG_{0.5}$ is independent of phosphorylation state [113]. At saturating G6P the apparent $UDPG_{0.5}$ is defined as $UDPG_{0.5,app} = UDPG_{0.5}/\alpha_{G6P}$. In order for $UDPG_{0.5,app}$ to remain constant despite phosphorylation, any increase in $UDPG_{0.5}$ must be matched by an equal increase in α_{G6P}. Others have only observed a significant difference in $UDPG_{0.5}$ for the I and D forms in the presence of high ATP concentrations (6 mM) [39]. Roach *et al.* [72] isolated nine samples of GS with phosphate contents ranging from 0.27 to 3.49 mol per mol subunit. In these samples $UDPG_{0.5}$ increased with the phosphate content from 1.3 to 9100 mM. In the presence of 5 mM G6P it increased from 65 to 160 μM. These high values obtained for the more phosphorylated forms are probably artefactual, as discussed by the authors, but the overall trend is nevertheless clear. Similarly, Guinovart *et al.* [90] recorded an increase in $UDPG_{0.5}$ from 1.5 to 200 mM as the number of phosphates per subunit increased from 0 to 4.3.

It should be noted that, in order to adhere to the thermodynamic constraints of the Haldane equation, phosphorylation must have equal effects on $UDPG_{0.5}$ and $UDP_{0.5}$. However, it has been noted in a few cases that phosphorylation strengthens UDP inhibition, i.e. it *decreases* $UDP_{0.5}$ [79, 118]. If this is indeed the case, phosphorylation should also be expected to have differential effects on the forward and reverse catalytic constants.

Piras *et al.* [39, 67] noted that higher G6P concentrations are necessary to reverse ATP inhibition in the D form than in the I form, and that the D form is much more strongly inhibited by ATP than the I form. Since they observed no effect of G6P on $UDPG_{0.5}$ at pH 6.6, the higher G6P requirements suggest that $G6P_{0.5}$ increases with phosphorylation, i.e., the affinity for G6P decreases, while the affinity for ATP increases. Without parameter fitting it cannot be determined whether the increase in ATP affinity is the result of decreased $ATP'_{0.5}$, $ATP_{0.5}$, or both. Roach *et al.* [72] showed that $G6P_{0.5}$ could increase by roughly three orders of magnitude as the phosphate content increased from 0.27 to 3.49 mol per mol subunit. Similarly, Nimmo *et al.* [119] observed an increase in $G6P_{0.5}$ from 0.05 to 10 mM as the number of phosphates per subunit increased from 0 to 1.95. Wang & Roach [120] found that complete phosphorylation by GSK3 increased $G6P_{0.5}$ ten-fold, whereas phosphorylation by PKA and CK1 increased $G6P_{0.5}$ 100-fold [56].

As discussed earlier, there is evidence that γ_{G6P} and α_{G6P} increase with phospho-

rylation such that the effects of phosphorylation on k_{cat} and $UDPG_{0.5}$ are cancelled by saturating G6P. However, although the specific activation of GS by G6P is well-established, it is much less certain whether G6P also increases the catalytic capacity (k_{cat}) of GS. However, if $k_{cat} \cdot \gamma_{G6P}$ is indeed independent of the phosphorylation state and if $\gamma_{G6P} > 1$, then it is implied that phosphorylation also affects k_{cat}. The effect of phosphorylation on α_{ATP} is not known. However, in analogy to α_{G6P}, we speculate that α_{ATP} approaches unity as phosphorylation increases; that is, ATP will bring about little further inhibition in GS states that are already substantially inhibited by phosphorylation.

It is generally accepted that UDPG binding is non-cooperative, i.e. $h = 1$, regardless of the phosphorylation state of GS. Hyperbolic kinetics have been reported for both the I form and D form [24, 41, 67]. Even in cases where negative cooperativity has been reported, h appears to be unaffected by phosphorylation. Roach *et al.* [72] reported an average h value of 0.8 for nine GS samples of varying phosphorylation degrees. In the presence of G6P, this value increased to unity for all phosphorylation states, thus restoring hyperbolic kinetics.

Roach *et al.* [72] reported an increase in sigmoidicity with regard to G6P with phosphorylation, i.e. h_{G6P} increased with phosphorylation. Hill plots of their data were, however, not linear. In support of these findings, Piras *et al.* [67] observed steeper Hill plots for the D form than the I form. This effect was potentiated in the presence of ATP. ATP did not seem to affect h_{G6P} in the I form. Similar results were observed for the D form in bovine heart [69]. Phosphorylation of sites in the N-terminal region, however, appears to have little effect on h_{G6P} [56]. Plesner *et al.* [82] observed sigmoid kinetics with regard to G6P only at low substrate concentrations.

The converse was observed with regard to h_{ATP}, i.e. sigmoidicity with respect to ATP binding decreases with phosphorylation [67]. In the I form, G6P increased h_{ATP}, but in the D form G6P had little effect.

Importance of individual phosphorylation sites

Thus far we have discussed the general effect of phosphorylation on GS kinetics without considering the importance of specific phosphorylation sites towards the observed change in kinetic parameters. Much time has been devoted to determine which phosphorylation sites have the greatest influence on GS kinetics. The relative importance of a particular site can be assigned by considering the effect that phosphorylation of the site has on the activity ratio.

Two methods have been used to determine the activity ratio and, in a few cases, kinetics for various GS phosphorylation states: phosphorylation with site-specific kinases, and site-directed mutagenesis. The first method relies on the hierarchical and sequential nature of GS phosphorylation. By using a primary and secondary kinase pair a specific phosphorylation cluster can be systematically phosphorylated. A disadvantage of this method is that the kinases are not all specific for only one site. PKA, for instance, will phosphorylate sites 2, 1a, and 1b. This particular case can be overcome by using PhK, which only phosphorylates site 2. A greater limitation of this method is that intermediate secondary phosphorylation states cannot be obtained. That is, secondary phosphorylation sites are all phosphorylated by the same kinase and it is thus difficult to prevent phosphorylation of the entire cluster in order to study intermediate states. Furthermore, regardless of promoting dephosphorylation, isolated GS usually still contains low amounts of residual phosphate [107]. By using site-directed mutagenesis, on the other hand, phosphorylation sites can be destroyed by replacing the serine residues of interest with alanine residues. This method too relies on sequential phosphorylation in that phosphorylation of a cluster cannot proceed past a mutated site. When using this method it must be kept in mind that kinases such as those from the DYRK family, PASK, and p38 MAPK are able to circumvent hierarchical phosphorylation and could phosphorylate sites past the mutated residues.

Studies using site-directed mutagenesis showed that no single phosphorylation site completely controls GS activity [114]. However, by mutating two phosphorylation sites simultaneously, a dramatic increase in activity ratio is usually observed. This is the case if both mutated sites are in the same cluster, but more so if sites from different clusters are mutated. The influence of a phosphorylation site must be interpreted both in terms of its intrinsic effect on GS activity and its role in sequential phosphorylation. Consider for instance site 5: in the first sense this site has virtually no influence, as it does not affect GS activity, but it is crucial in the latter sense in that it is a prerequisite for secondary phosphorylation. The experimentally determined activity ratios of GS phosphorylated at various sites are summarised in Table 2.3.

Brown *et al.* [56] used PKA and CK1 to systematically phosphorylate the N-terminal phosphorylation sites. They found that phosphorylation at site 2a (using only CK1) has a much greater effect on the activity ratio than phosphorylation at site 2 (using only PKA). Phosphorylation at both sites did not further decrease the activity ratio significantly. Kinetic analysis of these forms showed a mild increase in

$G6P_{0.5}$ for both the forms phosphorylated at sites 2 or 2a, but a significant further increase when both sites were phosphorylated. This increase in $G6P_{0.5}$ when both sites are phosphorylated does not correspond to a decrease in activity ratio below what is already seen for phosphorylation at only site 2a. As these workers used PKA, sites 1a and 1b were likely also phosphorylated. In contrast, more recent findings [106], or studies using PhK instead of PKA [109], recombinant GS (in an effort to limit residual phosphorylation) [107], or site-directed mutagenesis [114] indicate that site 2 is the more important site and that phosphorylation at only site 2a, or phosphorylation of this site in addition to phosphorylation at site 2, has a less significant effect on the activity ratio. In the N-terminal region, then, site 2 is probably the most important site in terms of both its intrinsic effect and its potentiation of phosphorylation at site 2a.

Incorporation of one phosphate per GS subunit by CK1 at site 5 has no effect on the activity ratio [107]. However, phosphorylation at this site is an absolute prerequisite for phosphorylation of the secondary sites in the rest of the cluster. Subsequent phosphorylation by GSK3 over 50 minutes resulted in the incorporation of an additional four phosphates per GS subunit and a marked decrease (from roughly 0.7 to 0.1) in activity ratio. Using site-directed mutagenesis, Wang and Roach [120] showed that only phosphorylation at sites 3b and 3a have significant effects on the activity ratio. Kuma *et al.* [94] reported that phosphorylation at site 3b had no inhibitory effect, but that subsequent phosphorylation at site 3a decreased GS activity. It appears then that the sole function of sites 5, 4, 3c, and, to some extent, 3b is to facilitate phosphorylation at site 3a, which results in potent inhibition. The existence of kinases, such as the DYRK family, PASK, and p38 MAPK, that directly phosphorylate site 3a supports this view. It is also interesting to note that in the C-terminal region only sites 3a and 3b are conserved between the yeast and mammalian enzymes [121].

As measured by their effect on the activity ratio, sites 1a and 1b do not appear to be important in terms of inhibition [114].

While complete phosphorylation of the clusters in the N- or C-terminal regions leads to substantial inactivation of GS, complete inactivation is only attained when both clusters are phosphorylated fully or at the important sites [107, 114]. The effects of phosphorylating various sites in combination on GS activity has been the topic of extensive site-directed mutagenesis studies [114, 115, 122]. These studies have, however, been complicated by the presence of kinases that circumvent hierarchical phosphorylation, the existence of which was not known at the time. The experi-

Table 2.3: Activity ratios (Eq. 2.8) of various GS phosphorylation states. Unless stated otherwise, the G6P concentration, when present, was 7.2 mM. UDPG was present at 4.4 mM. Lower values indicate greater inhibition. [a] [G6P] = 10 mM. [b] Sites 1a and 1b possibly phosphorylated; average of soluble and pellet fractions.

Phosphorylated sites	Activity ratio	Reference
none	0.8	[120]
2	0.45[a]	[109]
2+2a	0.17[a]	[109]
5	0.8	[120]
5+4	0.8	[120]
5+4+3c	0.8	[120]
5+4+3c+3b	0.6	[120]
5+4+3c+3b+3a	0.1	[120]
2+5+4+3c+3b	0.166[b]	[114]
2+5+4+3c+3b+3a	0.02[b]	[114]
2a+5+4+3c+3b	0.019[b]	[114]
2a+5+4+3c+3b+3a	0.011[b]	[114]

mentally determined activity ratio values of GS phosphorylated at various sites are summarised in Table 2.3.

Phosphorylation-dependent translocation

It is becoming increasingly clear that subcellular compartmentalization and translocation are major factors in the regulation of glycogen metabolism [123, 124]. Glycogen and many enzymes associated with it have been shown to be targeted to various intracellular compartments.

Recent studies suggest a strong link between GS phosphorylation state and subcellular localization. Prats *et al.* [125], working with rabbit muscle, found that GS phosphorylated at site 1b was exclusively associated with myofibrillar cross-striations (sarcomere I-bands). This was observed under both basal and exercise-stimulated conditions. Under basal conditions, GS phosphorylated at sites 1a or 3a+3b was found mainly in a perinuclear region and at cross-striations. Under exercise-stimulated conditions, however, GS phosphorylated at these sites was associated with actinin-containing spherical structures. No association with these spherical structures was observed for GS phosphorylated at sites 1b or 2+2a. GS phosphorylated at sites 2+2a was found in intermyofibrillar clusters, regardless of exercise stimulation. Similar results were obtained for human muscle [126]. In summary, phosphorylation at site 1b

Table 2.4: Phosphorylation-dependent intracellular distribution of GS [125, 126]

Phosphorylated sites	Basal	Exercise-stimulated
2, 3a, 3a+3b, 1a	perinuclear region cross-striations	spherical structures
2+2a	intermyofibrillar clusters	intermyofibrillar clusters
1b	cross-striations	cross-striations

exclusively targets GS to the intramyofibrillar cross-striations, whereas phosphorylation at site 2+2a targets GS to intermyofibrillar clusters (Table 2.4). Prats *et al.* [124] proposes that phosporylation at sites 2+2a, and the subsequent translocation, is the result of AMPK-dependent sensing of glycogen depletion in the intermyofibrillar region. Similarly, they argue that, since intramyofibrillar glycogen is preferentially used during exercise, phosphorylation at site 1b by PKA in response to adrenaline stimulation targets GS to this compartment to replete glycogen after exercise. Site 1b has been shown to be phosphorylated by CaMKII, suggesting a role for Ca^{2+} in GS translocation. From a kinetic perspective we have seen that phosphorylation at site 1b and, to a lesser extent, site 2a have little effect on GS activity. The above findings, however, suggest major roles for these two sites in GS translocation, which in turn regulates GS activity.

Insulin and glycogen content have also been shown to affect the subcellular localization of GS. Brady *et al.* [127] reported an insulin-induced decrease in cytosolic GS and ascribed it to G6P-mediated activation of PP1. Similarly, in human muscle cells insulin treatment results in dephosphorylation at sites 3a and 3b and a concomitant translocation to a particulate subcellular fraction [128]. The effect is abolished by insulin pre-treatment, possibly because under these conditions glycogen accumulates and overrides the insulin signal [128]. However, in rhesus monkey muscle, insulin treatment does not result in GS translocation [129]. Cid *et al.* [130] found that the distribution of GS is not affected by phosphorylation, but that deletion of the region enclosing the regulatory arginine cluster, which is implicated in regulation by G6P and phosphorylation, affected the nuclear accumulation of GS. There was also an inverse correlation between glycogen content and nuclear accumulation. Nielsen *et al.* [131] showed that at low glycogen levels GS translocated to a cytoskeleton fraction from a glycogen-rich membrane fraction. Low glycogen levels were also associated with smooth immunofluorescent stains at what corresponds to I-bands.

Function of GS multisite phosphorylation

Compared to GP, which is phosphorylated at only a single site, the multisite phosphorylation of GS seems almost excessive. Multisite phosphorylation is, however, not uncommon. Its prevalence and general function have been reviewed extensively [91, 132, 133]. Here we will discuss its function as it pertains to GS. As discussed, GS has both dispersed sites and clusters, and within clusters phosphorylation is hierarchical, sequential, and mostly distributive.

Multisite phosphorylation facilitates the integration of signals from the various endocrine, neural, and metabolic stimuli. As regards GS, signal integration is manifested on the level of both individual phosphorylation sites and clusters. Multiple kinases phosphorylate the same sites or clusters, and many sites share the same kinase. Site 2 is a substrate for numerous kinases regulated by different signals. Similarly, site 3a can be phosphorylated directly by a number of kinases, or via hierarchical and sequential phosphorylation by GSK3. Site 1b is likewise phosphorylated both by PKA and CaMKII. The adrenaline-stimulated cAMP-dependent pathway and the insulin-stimulated PI3K-dependent pathway—arguably the most prominent GS phosphorylation pathways—each affects different phosphorylation clusters.

Hierarchical phosphorylation is not a prerequisite for sequential phosphorylation. Appropriately positioned anionic amino acids are able to mimic phosphorylated primary phosphorylation sites and thus allow for sequential secondary phosphorylation [91]. However, hierarchical phosphorylation facilitates regulation at two levels: primary phosphorylation and secondary phosphorylation [86]. As both are catalysed by different kinases, each kinase can be regulated independently. In the N-terminal cluster of GS, it is the primary kinases that are regulated; either by the cAMP-dependent pathway (PKA) or by metabolic signals (AMPK). In the C-terminal cluster, on the other hand, the secondary kinase, GSK3, is regulated via the PI3K-dependent pathway. In addition, phosphorylation can also be regulated at the phosphatase level. Both adrenaline- and insulin-stimulation regulate PP1 activity.

In a random phosphorylation mechanism, the number of phosphorylation states per subunit increases exponentially with the number of phosphorylation sites. A protein subunit with n phosphorylation sites can result in up to 2^n phosphorylation states. In sequential phosphorylation, on the other hand, the number of phosphorylation states is a linear function $(n + 1)$ of the number of sites. If one assumes strict sequential phosphorylation (and dephosphorylation), the number of distinct GS phosphorylation states per subunit amounts to $(2 + 1) \times (5 + 1) \times 2 \times 2 = 72$. Were a

random mechanism employed, the number of states would amount to $2^9 = 512$. Sequential phosphorylation therefore severely limits the number of phosphorylation states and brings about an orderly transition between different states. This is beneficial if, as in the case of GS, only specific phosphorylation sites (for example, site 3a) elicit a particular effect. Phosphorylation of site 3a can be achieved and reversed with precision by adjusting the ratio of kinases to phosphatases appropriately in a sequential mechanism. In a random mechanism, on the other hand, phosphorylation of a particular site cannot be achieved with precision. However, a number of kinases circumvents sequential GS phosphorylation, obscuring any benefit it might entail. The number of states per cluster is therefore also likely significantly more than 72.

It has been argued (as discussed by Gunawardena [134]) that multisite phosphorylation, particularly if it proceeds distributively and sequentially, results in an ultrasensitive response to the ratio of kinase to phosphate, so that below a certain threshold the protein in question would be almost completely dephosphorylated, whereas above the threshold complete phosphorylation is rapidly attained. According to this view, more phosphorylation sites result in higher sensitivity, approaching switch-like behaviour. However, it has been demonstrated [134] that, although multiple phosphorylation creates a sharp threshold, an increase of the kinase to phosphatase ratio beyond the threshold does not result in switch-like behaviour, i.e., complete phosphorylation does not ensue rapidly. On the contrary, beyond the threshold, the response becomes milder as the number of phosphorylation sites increases. It seems feasible then that a function of the sequential phosphorylation of GS is to fine-tune the threshold at which the ratio of kinase to phosphatase elicits a response. This is particularly of interest if one considers that, apart from GS, GSK3 has numerous substrates in various signalling pathways [135]; regulation of GSK3 affects all these pathways, but by employing multiple phosphorylation to different extents, each pathway can refine its response to changes in GSK3 levels.

2.4 Regulation by glucose-6-phosphate

In 1959 Leloir *et al.* [22] were the first to show that G6P activates GS. They continued to show that G6P, which can appear to be a requirement for catalysis by highly phosphorylated GS, does not take part in the reaction and presumably binds to an allosteric site. This initial work was followed by kinetic studies in a variety of species

[71, 116, 117, 136, 137], which suggested that GS activation by G6P is a universal feature in eukaryotes. The regulation of GS by G6P is multifaceted and the initial assessment of Leloir *et al.* [22] is no surprise:

> "As to the mechanism by which G-6-P increases the activity of the glycogen-forming enzyme, no clue was obtained."

To date five mechanisms have been described by which G6P affects GS activity: it is 1) a substrate precursor, 2) an allosteric GS activator, 3) a GS kinase inhibitor, 4) a GS phosphatase activator, and 5) it enhances the export of GS from the nucleus. In this section we will discuss the binding of G6P to GS and the resulting conformational change that leads to activation (both allosteric and covalent) and possibly translocation of GS.

G6P-induced conformational change

The activation of GS by G6P must ultimately be the result of some conformational change, but little is known about such a conformational change in the muscle enzyme. However, due to the high degree of conservation between the yeast and muscle enzymes, it is instructive to consider the conformational change induced in ScGS upon G6P binding as revealed by the crystal structure of this enzyme in the presence of G6P [51]. In ScGS, G6P binds between the R helix (α22) and helix α13. The former contains the regulatory arginine cluster and links the crossed-over C-terminus and the phosphorylation sites to the C-terminal Rossmann fold domain. Helix α13 (together with α12) forms the main connection between the N- and C-terminal Rossmann fold domains. The phosphate moiety of G6P binds tightly in a pocket formed by amino acid residues from both the R helix and α13—including Arg582 and Arg586, residues that have been shown to be essential for G6P activation of the yeast [51, 63] and muscle [18, 64] enzymes. This pocket is ordered in the unbound state, and undergoes little change upon G6P binding. The G6P glucose moiety, on the other hand, forms hydrogen bonds with His280 and Gln283, which reorders the region between residues 278 and 284, allowing Asn284 to hydrogen bond with the corresponding residue of the subunit across the dimer pair two-fold symmetry (i.e. the A/B or C/D interface). The arginine residues therefore likely act as anchors of the G6P molecule so that the glucose moiety can bond with His280 and Gln283 [51]. It is tempting to speculate that the phosphate of ATP is similarly

anchored by Arg582 and Arg586, with the difference that the adenosine moiety stabilizes an inactive conformation.

G6P binding and the subsequent reordering of residues 278–284 bring about significant conformational change [51, 53] (Fig. 2.1d). The R helices within the A/B and C/D dimers are forced apart by 3.4 Å and the intersubunit helices (α15 and α16) of the B/D dimer pairs are translated by 14.2 Å away from that of the A/C pair and rotated by 7 °. Within subunits, the C-domain is rotated by 8.5 ° relative to the intersubunit helix pair, and the N-domain is rotated a further 4.5 ° relative to the C-domain. The overall effect of the conformational change is that the association between the N-domain insert (α2 and the loop between β4 and β5) and C-domain insert (α16), which locks the subunits in an inactive open conformation, as well as the reciprocal intersubunit interaction of the loops between β15 and α18 within the A/D and B/C interfaces are abrogated (Fig. 2.1c). In the G6P-bound form, α16 instead associates with the loop between β15 and α18 of its partner subunit in the dimer, allowing the interdomain closure that is required for catalysis.

Comparing the structures of the G6P insensitive mutant R580A/R581A/R583A (yeast enzyme numbering) to the inactive, but G6P sensitive, mutant R589A/R592A in the presence of G6P, Baskaran [53] observed a closure of the active site of subunit B relative to the G6P insensitive mutant over and above of that witnessed in the remaining three subunits. This additional closure was the result of G6P binding in the active site of subunit B. Although generally acting as a GS activator, this observation suggests that G6P could also compete with GS substrates, presumably UDPG, for the active site and therefore inhibit GS. Slight inhibition by G6P has been noted before for the dephosphorylated enzyme [64].

Effect of G6P on GS kinetics

In agreement with the extensive conformational change resulting from G6P binding, G6P affects the kinetics of GS significantly.

Several workers have observed higher apparent k_{cat} values in the presence of G6P. Such catalytic activation is described by $\gamma_{G6P} > 1$. In many cases the extent to which k_{cat} is affected seems to depend on the degree of phosphorylation. Rosell-Perez *et al.* consistently found an increase in the k_{cat} of the phosphorylated D enzyme from rat [71], rabbit [116], and dog [117], but observed no or little change in the k_{cat} for the dephosphorylated I form. The effect was independent of Mg^{2+}. Kornfeld & Brown [32], however, only reported an increase in k_{cat} in the presence of Mg^{2+}.

Others, working with the I form, reported no change in k_{cat}, but did observe that contamination with the D form resulted in catalytic activation of GS [42]. Catalytic activation was also observed for the D form from rat adipose tissue [68], bovine heart [69], and pig brain [70]. More recently, Lai *et al.* [138] found that catalytic activation increases with glycogen content, which in turn correlates with degree of phosphorylation. However, several workers have found no increase in k_{cat} in the presence of G6P, regardless of the phosphorylation state. Piras *et al.* [67] found no increase in k_{cat} for both the I and D forms of the rat muscle enzyme in response to G6P. Similarly, Roach *et al.* [72] observed essentially the same V_{max}, and thus k_{cat}, in the presence and absence of G6P for a range of phosphorylation states of the rabbit muscle enzyme.

The apparent effect of G6P on $UDPG_{0.5}$, on the other hand, is well-established (see for example [72]). Even for the most phosphorylated forms, G6P decreases the apparent $UDPG_{0.5}$ dramatically. This potent activation potential is indicative of a large α_{G6P} value. In most cases where catalytic activation was observed, specific activation was also observed.

G6P further activates GS by suppressing ATP binding at the allosteric site. This effect manifests as an apparent increase in $ATP_{0.5}$. Several secondary effects on k_{cat} and $UDPG_{0.5}$ could ensue, depending on the type of inactivation (specific or catalytic) that results from ATP binding. If, for instance, ATP inhibited GS by increasing the apparent $UDPG_{0.5}$ (i.e. $\alpha_{G6P} < 1$), then G6P would enhance substrate binding in the presence of ATP over and above its own direct activation of GS. Indeed, Piras *et al.* [67] argue that this indirect activation of GS has more physiological relevance than the direct effect of G6P on $UDPG_{0.5}$, since even the phosphorylated forms are often saturated with G6P at physiological concentrations, thus obscuring both the function of phosphorylation and G6P activation. In their view, ATP, which binds preferentially to the phosphorylated enzyme, restores the necessary G6P sensitivity in inactive GS. Moreover, G6P increases h_{ATP}, especially in the dephosphorylated enzyme, suggesting that, in addition to competing with ATP, G6P also stabilizes a conformation with a low affinity for ATP.

Finally, it is generally accepted that high G6P concentrations activate even the most phosphorylated forms of GS to the same level as the dephosphorylated enzyme [31, 89, 113]. This, as discussed earlier, is equivalent to stating that both $k_{cat} \cdot \gamma_{G6P}$ and $UDPG_{0.5}/\alpha_{G6P}$ are constants that are independent of phosphorylation state. Any effect of phosphorylation on k_{cat} or $UDPG_{0.5}$ is therefore reversed by G6P.

G6P-dependent covalent activation

Apart from reversing the effects of phosphorylation on the kinetics of GS, it has been demonstrated in a few cases that G6P also enhances the reversal of covalent phosphorylation itself; either by inhibiting GS kinases, or by activating GS phosphatases.

Phosphorylation by PKA at site 2 potently inactivates GS. It has, however, been observed that in rabbit skeletal muscle insulin inhibits PKA in a seemingly competitive fashion with regard to cyclic AMP (cAMP) [139]. At least one mechanism by which insulin inhibits PKA is by increasing the G6P concentration [139]. PKA (or R_2C_2) is a tetrameric enzyme consisting of two catalytic (C) subunits, each associated with a regulatory (R) subunit [140]. The R subunit is a pseudosubstrate that inhibits the C subunit by blocking its active site. Each R subunit has two binding sites for cAMP, which binds to it sequentially, leading to the stepwise dissociation of the R and C subunits and thus activation of PKA. Several PKA substrates are able to activate PKA in a cAMP-independent fashion [139]. These substrates compete with the R subunit for the active site. In the absence of cAMP, GS is able to stimulate PKA to an activity that is roughly 50% of that in the presence of 2 μM cAMP. When G6P is bound to GS, however, the ability of GS to activate PKA is abolished.

G6P inhibition of phosphorylation appears to be specific to PKA and GS [139]. No other GS kinases are inhibited by G6P, neither is the phosphorylation of other PKA substrates affected. The possibility that G6P brings about the inhibition by binding to the C or R subunits of PKA is thus ruled out and the inactivation must be the result of G6P binding to the allosteric site on GS. Since GS activates PKA by competing with the R subunit, one would expect that G6P decreases the C subunit's affinity for GS. No changes in the K_m or V_{max} were however found in the presence or absence of G6P. G6P appears then, by causing a conformational change in GS, to only hinder its ability to activate PKA and not the kinetics of PKA. This hints at an activation mechanism other than pure competition of GS with the R subunit. It has been suggested that the protein substrates of PKA could activate it by interaction with the R subunit [139].

G6P also inhibits one or more yeast GS kinases [141].

Traut & Lipmann [142] observed that incubation with G6P increased the activity of lamb muscle GS in the absence of G6P. GS activated in this way retained the activation after several days in cold storage. The activation by G6P was reversed by incubation with ATP. Therefore, apart from allosterically activating GS, it also activated the enzyme in a, presumably, covalent fashion. Kinase inhibition by G6P, as

discussed above, does not appear to have contributed significantly to the results obtained by Traut & Lipmann, as their preparations were, judging by the activity ratio, already extensively phosphorylated. This suggests that G6P also has the potential to enhance the dephosphorylation of GS. These findings have subsequently been verified by various other workers. Kato & Bishop [143] showed that G6P enhances the D to I form conversion of rabbit muscle GS by a protein phosphatase. This effect of G6P was not observed in the absence of the phosphatase. G6P analogues such as glucosamine-6-phosphate and galactose-6-phosphate, which also activate GS, had a similar effect on the dephosphorylation of GS. No effect was seen for the dephosphorylation of histone by the same phosphatase in the presence of G6P, suggesting that the activation of the phosphatase by G6P is mediated by the binding of G6P to GS. Others have shown that activation of the phosphatase reaction by G6P is inhibited by inorganic phosphate and sulphate [144], and ATP [145]. ATP was also shown to inhibit dephosphorylation of GS in human muscle [145].

More recently, Villar-Palasi [146] found that, in rabbit muscle, G6P activates the D form of GS covalently by promoting dephosphorylation. This effect was observed for both PP1 and protein phosphatase 2A (PP2A). Except for a slight activation at low G6P concentrations of GP dephosphorylation by PP1, G6P did not enhance the dephosphorylation of any other tested PP1 or PP2A substrates. This suggests that G6P does not directly activate the phosphatases in question, but rather causes a conformational change in GS, rendering it a better substrate. G6P activated dephosphorylation by PP1 and PP2A to the same degree. The G6P phosphatase activation was observed by measuring both the change in GS activity ratio and phosphate release. From both methods a K_a of 0.2 mMwas calculated for phosphatase activation. This coincided with the K_a for GS activation as determined for the preparation used in the study, strengthening the argument that the activation is caused by G6P binding to GS. Intriguingly, the affinity of the phosphatases for GS was not altered by G6P. The activation appears to rather involve an increase in the V_{max} and thus presumably the catalytic constant k_{cat}. It has been suggested that the GS conformational change resulting from G6P binding *exposes* the phosphorylation sites to PP1 [147]. Although such a view is a useful metaphor, it is not strictly in agreement with the observation that only the k_{cat} of the phosphatase is affected. Several other sugar phosphates that are known to activate GS were tested [146]. Those with the highest affinities for GS, such as fructose-6-phosphate and galactose-6-phosphate, yielded the highest covalent activation, with the former matching G6P, but there appeared to be no direct

relationship between GS affinity and phosphatase activation [146]. Note that even though PP2A is not generally considered a major *in vivo* GS phosphatase, we include it here to better illustrate that the reported activation of GS dephosphorylation by G6P is substrate-specific, i.e., independent of the particular phosphatase.

Nucleocytoplasmic shuttling

There is mounting evidence that the subcellular distribution of GS, from both liver and muscle, is regulated by glucose. In liver, incubation with glucose results in the translocation of GS from the cytosol to a region near the cell membrane [148, 149]. Similarly, Cid *et al.* [130] have shown that muscle GS translocates from the nucleus to the cytosol when incubated with glucose. Under conditions of glycogen and glucose depletion, GS conversely translocates to the nucleus. In addition to mediating the allosteric and covalent regulation of GS, the arginine cluster also functions as a nuclear localization sequence. Arginine cluster mutants, in which G6P sensitivity and presumably nuclear localization are abrogated, exhibited little or no nuclear accumulation. Systematic mutation of the GS phosphorylation sites indicated that phosphorylation does not affect nucleocytosolic GS translocation, suggesting that only G6P stimulates translocation to the cytosol. Moreover, based on the observation that 6-deoxyglucose does not stimulate translocation to the cytosol, Cid *et al.* [130] suggest that it is in fact G6P, and not glucose, that elicits the translocation. If this is indeed the case, G6P-stimulated translocation of GS to the cytosol would effectively increase the total GS concentration, $[\mathrm{E}]_{\mathrm{tot}}$, in the cytosol.

As G6P stimulates net dephosphorylation of GS, it is expected that it would also influence the subcytosolic distribution of GS by promoting the dephosphorylation of sites, such as 2a and 1b, that are associated with targeting GS to various fractions in the cytosol.

Function of G6P feedforward activation

G6P is a precursor of UDPG, one of the GS substrates. Activation of GS by G6P therefore constitutes a feedforward activation loop. Hofmeyr & Cornish-Bowden [15] have previously demonstrated that a similar regulatory mechanism, the feedback inhibition loop, does not function to control the flux through the regulated enzyme, but rather to maintain the concentration of the regulatory metabolite within a narrow range. In terms of GS, supposing a function of feedforward activation simi-

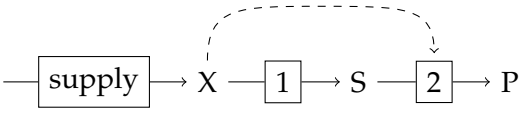

Figure 2.4: Minimal feedforward activation mechanism. Metabolite X is a product of the supply system, a substrate of enzyme 1, and an allosteric activator of enzyme 2. In order for the feedforward activation of enzyme 2 by X to be effective, enzyme 2 must hold the majority of flux control within the isolated block that excludes the supply system.

lar to that of feedback inhibition, the function of G6P activation is not to regulate the flux through GS, but rather to maintain G6P homeostasis. However, Hofmeyr *et al.* [16] argue that, unlike the situation in feedback inhibition, the type of activation—whether by increasing k_{cat} or decreasing K_m—has important consequences for the effectiveness of the mechanism in maintaining the concentration of the regulatory metabolite homeostatically. We will only briefly consider these consequences here. See [16] for a thorough mathematical exposition.

Consider the minimal feedforward activation loop portrayed in Fig. 2.4. Enzyme 2, the regulated enzyme, is activated allosterically by metabolite X, the regulatory metabolite. In order for the feedforward loop to be effective—that is, for activation of enzyme 2 to have any significant effect on the pathway—enzyme 2 should control the flux through the isolated subpathway (that part of the pathway that excludes the supply enzyme). One way in which complete flux control by enzyme 2 can be achieved is if it is saturated by its immediate substrate, S. However, in such a scenario any increase in the affinity of enzyme 2 for S resulting from activation by X is clearly futile, as enzyme 2 is already saturated by S and cannot bind more substrate in order to operate faster; enzyme 2 has reached its maximal velocity. Alternatively, if the action of X is to increase the catalytic rate, k_{cat} (and V_{max} by extension), of enzyme 2, the enzyme could operate faster despite being saturated by its substrate. Hofmeyr *et al.* [16] thus argue that catalytic activation (increase in k_{cat}) is expected to be the dominant type of activation in feedforward mechanisms.

In terms of GS, then, it is expected that G6P should be a catalytic—and not necessarily a specific—activator of GS, i.e., $\gamma_{G6P} > 1$ should hold. This is indeed the case for the major yeast GS [63]. However, it is much less certain whether this is also the case for the mammalian muscle enzyme. As discussed, many of the earlier studies found catalytic activation for the D form and specific activation for the I form. It can however be argued, that, since the I form already has a high affinity for UDPG, it is in fact the I form that would benefit most from catalytic activation, whereas the

D form, with a lower UDPG affinity, would benefit from specific (and catalytic) activation. There are two solutions not considered explicitly by Hofmeyr *et al.* [16] in which pure specific activation could still result in efficient feedforward activation. First, GS is a bisubstrate enzyme. In bisubstrate kinetics specific activation (and, trivially, catalytic activation) with regard to one substrate, say glycogen, manifests as catalytic activation with regard to the other, say UDPG, with the condition that the first substrate is not saturating. Therefore, if G6P enhances glycogen binding, which is likely the case, it would appear to increase the apparent k_{cat} if considered with respect to UDPG, even if kinetically G6P were only a specific activator. However, it is not clear to what extent such a situation is relevant physiologically, as GS is likely saturated by glycogen *in vivo*. Second, saturation by UDPG is not the only device by which flux control can be retained by GS; the same outcome would be achieved if the enzyme preceding GS operated near equilibrium. Since GS need no longer be saturated by UDPG, a G6P-induced increase in the affinity for UDPG becomes an effective form of activation.

We must however not only consider the direct effects of G6P on GS. As mentioned, G6P also activates GS by reversing inhibition by ATP and phosphorylation. If either ATP or phosphorylation decreases the apparent k_{cat}, then by reversing this decrease, G6P would appear to be a catalytic activator even if it exhibits no such activation in the absence of ATP or phosphorylation. The observation that G6P is a catalytic activator of the D form probably indicates a reversal of inhibition by phosphorylation, but there is no definitive evidence that either ATP or phosphorylation decreases the apparent k_{cat}. Finally, in what is effectively catalytic activation, G6P increases the total cytosolic concentration of GS by inducing its translocation from the nucleus. However, as glycogen depletion is a requirement for nuclear retention of GS, this mechanism of activation would likely only be relevant during the onset of glycogen resynthesis after exercise.

The effectiveness of G6P feedforward activation, whether specific or catalytic, appears to depend strongly on such cellular conditions as the concentrations of UDPG and ATP, the degree of GS phosphorylation, and glycogen content. In order to understand the function of GS feedforward regulation by G6P, it must be established definitively whether G6P is a catalytic or specific activator of GS, to what extent GS is saturated by its substrate *in vivo*, and to what extent ATP and phosphorylation affect the apparent catalytic capacity of GS.

2.5 A unifying view of covalent and allosteric regulation

The complex kinetics and regulation of GS, as discussed in the previous two sections, continue to evade description by a succinct mechanistic model. The sheer number of phosphorylation states and an incomplete understanding of how GS kinetics is altered by phosphorylation makes it near impossible to capture the enzyme's behaviour with conventional enzyme kinetic rate equations. In this section we will argue that, without deriving any form of rate equation yet, the MWC model could provide an adequate description of the nuances of GS kinetics and regulation—both allosteric and covalent—as reviewed in this writing.

Let us briefly summarize the interplay between G6P, ATP and phosphorylation. In many respects the effects of regulation by G6P and phosphorylation are reciprocal (Fig. 2.5A). G6P binding activates GS (a) in a cooperative fashion (b). It not only reverses the inhibitory effects of phosphorylation, but also reverses phosphorylation itself (c). Phosphorylation, on the other hand, inhibits GS (e). It also inhibits G6P binding (g), but intriguingly enhances G6P binding cooperativity (h). Conversely, the effects of ATP and phosphorylation on GS and each other appear to be qualitatively identical (Fig. 2.5B). Both inhibit GS (a, e). ATP enhances phosphorylation (c) and phosphorylation enhances ATP binding (g). In addition, phosphorylation decreases ATP binding cooperativity (h). Finally, G6P binding affects ATP binding and phosphorylation similarly; and ATP binding and phosphorylation affect G6P binding in similar ways (Fig. 2.5C). G6P and ATP decrease each other's binding affinity (c, g), but enhance each other's binding cooperativity (h, d).

Several trends concerning the interplay between activation and inhibition of GS emerge. Activators and inhibitors inhibit each other's binding, but enhance each other's binding cooperativity. Inhibitors, on the other hand, enhance each other's binding, but each decreases the degree of cooperativity to which the other binds. It is evident, therefore, that phosphorylation—though covalent—exhibits exactly the same qualitative behaviour with respect to G6P as ATP—a classic allosteric inhibitor.

We arrived at this picture of GS regulation with the aid of the Hill equation. However, as we have seen, the Hill equation cannot account for the heterotropic cooperativity that is observed between activators and inhibitors; that is, in the Hill equation h, the degree of cooperativity, is constant. It has been proposed that a modification term be incorporated in the Hill equation that would allow h to be a function of

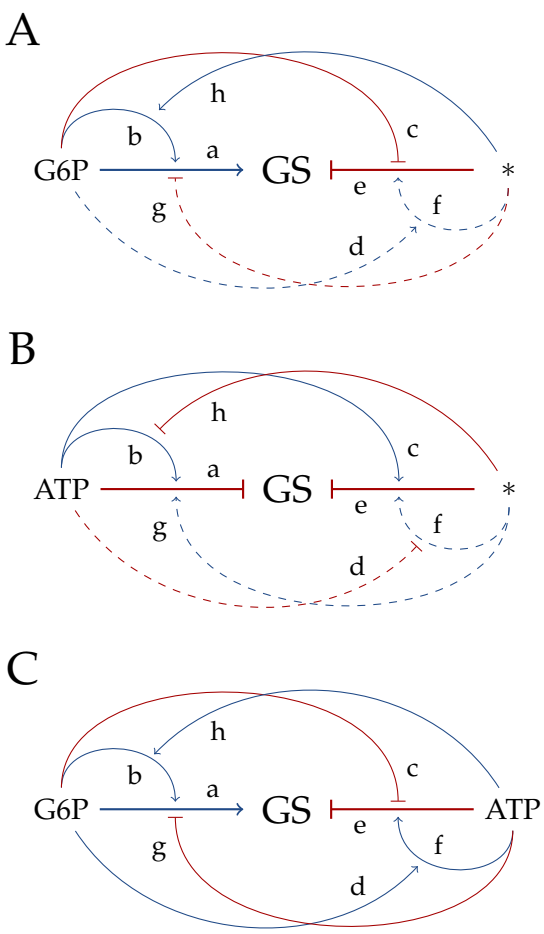

Figure 2.5: Regulation of GS by G6P, ATP, and phosphorylation (∗). Blue arrows indicate activation, red arrows indicate inhibition, and dashed lines indicate predicted, but as of yet unobserved, effects. (*A*) G6P binding activates GS (a) and is positively cooperative (b). While phosphorylation inhibits G6P binding (g), it increases the degree of G6P binding cooperativity (h). Phosphorylation inhibits GS (e), but phosphorylation and its effects are reversed by G6P (c). It is predicted that, in addition to hierarchical phosphorylation, phosphorylation is also cooperative (f) and that the degree of this cooperativity is increased in the presence of G6P (d). (*B*) ATP inhibits GS (a) in a cooperative manner (b). Phosphorylation enhances ATP binding (g), but decreases the degree of ATP cooperativity (h). ATP is predicted to decrease the degree of cooperative phosphorylation (g). (*C*) G6P inhibits ATP binding (c), but increases the degree of ATP cooperativity (d). Similarly, ATP inhibits G6P binding (g) and enhances the degree of G6P cooperativity (h). Note that the arrows in *A* are isomorphic to the arrows in *C*, and that within *B* the arrows originating from ATP are symmetrical with respect to the arrows originating from ∗. This indicates that phosphorylation behaves qualitatively like a classic MWC-type allosteric inhibitor.

other modifiers [150]. Such a modification term would however soon lapse into an infinite regress, as it would have to contain binding terms that are themselves raised to yet another modified Hill coefficient. Another shortcoming of the Hill equation is that the ability of G6P to completely reactivate GS of any phosphorylation state can only be described by imposing explicit constraints on the equation parameters. For instance, k_{cat} and γ_{G6P} must be constrained by the relationship $k_{cat} \cdot \gamma_{G6P} = C$, where C is a constant.

The MWC model does not suffer these shortcomings and readily explains the trends observed in GS regulation. Piras *et al.* [67] offered an explanation of the interplay between G6P, ATP, and phosphorylation using the MWC model. Noting that phosphorylation enhanced G6P cooperativity, but decreased ATP cooperativity, they suggested that the covalent modification of GS exerts its effects in exactly the same way as classic MWC-type allosteric modification does: by altering the equilibrium constant L_0 between an active R conformation and an inactive T conformation. In the MWC model cooperativity arises due to the simultaneous or concerted conformational change of all subunits of the enzyme. By binding preferentially to a particular conformation, modifiers shift the equilibrium of all subunits, regardless of whether they are occupied, towards that conformation and thus enhance subsequent modifier binding. However, cooperativity is only observed if the majority of the enzyme is in the conformation not favoured by the modifier in question. The results of Piras *et al.* [67] are then explained if the majority of the dephosphorylated I form is already in the active form so that G6P binding is only mildly cooperative. Phosphorylation, which favours the T conformation, would then enhance G6P cooperativity. The converse would be true with regard to ATP cooperativity. This model is depicted in Fig. 2.6.

Sølling [42] also described the kinetics of GS by employing two enzyme conformations and suggested that the MWC model might account for his findings. However, since he worked with the I form which shows little G6P cooperativity, normal Michaelian kinetics for each conformation provided an adequate description. Kinetic [63] and crystal structure [51] studies of the yeast enzyme lend further support to a discrete state model such as the MWC model. A three-state model has been suggested in which the enzyme is normally present in a basal I conformation (not to be confused with the I form of the I/D nomenclature). Phosphorylation would then stabilize an inactive T conformation, whereas G6P would stabilize an active R conformation. Conformational change, particularly involving the interdomain closure

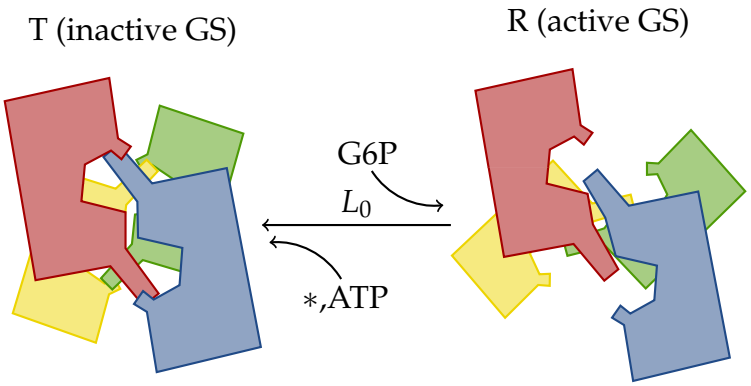

Figure 2.6: Monod-Wyman-Changeux-type model of allosteric and covalent GS regulation. Dephosphorylated GS is predominantly in the R conformation. Activation by G6P shifts the equilibrium between the two conformations towards R, but inhibition by ATP and phosphorylation (∗) shifts the equilibrium towards T. Both allosteric and covalent regulation then manifests as an apparent change to L_0, the equilibrium between T and R. Not all phosphorylation sites would contribute equally to a change in L_0; phosphorylation at sites that do not affect GS activity will also not alter L_0. No crystal structure of phosphorylated GS is available and it is thus possible that a second inactive conformation exists. The cartoons used here are based on the crystal structures of basal and activated yeast GS [51].

of subunits, is a recurring theme in GS from various crystal structure studies.

The complete activation of any GS phosphorylation state by saturating levels of G6P is readily described by the MWC model. If the affinity of the R conformation for G6P were such that G6P binding lowers the apparent value of L_0 more than phosphorylation increases it, G6P binding would completely overcome inhibition by phosphorylation. Note also that in such a scenario saturating G6P would activate any phosphorylation state, including the dephosphorylated state, to the same level, which is equivalent to constraining the values of $k_{cat} \cdot \gamma_{G6P}$ and $UDPG_{0.5}/\alpha_{G6P}$. If ATP were also able to bind to the catalytic site, then the MWC model would, like the Hill model, be compatible with the observation that G6P does not completely overcome ATP inhibition [42, 67].

Not only does the MWC model account for the reversal of the effects of phosphorylation by G6P but it also predicts the observed inhibition of phosphorylation itself as manifested by G6P-induced GS kinase inhibition and activation of PP1. If, as proposed, phosphorylation stabilizes the inactive T conformation, then by extension the T conformation is more readily phosphorylated. Hence, all modifiers that stabilize the R conformation will not only activate GS kinetically, but will also promote its covalent activation by stabilizing the conformation that is less readily phosphorylated. Kinase inhibition by G6P has only been observed for PKA; whereas GSK3, PhK, and

CK1 showed no activation by G6P. The MWC model, however, predicts that only kinases that phosphorylate sites that affect GS activity should be inhibited by G6P and thus little, if any, inhibition is expected for PhK and CK1, if used alone. Similarly, the majority of sites phosphorylated by GSK3 have no effect on GS activity and no inhibition by G6P is expected for the phosphorylation of these sites. Inhibition by G6P is however expected for phosphorylation of site 3a by GSK3, but was not observed [139]. No explanation can be offered in this regard, except that site 3a might have already been phosphorylated substantially, given that the phosphorylation state was not known. Similarly, ATP is predicted to enhance net GS phosphorylation over and above its contribution as kinase cosubstrate (c in Fig. 2.5B). Embi *et al.* [151] have indeed observed stimulation of GSK3 by ATP even after the kinase was already saturated with ATP, suggesting a substrate-specific effect. Inhibition of PP1 by ATP, in a manner reversible by G6P, is well-established [142, 145, 152–154].

In the majority of kinetic treatments that incorporate modifier effects, it is assumed that specific modification affects binding of substrate-product pairs to the same extent and that catalytic modification affects forward and reverse rate constants to the same extent. These assumptions are sufficient but not necessary to satisfy the constraints of the Haldane relationship. Differential modification of the binding affinities of substrates and products is allowed by the Haldane relationship, but with the condition that the forward and reverse rate constants are also modified differentially and to the same extent. Describing differential modification of rate constants and binding affinity in the Michaelian or Hill models, however, leads to complicated rate equations; whereas in the MWC model the behaviour can be accounted for without the introduction of additional parameters. This advantage of the MWC model is, however, not an argument for its applicability to GS kinetics.

A few objections have been levelled against the MWC model as a model for GS regulation. First, Piras *et al.* [67] argued that non-cooperative substrate binding is seemingly incompatible with this model. Non-cooperative substrate binding can, however, be achieved by making the usual assumption that only the R conformation is catalytically active, as well as the assumption that the UDPG substrate binds with equal (or only slightly different) affinities to the R conformation and to the T conformation. These assumptions lead to no, or very mild, substrate binding cooperativity (comparable to that seen for G6P in the dephosphorylated form) for both the dephosphorylated and phosphorylated states, but also impose catalytic activation by G6P. Modifier binding cooperativity is retained, as modifiers bind with vastly dif-

ferent affinities to the two conformations. This mechanism is predicted to exhibit positive substrate cooperativity if the apparent affinity of the two conformations for UDPG is affected to different extents by a competitive inhibitor. This has indeed been observed for the bovine heart enzyme, in which UTP elicited positive cooperativity with respect to UDPG binding [69]. These assumptions are also supported by Sølling [42] who was unable to detect significant conformational change induced by UDPG or UDP. Non-cooperative substrate binding can also be achieved if it is assumed that glycogen can bind to only one subunit at a time due to steric constraints and that UDPG can only bind to the subunit that is already bound to glycogen. These two assumptions are equivalent to assuming infinite negative cooperativity, which is kinetically indistinguishable from hyperbolic kinetics. This mechanism is, however, incompatible with random order bi-bi kinetics, the favoured kinetic mechanism for GS. Although glycogen saturation alters the random bi-bi mechanism to an apparent ordered mechanism, the assumptions here imply a true ordered mechanism that would affect even the sites not occupied by glycogen.

In a further objection, Plesner *et al.* [82] argue that G6P cooperativity is an artefact that disappears at high substrate concentrations and they thus reject the MWC model. Their observation is however in agreement with the model proposed here. UDPG is expected to bind preferentially to the R conformation (otherwise specific activation would not be observed). High substrate concentrations would therefore stabilize the R conformation and so abrogate G6P cooperativity. The disappearance of G6P cooperativity is thus not an artefact, but a characteristic, of the model.

Some aspects of GS regulation suggest that a MWC model with more than two conformations might be required. Many earlier GS kinetic studies found that catalytic activation by G6P was restricted to the D form, whereas specific activation was restricted to the I form. Unless these finding were artefactual, they can only be accounted for by a MWC model with at least three conformations. In a similar vein, Piras *et al.* [39] noted that the specific activation of GS by G6P was pH-dependent, which could indicate that an additional pH-dependent conformational transition occurs. Some workers [42, 82] have also found that inorganic phosphate and sulphate are inhibitors of the D form, but activate the I form. This situation could perhaps be explained with a two-state MWC model if phosphate and sulphate prefer to bind to the R conformation. In the I form, which is often assayed in the absence of G6P, they would result in slight activation, whereas in the D form, which is rarely assayed in the absence of G6P, they would impair G6P activation by competing for the allosteric

site. However, if phosphate and sulphate are true inhibitors of the D form, that is, not only with respect to G6P, additional conformations would be required to explain the behaviour. Based on crystal structure data, a three-state MWC type model has indeed been proposed for yeast GS [51], but no rigorous kinetic studies have yet confirmed this proposal. Until a two-state MWC model is shown to be inadequate, however, little is gained by considering additional conformational states.

The MWC model proposed here, in which phosphorylation increases L_0, makes a few predictions that have, to our knowledge, not been tested experimentally. First, it predicts that phosphorylation is cooperative (see f in Fig. 2.5A). That is, phosphorylation of, say, site 2 on one subunit must enhance phosphorylation of site 2 on the next subunit. And more generally, phosphorylation of any site that increases L_0 should enhance subsequent phosphorylation of any other phosphorylation site—on the same or other subunits of the oligomeric enzyme—that also increases L_0. In simpler terms, if phosphorylation at two different sites, whether on the same or different subunits, both stabilize the T conformation, then phosphorylation of one site should enhance phosphorylation at the other site. Similarly, dephosphorylation should also proceed cooperatively. Not all phosphorylation sites affect the activity, and thus L_0, of GS. Phosphorylation sites like 1a, 1b, and 5–3c have little if any effect on GS activity and thus no cooperative phosphorylation of these sites is expected. Hierarchical sequential phosphorylation is not equivalent to cooperative phosphorylation; however, in a MWC model, these two mechanisms could be difficult to tell apart in phosphorylation assays. Suppose for instance that phosphorylation at both sites 2 and 2a stabilizes the T conformation. Phosphorylation of site 2a would then be enhanced by prior phosphorylation at site 2 by virtue of the recognition motif of CK1 containing a phosphorylated serine residue, but also because phosphorylation at site 2 stabilizes the same conformation that is favoured by phosphorylation at site 2a. It has been noted that phosphorylation of sites 2 and 2a is synergistic [106]: prior phosphorylation at site 2 greatly enhances, but is not a requirement for, phosphorylation at site 2a. If regulation of GS is indeed adequately described by a MWC-type model, this enhanced phosphorylation at site 2a cannot purely be the result of hierarchical sequential phosphorylation.

Second, it is predicted that G6P would enhance the degree of cooperative phosphorylation by stabilizing the conformation not favoured by phosphorylation (d in Fig. 2.5A). ATP, on the other hand, will decrease the degree of cooperativity of phosphorylation (d in Fig. 2.5B), despite the fact that it enhances phosphorylation itself

(c in Fig. 2.5B).

The kinetics and regulation of GS seem to be adequately described by a MWC model in which phosphorylation acts like a classic allosteric modifier. The sequential or Koshland-Némethy-Filmer (KNF) model [155] is, however, expected to provide an equally adequate description. However, an equation derived from the assumptions of the KNF model for a tetramer in a tetrahedral arrangement with product inhibition and two allosteric modifiers would be too complicated to be useful. Moreover, in the KNF model it is not immediately clear which parameters would be influenced by phosphorylation. The MWC-type model proposed here is almost certainly a gross over-simplification of the true regulation of GS, but is nevertheless a useful working model.

2.6 Conclusion

In this chapter we discussed the general kinetic properties of GS and how these properties are affected by allosteric and covalent regulation. The covalent regulation of GS is particularly elaborate, allowing the enzyme to be sensitive to multiple regulatory signals. However, only a few of the phosphorylation sites have direct effects on the enzyme's activity. The majority appear to rather fulfil auxiliary roles such as targeting the enzyme to appropriate sub-cellular compartments or to facilitate the phosphorylation of those sites that do directly affect activity. In this regard the sites phosphorylated by GSK3 are of particular interest, as this kinase can be considered a hub in signal transduction, regulating several downstream processes. We postulate that the multiple GSK3 sites on GS function to calibrate the response of GS to changes in the activity of GSK3. The allosteric regulation of GS also appears to be multifaceted. Not only is the enzyme's activity directly influenced by its allosteric modifiers, its sub-cellular and nucleocytoplasmic distribution is also affected. Moreover, the allosteric and covalent regulation of GS is tightly intertwined. It is clear that no discussion of the covalent regulation of GS is complete without mention of its effect on G6P activation, and no treatment of its allosteric regulation is complete without also considering its effect on phosphorylation. Part of the function of either regulatory mechanism, it seems, is to regulate the other.

There is no *a priori* reason why covalent and allosteric modification of an enzyme should be considered to be qualitatively different. In fact, both kinds of interaction are, as it were, *allosteric*; in either case the enzyme's activity is affected by modifiers

binding (whether covalently, or through ionic or hydrophobic interactions) to a site other than the catalytic site. Notwithstanding, earlier studies on GS kinetics were usually entirely devoted to either the I or D form, with little attempt to sketch an integrated view. In an effort to remedy this situation, we here proposed a unifying view of GS regulation in which covalent modification is considered to be qualitatively identical to classic allosteric modification as per the MWC model. This is indeed the standard depiction of the regulation of GS in textbooks: phosphorylation favours an inactive T conformation, whereas G6P favours the active R conformation. However, to our knowledge, this model has never been applied in a kinetic treatment of GS and its implications for the function of the extensive phosphorylation of GS has not been considered. Our own endeavours in this regard is the theme of the next chapter. A major advantage of this model is that it eliminates the need to determine the kinetic parameters for GS in all its possible phosphorylation states, leaving only the requirement to establish the relationship between a particular phosphorylation state and L the equilibrium constant between the T and R conformers in the absence of ligands.

We have discussed the function of G6P as a feedforward activator of GS and suggested that this feedforward mechanism plays a role in G6P homeostasis in that it increases the response of the flux local to the glycogen synthesis pathway to G6P. One reason for this elevated response is the fact that G6P binds cooperatively to GS. In the unifying model of GS regulation that we here propose, both ATP (h in Fig. 2.5C) and phosphorylation (h in Fig. 2.5A) increase the degree of G6P binding cooperativity and are thus expected to enhance the response of the glycogen synthesis pathway to G6P. If the feedforward loop is indeed a mechanism of G6P homeostasis, then physiological concentrations of ATP, as demonstrated by Piras *et al.* [67], and phosphorylation should be expected to enhance G6P homeostasis.

The model we propose here has interesting implications regarding the relative importance of allosteric and covalent regulation. Using knock-in mice in which GS was desensitized to G6P, Bouskila *et al.* [18] recently reported that allosteric, and not covalent, regulation is the major mechanism by which insulin activates glycogen synthesis. From Fig. 2.5A it is clear that if GS is desensitized to activation by G6P, i.e., if arrow (a) is removed, several functions of phosphorylation also disappear (h, g), leading to a possible underestimation of the importance of phosphorylation. In particular, only the direct effect of phosphorylation on the activity of GS would be observed, but its role in increasing the sensitivity of GS towards G6P would be ne-

glected. Similarly, if one were to remove the phosphorylation sites on GS, the function of G6P to inhibit phosphorylation is obscured. It is our opinion that mathematical modelling and metabolic control analysis (MCA) [10, 11] could provide insights into the relative contributions of allosteric and covalent regulation towards the activation of GS, if indeed these contributions can be considered in isolation. It could also provide valuable insights regarding the regulatory design of muscle glycogen metabolism and its involvement in the onset of insulin resistance. One of the central aims of MCA is to relate properties of individual enzymes to global pathway responses. It is therefore essential to obtain a quantitative grasp of the precise effects of regulation on the kinetics of GS, a grasp that can only be obtained by returning to enzyme kinetics. We thus echo the call by Jensen & Lai [5] for a detailed quantitative investigation of the effects of allosteric and covalent regulation on the kinetic properties of GS.

Chapter 3

Development of a glycogen synthase rate equation

3.1 Introduction

In the previous chapter, borrowing the terminology of the Hill model, we discussed the kinetics and regulation of glycogen synthase (GS) in detail. The Hill model is independent of the kinetic mechanism and mechanism of cooperativity of the enzyme it describes and its parameters have clear operation meanings. We argued that the effects of allosteric and covalent regulation of GS on its kinetic parameters, as defined by the Hill model, are consistent with an Monod-Wyman-Changeux (MWC)-type model in which not only allosteric modification, but also covalent modification, alters the equilibrium constant, L_0, between the classic T and R conformations. In this chapter we set out to develop a rate equation for GS based on such a MWC-type model. Considering only the interconversion between GS phosphorylation states, a general form of the rate equation is provided. Several specific forms are then proposed for the rate equation, based on the observed GS kinetics. Parameter optimization is used to determine which forms provide the best description of experimental kinetic data. Finally, we investigate the relationship between L_0 and the fractional velocity and show how L_0 can be determined from the fractional velocity.

3.2 Phosphorylation states

The total number of distinct phosphorylation states, s, for a protein subunit with n phosphorylation sites grouped together in the same phosphorylation cluster that are

phosphorylated randomly is given by the function

$$s = 2^n \tag{3.1}$$

In the case of strict sequential phosphorylation and dephosphorylation, the number of states is given by

$$s = n + 1 \tag{3.2}$$

Since several independent phosphorylation clusters, some randomly phosphorylated and some sequentially phosphorylated, can be present on a subunit, the total number of states is the product of states in each cluster

$$s = \prod_i s_i \tag{3.3}$$

where i denotes a particular phosphorylation cluster.

Let C_{22a}, C_{543abc}, C_{1a}, and C_{1b} designate the four phosphorylation clusters of GS (subscripts indicate the phosphorylation sites in each cluster). According to Eq. 3.3, and assuming random phosphorylation for the sites in each cluster, the number of phosphorylation states for a single GS subunit is

$$\begin{aligned} s &= s_{C_{22a}} \cdot s_{C_{543abc}} \cdot s_{C_{1a}} \cdot s_{C_{1b}} && (3.4)\\ &= 2^2 \cdot 2^5 \cdot 2 \cdot 2 && (3.5)\\ &= 2^9 && (3.6)\\ &= 512 && (3.7) \end{aligned}$$

Assuming strict sequential phosphorylation and dephosphorylation, on the other hand, the number of phosphorylation states per GS subunit is

$$\begin{aligned} s &= s_{C_{22a}} \cdot s_{C_{543abc}} \cdot s_{C_{1a}} \cdot s_{C_{1b}} && (3.8)\\ &= (2+1)(5+1)(1+1)(1+1) && (3.9)\\ &= 72 && (3.10) \end{aligned}$$

As discussed earlier, the majority of evidence suggests, however, that GS is a tetramer. The number of states for a random mechanism and sequential mechanism is then respectively 512^4 and 72^4. But if it is assumed, as in the MWC-model, that

the four subunits are equivalent and that enzyme forms to which the same number and type of ligand (and thus also covalent bonds) are bound are kinetically equivalent, the number of kinetically distinct states decreases dramatically. Granted this assumption, the number of kinetically distinct states for an enzyme with m subunits and n phosphorylation sites grouped in the same cluster and phosphorylated randomly (assuming phosphorylation at all sites affect the kinetics) is given by the function

$$s = (m+1)^n \tag{3.11}$$

In the case of sequential phosphorylation, on the other hand, the number of states is given by the formula for the $(n+1)^{\text{th}}$ element of the r-topic numbers (the numbers in the $(r+1)^{\text{th}}$ diagonal of Pascal's Triangle) with $r = m$:

$$s = \frac{(n+1)^{(m)}}{m!} \tag{3.12}$$

where $(n+1)^{(m)}$ is the rising factorial. Setting $m = 1$, Eqs. 3.11 and 3.12 simplify to Eqs. 3.1 and 3.2 as expected. As before, if multiple phosphorylation clusters can exist per subunit, the number of states is given by the product of the states for each cluster (Eq. 3.3).

Assuming a random phosphorylation mechanism, the number of kinetically distinct states in which tetrameric GS ($m = 4$) can exist is

$$\begin{aligned} s &= s_{C_{22a}} \cdot s_{C_{543abc}} \cdot s_{C_{1a}} \cdot s_{C_{1b}} && (3.13)\\ &= (4+1)^2 \cdot (4+1)^5 \cdot (4+1) \cdot (4+1) && (3.14)\\ &= 5^9 && (3.15)\\ &= 1953125 && (3.16) \end{aligned}$$

and for a sequential mechanism

$$\begin{aligned} s &= s_{C_{22a}} \cdot s_{C_{543abc}} \cdot s_{C_{1a}} \cdot s_{C_{1b}} && (3.17)\\ &= \frac{3\times4\times5\times6}{4!} \cdot \frac{6\times7\times8\times9}{4!} \cdot \frac{2\times3\times4\times5}{4!} \cdot \frac{2\times3\times4\times5}{4!} && (3.18)\\ &= 15\times126\times5\times5 && (3.19)\\ &= 47250 && (3.20) \end{aligned}$$

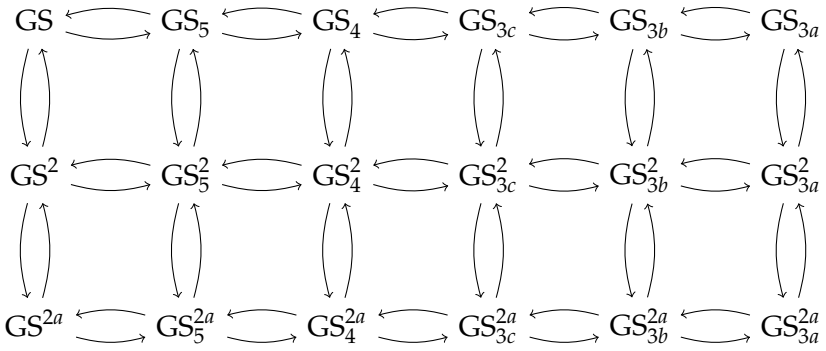

Figure 3.1: Interconversion between 18 GS phosphorylation states. Phosphorylation within each phosphorylation cluster is assumed to proceed strictly sequentially. Phosphorylation of sites 1a and 1b is neglected.

Finally, if sites 1a and 1b, which do not significantly affect GS activity, are neglected the numbers of GS states for a random and sequential mechanism decrease to 5^7 and 1890 respectively. Still, regardless of whether a random or sequential phosphorylation mechanism is considered, it is by no means feasible to develop a single MWC-type equation that will incorporate all the phosphorylation states of tetrameric GS. Neither is it feasible to model the interconversion between these states with the appropriate kinase and phosphatase reactions. In the present treatment of GS kinetics, we have therefore decided on the following simplifying assumptions: 1) both phosphorylation and dephosphorylation of all the phosphorylation clusters proceed strictly sequentially, 2) phosphorylation at each site is *all-or-nothing*, that is, if for instance site 2 is phosphorylated, it is simultaneously phosphorylated on all four subunits. The same holds for dephosphorylation. 3) Sites 1a and 1b are neglected, because phosphorylation at these sites does not result in kinetically distinct phosphorylation states. Although sites 5, 4, 3c, and 3b also have little effect on GS kinetics, they are included, because they are required for phosphorylation at site 3a.

Given these assumptions, GS is modelled as existing in only $(2+1)(5+1) = 18$ states . Even though these 18 states are the result of simplifying assumptions, they represent a subset of the total number of possible states and are therefore *real* phosphorylation states in which GS can exist. Indeed many of these states have been the subject in site-directed mutagenesis and sequential phosphorylation studies. Kinetic data, albeit limited, are therefore available for some of these states. Moreover, kinetic data for the interconversion between some of these states are also available.

With 18 phosphorylation states it is feasible to explicitly model the interconversion between the states with separate kinase and phosphatase reactions (Fig. 3.1).

Unlike for the allosteric modification of GS, there will therefore be no explicit terms for covalent modification in the GS rate equation. As we have chosen to represent each phosphorylation state as a separate species, the general form of the GS rate equation is the sum of the rates of all the GS states:

$$v = \sum_i v_i \tag{3.21}$$

where i is a particular phosphorylation state. In the next section, several models of allosterism and cooperativity are considered in order to arrive at an appropriate expression for v_i.

3.3 Kinetic models

Based on the detailed review of GS kinetics in the previous chapter, the following assumptions are made:

- GS is a tetrameric enzyme
- reagents bind according to a random order bi-bi mechanism, but due to glycogen saturation the mechanism simplifies to a uni-reactant mechanism
- glycogen binding is non-cooperative or, equivalently, infinitely negatively cooperative
- UDP-glucose (UDPG) binding is non-cooperative in the absence of inhibitors
- glucose-6-phosphate (G6P) is an allosteric activator that binds cooperatively to the phosphorylated enzyme
- G6P activation could be catalytic or specific, or both catalytic and specific
- ATP is an allosteric inhibitor that binds cooperatively to the dephosphorylated enzyme
- ATP is a specific inhibitor, but the inhibition could also have a catalytic component
- ATP and G6P compete for the same allosteric site, but the possibility that they bind to different sites cannot be ruled out
- ATP possibly competes with UDPG at the active site

Hill model

We have stated previously that the Hill model does not describe the kinetics of GS adequately. Here we will show more concretely why this is indeed the case. Adapting the Hill-type equation proposed earlier (Eq. 2.4) to also allow for the possibility that ATP could be a catalytic inhibitor, to reflect which parameters depend on the phosphorylation state, and setting $h = 1$, an expression for v_i can be written as

$$v_i = k_{\text{cat}i} \cdot [\text{E}]_{\text{tot}i} \cdot \mu_{\text{cat}_i} \times \frac{\sigma_i}{\mu_{\text{spec}_i} + \sigma_i + \pi_i} \times \left(1 - \frac{\Gamma}{K_{\text{eq}}}\right) \tag{3.22}$$

where

$$\mu_{\text{cat}_i} = \frac{1 + \gamma_{\text{G6P}i} \cdot \alpha_{\text{G6P}i} \cdot \xi_{\text{G6P}_i}^{h_{\text{G6P}i}} + \gamma_{\text{ATP}i} \cdot \alpha_{\text{ATP}i} \cdot \xi_{\text{ATP}_i}^{h_{\text{ATP}i}}}{1 + \alpha_{\text{G6P}i} \cdot \xi_{\text{G6P}_i}^{h_{\text{G6P}i}} + \alpha_{\text{ATP}i} \cdot \xi_{\text{ATP}_i}^{h_{\text{ATP}i}}} \tag{3.23}$$

and

$$\mu_{\text{spec}_i} = \left(1 + \xi_{\text{ATP}'_i}^{h_{\text{ATP}'i}}\right) \left(\frac{1 + \xi_{\text{G6P}_i}^{h_{\text{G6P}i}} + \xi_{\text{ATP}_i}^{h_{\text{ATP}i}}}{1 + \alpha_{\text{G6P}i} \cdot \xi_{\text{G6P}_i}^{h_{\text{G6P}i}} + \alpha_{\text{ATP}i} \cdot \xi_{\text{ATP}_i}^{h_{\text{ATP}i}}}\right) \tag{3.24}$$

where k_{cat} is the catalytic constant; $[\text{E}]_{\text{tot}}$ is the total GS concentration; $\sigma = \frac{[\text{UDPG}]}{\text{UDPG}_{0.5}}$; $\pi = \frac{[\text{UDP}]}{\text{UDP}_{0.5}}$; $\xi_{\text{G6P}} = \frac{[\text{G6P}]}{\text{G6P}_{0.5}}$; $\xi_{\text{ATP}} = \frac{[\text{ATP}]}{\text{ATP}_{0.5}}$; $\xi_{\text{ATP}'} = \frac{[\text{ATP}]}{\text{ATP}'_{0.5}}$; $\text{UDPG}_{0.5}$, $\text{UDP}_{0.5}$, $\text{G6P}_{0.5}$, $\text{ATP}_{0.5}$, and $\text{ATP}'_{0.5}$ are the UDPG, UDP, G6P, allosteric site ATP, and catalytic site ATP half-saturation concentrations in the absence of other ligands; $\gamma_{\text{G6P}} > 1$ is the degree of G6P catalytic activation; $\gamma_{\text{ATP}} < 1$ is the degree of ATP catalytic inhibition; $\alpha_{\text{G6P}} > 1$ and $\alpha_{\text{ATP}} < 1$ are reactant-modifier interaction factors; h_{G6P} is the degree of G6P binding cooperativity; h_{ATP} and $h_{\text{ATP}'}$ are the degrees of ATP binding cooperativity at the allosteric and catalytic sites, respectively; $\Gamma = \frac{[\text{UDP}]}{[\text{UDPG}]}$ is the mass-action ratio; and K_{eq} is the equilibrium constant. Parameters that depend on the phosphorylation state are indicated with the subscript i. Note that $[\text{E}]_{\text{tot}i}$ is not a parameter, but a variable species concentration.

In order to describe the kinetics of all 18 GS phosphorylation states a total of 253 parameters are required (14 phosphorylation-dependent parameters per state plus one phosphorylation-independent parameter). Obtaining values for this multitude of parameters from the limited kinetic data that are available is, however, not feasible.

The number of parameters can be slightly reduced by considering that, in the absence of ATP, saturating G6P appears to completely overcome the effect of phosphorylation on k_{cat} and $UDPG_{0.5}$, i.e., the apparent k_{cat} and $UDPG_{0.5}$ at saturating G6P have constant values that are independent of the phosphorylation state i:

$$k_{\text{cat}_{\text{app}}} = \gamma_{\text{G6P}_i} \cdot k_{\text{cat}_i} \tag{3.25}$$

and

$$\text{UDPG}_{0.5\text{app}} = \text{UDPG}_{0.5i} / \alpha_{\text{G6P}_i} \tag{3.26}$$

Rewriting these equations to have γ_{G6P_i} and α_{G6P_i} on the left hand side and substituting in Eq. 3.22 results in an equation with two more phosphorylation-independent parameters and two fewer parameters per state, decreasing the number of parameters to 219. Introducing similar constraints for ATP, which is harder to justify, further decreases the number of parameters to 185. However, even considering this reduced number of parameters, we have not been able to find a rich enough experimental data set in the literature that would allow fitting these parameters.

A more serious impediment to the application of the Hill model to GS kinetics, regardless of whether a rich enough experimental data set can be obtained, is its inability to account for variations in the degree of cooperativity (heterotropic cooperativity). It is well-established that G6P increases the degree of cooperativity with which ATP binds to GS, and the other way around. In an attempt to remedy this shortcoming, it has been proposed [150] that the Hill coefficient for a particular ligand be expressed as a function of the heterotropic ligand that alters it (assuming a hyperbolic relationship):

$$h_{\text{app}} = h \left(\frac{1 + \beta\xi}{1 + \xi} \right) \tag{3.27}$$

where $\xi = x/x_{0.5}$; x and $x_{0.5}$ are the heterotropic ligand concentration and half-saturation concentration; and β is the factor by which h is multiplied at saturating x. Given that both G6P and ATP bind cooperatively to GS, one would, however, expect a sigmoidal relationship, but a sigmoidal relationship would result in the mutually recursive expression of $h_{\text{G6P}_{\text{app}}}$ in terms of $h_{\text{ATP}_{\text{app}}}$:

$$h_{\text{G6P}_{\text{app}}} = h_{\text{G6P}} \left(\frac{1 + \beta\xi^{h_{\text{ATP}_{\text{app}}}}}{1 + \xi^{h_{\text{ATP}_{\text{app}}}}} \right) \tag{3.28}$$

where

$$h_{\text{ATPapp}} = h_{\text{ATP}} \left(\frac{1 + \beta \xi^{h_{\text{G6Papp}}}}{1 + \xi^{h_{\text{G6Papp}}}} \right) \tag{3.29}$$

These forms would be even more complicated if they also reflected the competition between ATP and G6P. Unless it can be shown that the dependence of the Hill coefficient for each ligand on the concentration of the other ligand is hyperbolic, we would not consider this approach to be workable, especially since two additional parameters, possibly depending on the phosphorylation state, would have to be introduced.

Monod-Wyman-Changeux model

The MWC model is probably the best-known model of cooperativity and allosterism. In the MWC model all n subunits of an enzyme are simultaneously in either the T or R conformation. The conversion of all subunits from one to the other conformation is thus concerted. The equilibrium ratio of the concentration of unliganded enzyme in the T conformation to that in the R conformation is given by L_0, the allosteric constant. Any ligand that preferentially binds to a particular conformation will by necessity shift the equilibrium between the liganded T and R conformations in the direction of the preferred conformation and thus appear to alter L_0. The subsequent binding of another ligand of the same or different type will therefore be enhanced, as the proportion of enzyme in this conformation is increased, thus giving rise to homotropic cooperativity. The subsequent binding of a different ligand that prefers the opposite conformation would, on the other hand, be hindered. There is, however, a greater potential for the second ligand to alter the equilibrium in favour of the opposite conformation, thus giving rise to heterotropic cooperativity.

Another attractive feature of the MWC model is that it describes cooperativity on a per ligand basis, even allowing complete non-cooperative binding for some ligands while others still bind cooperatively. There is no single parameter, as in the Hill model, that describes cooperativity. Instead the degree of cooperativity depends on L_0, the allosteric constant, n, the number of subunits, and on the relative affinities of the two conformations for a particular ligand. Consider the simple irreversible MWC equation for an enzyme with an allosteric modifier:

$$v = \frac{V_{\max t} n \sigma_t \left(1+\sigma_t\right)^{n-1} L_0 \left(\frac{1+\xi_t}{1+\xi_r}\right)^n + V_{\max r} n \sigma_r \left(1+\sigma_r\right)^{n-1}}{\left(1+\sigma_t\right)^n L_0 \left(\frac{1+\xi_t}{1+\xi_r}\right)^n + \left(1+\sigma_r\right)^n} \tag{3.30}$$

where t and r denote enzyme in the T and R conformations; $\sigma = s/K_s$; $\xi = x/K_x$; s and x are the substrate and modifier concentrations; K_s and K_x are intrinsic dissociation constants; and L_0 is the allosteric constant. Both conformations are catalytically active and substrate is allowed to bind to either the T or R conformation. Setting $n = 1$ results in

$$v = \frac{V_{\max t} \sigma_t L_0 \left(\frac{1+\xi_t}{1+\xi_r}\right) + V_{\max r} \sigma_r}{\left(1+\sigma_t\right) L_0 \left(\frac{1+\xi_t}{1+\xi_r}\right) + \left(1+\sigma_r\right)} \tag{3.31}$$

thereby abolishing cooperativity with respect to all ligands, regardless of the values of L_0 or the relative affinities of the two conformations for any particular ligand. Similarly, setting $L_0 = 0$, or letting $L_0 \to \infty$ results in

$$v = \frac{V_{\max} n \sigma \left(1+\sigma\right)^{n-1}}{\left(1+\sigma\right)^n} \tag{3.32}$$

$$= \frac{V_{\max} n \sigma}{1+\sigma} \tag{3.33}$$

thereby abolishing all cooperativity and modifier effects. Cooperativity is observed for all other values of L_0, with the maximum degree of cooperativity with respect to a particular ligand occurring when $L_0 = \sqrt{(K_t/K_r)^n}$. Alternatively, setting $\sigma = \sigma_r = \sigma_t$, i.e., assuming that substrate binds equally well to the T and R conformations, results in

$$v = \frac{V_{\max t} n \sigma L_0 \left(\frac{1+\xi_t}{1+\xi_r}\right)^n + V_{\max r} n \sigma}{\left(1+\sigma\right) L_0 \left(\frac{1+\xi_t}{1+\xi_r}\right)^n + \left(1+\sigma\right)} \tag{3.34}$$

In this form of the equation substrate binds non-cooperatively while cooperativity with respect to the allosteric modifier remains unaffected. The situation is slightly more complicated when ligands compete for the same site. Supposing that the modifier binds to the catalytic site, instead of the allosteric site, alters Eq. 3.34 to

$$v = \frac{V_{\max t} n\sigma \left(1+\sigma+\xi_t\right)^{n-1} L_0 + V_{\max r} n\sigma \left(1+\sigma+\xi_r\right)^{n-1}}{\left(1+\sigma+\xi_t\right)^n L_0 + \left(1+\sigma+\xi_r\right)^n} \tag{3.35}$$

showing that substrate binds cooperatively, but only in the presence of modifier.

Appreciation for the per-ligand description of cooperativity in the MWC model is often lost due to the assumption, which is practically always made, that substrate only binds to the R conformation ($\sigma_t = 0$), essentially forcing the condition $\sigma_t \neq \sigma_r$, so that substrate binding is always cooperative. Indeed, the supposed inability of the MWC model to describe non-cooperative substrate binding has been put forward as an argument against its applicability to GS kinetics [67].

As for the Hill model, an expression for v_i according to the MWC model could be formulated by considering each of the 18 phosphorylation states of GS to be described by a different set of parameter values. This would mean that each phosphorylation state is in equilibrium between a T and R conformation, but that T and R conformations in different states are not necessarily kinetically identical. There would thus be 18 possibly unique T conformations and R conformations. But we here run into the same problems as with the Hill model: a separate set of parameter values, with the exception of n and K_{eq}, will have to be obtained for each phosphorylation state. A simple solution entails treating all T conformations and all R conformations, regardless of phosphorylation states, as identical, but allowing each phosphorylation state to have a different value for L_0. In other words, a single T and R conformation is shared by all the phosphorylation states, but for each state the equilibrium T/R ratio will be potentially different. This simplification decreases the number of parameters significantly, as only L_0 and the concentration of the enzyme in a particular state will vary with phosphorylation. All other parameters have the same values, regardless of phosphorylation state.

Not only does the number of parameters decrease, but by treating covalent modification as equivalent to classic MWC-type allosteric modification, i.e., as an apparent change to the value of L_0 (albeit explicit in the case of covalent modification) it becomes possible to describe the experimentally observed changes in cooperativity with respect to G6P and ATP resulting from phosphorylation. In particular, if phosphorylation increases the apparent value of L_0, it will increase cooperativity with respect to G6P by virtue of decreasing the concentration of the conformation preferred by G6P. Conversely, phosphorylation will decrease the degree of cooperativity with respect to ATP binding. Admittedly, these phenomena would also be observed without assuming that all T conformations and all R conformations are

identical, but not making this assumption runs contrary to the central assumption of the MWC model that ligands do not affect the kinetics of any conformation, but rather affect the apparent equilibrium concentrations of conformations.

We will now proceed to investigate particular forms of the MWC equation, but let us first consider a generic form from which more specific forms can be obtained. The reversible uni-substrate MWC equation for an enzyme with n subunits, an arbitrary number of active site competitive inhibitors, allosteric sites, and ligands competing per allosteric site is given by [156, 157]:

$$v = \frac{\begin{array}{c} V_{\max t} n \sigma_t \left(1 + \sigma_t + \pi_t + \sum_j \xi_{tj}\right)^{n-1} L_0 \prod_k \left(1 + \sum_l \xi_{tkl}\right)^n + \\ V_{\max r} n \sigma_r \left(1 + \sigma_r + \pi_r + \sum_j \xi_{rj}\right)^{n-1} \prod_k \left(1 + \sum_l \xi_{rkl}\right)^n \end{array}}{\begin{array}{c} \left(1 + \sigma_t + \pi_t + \sum_j \xi_{tj}\right)^n L_0 \prod_k \left(1 + \sum_l \xi_{tkl}\right)^n + \\ \left(1 + \sigma_r + \pi_r + \sum_j \xi_{rj}\right)^n \prod_k \left(1 + \sum_l \xi_{tkl}\right)^n \end{array}} \times \left(1 - \frac{\Gamma}{K_{\text{eq}}}\right) \tag{3.36}$$

where t and r indicate parameters pertaining to the T and R conformations; j indicates a particular non-reactant catalytic site ligand; k indicates a particular allosteric site; l indicates a particular ligand that binds to allosteric site k; $\sigma = s/K_s$; $\pi = p/K_p$; $\xi = x/K_x$; s, p, and x are substrate, product and modifier concentrations; K_s, K_p, and K_x are intrinsic dissociation constants; L_0 is the equilibrium ratio of unliganded enzyme in the T conformation to unliganded enzyme in the R conformation; $\Gamma = p/s$ is the mass-action ratio; and K_{eq} is the equilibrium constant.

We considered several specific forms of Eq. 3.36 in order to obtain the most appropriate expression for v_i. In each case the enzyme was assumed to be a tetramer, i.e. $n = 4$. Furthermore, although we do not consider GS to be irreversible, we were unable to find an appropriate data set in which UDP is varied; we therefore only considered irreversible forms of Eq. 3.36. When applying Eq. 3.36 to the case of GS, the observation that saturating G6P concentrations do not completely reverse inhibition by ATP can be described in two ways. In the first description it is assumed that G6P and ATP compete for the same allosteric site, but that ATP also binds to the catalytic site in competition with the substrate UDPG, yielding the equation (DepCom):

$$v_i = \frac{V_{\max t} n \sigma_t \left(1 + \sigma_t + \xi_{\mathrm{ATP}'t}\right)^{n-1} L_{0i} \left(\frac{1 + \xi_{\mathrm{G6P}t} + \xi_{\mathrm{ATP}t}}{1 + \xi_{\mathrm{G6P}r} + \xi_{\mathrm{ATP}r}}\right)^{n} + V_{\max r} n \sigma_r \left(1 + \sigma_r + \xi_{\mathrm{ATP}'r}\right)^{n-1}}{\left(1 + \sigma_t + \xi_{\mathrm{ATP}'t}\right)^{n} L_{0i} \left(\frac{1 + \xi_{\mathrm{G6P}t} + \xi_{\mathrm{ATP}t}}{1 + \xi_{\mathrm{G6P}r} + \xi_{\mathrm{ATP}r}}\right)^{n} + \left(1 + \sigma_r + \xi_{\mathrm{ATP}'r}\right)^{n}} \tag{3.37}$$

The MWC equation is often simplified by adopting the assumption that substrate is unable to bind to the T conformation, i.e., $\sigma_t = 0$. However, as discussed above, this assumption only allows for strong cooperativity with respect to substrate binding, whereas in the case of GS only mild or no cooperativity is observed for UDPG binding. Alternatively, if it is assumed that only the R conformation exhibits any catalytic activity, i.e., $V_{\max t} = 0$, a much simpler form, but one which allows for mild or no substrate cooperativity, is obtained (terms that disappear as a result of this and subsequent assumptions are shown in gray, DepComR):

$$v_i = \frac{V_{\max t} n \sigma_t \left(1 + \sigma_t + \xi_{\mathrm{ATP}'t}\right)^{n-1} L_{0i} \left(\frac{1 + \xi_{\mathrm{G6P}t} + \xi_{\mathrm{ATP}t}}{1 + \xi_{\mathrm{G6P}r} + \xi_{\mathrm{ATP}r}}\right)^{n} + V_{\max r} n \sigma_r \left(1 + \sigma_r + \xi_{\mathrm{ATP}'r}\right)^{n-1}}{\left(1 + \sigma_t + \xi_{\mathrm{ATP}'t}\right)^{n} L_{0i} \left(\frac{1 + \xi_{\mathrm{G6P}t} + \xi_{\mathrm{ATP}t}}{1 + \xi_{\mathrm{G6P}r} + \xi_{\mathrm{ATP}r}}\right)^{n} + \left(1 + \sigma_r + \xi_{\mathrm{ATP}'r}\right)^{n}} \tag{3.38}$$

For the case in which ATP does not bind to the catalytic site, but still competes with G6P for the allosteric site (setting $\xi_{\mathrm{ATP}'r} = 0$ and $\xi_{\mathrm{ATP}'t} = 0$) Eq. 3.37 simplifies to (Dep)

$$v_i = \frac{V_{\max t} n \sigma_t \left(1 + \sigma_t + \xi_{\mathrm{ATP}'t}\right)^{n-1} L_{0i} \left(\frac{1 + \xi_{\mathrm{G6P}t} + \xi_{\mathrm{ATP}t}}{1 + \xi_{\mathrm{G6P}r} + \xi_{\mathrm{ATP}r}}\right)^{n} + V_{\max r} n \sigma_r \left(1 + \sigma_r + \xi_{\mathrm{ATP}'r}\right)^{n-1}}{\left(1 + \sigma_t + \xi_{\mathrm{ATP}'t}\right)^{n} L_{0i} \left(\frac{1 + \xi_{\mathrm{G6P}t} + \xi_{\mathrm{ATP}t}}{1 + \xi_{\mathrm{G6P}r} + \xi_{\mathrm{ATP}r}}\right)^{n} + \left(1 + \sigma_r + \xi_{\mathrm{ATP}'r}\right)^{n}} \tag{3.39}$$

and, further, if $V_{\max t} = 0$ (DepR):

$$v_i = \frac{V_{\max t} n \sigma_t \left(1 + \sigma_t + \xi_{\mathrm{ATP}' t}\right)^{n-1} L_{0i} \left(\frac{1 + \xi_{\mathrm{G6P}t} + \xi_{\mathrm{ATP}t}}{1 + \xi_{\mathrm{G6P}r} + \xi_{\mathrm{ATP}r}}\right)^{n} + V_{\max r} n \sigma_r \left(1 + \sigma_r + \xi_{\mathrm{ATP}' r}\right)^{n-1}}{\left(1 + \sigma_t + \xi_{\mathrm{ATP}' t}\right)^{n} L_{0i} \left(\frac{1 + \xi_{\mathrm{G6P}t} + \xi_{\mathrm{ATP}t}}{1 + \xi_{\mathrm{G6P}r} + \xi_{\mathrm{ATP}r}}\right)^{n} + \left(1 + \sigma_r + \xi_{\mathrm{ATP}' r}\right)^{n}} \tag{3.40}$$

We also considered the case in which UDPG binds equally well to the T and R conformations in the absence of other ligands, i.e. $\sigma = \sigma_r = \sigma_t$, resulting in the equation (DepComNoSpec):

$$v_i = \frac{V_{\max t} n \sigma \left(1 + \sigma + \xi_{\mathrm{ATP}' t}\right)^{n-1} L_{0i} \left(\frac{1 + \xi_{\mathrm{G6P}t} + \xi_{\mathrm{ATP}t}}{1 + \xi_{\mathrm{G6P}r} + \xi_{\mathrm{ATP}r}}\right)^{n} + V_{\max r} n \sigma \left(1 + \sigma + \xi_{\mathrm{ATP}' r}\right)^{n-1}}{\left(1 + \sigma + \xi_{\mathrm{ATP}' t}\right)^{n} L_{0i} \left(\frac{1 + \xi_{\mathrm{G6P}t} + \xi_{\mathrm{ATP}t}}{1 + \xi_{\mathrm{G6P}r} + \xi_{\mathrm{ATP}r}}\right)^{n} + \left(1 + \sigma + \xi_{\mathrm{ATP}' r}\right)^{n}} \tag{3.41}$$

or if only the R conformation is active (DepComNoSpecR):

$$v_i = \frac{V_{\max t} n \sigma \left(1 + \sigma + \xi_{\mathrm{ATP}' t}\right)^{n-1} L_{0i} \left(\frac{1 + \xi_{\mathrm{G6P}t} + \xi_{\mathrm{ATP}t}}{1 + \xi_{\mathrm{G6P}r} + \xi_{\mathrm{ATP}r}}\right)^{n} + V_{\max r} n \sigma \left(1 + \sigma + \xi_{\mathrm{ATP}' r}\right)^{n-1}}{\left(1 + \sigma + \xi_{\mathrm{ATP}' t}\right)^{n} L_{0i} \left(\frac{1 + \xi_{\mathrm{G6P}t} + \xi_{\mathrm{ATP}t}}{1 + \xi_{\mathrm{G6P}r} + \xi_{\mathrm{ATP}r}}\right)^{n} + \left(1 + \sigma + \xi_{\mathrm{ATP}' r}\right)^{n}} \tag{3.42}$$

In the second description, incomplete reversal of inhibition by ATP in the presence of saturating G6P is obtained by assuming that G6P and ATP do not in fact bind to same allosteric site, obviating the need to allow for ATP binding at the catalytic site (Independent):

Table 3.1: Summary of different MWC-type equations and assumptions considered as candidate GS rate equations.

Equation	Independent allosteric ligand binding	ATP catalytic site inhibition	$\sigma_r = \sigma_t$	Active T state
Dep				✓
DepR				
DepCom		✓		✓
DepComR		✓		
DepComNoSpec		✓	✓	✓
DepComNoSpecR		✓	✓	
Independent	✓			✓
IndependentR	✓			

$$v_i = \frac{V_{\max t} n \sigma_t \left(1+\sigma_t\right)^{n-1} L_{0i} \left(\frac{1+\xi_{\mathrm{G6P}_t}}{1+\xi_{\mathrm{G6P}_r}}\right)^n \left(\frac{1+\xi_{\mathrm{ATP}_t}}{1+\xi_{\mathrm{ATP}_r}}\right)^n + V_{\max r} n \sigma_r \left(1+\sigma_r\right)^{n-1}}{\left(1+\sigma_t\right)^n L_{0i} \left(\frac{1+\xi_{\mathrm{G6P}_t}}{1+\xi_{\mathrm{G6P}_r}}\right)^n \left(\frac{1+\xi_{\mathrm{ATP}_t}}{1+\xi_{\mathrm{ATP}_r}}\right)^n + \left(1+\sigma_r\right)^n} \tag{3.43}$$

Further assuming, as before, that only the R conformation is active yields (IndependentR):

$$v_i = \frac{V_{\max t} n \sigma_t \left(1+\sigma_t\right)^{n-1} L_{0i} \left(\frac{1+\xi_{\mathrm{G6P}_t}}{1+\xi_{\mathrm{G6P}_r}}\right)^n \left(\frac{1+\xi_{\mathrm{ATP}_t}}{1+\xi_{\mathrm{ATP}_r}}\right)^n + V_{\max r} n \sigma_r \left(1+\sigma_r\right)^{n-1}}{\left(1+\sigma_t\right)^n L_{0i} \left(\frac{1+\xi_{\mathrm{G6P}_t}}{1+\xi_{\mathrm{G6P}_r}}\right)^n \left(\frac{1+\xi_{\mathrm{ATP}_t}}{1+\xi_{\mathrm{ATP}_r}}\right)^n + \left(1+\sigma_r\right)^n} \tag{3.44}$$

To simplify reference to the eight cases considered above, we adopt the terminology summarized in Table 3.1.

3.4 Parameter optimization

Experimental data

In order to use Eq. 3.21 in parameter optimization, it is necessary to have knowledge of all the phosphorylation states and the concentrations at which they were present

in the assay used to obtain the experimental results. We have not been able to obtain an experimental data set from the literature in which both the exact phosphorylation states were known and in which the assay was repeated for all the conditions that would allow parameter optimization for any of the kinetic models proposed. However, we have been able to show that, for any of the MWC-type kinetic models, Eq. 3.21 can be rewritten as a single term, as opposed to a sum, that takes on the form of v_i, as defined for the particular kinetic model, but with L_0, which replaces L_{0i}, as a function of the concentrations of the GS phosphorylation states and the L_{0i} values for all the states (see Appendix A.1). In this form, if L_0 is treated as a parameter, it is not necessary to know in which phosphorylation states GS is present or at what concentrations. The only remaining requirement is that experimental data must be available for both extensively dephosphorylated and extensively phosphorylated enzymes states. In order to obtain values for the parameters of Eqs. 3.37 to 3.44, the enzyme must also be assayed for a range of UDPG, G6P, and ATP concentrations.

Exploiting the sequential and hierarchical phosphorylation of GS, various states of the C_{543} [107, 120] and C_{22a} [106] clusters have been assayed. However, as these studies did not have a complete kinetic characterization of GS kinetics as goal, the states were assayed at a single UDPG concentration and at only two G6P concentrations. Inhibition by ATP was also not considered. On the other hand, others like Sølling [42] assayed GS in the presence of several allosteric modifiers at various concentrations, but only considered a particular phosphorylation state.

The kinetic characterization of rat muscle GS by Piras *et al.* [39, 67] provides, to our knowledge, the only experimental data set in which GS was assayed at varying substrate, product, activator, and inhibitor concentrations for both the dephosphorylated (I form) and phosphorylated (D form) enzyme. Parameters for the various candidate definitions of v_i were therefore fitted to this data set. Note that the exact composition of the two enzyme forms in terms of phosphorylation state is unknown, but, judging by the ratio of activity in the absence and presence of 10 mM G6P, the I form (0.75–1) was essentially dephosphorylated, whereas the D form (0.05–0.15) was extensively phosphorylated.

There are a few shortcomings in using this data set. First, the enzyme concentrations used in the assays are unknown; it is thus not possible to obtain values for k_{cat}. Second, the dependence of activity on the concentration of UDPG at different ATP concentrations for the two phosphorylation states are represented as Lineweaver-

Burk plots. Using data linearized according to this transformation in parameter optimization increases the error in parameter values. To minimize this error and also to avoid forcing hyperbolic kinetics on UDPG binding, we chose to reverse this linearization, but in so doing ran the risk of enlarging any error introduced during the digitization of the data. Third, the exact x coordinates of many data points are unknown, so that error is introduced in both the x and y coordinates during digitization. Fourth, Piras *et al.* [39] considered the D form to be contaminated with 10% of the I form and therefore applied a correction to the D form data. Their conclusion was probably based on the misconception that the D form is entirely dependent on G6P; they therefore ascribed any observed activity in the absence of G6P to contamination with I form. We have not attempted to reverse this correction, but expect that it will only affect the value of L_0. Since no L_0 value fitted to the data of Piras *et al.* [67] corresponds to a known phosphorylation state, error in this value is not a concern.

Data points were extracted from the graphs in [67] with the program *Engauge Digitizer* (http://digitizer.sourceforge.net). High-resolution PNG images of the graphs were obtained from a PDF version of the paper. These images were imported into *Engauge* individually and zoomed to an appropriate size. The coordinates for each data point were set manually at what was judged to be the centre of the associated symbol. Where values were clearly given in the text, digitized x coordinates were adjusted accordingly.

Methods

Algorithm and weighting

The Levenberg-Marquardt algorithm [158] was used to minimize the sum of squared residuals S:

$$S = \sum_{i=1}^{n} r_i^2 \tag{3.45}$$

where $r_i^2 = (v_i - \hat{v}_i)^2$, with v the observed rate and $\hat{v}$ the rate calculated from the rate equation.

We found this algorithm to be considerably faster than global optimization algorithms such as *simulated annealing* (SciPy, http://www.scipy.org) or *particle swarm* [159], but it is less likely to find the global minimum. To increase the likelihood of obtaining a global minimum, we seeded each optimization with random initial pa-

rameter values for 1000 repetitions. This method does, however, not guarantee that a global minimum is found. To avoid the assignment of negative parameter values, all parameters were constrained to be positive ($> 1 \times 10^{-25}$).

Separate V_{max} values were fitted for the four data sets, as the concentrations of I and D form are unknown and unlikely to be equal. Moreover, it is not clear whether the same enzyme concentration was used in assays in which UDPG or G6P was varied, even for the same enzyme form. Separate values were also fitted for L_0 for enzyme in the I and D forms.

Each residual should ideally be weighted by the standard deviation of the observed rate so that data points with greater error contribute less towards S. As no information is available regarding the error in the data sets of Piras *et al.* [67], we considered two weighting strategies: *scaled* residuals and *half-scaled* residuals. In the first the residuals are normalized by the calculated rate $\hat{v}$ before squaring:

$$r_i^2 = \left(\frac{v_i - \hat{v}_i}{\hat{v}_i} \right)^2 \tag{3.46}$$

In the second the residuals are essentially weighted by the square root of the calculated rate and then squared:

$$r_i^2 = \frac{(v_i - \hat{v}_i)^2}{\hat{v}_i} \tag{3.47}$$

The appropriate weighting strategy was chosen, as discussed later, by inspection of residuals plots.

Statistics

The coefficient of determination, R^2, the adjusted coefficient of determination, $\bar{R}^2$, and the F-statistic were used to identify the best-fit equation. $\bar{R}^2$ is a variant of R^2 that is adjusted for the number of observations and parameters:

$$\bar{R}^2 = 1 - (1 - R^2) \frac{n - 1}{n - p - 1} \tag{3.48}$$

The F-statistic was calculated according to the formula

$$F = \left(\frac{S_{spec} - S_{gen}}{p_{gen} - p_{spec}} \right) \left(\frac{n - p_{gen}}{S_{gen}} \right) \tag{3.49}$$

where S is the sum of squared residuals; n is the number of observations; p is the number of parameters; and *gen* and *spec* distinguish between the more generic and

the more specific rate equation. The critical F-value with degrees of freedom $p_{\text{gen}} - p_{\text{spec}}$ and $n - p_{\text{gen}}$ for $p = 0.01$ was obtained from a table. The null hypothesis was that the more generic equation does not provide a significantly better fit than the more specific equation. The null hypothesis was rejected if the F-statistic was greater than the critical F-value. In cases where the null hypothesis was rejected or $\bar{R}^2$ had a lower value for the more generic equation, the more specific equation was considered the best-fit equation.

Software

The optimization was carried out using a combination of Python programming language modules: *NumPy* (http://numpy.scipy.org) and *SciPy* for numeric procedures; *LMfit-py* (http://newville.github.com/lmfit-py), a wrapper around the SciPy implementation of the Levenberg-Marquardt algorithm with added support for constraints; and *matplotlib* (http://matplotlib.org) for visualization. *IPython* [160] was used as an interactive shell for Python. IPython's built-in support for parallel computing was used to speed up optimizations.

To ease the optimization procedure, we developed an extensible optimization framework as a Python module that interfaces with the above modules. This framework will be discussed in detail elsewhere. Briefly, the framework was developed to be independent of the format of experimental data, optimization algorithm, weighting strategy, calculation of the predicted rate (whether using an equation or a simulation environment like PySCeS), and output format. In each case a sensible default is provided, but custom implementations can easily be substituted.

Results

In all cases, regardless of the weighting strategy employed, and despite some equations providing fits with high R^2 values, the parameter error estimates of the rate equations in which both the T and R conformations were allowed to exhibit catalytic activity were very large or no error estimates could be calculated due to some parameters violating the constraint, $> 1 \times 10^{-25}$. Only those rate equations that limit activity to the R conformation (DepComR, DepR DepComNoSpecR, IndependentR) were therefore considered.

In the case where no weighting strategy was applied, DepComR had the highest R^2 value (Table 3.2), but did not provide a significantly better fit than DepCom-

Table 3.2: Optimized kinetic parameters obtained using no weighting strategy

	DepComR		DepR		DepComNoSpecR		IndependentR	
Parameter	value	error	value	error	value	error	value	error
R^2	0.9477	–	0.90894	–	0.94763	–	0.93728	–
$\bar{R}^2$	0.93918	–	0.89652	–	0.9398	–	0.92872	–
$K_{\mathrm{UDPG}r}$	0.98	0.29	2.82	1.14	1.07	0.13	0.84	0.13
$K_{\mathrm{UDPG}t}$	1.06	0.13	2.05	0.59	–	–	1.46	0.22
$K_{\mathrm{G6P}r}$	$7.12 \cdot 10^{-2}$	$2.19 \cdot 10^{-2}$	0.14	$5.08 \cdot 10^{-2}$	$7.95 \cdot 10^{-2}$	$2.23 \cdot 10^{-2}$	0.17	$2.72 \cdot 10^{-2}$
$K_{\mathrm{G6P}t}$	0.23	0.11	0.16	$6.8 \cdot 10^{-2}$	0.23	$8.1 \cdot 10^{-2}$	0.6	0.12
$K_{\mathrm{ATP}r}$	4.92	2.47	7.33	5.04	5.72	2.8	26.2	16.67
$K_{\mathrm{ATP}t}$	2.28	1.17	2.13	0.94	2.59	0.96	3.21	0.82
$K'_{\mathrm{ATP}r}$	25.42	11.89	–	–	29.12	15.13	–	–
$K'_{\mathrm{ATP}t}$	6.44	2.69	–	–	6.69	1.78	–	–
L_0^{I}	0.45	0.16	0.24	0.12	0.38	0.12	0.69	0.24
L_0^{D}	13.21	6.98	$1.64 \cdot 10^{6}$	$6.03 \cdot 10^{11}$	10.21	4.29	7.61	3.33
$V_r^{\mathrm{I;G6P}}$	0.65	0.14	1.61	0.61	0.69	$6.62 \cdot 10^{-2}$	0.58	$6.17 \cdot 10^{-2}$
$V_r^{\mathrm{D;G6P}}$	0.54	$9.09 \cdot 10^{-2}$	$8.73 \cdot 10^{5}$	$3.21 \cdot 10^{11}$	0.59	$9.01 \cdot 10^{-2}$	0.44	$4.79 \cdot 10^{-2}$
$V_r^{\mathrm{I;UDPG}}$	0.52	0.13	0.86	0.27	0.54	$5.23 \cdot 10^{-2}$	0.43	$2.9 \cdot 10^{-2}$
$V_r^{\mathrm{D;UDPG}}$	0.35	$5.18 \cdot 10^{-2}$	$8.11 \cdot 10^{5}$	$2.99 \cdot 10^{11}$	0.38	$5.28 \cdot 10^{-2}$	0.28	$1.97 \cdot 10^{-2}$

NoSpecR, which had the highest $\bar{R}^2$ value. DepComR was significantly better than DepR. DepComNoSpecR could not be compared to DepR using the *F*-test, as DepR is not a simplified form of DepComNoSpecR, but DepR had a much lower $\bar{R}^2$. Likewise, Independent could not be compared with the *F*-test to any of the equations in which G6P competes with ATP, because they represent different simplifications of the same generic equation. Nevertheless, based on the $\bar{R}^2$ value, Independent, though better than DepR, provides a worse fit than either DepComR and DepComNoSpecR.

Similar results were consistently found for *scaled* (Table 3.3) and *half-scaled* (Table 3.4). In all cases DepComR provided the best fit, but was not significantly better than DepComNoSpecR. DepR provided the worst fit and in all cases no error estimates could be calculated. Independent provided the second worst fit. These results led us to choose DepComNoSpecR as the simplest model to provide an adequate description of the experimental data (Fig. 3.2).

To identify the weighting strategy that minimizes the effects of experimental error on the fitted parameters and any error introduced during the digitization of data, especially those resulting from inverting the Lineweaver-Burk plots, graphs of the weighted residuals against the calculated rate were plotted (Fig. 3.3). Although the availability of more data points would aid the interpretation, several trends can be observed. For the data depicting the dependence of I form activity on UDPG and ATP, the variance in both *unscaled* and *half-scaled* appears to increase with the calculated rate. These weighting strategies therefore neglect data points with small calcu-

Table 3.3: Optimized kinetic parameters obtained using a scaled weighting strategy

	DepComR		DepR		DepComNoSpecR		IndependentR	
Parameter	value	error	value	error	value	error	value	error
R^2	0.93702	–	0.8944	–	0.93694	–	0.915	–
$\bar{R}^2$	0.92676	–	0.88	–	0.92752	–	0.90341	–
K_{UDPG_r}	1.07	0.39	0.92	–	1	0.19	0.78	0.19
K_{UDPG_t}	1.02	0.22	1.69	–	–	–	1.6	0.29
K_{G6P_r}	$6.62 \cdot 10^{-2}$	$1.94 \cdot 10^{-2}$	0.12	–	$6.41 \cdot 10^{-2}$	$1.88 \cdot 10^{-2}$	0.22	$2.88 \cdot 10^{-2}$
K_{G6P_t}	0.19	$7.38 \cdot 10^{-2}$	$1.83 \cdot 10^{-7}$	–	0.18	$5.79 \cdot 10^{-2}$	1.07	0.14
K_{ATP_r}	3.17	1.31	5.01	–	3.05	1.26	23.53	10.03
K_{ATP_t}	1.57	0.7	$7.5 \cdot 10^{-7}$	–	1.48	0.56	2.01	0.59
K'_{ATP_r}	30.65	27.06	–	–	30.17	25.71	–	–
K'_{ATP_t}	6.97	2.79	–	–	7.13	2.27	–	–
L_0^{I}	0.31	0.12	$1 \cdot 10^{-25}$	–	0.31	0.12	0.21	0.14
L_0^{D}	8.28	3.35	$2.13 \cdot 10^{-24}$	–	8.29	3.46	4.58	3.04
$V_r^{\mathrm{I;G6P}}$	0.7	0.2	0.58	–	0.67	$9.38 \cdot 10^{-2}$	0.52	$8.39 \cdot 10^{-2}$
$V_r^{\mathrm{D;G6P}}$	0.59	0.15	0.45	–	0.57	0.1	0.39	$6.49 \cdot 10^{-2}$
$V_r^{\mathrm{I;UDPG}}$	0.46	0.15	0.33	–	0.44	$5.64 \cdot 10^{-2}$	0.33	$4.59 \cdot 10^{-2}$
$V_r^{\mathrm{D;UDPG}}$	0.51	0.13	0.39	–	0.49	$8.93 \cdot 10^{-2}$	0.33	$5.29 \cdot 10^{-2}$

Table 3.4: Optimized kinetic parameters obtained using a half-scaled weighting strategy

	DepComR		DepR		DepComNoSpecR		IndependentR	
Parameter	value	error	value	error	value	error	value	error
R^2	0.96278	–	0.92523	–	0.96274	–	0.94666	–
$\bar{R}^2$	0.95672	–	0.91503	–	0.95718	–	0.93938	–
K_{UDPG_r}	0.74	0.2	0.69	–	0.77	$9.71 \cdot 10^{-2}$	0.6	0.1
K_{UDPG_t}	0.77	$9.71 \cdot 10^{-2}$	1.38	–	–	–	1.25	0.18
K_{G6P_r}	$7.14 \cdot 10^{-2}$	$1.65 \cdot 10^{-2}$	$8.83 \cdot 10^{-2}$	–	$7.38 \cdot 10^{-2}$	$1.63 \cdot 10^{-2}$	0.2	$2.48 \cdot 10^{-2}$
K_{G6P_t}	0.24	$8.45 \cdot 10^{-2}$	$1.52 \cdot 10^{-7}$	–	0.25	$6.19 \cdot 10^{-2}$	0.93	0.13
K_{ATP_r}	4.68	1.72	3.42	–	4.91	1.75	24	10.86
K_{ATP_t}	2.18	0.86	$5.47 \cdot 10^{-7}$	–	2.3	0.66	2.42	0.54
K'_{ATP_r}	20.95	9	–	–	21.63	9.31	–	–
K'_{ATP_t}	5.38	1.74	–	–	5.31	1.05	–	–
L_0^{I}	0.36	0.11	$1 \cdot 10^{-25}$	–	0.34	$9.42 \cdot 10^{-2}$	0.5	0.23
L_0^{D}	13.16	5.11	$2.74 \cdot 10^{-24}$	–	12.28	4.13	9.63	4.61
$V_r^{\mathrm{I;G6P}}$	0.53	$9.64 \cdot 10^{-2}$	0.46	–	0.54	$4.92 \cdot 10^{-2}$	0.45	$4.75 \cdot 10^{-2}$
$V_r^{\mathrm{D;G6P}}$	0.43	$6.37 \cdot 10^{-2}$	0.34	–	0.44	$5.11 \cdot 10^{-2}$	0.34	$3.63 \cdot 10^{-2}$
$V_r^{\mathrm{I;UDPG}}$	0.45	$9.77 \cdot 10^{-2}$	0.33	–	0.46	$4.04 \cdot 10^{-2}$	0.35	$2.58 \cdot 10^{-2}$
$V_r^{\mathrm{D;UDPG}}$	0.36	$4.78 \cdot 10^{-2}$	0.28	–	0.36	$3.76 \cdot 10^{-2}$	0.27	$2.22 \cdot 10^{-2}$

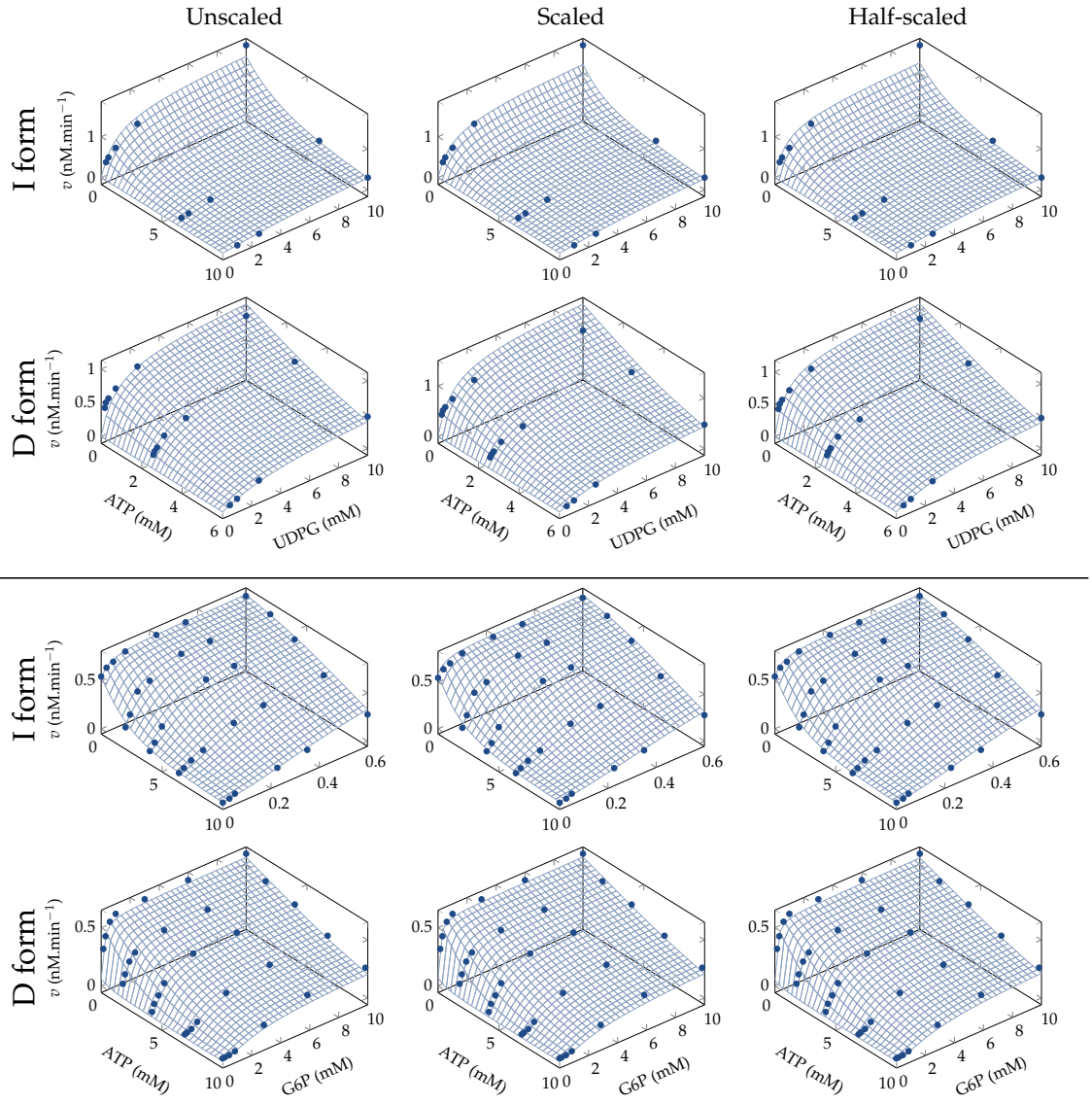

Figure 3.2: Comparison of experimental data points [67] to the rates calculated from the best-fit equations (DepComNoSpecR in all cases) for the *unscaled*, *scaled*, and *half-scaled* weighting strategies.

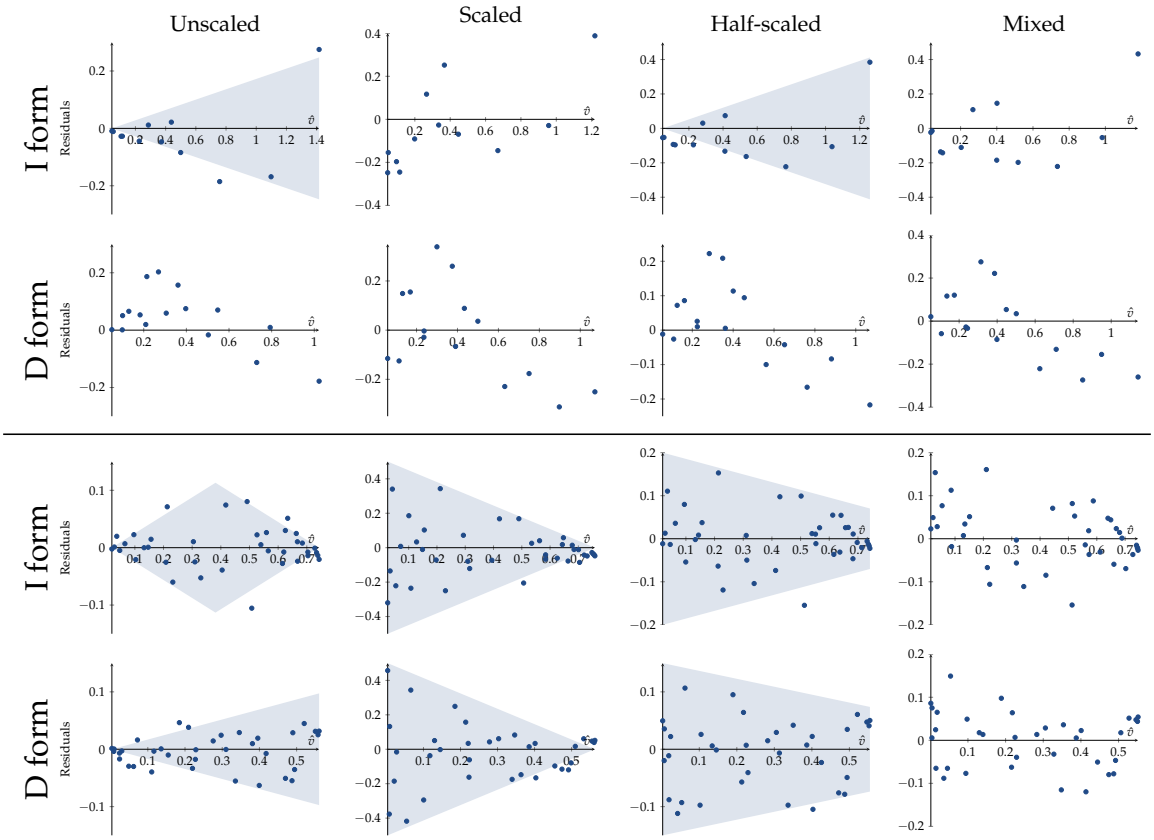

Figure 3.3: Weighted residual plots with respect to the calculated rate $\hat{v}$. UDPG and ATP are varied in the first two rows, whereas G6P and ATP are varied in the last two rows. Shaded areas indicate trends in residual distribution.

lated values, whereas the *scaled* strategy gives a more even weight to all data points, regardless of the calculated rate. For the D form no clear trend can be observed, but the residuals appear to be more randomly distributed for the *scaled* strategy. For the data depicting the dependence of D form activity on G6P and ATP, *unscaled* is biased towards the mid-range residuals, whereas *scaled* is biased towards the low-range residuals. For *half-scaled* the weighting is more even, but high-range residuals are still neglected. For the D form, *unscaled* is biased towards the high-range residuals, *scaled* is biased towards the low-range residuals, and *half-scaled* slightly neglects the high-range residuals. Based on these results, we chose *scaled* for the data depicting the dependence of I and D form activity on UDPG and ATP, and *half-scaled* for the data depicting the dependence of I and D form activity on G6P and ATP.

We next repeated the parameter optimization, but with the appropriate weighting strategies applied. The optimized parameters are listed in Table 3.5. Again, only the rate equations in which only the R conformation is active provided useful fits.

Table 3.5: Optimized kinetic parameters obtained using a scaled weighting strategy for data obtained by varying UDPG and a half-scaled strategy for data obtained by varying G6P

	DepComR		DepR		DepComNoSpecR		IndependentR	
Parameter	value	error	value	error	value	error	value	error
R^2	0.97008	–	0.94123	–	0.97008	–	0.94864	–
$\bar{R}^2$	0.96521	–	0.93321	–	0.96561	–	0.94163	–
$K_{\mathrm{UDPG}r}$	0.72	0.16	0.76	–	0.72	$9.14 \cdot 10^{-2}$	0.7	0.12
$K_{\mathrm{UDPG}t}$	0.72	$9.52 \cdot 10^{-2}$	1.63	–	–	–	1.63	0.18
$K_{\mathrm{G6P}r}$	$6.75 \cdot 10^{-2}$	$1.49 \cdot 10^{-2}$	0.1	–	$6.76 \cdot 10^{-2}$	$1.44 \cdot 10^{-2}$	0.19	$2.73 \cdot 10^{-2}$
$K_{\mathrm{G6P}t}$	0.29	$9.34 \cdot 10^{-2}$	$2.15 \cdot 10^{-7}$	–	0.29	$7.18 \cdot 10^{-2}$	1.09	0.19
$K_{\mathrm{ATP}r}$	4.93	1.59	4.51	–	4.94	1.49	13.09	5.36
$K_{\mathrm{ATP}t}$	2.33	0.89	$6.2 \cdot 10^{-7}$	–	2.33	0.59	1	0.5
$K'_{\mathrm{ATP}r}$	15.9	6.08	–	–	15.92	6.04	–	–
$K'_{\mathrm{ATP}t}$	3.93	1.13	–	–	3.93	0.7	–	–
L_0^{I}	0.3	$9.74 \cdot 10^{-2}$	$1 \cdot 10^{-25}$	–	0.3	$9.35 \cdot 10^{-2}$	$6.28 \cdot 10^{-2}$	$8.07 \cdot 10^{-2}$
L_0^{D}	15.5	6.53	$3.36 \cdot 10^{-24}$	–	15.45	6.16	1.74	2.27
$V_r^{\mathrm{I;G6P}}$	0.52	$8.16 \cdot 10^{-2}$	0.49	–	0.52	$4.67 \cdot 10^{-2}$	0.47	$5.3 \cdot 10^{-2}$
$V_r^{\mathrm{D;G6P}}$	0.41	$5.86 \cdot 10^{-2}$	0.34	–	0.41	$4.26 \cdot 10^{-2}$	0.35	$4.05 \cdot 10^{-2}$
$V_r^{\mathrm{I;UDPG}}$	0.41	$8.14 \cdot 10^{-2}$	0.32	–	0.41	$3.88 \cdot 10^{-2}$	0.32	$2.72 \cdot 10^{-2}$
$V_r^{\mathrm{D;UDPG}}$	0.36	$4.75 \cdot 10^{-2}$	0.32	–	0.36	$3.56 \cdot 10^{-2}$	0.3	$3.09 \cdot 10^{-2}$

DepComR and DepComNoSpecR provided equally good fits, followed by IndependentR and DepR, for which no errors could be estimated. Being the more simple model, DepComNoSpecR had a smaller $\bar{R}^2$ value than DepComR. Its estimated errors were also smaller than that of DepComR. These results indicate that, of the tested equations, DepComNoSpecR best describes the experimental data obtained by Piras *et al.* [67].

Discussion

Piras *et al.* [67] found that ATP inhibition of GS is formally of the competitive type, but that reversal of this inhibition by G6P does not affect the K_{m} for UDPG, indicating that ATP binds to an allosteric site. They also found that the reversal of inhibition by G6P is not complete and therefore argue that ATP and G6P possibly bind to different allosteric sites. Sølling [42] also found that G6P is unable to completely reverse ATP inhibition and suggested that, in addition to competing with G6P for the same allosteric site, ATP also competes with UDPG for the catalytic site. To determine which of these scenarios provided the best description of GS kinetics, we considered several forms of the MWC equation. In one set of equations, G6P and ATP binding was considered dependent, i.e., binding to the same allosteric site. Within this group we further distinguished between forms in which a.) ATP does not bind to the catalytic site (Dep), and b.) ATP does bind to the catalytic site (DepCom). In the other set, ATP and G6P were considered to bind to separate allosteric sites (Independent).

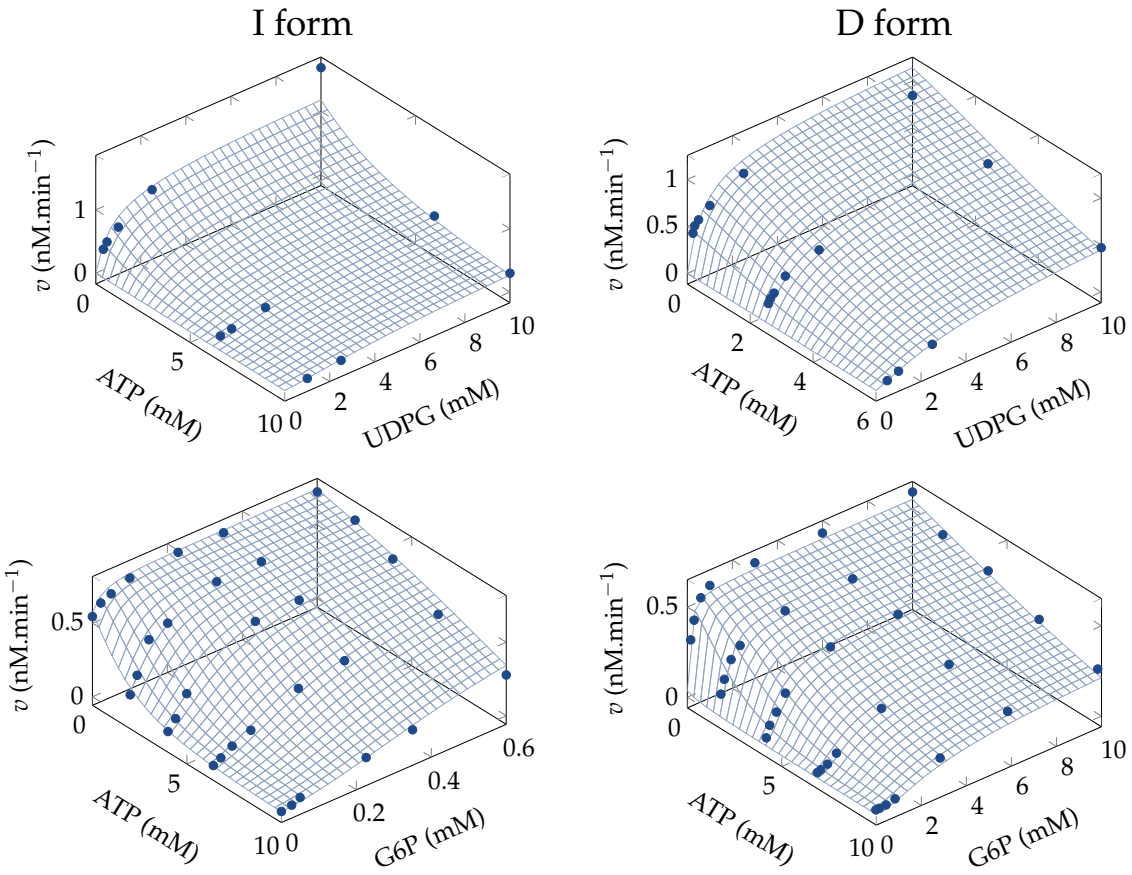

Figure 3.4: Comparison of experimental data points [67] to the rates calculated from the best-fit equation (DepComNoSpecR) for the *mixed* weighting strategy

The fitted values of σ_r and σ_t were very similar for DepCom, we therefore also considered a form in which it was assumed that $\sigma_r = \sigma_t$ (DepComNoSpec). Finally, from these four rate equations a further four were obtained by assuming in each case that only the R conformation is catalytically active.

Several weighting strategies were employed in an effort to minimize the contribution of outliers. Based on graphs in which the scaled residuals were plotted against the calculated rate, we chose the *scaled* strategy for data in which UDPG and ATP were varied, and the *half-scaled* strategy for data in which G6P and ATP were varied.

Of the tested equations, DepR provided the worst fit, indicating that mere competition for the same allosteric site by G6P and ATP is not sufficient to describe the kinetics of GS. This finding is in agreement with both Piras *et al.* [67] and Sølling

[42], who found that G6P does not completely reverse ATP inhibition as is assumed in DepR. IndependentR provided the second worst fit, ruling out the suggestion by Piras *et al.* [67] that ATP and G6P bind to different allosteric sites. Finally, DepComR and DepComNoSpecR provided equally good fits and equivalent parameter values. Having one less parameter than DepComR, DepComNoSpecR is the simplest equation that provides a good description of GS kinetics. Our data therefore indicate that the kinetics of GS is best described by a rate equation in which ATP competes with G6P for the allosteric site but also with UDPG for the catalytic site. In all cases, the rate equations in which both the T and R conformations were catalytically active resulted in either very large errors in the fitted parameters or in negative parameter values.

The application of DepComNoSpecR to GS kinetics implies that G6P is not in itself a specific activator of GS, i.e., it does not affect the enzyme's affinity for UDPG, but merely reverses specific inhibition by ATP. This finding, although in good agreement with the analysis of Piras *et al.* [67], differs from the conventional view that G6P is a specific activator even in the absence of ATP. These contradictory findings are explained by recalling that Piras *et al.* [67] worked at pH 6.6. When working at pH 7.8 their findings essentially agreed with the conventional view. Given the physiological muscle pH range (6.6–7.1), it must be stressed that our findings and those of Piras *et al.* [67] only apply to one end of the spectrum. Most other studies (see for example [42, 79, 90]) have worked at higher pH concentrations, often exceeding the physiological limit. Since inhibition of GS by ATP is known to increase as the pH decreases [67], working at a high pH has the advantage of minimizing ATP inhibition in experimental set-ups. A more complete description of GS kinetics would also have to consider the effect of pH, possibly by including an additional pH-dependent conformational change. Note, however, that the lack of specific activation by G6P does not mean that G6P results in no activation in the absence of ATP, it merely implies that all activation in the absence of ATP must be the result of catalytic activation, i.e., an apparent increase in the rate constant.

3.5 Estimation of L_0 for each phosphorylation state

Fractional velocity is frequently reported in the GS literature as an indication of the phosphorylation state of GS or its sensitivity towards G6P. In Chapter 2 we provided an expression for the fractional velocity according to the Hill model (Eq. 2.12) to pro-

vide insight into the relationship between the fractional velocity and kinetics parameters. We can now provide an expression according to Eq. 3.42 (DepComNoSpecR). In the absence of ATP Eq. 3.42 simplifies to

$$v_i = \frac{V_{\max r} n\sigma(1+\sigma)^{n-1}}{(1+\sigma)^n L_{0i}\left(\frac{1+\xi_{\mathrm{G6P}t}}{1+\xi_{\mathrm{G6P}r}}\right)^n + (1+\sigma)^n} \tag{3.50}$$

$$= V_{\max r} n\sigma(1+\sigma)^{-1}\left[L_{0i}\left(\frac{1+\xi_{\mathrm{G6P}t}}{1+\xi_{\mathrm{G6P}r}}\right)^n + 1\right]^{-1} \tag{3.51}$$

The fractional velocity is thus expressed as follows

$$\begin{aligned} FV_x &= \frac{v_{i,\mathrm{G6P}=x}}{v_{i,\mathrm{G6P}\gg K_{\mathrm{G6P}t,r}}} \\ &= \frac{V_{\max r} n\sigma(1+\sigma)^{-1}\left[L_{0i}\left(\frac{1+\xi_{\mathrm{G6P}t}}{1+\xi_{\mathrm{G6P}r}}\right)^n + 1\right]^{-1}}{V_{\max r} n\sigma(1+\sigma)^{-1}\left[L_{0i}\left(\frac{\xi_{\mathrm{G6P}t}}{\xi_{\mathrm{G6P}r}}\right)^n + 1\right]^{-1}} \\ &= \frac{L_{0i}\left(\frac{K_{\mathrm{G6P}r}}{K_{\mathrm{G6P}t}}\right)^n + 1}{L_{0i}\left(\frac{1+\xi_{\mathrm{G6P}t}}{1+\xi_{\mathrm{G6P}r}}\right)^n + 1} \end{aligned} \tag{3.52}$$

showing that it is independent of the UDPG concentration and affinity. Setting $x = 0$, the activity ratio is also obtained:

$$AR = FV_0 \tag{3.53}$$

$$= \frac{L_{0i}\left(\frac{K_{\mathrm{G6P}r}}{K_{\mathrm{G6P}t}}\right)^n + 1}{L_{0i} + 1} \tag{3.54}$$

Since $(K_{\mathrm{G6P}r}/K_{\mathrm{G6P}t})^n \simeq 0.003$, the activity ratio is an approximation of $1/(L_{0i}+1)$ or $R_i/(T_i+R_i)$, the fraction of enzyme in state i present in the R conformation in the absence of ligands. This result is particularly interesting, as the initial definition of the activity ratio was indeed that of a mole fraction, namely the fraction of enzyme in the I form: $I/(D+I)$.

More importantly, by rewriting Eq. 3.52, L_{0i} can be expressed in terms of fractional velocity, so that L_{0i} can be calculated for any phosphorylation state of GS for which the fractional velocity (or activity ratio) is known:

$$L_{0i} = \frac{1 - FV}{FV\left(\frac{1 + \xi_{\text{G6P}t}}{1 + \xi_{\text{G6P}r}}\right)^n - \left(\frac{K_{\text{G6P}r}}{K_{\text{G6P}t}}\right)^n} \tag{3.55}$$

The fractional velocity or activity ratio is only available for a few of the 18 phosphorylation states considered here. Following the principles explained below, however, we were able to calculate all 18 L_{0i} values. The left-hand side of Fig. 3.5 depicts an MWC-type enzyme that is phosphorylated in random order at two phosphorylation sites denoted 1 and 2. Phosphorylation is assumed to alter the apparent T/R equilibrium in a manner analogous to any classic allosteric modifier. It is further assumed that in all phosphorylation events all the subunits are phosphorylated simultaneously at the site in question. For the unliganded dephosphorylated form the equilibrium between the T and R conformations is then given by L_0. For the unliganded form phosphorylated at site 1, the corresponding equilibrium is given by L_{01}, and so on. K is the equilibrium constant of phosphorylation for a particular form as denoted by the subscripts. However, since the overall equilibrium constant must be the same regardless of whether a particular site is phosphorylated before or after the T/R transition occurs, it is clear that not all the equilibria can be independent. In particular, if L_{01} differs from L_0 by a factor α_1 as in the right-hand side of Fig. 3.5, then since $K_{1r}L_{01} = L_0K_{1t}$ must hold, $K_{1t} = \alpha_1K_{1r}$ must also hold. If we further define $L_{02} = \alpha_2L_0$, then since $K_{1r}L_{012} = L_{02}K_{1t}$, it can be shown that $L_{012} = \alpha_1\alpha_2L_0$. It thus follows that if L_0, L_{01} and L_{02} are available L_{012} can be calculated. The same result is readily but tediously obtained for more elaborate phosphorylation schemes. The general rule is that if a value of L_0 is available for each phosphorylation state in a sequentially phosphorylated cluster, then values can be calculated for states that result from combinations of phosphorylation in different clusters.

L_0 could be calculated from the activity ratio for 12 of the 18 phosphorylation states (Table 3.6). As not all the activity ratios were calculated at the same saturating G6P concentration, we used an adapted form of Eq. 3.55 that explicitly contains the saturating G6P concentration:

$$L_0 = \frac{1 - FV_0}{FV_0 - \left(\frac{K_{\text{G6P}r}K_{\text{G6P}r} + [\text{G6P}]_{\text{sat}}K_{\text{G6P}r}}{K_{\text{G6P}r}K_{\text{G6P}r} + [\text{G6P}]_{\text{sat}}K_{\text{G6P}t}}\right)^n} \tag{3.56}$$

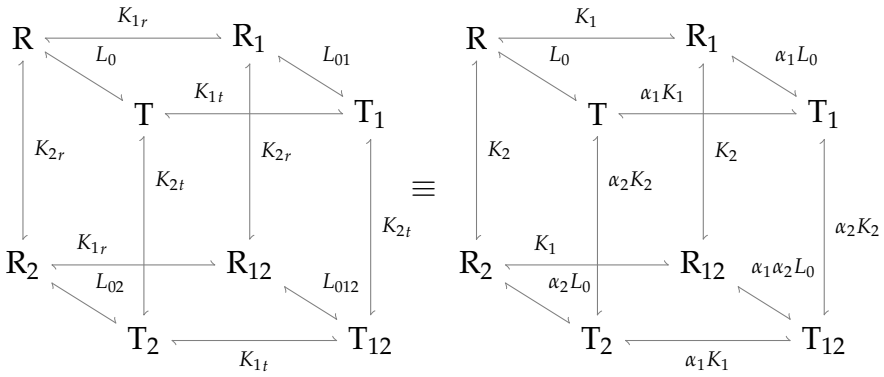

Figure 3.5: Kinetic model of a MWC-type enzyme phosphorylated at independent phosphorylation sites. All-or-none phosphorylation is assumed so that all subunits of a particular form are in the same phosphorylation state. Phoshorylation is assumed to alter the apparent equilibrium between the T and R conformations.

Table 3.6: Activity ratios for various phosphorylation states obtained from literature data and the corresponding values of L_0 calculated using Eq. 3.56. A few L_0 values calculated according to the expressions in Table 3.8 are included here for comparison.

Phosphorylated sites	$[G6P]_{sat}$ (mM)	Activity ratio	Ref.	L_{0i} (from activity ratio)	L_{0i} (from component L_{0i} values)
none	7.2	0.8	[120]	0.25	–
2	10	0.45	[109]	1.23	–
2–2a	10	0.17	[109]	4.98	–
5	7.2	0.8	[120]	0.25	–
5–4	7.2	0.8	[120]	0.25	–
5–3c	7.2	0.8	[120]	0.25	–
5–3b	7.2	0.6	[120]	0.67	–
5–3a	7.2	0.1	[120]	9.31	–
2; 5–3b	7.2	0.17	[114]	5.13	3.29
2; 5–3a	7.2	$2 \cdot 10^{-2}$	[114]	58.96	45.68
2–2a; 5–3b	7.2	$1.9 \cdot 10^{-2}$	[114]	62.79	13.29
2–2a; 5–3a	7.2	$1.1 \cdot 10^{-2}$	[114]	129.74	184.69

Table 3.7: Factors from which all values of L_0 can be calculated according to the expressions in Table 3.8

Factor	Value
α_2	4.9
α_{2a}	4.04
α_5	1
α_4	1
α_{3c}	1
α_{3b}	2.67
α_{3a}	13.89

Table 3.8: Calculated L_0 values for all 18 GS phosphorylation states

Phosphorylation state	Expression	L_{0i}
dephosphorylated	L_0	0.25
2	$\alpha_2 L_0$	1.23
2–2a	$\alpha_2\alpha_{2a} L_0$	4.98
5	$\alpha_5 L_0$	0.25
2;5	$\alpha_2\alpha_5 L_0$	1.23
2–2a;5	$\alpha_2\alpha_{2a}\alpha_5 L_0$	4.98
5–4;	$\alpha_5\alpha_4 L_0$	0.25
2;5–4	$\alpha_2\alpha_5\alpha_4 L_0$	1.23
2–2a;5–4	$\alpha_2\alpha_{2a}\alpha_5\alpha_4 L_0$	4.98
5–3c	$\alpha_5 \ldots \alpha_{3c} L_0$	0.25
2;5–3c	$\alpha_2\alpha_5 \ldots \alpha_{3c} L_0$	1.23
2–2a;5–3c	$\alpha_2\alpha_{2a}\alpha_5 \ldots \alpha_{3c} L_0$	4.98
5–3b	$\alpha_5 \ldots \alpha_{3b} L_0$	0.67
2;5–3b	$\alpha_2\alpha_5 \ldots \alpha_{3b} L_0$	3.29
2–2a;5–3b	$\alpha_2\alpha_{2a}\alpha_5 \ldots \alpha_{3b} L_0$	13.29
5–3a	$\alpha_5 \ldots \alpha_{3a} L_0$	9.31
2;5–3a	$\alpha_2\alpha_5 \ldots \alpha_{3a} L_0$	45.68
2–2a;5–3a	$\alpha_2\alpha_{2a}\alpha_5 \ldots \alpha_{3a} L_0$	184.69

The factors (denoted by α) by which each phosphorylation site apparently alters L_0, calculated from the values in Table 3.6, are listed in Table 3.7. The remaining six L_0 values were calculated from the expressions in Table 3.8. For four states (2; 5–3b, 2; 5–3a, 2–2a; 5-3b, and 2–2a; 5-3a) the value of L_0 could be calculated both directly from the activity ratio and according to the expressions in Table 3.8, allowing us to validate this method of calculation and, by implication, the assumption that GS kinetics is described by a MWC-type model in which phosphorylation alters the apparent L_0. In all four cases the values obtained from the two methods were of the same order of magnitude (Table 3.6).

3.6 Fractional velocity as a function of phosphorylation degree

Guinovart *et al.* [90] determined the fractional velocities for GS in a range of phosphorylation states (Fig. 3.6). They calculated the GS fractional velocity as the ratio of the activity in the presence of a low non-saturating G6P concentration to that in the presence of 10 mM G6P. The UDPG concentration for both activities was held constant at 0.2 mM. Using our 18-state model of GS, we attempted to reproduce the findings of Guinovart *et al.* [90].

The degree of phosphorylation (or average number of phosphates per subunit) is defined as

$$P_{deg} = \sum_i p_i \frac{[\mathrm{GS}_i]}{[\mathrm{GS}]_{tot}} \tag{3.57}$$

where p_i is the number of phosphorylated sites of GS in phosphorylation state i. The degree of phosphorylation is not a parameter, but a variable and cannot be manipulated directly. We therefore used a stochastic method to obtain sets of GS state concentrations that span the entire range (0 to 7) of possible degrees of phosphorylation. For each set the fractional velocity was calculated for the appropriate non-saturating G6P concentrations. The fractional velocities were then plotted against degree of phosphorylation (Fig. 3.6).

Good agreement was found between our model prediction and the experimental data obtained by Guinovart *et al.* [90]. However, a few discrepancies warrant discussion. First, full inactivation occurs at a much lower degree of phosphorylation in the experimental data of Guinovart *et al.* [90] than in the simulated data. This most likely reflects the fact that phosphorylation of GS is not strictly sequential in all phosphorylation clusters. In particular, it has been reported that sites 3a and possibly 3b can be phosphorylated by members of the dual specificity tyrosine phosphorylation regulated protein kinase (DYRK) kinase family without the requirement of prior phosphorylation at sites 5, 4 and 3c [92]. As phosphorylation at these sites results in potent inhibition, a decrease in the fractional velocity is expected to occur at lower degrees of phosphorylation than predicted if strict sequential phosphorylation is assumed. Second, the predicted fractional velocities are somewhat higher than the experimental values. This could be explained by the fact that our simulated values do not allow for the possibility of product inhibition or other phenomena that could

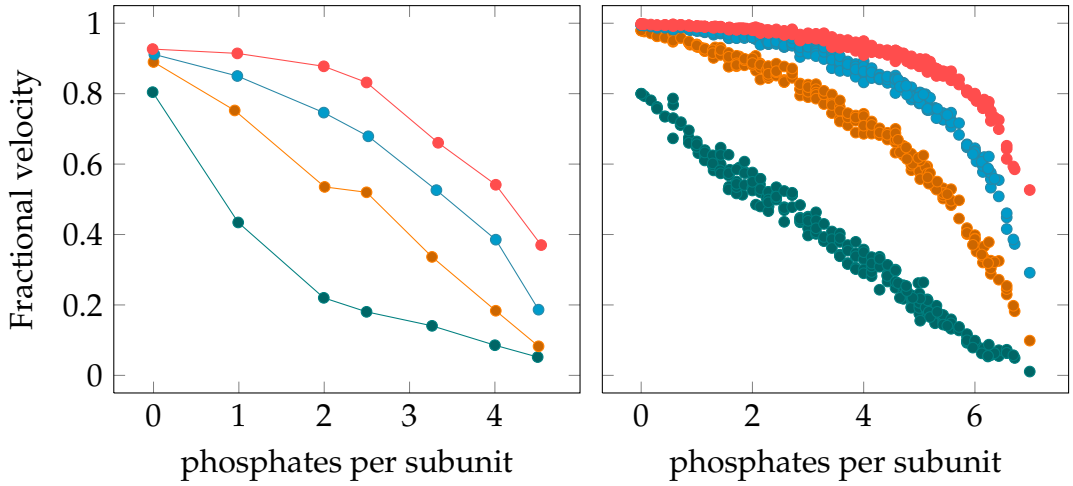

Figure 3.6: Relationship between fractional velocity and degree of phosphorylation as obtained from Guinovart *et al.* [90] (left) and reproduced from our optimized parameters and calculated L_{0i} values (right). The non-saturating G6P concentrations were: 0 mM (—●—), 0.1 mM (—●—), 0.25 mM (—●—), and 0.5 mM (—●—). The saturating G6P concentration was 10 mM in all cases. UDPG was present at 0.2 mM.

have affected the experimental values. In addition, the fact that no UDPG binding terms are present in Eq. 3.52 could result in the simulated values being higher.

In the next chapter we consider the implications that the GS rate equation developed in this chapter has for the interaction of allosteric and covalent modification.

Chapter 4

Interaction of allosteric and covalent enzyme modification

4.1 Introduction

We have argued that the observed effects of phosphorylation on glycogen synthase (GS) kinetics is qualitatively the same as would be expected if GS were a Monod-Wyman-Changeux (MWC)-type enzyme in which phosphorylation, in addition to allosteric modification, resulted in a shift in the apparent equilibrium between enzyme in the T and R conformations. We then proceeded to show that a rate equation based on such a MWC-type model does indeed provide a good description of the experimental data published by Piras *et al.* [67]. In this chapter we will show that this model has far-reaching implications, affecting not only the GS rate equation, but also the rate equations of enzymes that catalyse the covalent modification of GS. The significance of these implications are demonstrated by analysing a minimal feed-forward activation system in which the regulated enzyme is inhibited by covalent modification. Finally, the findings are applied to GS and glycogen synthesis.

A central principle employed throughout this chapter is that the free energy change, and thus K_{eq}, for the conversion of one substance to another is constant regardless of which other states served as intermediates. Consider, for example, the conversion of protein A to protein B as in the left hand side of Fig. 4.1. The overall equilibrium constant K_{eq} for the conversion of A to B remains unaffected whether the conversion took place via intermediate I or intermediate I′, so that $K_{eq} = K_{eq1} \cdot K'_{eq2} = K'_{eq1} \cdot K_{eq2}$. It follows that $\frac{K'_{eq1}}{K_{eq1}} = \frac{K'_{eq2}}{K_{eq2}} = \alpha$, where α is a constant, so that the left hand side of Fig. 4.1 can also be shown as in the right hand side. In

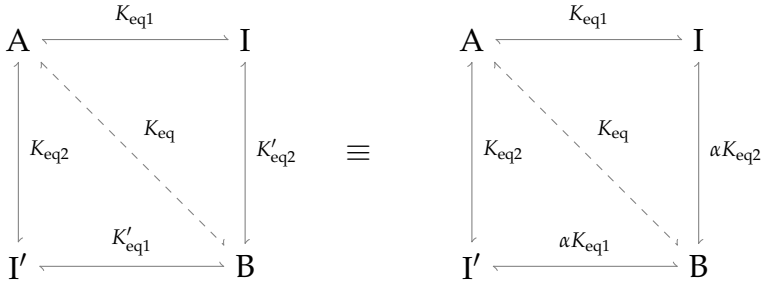

Figure 4.1: Reaction scheme of conversion of protein A to protein B via intermediates I and I′. The K_{eq} is constant and independent of whether I or I′ served as intermediate. The left hand scheme is therefore equivalent to the right hand scheme.

what follows, where applicable, we will immediately write equilibrium constants in terms of factors as in the right hand side of Fig. 4.1.

4.2 Interaction of allosteric and covalent modification

In Chapter 3 we have seen that if phosphorylation is considered to alter L_0 by a factor α, then by necessity the equilibrium constant of phosphorylation of the T conformation differs from the equilibrium constant of phosphorylation of the R conformation by the same factor α. We will now investigate this matter further. In contrast to the earlier treatment, however, we will not assume *all-or-none* modification.

Conformational change alters the apparent equilibrium constant of covalent modification

Consider a monomeric enzyme in equilibrium between a T and R conformation that undergoes covalent modification at a single site:

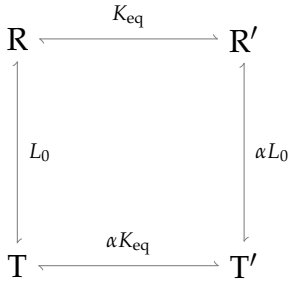

(4.1)

where R and T represent the classic "relaxed" and "taut" conformations of the MWC model, prime (′) denotes the enzyme form that is covalently modified, K_{eq} is the

equilibrium constant of covalent modification, and α is the factor by which covalent modification alters L_0. The concentration of the group that is transferred to the enzyme is considered constant and thus omitted. The apparent equilibrium constant of covalent modification is therefore defined as:

$$\begin{aligned} K_{\text{eq,app}} &= \frac{[\text{T}'] + [\text{R}']}{[\text{T}] + [\text{R}]} \\ &= \frac{[\text{R}'](\alpha L_0 + 1)}{[\text{R}](L_0 + 1)} \\ &= K_{\text{eq}} \left(\frac{\alpha L_0 + 1}{L_0 + 1} \right) \end{aligned} \tag{4.2}$$

If $\alpha < 1$, then $K_{\text{eq,app}} < K_{\text{eq}}$, otherwise if $\alpha > 1$, then $K_{\text{eq,app}} > K_{\text{eq}}$. If covalent modification has no effect whatsoever on the apparent L_0, i.e., $\alpha = 1$, then $K_{\text{eq,app}} = K_{\text{eq}}$. For any given covalent modification state, α has a fixed value, but L_0 can potentially undergo an apparent alteration by additional modification, whether covalent or allosteric. As the apparent value of L_0 decreases, $K_{\text{eq,app}}$ approaches K_{eq}. If L_0 is very large, on the other hand, $K_{\text{eq,app}}$ approaches αK_{eq}. Note, however, that the equilibrium constants for the reactions $\text{R} \rightarrow \text{R}'$ and $\text{T} \rightarrow \text{T}'$, K_{eq} and αK_{eq}, remain constant; it is only their relative contribution towards the K_{eq} of the *apparent* reaction $\text{E} \rightarrow \text{E}'$ (where E and E′ are the total unmodified and modified proteins) that changes with L_0.

Adding an allosteric modification layer to Eq. 4.1 yields:

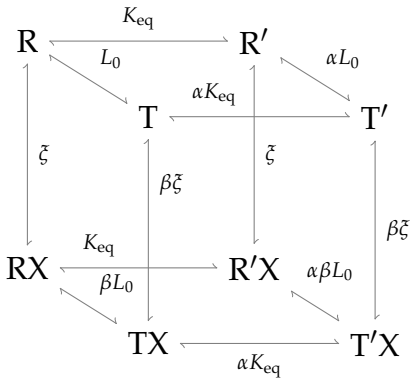

(4.3)

where X denotes an allosteric modifier with concentration x; $\xi = x/K_{\text{x}}$; K_{x} is the modifier dissociation constant; and β is the factor by which L_0 is apparently altered upon modifier binding. The expression for $K_{\text{eq,app}}$ now reads

$$K_{\text{eq,app}} = \frac{[\text{T}'] + [\text{R}'] + [\text{R}'\text{X}] + [\text{T}'\text{X}]}{[\text{T}] + [\text{R}] + [\text{RX}] + [\text{TX}]} = K_{\text{eq}} \left(\frac{\alpha L_0 (1 + \beta\xi) + 1 + \xi}{L_0 (1 + \beta\xi) + 1 + \xi} \right) \tag{4.4}$$

In the absence of allosteric modifier, Eq. 4.4 simplifies to Eq. 4.2, but at saturating modifier concentrations it is transformed to

$$K_{\text{eq,app}} = K_{\text{eq}} \left(\frac{\alpha\beta L_0 + 1}{\beta L_0 + 1} \right) \tag{4.5}$$

$$= K_{\text{eq}} \left(\frac{\alpha L_0 + \frac{1}{\beta}}{L_0 + \frac{1}{\beta}} \right) \tag{4.6}$$

showing that if X binds preferentially to the T conformation ($\beta > 1$) it increases the apparent value of L_0 and thus displaces $K_{\text{eq,app}}$ towards αK_{eq}. If, however, X prefers to bind to the R conformation ($\beta < 1$), then $K_{\text{eq,app}}$ approaches K_{eq} as x increases. Note that X need not be an allosteric modifier; any ligand that prefers binding to either the T or R conformation ($\beta \neq 1$) will affect $K_{\text{eq,app}}$. In fact, any process whatsoever (including additional covalent modification) that has an apparent effect on L_0 will also affect $K_{\text{eq,app}}$.

Covalent modification is positively cooperative

Similar results are obtained for a dimeric enzyme. Figure 4.2 depicts the kinetic model of a dimeric MWC-type enzyme with a single covalent modification site per subunit. The statistical factors 2 and $\frac{1}{2}$ must be included to show that, for instance, R′ can be formed by modifying any of the two sites of R, or by eliminating modification from any of the two sites of R″. The same is true with regard to T′.

The expression for the overall apparent equilibrium constant is

$$K^2_{\text{eq,app}} = \frac{[\text{T}''] + [\text{R}'']}{[\text{T}] + [\text{R}]} = K^2_{\text{eq}} \left(\frac{\alpha^2 L_0 + 1}{L_0 + 1} \right)$$

$$K_{\text{eq,app}} = K_{\text{eq}} \sqrt{\frac{\alpha^2 L_0 + 1}{L_0 + 1}} \tag{4.7}$$

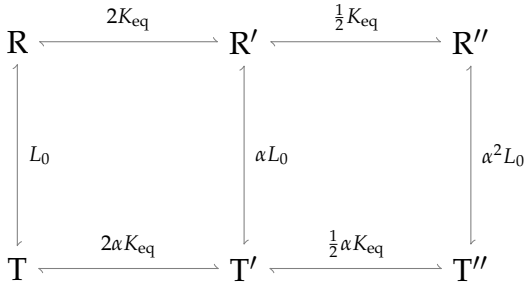

Figure 4.2: Reaction scheme for the covalent modification of a dimeric Monod-Wyman-Changeux-type enzyme. Each covalent modification (indicated by ′) alters the equilibrium between the T and R conformations by a factor α. See text for details.

$K_{eq,app}$ thus varies with L_0 and α in a manner qualitatively the same as for the monomeric enzyme.

Considering only the first covalent modification the apparent equilibrium constant is given by

$$\begin{aligned} 2K_{eq1,app} &= \frac{[T'] + [R']}{[T] + [R]} \\ &= 2K_{eq}\left(\frac{\alpha L_0 + 1}{L_0 + 1}\right) \\ K_{eq1,app} &= K_{eq}\left(\frac{\alpha L_0 + 1}{L_0 + 1}\right) \end{aligned} \tag{4.8}$$

and for the second modification by

$$\begin{aligned} \frac{1}{2}K_{eq2,app} &= \frac{[T''] + [R'']}{[T'] + [R']} \\ &= \frac{1}{2}K_{eq}\left(\frac{\alpha^2 L_0 + 1}{\alpha L + 1}\right) \\ K_{eq2,app} &= K_{eq}\left(\frac{\alpha^2 L_0 + 1}{\alpha L_0 + 1}\right) \end{aligned} \tag{4.9}$$

It can be shown that $K_{eq2,app} > K_{eq1,app}$ for all $\alpha \in (0,\infty), \alpha \neq 1$ and $L_0 \in (0,\infty)$:

$$\Delta K_{eq,app} = K_{eq2,app} - K_{eq1,app} \tag{4.10}$$

$$= K_{eq}\frac{L_0(1-\alpha)^2}{(1+\alpha L_0)(1+L_0)} > 0 \tag{4.11}$$

It follows that the second modification proceeds more readily than the first, i.e., covalent modification is positively cooperative. If $\alpha = 1$ (if covalent modification has no apparent effect on L_0), then $K_{\text{eq2,app}} = K_{\text{eq1,app}}$ and no cooperativity is observed.

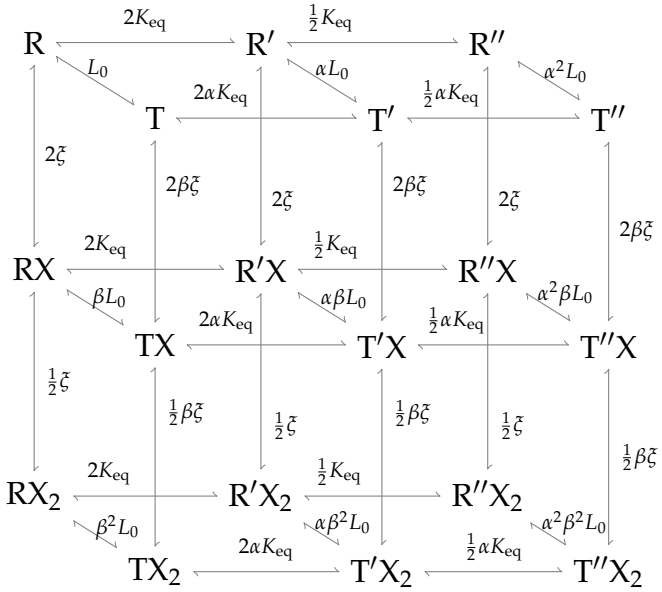

Figure 4.3: Reaction scheme for the covalent and allosteric modification of a dimeric Monod-Wyman-Changeux-type enzyme. Each covalent modification (indicated by ′) alters the equilibrium between the T and R conformations by a factor α, whereas binding of the allosteric modifier X alters the T and R equilibrium by a factor β. See text for details.

Adding an allosteric site, Fig. 4.2 is extended to Fig. 4.3. The overall apparent equilibrium constant then becomes

$$K_{\text{eq,app}} = K_{\text{eq}} \sqrt{\frac{\alpha^2 L_0 (1+\beta\xi)^2 + (1+\xi)^2}{L_0 (1+\beta\xi)^2 + (1+\xi)^2}} \tag{4.12}$$

or

$$K_{\text{eq,app}} = K_{\text{eq}} \sqrt{\frac{\alpha^2 \beta^2 L_0 + 1}{\beta^2 L_0 + 1}} \tag{4.13}$$

if the modifier is saturating. The $K_{\text{eq,app}}$ for the first covalent modification is

$$
\begin{aligned}
2K_{\text{eq1,app}} &= \frac{[\text{T}'] + [\text{R}'] + [\text{T}'\text{X}] + [\text{R}'\text{X}] + [\text{T}'\text{X}_2] + [\text{R}'\text{X}_2]}{[\text{T}] + [\text{R}] + [\text{TX}] + [\text{RX}] + [\text{TX}_2] + [\text{RX}_2]} \\
&= 2K_{\text{eq}} \left(\frac{\alpha L_0 (1+\beta\xi)^2 + (1+\xi)^2}{L_0(1+\beta\xi)^2 + (1+\xi)^2} \right) \\
K_{\text{eq1,app}} &= K_{\text{eq}} \left(\frac{\alpha L_0 (1+\beta\xi)^2 + (1+\xi)^2}{L_0(1+\beta\xi)^2 + (1+\xi)^2} \right)
\end{aligned} \tag{4.14}
$$

and

$$
\begin{aligned}
\frac{1}{2}K_{\text{eq2,app}} &= \frac{[\text{T}''] + [\text{R}''] + [\text{T}''\text{X}] + [\text{R}''\text{X}] + [\text{T}''\text{X}_2] + [\text{R}''\text{X}_2]}{[\text{T}'] + [\text{R}'] + [\text{T}'\text{X}] + [\text{R}'\text{X}] + [\text{T}'\text{X}_2] + [\text{R}'\text{X}_2]} \\
&= \frac{1}{2}K_{\text{eq}} \left(\frac{\alpha^2 L_0 (1+\beta\xi)^2 + (1+\xi)^2}{\alpha L_0(1+\beta\xi)^2 + (1+\xi)^2} \right) \\
K_{\text{eq2,app}} &= K_{\text{eq}} \left(\frac{\alpha^2 L_0 (1+\beta\xi)^2 + (1+\xi)^2}{\alpha L_0(1+\beta\xi)^2 + (1+\xi)^2} \right)
\end{aligned} \tag{4.15}
$$

for the second covalent modification. The difference between $K_{\text{eq2,app}}$ and $K_{\text{eq1,app}}$ is, given the same constraints as earlier, also positive:

$$
\Delta K_{\text{eq,app}} = K_{\text{eq}} \frac{L_0(1+\beta\xi)^2(1-\alpha)^2}{[(1+\xi)^2 + \alpha L_0(1+\beta\xi)^2]\,[(1+\xi)^2 + L_0(1+\beta\xi)^2]} > 0 \tag{4.16}
$$

Cooperativity with respect to covalent modification is therefore observed regardless of the concentration of allosteric modifier. However, the allosteric modifier and its preference for the T or R conformation does affect the *degree* of cooperativity with respect to covalent modification. This effect can be investigated by considering the difference between $\Delta K_{\text{eq,app}}$ in the presence of allosteric modifier and $\Delta K_{\text{eq,app}}$ in the absence of modifier. To simplify the calculation we assume allosteric modifier, if present, is saturating:

$$
\begin{aligned}
\Delta K_{\text{eq,app}}^{\xi\to\infty} - \Delta K_{\text{eq,app}}^{\xi=0} &= K_{\text{eq}} \frac{\beta^2 L_0 (1-\alpha)^2}{(1+\alpha\beta^2 L_0)(1+\beta^2 L_0)} - K_{\text{eq}} \frac{L_0(1-\alpha)^2}{(1+\alpha L_0)(1+L_0)} \\
&= -K_{\text{eq}} \frac{(\alpha-1)^2(\beta^2-1)(\alpha\beta^2 L_0^2 - 1)}{(1+L_0)(1+\alpha L_0)(1+\beta^2 L_0)(1+\alpha\beta^2 L_0)}
\end{aligned} \tag{4.17}
$$

For positive values of Eq. 4.17, binding of the allosteric modifier leads to an increase in the degree of cooperativity with respect to covalent modification. Conversely, a decrease in degree of cooperativity is seen for solutions where Eq. 4.17 is

negative. Finally, where Eq. 4.17 is zero, the allosteric modifier has no effect on the degree of cooperativity. There are five cases to consider.

1. If the allosteric modifier is an inhibitor ($\beta > 1$) and covalent modification is inhibitory ($\alpha > 1$) or only mildly activating ($\alpha\beta^2 > 1$), then the allosteric modifier will decrease the cooperativity with respect to covalent modification for all $L_0 > \sqrt{\frac{1}{\alpha\beta^2}}$ and increase the cooperativity for all $L_0 < \sqrt{\frac{1}{\alpha\beta^2}}$ where $\sqrt{\frac{1}{\alpha\beta^2}} < 1$ (Fig. 4.4A).

2. If the allosteric modifier is an activator ($\beta < 1$) and covalent modification is also activating ($\alpha < 1$) or only mildly inhibitory ($\alpha\beta^2 < 1$), then the allosteric modifier will decrease the cooperativity with respect to covalent modification for all $L_0 < \sqrt{\frac{1}{\alpha\beta^2}}$ and increase the cooperativity for all $L_0 > \sqrt{\frac{1}{\alpha\beta^2}}$ where $\sqrt{\frac{1}{\alpha\beta^2}} > 1$ (Fig. 4.4B).

3. If the allosteric modifier is an activator ($\beta < 1$) and covalent modification is strongly inhibitory ($\alpha > 1$, $\alpha\beta^2 > 1$), then the allosteric modifier will increase the cooperativity with respect to covalent modification for all $L_0 > \sqrt{\frac{1}{\alpha\beta^2}}$ and decrease the cooperativity for all $L_0 < \sqrt{\frac{1}{\alpha\beta^2}}$ where $\sqrt{\frac{1}{\alpha\beta^2}} < 1$ (Fig. 4.4C).

4. If the allosteric modifier is an inhibitor ($\beta > 1$) and covalent modification is strongly activating ($\alpha < 1$, $\alpha\beta^2 < 1$), then the allosteric modifier will increase the cooperativity with respect to covalent modification for all $L_0 < \sqrt{\frac{1}{\alpha\beta^2}}$ and decrease the cooperativity for all $L_0 > \sqrt{\frac{1}{\alpha\beta^2}}$ where $\sqrt{\frac{1}{\alpha\beta^2}} > 1$ (Fig. 4.4D).

5. In the trivial case where only the R conformation can be phosphorylated ($\alpha = 0$), the allosteric modifier will increase cooperativity with respect to covalent modification for all values of L_0 if it is an inhibitor ($\beta > 1$) or decrease it if it is an activator ($\beta < 1$). The converse is true if only the T conformation can be phosphorylated.

In all five cases β can be replaced with $\frac{1+\beta\xi}{1+\xi}$ to evaluate the effect of non-saturating allosteric modifier on the degree of cooperativity with respect to covalent modification.

Although it depends on the exact values of α, β and L_0 whether the allosteric modifier increases or decreases the degree of cooperativity with respect to covalent

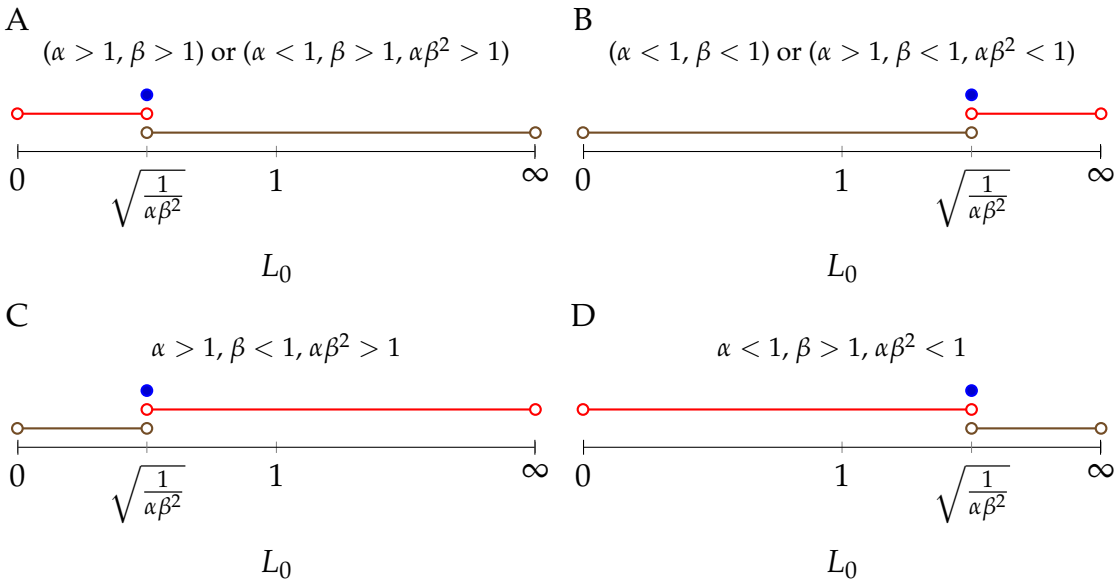

Figure 4.4: Influence of saturating allosteric modifier on the degree of cooperativity with respect to covalent modification. Depending on the value of L_0, the allosteric modifier will either have no effect (●) on the cooperativity of covalent modification, increase it (—●—), or decrease it (—●—).

modification, the following general conclusions can be drawn. If covalent and allosteric modification both prefer the same conformation, then if the enzyme is already predominantly present in that conformation, the degree of cooperativity with respect to covalent modification is decreased in the presence of allosteric modifier. If, however, covalent and allosteric modification prefer opposite conformations, then if the enzyme is already predominantly present in the conformation preferred by covalent modification and given that covalent modification is the stronger effect, the degree of cooperativity with respect to covalent modification is increased in the presence of allosteric modifier. The same overall conclusions can be drawn for enzymes with more than two subunits.

Half-saturation and half-alteration

Further extending the kinetic model in Fig. 4.3 to an arbitrary number of subunits, n, the overall equilibrium constant becomes

$$K_{\text{eq,app}} = K_{\text{eq}} \sqrt[n]{\frac{\alpha^n L_0(1+\beta\xi)^n + (1+\xi)^n}{L_0(1+\beta\xi)^n + (1+\xi)^n}} \tag{4.18}$$

The extent γ_x to which a particular allosteric modifier concentration x alters the overall $K_{\text{eq,app}}$ relative to the alteration seen with saturating allosteric modifier can be defined as follows:

$$\gamma_x = \frac{K_{\text{eq,app}} - K_{\text{eq,app}}^{\xi=0}}{K_{\text{eq,app}}^{\xi\to\infty} - K_{\text{eq,app}}^{\xi=0}} \tag{4.19}$$

γ_x ranges from 0 to 1 as x increases from zero to saturation. Setting $\gamma_x = \frac{1}{2}$ and $\xi = \xi_{\frac{1}{2}}$, an expression can be obtained for the dimensionless concentration, $\xi_{\frac{1}{2}}$, at which half the maximal alteration to $K_{\text{eq,app}}$ is observed.

$$\begin{aligned}
\gamma_x &= \frac{1}{2} \\
\frac{K_{\text{eq,app}} - K_{\text{eq,app}}^{\xi=0}}{K_{\text{eq,app}}^{\xi\to\infty} - K_{\text{eq,app}}^{\xi=0}} &= \frac{1}{2} \\
K_{\text{eq,app}} &= \frac{1}{2}\left(K_{\text{eq,app}}^{\xi\to\infty} + K_{\text{eq,app}}^{\xi=0}\right) && (4.20) \\
K_{\text{eq}}\sqrt[n]{\frac{\alpha^n L_0(1+\beta\xi_{\frac{1}{2}})^n + (1+\xi_{\frac{1}{2}})^n}{L_0(1+\beta\xi_{\frac{1}{2}})^n + (1+\xi_{\frac{1}{2}})^n}} &= \frac{1}{2}K_{\text{eq}}\left(\sqrt[n]{\frac{\alpha^n L_0\beta^n + 1}{L_0\beta^n + 1}} - \sqrt[n]{\frac{\alpha^n L_0 + 1}{L_0 + 1}}\right) && (4.21) \\
\xi_{\frac{1}{2}} &= \frac{L_0 + 1}{L_0\beta + 1} \quad \text{(assuming } n = 1\text{)} && (4.22)
\end{aligned}$$

Unfortunately, an analytical solution does not exist for arbitrary values of n. The half-saturation concentration is similarly defined as [161]:

$$\begin{aligned}
L_0 &= \frac{\xi_{\frac{1}{2}} - 1}{1 - \beta\xi_{\frac{1}{2}}}\left(\frac{1+\xi_{\frac{1}{2}}}{1+\beta\xi_{\frac{1}{2}}}\right)^{n-1} && (4.23) \\
\xi_{\frac{1}{2}} &= \frac{L_0 + 1}{L_0\beta + 1} \quad \text{(assuming } n = 1\text{)} && (4.24)
\end{aligned}$$

Again, a general analytical solution does not exist. Nevertheless, we see that for a monomeric enzyme the allosteric modifier half-saturation concentration for the covalently unmodified enzyme is equal to the concentration that results in half-maximal alteration of the apparent equilibrium constant for covalent modification. All that can be said for oligomeric enzymes ($n > 1$) is that both the half-saturation and half-alteration concentrations are between K_x and K_x/β and not necessarily equal.

4.3 Rate equations for covalent modification

In the previous section we have shown that the equilibrium constant for the covalent modification of an MWC-type protein, in which covalent modification brings about a shift in the equilibrium between the unliganded T and R conformations, undergoes an apparent change as a result of allosteric and covalent modification of the protein. Covalent modification of such a protein would typically be catalysed by an enzyme. It would therefore be of interest to derive a rate equation for such a reaction. The Haldane relationship

$$K_{\text{eq}} = \frac{V_{\text{f}} K_{\text{p}}}{V_{\text{r}} K_{\text{s}}} \tag{4.25}$$

requires that any change in the equilibrium constant (left hand side of Eq. 4.25) must be accompanied by compensating changes in the kinetic parameters on the right hand side of Eq. 4.25. Here we will derive rate equations for the forward and reverse covalent modification reactions. A critical step in the derivation of a rate equation is the expression of all enzyme forms in terms of only intrinsic equilibrium constants, the free enzyme concentration, and unbound ligand concentrations. This step can only be performed if it is assumed that all species are in equilibrium. This assumption, however, cannot be made if the interconversion between enzyme forms is itself enzyme-catalysed. Note that the assumption is valid if one is interested in equilibrium conditions as in the previous sections where an expression for the apparent equilibrium constant was sought. In order to derive a rate equation, then, one is forced to derive a separate equation for each covalent enzyme state and to subsequently describe the interconversion between states with additional rate equations. The overall rate is then the sum of the rates of the constituent enzyme states. In the previous chapter we were concerned with finding an expression for such a sum of rates. Here our focus turns to the interconversion between covalent enzyme states. The interconversion between the two covalent states of a monomeric protein with a single covalent modification site and one allosteric site will be used as an example (Fig. 4.5). Since the forward and reverse interconversions are usually catalysed by different enzymes, two rate equations are required to describe the interconversion.

Forward covalent modification

Assuming that the forward covalent modification reaction is a bi-substrate coupled reaction with a random binding order that is catalysed by enzyme A, the kinetic

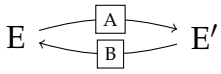

Figure 4.5: Forward and reverse covalent modification of a monomeric Monod-Wyman-Changeux-type enzyme by enzymes A and B. This scheme is obtained by *collapsing* all the conformations of a particular state in Eq. 4.3 into a single entity, so that, for instance, E collectively represents R, T, RX, and TX.

model is given in Fig. 4.6. During catalysis, unmodified protein E is converted to modified protein E′ by the transfer of the group (′) from the co-substrate, C′, to the co-product, C. Covalent modification alters the T/R equilibrium, L_0, by a factor α. A modifier X binds to the allosteric site of both covalent states of protein E, so that each covalent state exists in four forms (the T and R conformations and the two corresponding liganded forms). Binding of modifier X alters L_0 by a factor β. In addition, binding of protein E to enzyme A alters L_0 by a factor γ, or stated otherwise, the affinity of enzyme A for the R conformation differs from that for the T conformation by a factor γ. The parameters k_f and k_r are the forward and reverse rate constants of covalent modification. See Fig. 4.6 for additional parameter definitions.

The overall equilibrium constant for the conversion of ARC′ to AT′C is constant and independent of whether AR′C or ATC′ serves as an intermediate. Similarly, the equilibrium constant for the conversion of ARXC′ to AT′XC is independent of whether AR′XC or ATXC′ serves as intermediate. It follows that the forward rate constants for covalent modification of the complexes ATC′ and ATXC′ must be multiplied by α. Alternatively, the reverse rate constants must be multiplied by $\frac{1}{\alpha}$. These thermodynamic requirements can, of course, also be satisfied by combined changes in the forward and reverse constants. In what follows, however, we will only consider changes to the forward rate constants as shown in Fig. 4.6.

The total concentration of A can be expressed as

$$[\mathrm{A}]_{\mathrm{tot}} = [\mathrm{A}] + [\mathrm{AE}] + [\mathrm{AC}'] + [\mathrm{AEC}'] + [\mathrm{AEC}] + [\mathrm{AE}'] + [\mathrm{AC}] + [\mathrm{AE}'\mathrm{C}] + [\mathrm{AE}'\mathrm{C}'] \tag{4.26}$$

where

$$[\mathrm{AE}] = [\mathrm{AR}] + [\mathrm{AT}] + [\mathrm{ARX}] + [\mathrm{ATX}] \tag{4.27}$$

$$[\mathrm{AEC}] = [\mathrm{ARC}] + [\mathrm{ATC}] + [\mathrm{ARXC}] + [\mathrm{ATXC}] \tag{4.28}$$

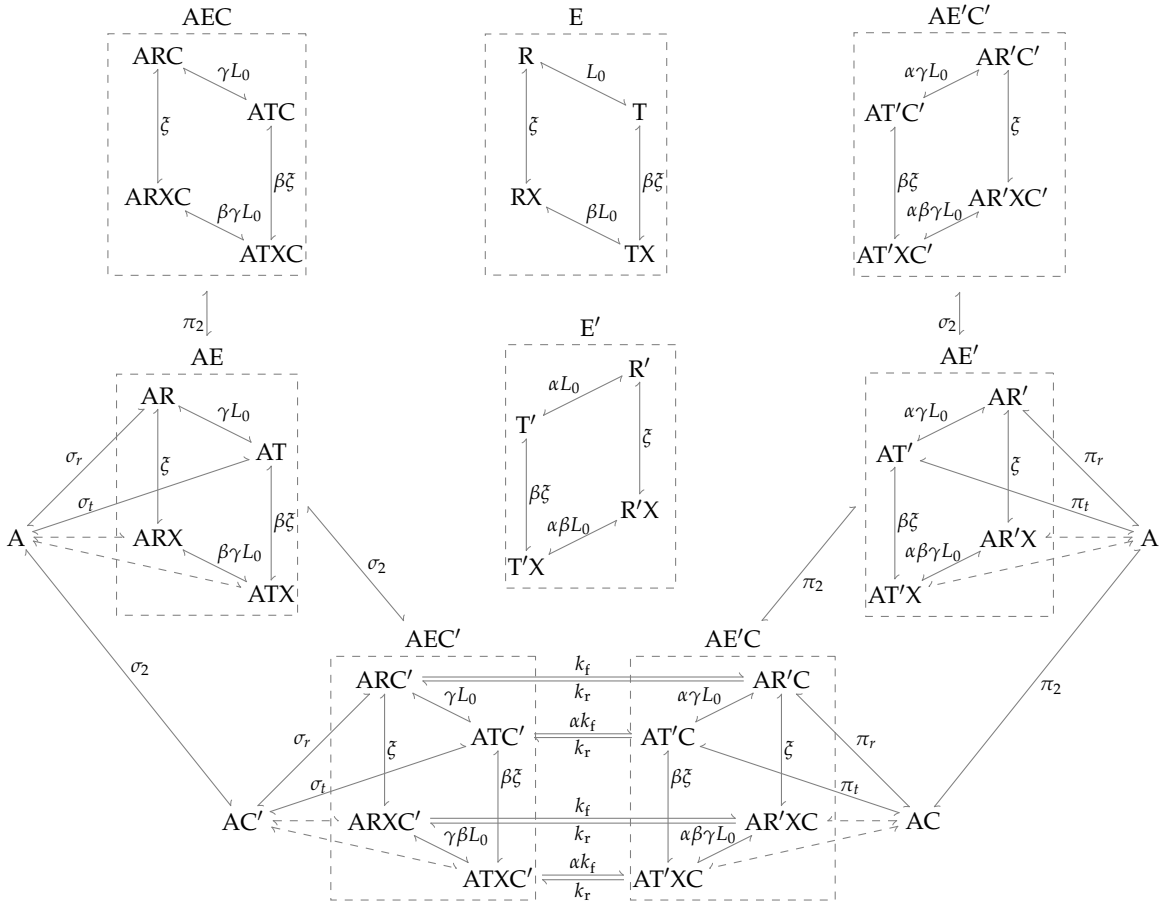

Figure 4.6: Kinetic model for the forward covalent modification ($E + C' \rightleftharpoons E' + C$) of protein E by enzyme A. Reactants are assumed to bind in random order. The formation of two dead-end complexes, AEC and AE′C′, is allowed. The forward and reverse catalytic constants are denoted by k_f and k_r; $\sigma_r = \frac{r}{K_{s_1}}$; $\sigma_t = \frac{t\gamma}{K_{s_1}}$; $\pi_r = \frac{r'}{K_{p_1}}$; $\pi_t = \frac{t'\gamma}{K_{p_1}}$; t and r are the concentrations of the T and R conformations of free protein E; $\sigma_2 = \frac{c'}{K_{s_2}}$; $\pi_2 = \frac{c}{K_{p_2}}$; and K denotes intrinsic substrate (s) and product (p) dissociation constants for the substrate/product pair (1) and for the co-substrate/co-product pair (2). The factors α, β, and γ quantify the apparent changes to L_0 as a result of covalent modification, allosteric modification, and binding to enzyme A. The four non-covalent forms in which any covalent state can exist can be represented as a single form that is able to complex with A (dashed boxes).

$$[\mathrm{AEC}'] = [\mathrm{ARC}'] + [\mathrm{ATC}'] + [\mathrm{ARXC}'] + [\mathrm{ATXC}'] \tag{4.29}$$

$$[\mathrm{AE}'\mathrm{C}] = [\mathrm{AR}'\mathrm{C}] + [\mathrm{AT}'\mathrm{C}] + [\mathrm{AR}'\mathrm{XC}] + [\mathrm{AT}'\mathrm{XC}] \tag{4.30}$$

$$[\mathrm{AE}'] = [\mathrm{AR}'] + [\mathrm{AT}'] + [\mathrm{AR}'\mathrm{X}] + [\mathrm{AT}'\mathrm{X}] \tag{4.31}$$

$$[\mathrm{AE}'\mathrm{C}'] = [\mathrm{AR}'\mathrm{C}'] + [\mathrm{AT}'\mathrm{C}'] + [\mathrm{AR}'\mathrm{XC}'] + [\mathrm{AT}'\mathrm{XC}'] \tag{4.32}$$

or in terms of intrinsic equilibria:

$$[\mathrm{A}]_{\mathrm{tot}} = [\mathrm{A}]\left(1 + \sigma_r\left[(1+\xi) + \gamma L_0(1+\beta\xi)\right] + \pi_r\left[(1+\xi) + \alpha\gamma L_0(1+\beta\xi)\right]\right)\left(1 + \sigma_2 + \pi_2'\right) \tag{4.33}$$

The total concentration of unbound protein E is given by

$$e = [\mathrm{R}] + [\mathrm{T}] + [\mathrm{RX}] + [\mathrm{TX}] \tag{4.34}$$

$$= [\mathrm{R}]\left[(1+\xi) + L_0(1+\beta\xi)\right] \tag{4.35}$$

and the total concentration of unbound protein E′ is given by

$$e' = [\mathrm{R}'] + [\mathrm{T}'] + [\mathrm{R}'\mathrm{X}] + [\mathrm{T}'\mathrm{X}] \tag{4.36}$$

$$= [\mathrm{R}']\left[(1+\xi) + \alpha L_0(1+\beta\xi)\right] \tag{4.37}$$

It thus follows that, $[\mathrm{R}] = \dfrac{e}{(1+\xi) + L_0(1+\beta\xi)}$ and $[\mathrm{R}'] = \dfrac{e'}{(1+\xi) + \alpha L_0(1+\beta\xi)}$, so that

$$\sigma_r = \frac{\sigma_1}{(1+\xi) + L_0(1+\beta\xi)} \tag{4.38}$$

and

$$\pi_r = \frac{\pi_1}{(1+\xi) + \alpha L_0(1+\beta\xi)} \tag{4.39}$$

where $\sigma_1 = \frac{e}{K_{\mathrm{s}_1}}$ and $\pi_1 = \frac{e'}{K_{\mathrm{p}_1}}$. Substituting Eqs. 4.38 and 4.39 into Eq. 4.33 gives

$$[\mathrm{A}]_{\mathrm{tot}} = [\mathrm{R}]\left(1+\sigma_1\left[\frac{(1+\xi)+\gamma L_0(1+\beta\xi)}{(1+\xi)+L_0(1+\beta\xi)}\right]+\pi_1\left[\frac{(1+\xi)+\alpha\gamma L_0(1+\beta\xi)}{(1+\xi)+\alpha L_0(1+\beta\xi)}\right]\right)(1+\sigma_2+\pi_2) \tag{4.40}$$

The rate of covalent modification is described by

$$\begin{aligned} v_{\mathrm{A}} = {} & k_{\mathrm{f}}[\mathrm{ARC}'] + k_{\mathrm{f}}[\mathrm{ARXC}'] + \alpha k_{\mathrm{f}}[\mathrm{ATC}'] + \alpha k_{\mathrm{f}}[\mathrm{ATXC}'] \\ & - \left(k_{\mathrm{r}}[\mathrm{AR}'\mathrm{C}] + k_{\mathrm{r}}[\mathrm{AR}'\mathrm{XC}] + k_{\mathrm{r}}[\mathrm{AT}'\mathrm{C}] + k_{\mathrm{r}}[\mathrm{AT}'\mathrm{XC}]\right) \end{aligned} \tag{4.41}$$

$$= \frac{[\mathrm{A}]_{\mathrm{tot}}\left[\begin{array}{l} k_{\mathrm{f}}[\mathrm{ARC}'] + k_{\mathrm{f}}[\mathrm{ARXC}'] + \alpha k_{\mathrm{f}}[\mathrm{ATC}'] + \alpha k_{\mathrm{f}}[\mathrm{ATXC}'] \\ \quad - \left(k_{\mathrm{r}}[\mathrm{AR}'\mathrm{C}] + k_{\mathrm{r}}[\mathrm{AR}'\mathrm{XC}] + k_{\mathrm{r}}[\mathrm{AT}'\mathrm{C}] + k_{\mathrm{r}}[\mathrm{AT}'\mathrm{XC}]\right) \end{array}\right]}{[\mathrm{A}]_{\mathrm{tot}}} \tag{4.42}$$

$$= \frac{V_{\mathrm{f}}\sigma_1\left[\frac{(1+\xi)+\alpha\gamma L_0(1+\beta\xi)}{(1+\xi)+L_0(1+\beta\xi)}\right]\sigma_2 - V_{\mathrm{r}}\pi_1\left[\frac{(1+\xi)+\alpha\gamma L_0(1+\beta\xi)}{(1+\xi)+\alpha L_0(1+\beta\xi)}\right]\pi_2}{\left(1+\sigma_1\left[\frac{(1+\xi)+\gamma L_0(1+\beta\xi)}{(1+\xi)+L_0(1+\beta\xi)}\right]+\pi_1\left[\frac{(1+\xi)+\alpha\gamma L_0(1+\beta\xi)}{(1+\xi)+\alpha L_0(1+\beta\xi)}\right]\right)(1+\sigma_2+\pi_2)} \tag{4.43}$$

where $V_{\mathrm{f}} = k_{\mathrm{f}}[\mathrm{A}]_{\mathrm{tot}}$ and $V_{\mathrm{r}} = k_{\mathrm{r}}[\mathrm{A}]_{\mathrm{tot}}$. Equation 4.43 can be written in the form of the classic bi-substrate random order rate equation:

$$v_{\mathrm{A}} = \frac{V_{\mathrm{f,app}}\sigma_{1,\mathrm{app}}\sigma_2 - V_{\mathrm{r}}\pi_{1,\mathrm{app}}\pi_2}{\left(1+\sigma_{1,\mathrm{app}}+\pi_{1,\mathrm{app}}\right)(1+\sigma_2+\pi_2)} \tag{4.44}$$

with $V_{\mathrm{f,app}} = V_{\mathrm{f}}\left[\frac{(1+\xi)+\alpha\gamma L_0(1+\beta\xi)}{(1+\xi)+\gamma L_0(1+\beta\xi)}\right]$, $\sigma_{1,\mathrm{app}} = \sigma_1\left[\frac{(1+\xi)+\gamma L_0(1+\beta\xi)}{(1+\xi)+L_0(1+\beta\xi)}\right]$, and $\pi_{1,\mathrm{app}} = \pi_1\left[\frac{(1+\xi)+\alpha\gamma L_0(1+\beta\xi)}{(1+\xi)+\alpha L_0(1+\beta\xi)}\right]$. Note that, since we have considered k_{r} to be unaltered by covalent modification, there are no terms that modify V_{r}.

Setting $v_{\mathrm{A}} = 0$ in Eq. 4.44, an expression for the equilibrium constant is obtained:

$$\begin{aligned}
\frac{V_{\mathrm{f,app}}\sigma_{1,\mathrm{app}}\sigma_2 - V_{\mathrm{r}}\pi_{1,\mathrm{app}}\pi_2}{\left(1+\sigma_{1,\mathrm{app}}+\pi_{1,\mathrm{app}}\right)\left(1+\sigma_2+\pi_2\right)} &= 0 \\
V_{\mathrm{f,app}}\sigma_{1,\mathrm{app}}\sigma_2 &= V_{\mathrm{r}}\pi_{1,\mathrm{app}}\pi_2 \\
\frac{c_{\mathrm{eq}}\cdot e'_{\mathrm{eq}}}{c'_{\mathrm{eq}}\cdot e_{\mathrm{eq}}} &= \frac{V_{\mathrm{f,app}}K_{\mathrm{p}_1,\mathrm{app}}K_{\mathrm{p}_2}}{V_{\mathrm{r}}K_{\mathrm{s}_1,\mathrm{app}}K_{\mathrm{s}_2}} \\
K_{\mathrm{eq,app}} &= \frac{V_{\mathrm{f,app}}K_{\mathrm{p}_1,\mathrm{app}}K_{\mathrm{p}_2}}{V_{\mathrm{r}}K_{\mathrm{s}_1,\mathrm{app}}K_{\mathrm{s}_2}} \\
K_{\mathrm{eq,app}} &= \frac{V_{\mathrm{f}}K_{\mathrm{p}_1}K_{\mathrm{p}_2}}{V_{\mathrm{r}}K_{\mathrm{s}_1}K_{\mathrm{s}_2}}\left[\frac{(1+\xi)+\alpha L_0(1+\beta\xi)}{(1+\xi)+L_0(1+\beta\xi)}\right] \\
K_{\mathrm{eq,app}} &= K_{\mathrm{eq}}\left[\frac{(1+\xi)+\alpha L_0(1+\beta\xi)}{(1+\xi)+L_0(1+\beta\xi)}\right] \qquad (4.45)
\end{aligned}$$

The expression of $K_{\mathrm{eq,app}}$ in Eq. 4.45 is, as expected, identical to the expression in Eq. 4.4. Writing Eq. 4.44 in terms of $K_{\mathrm{eq,app}}$ yields

$$v_{\mathrm{A}} = \frac{V_{\mathrm{f,app}}\sigma_{1,\mathrm{app}}\sigma_2\left(1-\dfrac{e'\cdot c/(e\cdot c')}{K_{\mathrm{eq,app}}}\right)}{\left(1+\sigma_{1,\mathrm{app}}+\pi_{1,\mathrm{app}}\right)\left(1+\sigma_2+\pi_2\right)} \qquad (4.46)$$

or, in expanded form:

$$v_{\mathrm{A}} = \frac{V_{\mathrm{f}}\sigma_1\left[\dfrac{(1+\xi)+\alpha\gamma L_0(1+\beta\xi)}{(1+\xi)+L_0(1+\beta\xi)}\right]\sigma_2\left(1-\dfrac{e'\cdot c/(e\cdot c')}{K_{\mathrm{eq}}\left[\dfrac{(1+\xi)+\alpha L_0(1+\beta\xi)}{(1+\xi)+L_0(1+\beta\xi)}\right]}\right)}{\left(1+\sigma_1\left[\dfrac{(1+\xi)+\gamma L_0(1+\beta\xi)}{(1+\xi)+L_0(1+\beta\xi)}\right]+\pi_1\left[\dfrac{(1+\xi)+\alpha\gamma L_0(1+\beta\xi)}{(1+\xi)+\alpha L_0(1+\beta\xi)}\right]\right)\left(1+\sigma_2+\pi_2\right)} \qquad (4.47)$$

If we now suppose that covalent modification does not bring about any conformational change to protein E, i.e., that $\alpha = 1$, then a factor $\left[\dfrac{(1+\xi)+\gamma L_0(1+\beta\xi)}{(1+\xi)+L_0(1+\beta\xi)}\right]$ can be cancelled from the numerator and denominator of Eq. 4.47, resulting in the rate equation for the classic bi-substrate random order mechanism. Therefore, even if enzyme A binds the T and R conformations with different affinities ($\gamma \neq 1$), no kinetic parameters are modified. On the other hand, if we suppose that enzyme A binds the T and R conformations with equal affinity ($\gamma = 1$), then $\sigma_{1,\mathrm{app}} = \sigma_1$ and $\pi_{1,\mathrm{app}} = \pi_1$, showing that only the maximal forward carrying capacity, V_{f}, undergoes apparent modification:

$$v_A = \frac{\phi V_f \sigma_1 \sigma_2 \left(1 - \frac{e' \cdot c/(e \cdot c')}{\phi K_{eq}}\right)}{(1 + \sigma_1 + \pi_1)(1 + \sigma_2 + \pi_2)} \tag{4.48}$$

where $\phi = \left[\frac{(1+\xi) + \alpha L_0(1+\beta\xi)}{(1+\xi) + L_0(1+\beta\xi)}\right]$.

Any change in the apparent Michaelis constants in response to allosteric modification of the substrate and product is solely the result of the differential affinities of the enzyme for the two substrate and product conformations and is not directly linked to the fact that covalent modification alters the value of L_0. Changes to the forward maximal rate is, however, solely the result of the fact that covalent modification alters L_0. In what follows, we will assume that enzyme A has an equal affinity for both conformations of its substrate and product, so that allosteric modification can only affect the forward maximal rate as in Eq. 4.48.

Note that modification is absent from the reverse maximal rate as a result of an assumption; equations can also be derived in which only V_r is apparently modified, or in which both V_f and V_r are modified. The important point is that catalytic modification, whether in the forward or reverse directions, is the result of covalent modification changing the value of L_0, and is independent of whether enzyme A has different affinities for the T and R conformations. Note also that the values of α and β are specific to protein E, and must have the same values in the rate equations for forward and reverse covalent modification. The value of γ, on the other hand, is specific to the enzyme that catalyses the modification; it should generally differ for forward and reverse covalent modification and even for different enzymes catalysing covalent modification in the same direction.

Reverse covalent modification

Assuming that the reverse covalent modification reaction is a uni-bi reaction with a random binding order catalysed by enzyme B, the kinetic model is given in Fig. 4.7. G is the group released upon reversing the covalent modification. Following a similar method as in the derivation of the forward reaction rate equation, the rate for the reverse covalent modification reaction can be shown to be described by

$$v_B = \frac{\phi^{-1} V_f \sigma' \left(1 - \frac{e \cdot g/e'}{\phi^{-1} K_{eq}}\right)}{\sigma + (1 + \pi_2)(1 + \pi_1)} \tag{4.49}$$

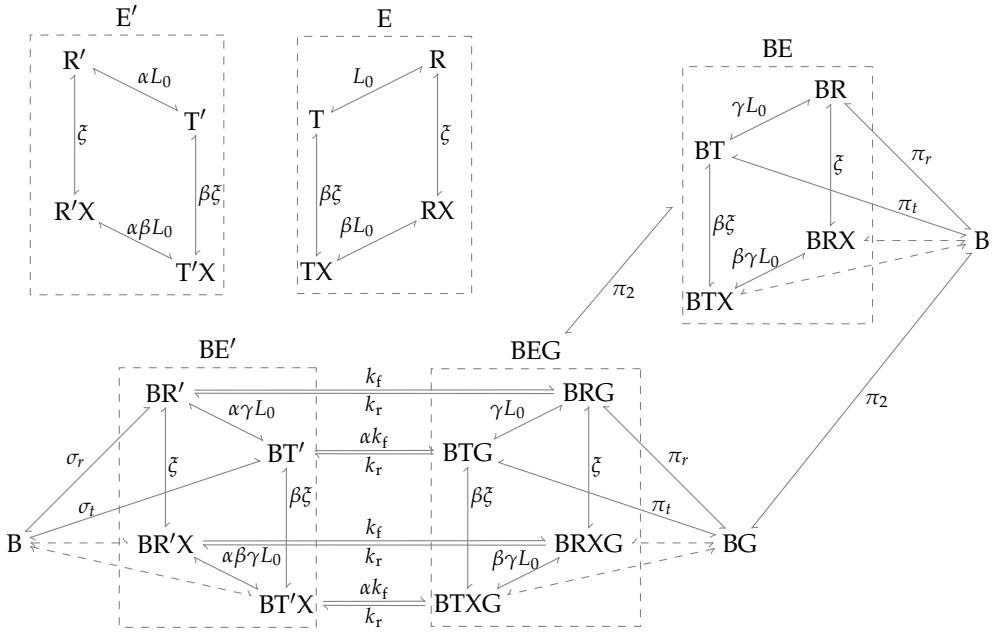

Figure 4.7: Kinetic model for the reverse covalent modification ($E' \rightleftharpoons E + G$) of protein E by enzyme A. Reactants are assumed to bind in random order. The formation of non-productive ternary complexes is ignored. The forward and reverse catalytic constants are denoted by k_f and k_r; $\sigma_r = \frac{r'}{K_s}$; $\sigma_t = \frac{t'\gamma}{K_s}$; $\pi_r = \frac{r}{K_{p_1}}$; $\pi_t = \frac{t'\gamma}{K_{p_1}}$; t and r are the concentrations of the T and R conformations of free protein E; $\pi_2 = \frac{g}{K_{p_2}}$; and K denotes intrinsic substrate (s) and product (p) dissociation constants. The factors α, β, and γ quantify the apparent changes to L_0 as a result of covalent modification, allosteric modification, and binding to enzyme A. The four non-covalent forms in which any covalent state can exist can be represented as a single form that is able to complex with A (dashed boxes).

where $V_f = k_f[B]_{tot}$, $\sigma = \dfrac{e'}{K_s}$, and $\pi_1 = \dfrac{e}{K_{p_1}}$. See legend of Fig. 4.7 for additional parameter definitions.

Generalization to n subunits

The kinetic model becomes significantly more complicated for proteins with more than one subunit. Since an additional covalent modification site is gained with each additional subunit, the number of forward and reverse covalent modification reactions equals the number of subunits. The covalent modification of a protein with n subunits therefore requires n forward and n reverse rate equations. Moreover, protein states that are the reagents in one reaction act as competitors in other reactions. Finally, the number of allosteric sites also increases and thus the number of non-covalent states.

In what follows we will derive the general forms of the n forward and reverse rate equations required to describe the covalent modification of a protein with n subunits. We will not attempt a detailed derivation, but, with the aid of simplifying principles, instead broadly describe how the rate equations were obtained. We begin with the derivation of the forward rate equations, and then also provide the equations for the reverse reactions.

As was shown in the derivation for the forward reaction with a monomeric protein, it is not necessary to explicitly consider all the non-covalent forms of a particular covalent state. For instance, binding of R, T, RX, and TX may be described collectively as the binding of E, so that the binding constant is really an apparent constant of which the value depends on the allosteric and covalent modification state of the protein.

We thus only have to consider the $n+1$ covalent modification states in which protein E can exist:

$$\mathrm{E}'^{(0)}, \mathrm{E}'^{(1)}, \ldots, \mathrm{E}'^{(n)} \tag{4.50}$$

where $'^{(i)}$ indicates the number of covalently modified subunits of the particular state. All the states in Eq. 4.50 can exist in free form and in complexes with A. The concentration of free $\mathrm{E}'^{(i)}$ is expressed by

$$e'^{(i)} = r'^{(i)} \left[(1+\xi)^n + \alpha^i L_0 (1+\beta\xi)^n \right] \tag{4.51}$$

where $r'^{(i)}$ is the concentration of state $\mathrm{E}'^{(i)}$ that is present in the R conformation, and hence

$$r'^{(i)} = \frac{e'^{(i)}}{(1+\xi)^n + \alpha^i L_0 (1+\beta\xi)^n} \tag{4.52}$$

A particular state $\mathrm{E}'^{(i)}$ can complex with A as either a substrate or a product. $\mathrm{E}'^{(i)}$ has $(n-i)$ unmodified subunits and and i modified subunits. As a substrate, the concentration of $\mathrm{E}'^{(i)}$ is then effectively multiplied by $(n-i)$, whereas in its capacity as product the concentration of $\mathrm{E}'^{(i)}$ is effectively multiplied by i. It is thus clear that $\mathrm{E}'^{(0)}$ can only function as a substrate (its concentration as product is multiplied by zero), whereas $\mathrm{E}'^{(n)}$ can only function as a product (its concentration as substrate is multiplied by zero). All other states function as both substrates and products.
The concentration of $\mathrm{E}'^{(i)}$ complexed as a substrate with A is expressed by

$$[\mathrm{AE}'^{(i)}]_\mathrm{s} = \sum_j^n [\mathrm{AR}'^{(i)}\mathrm{X}_j]_\mathrm{s} + \sum_j^n [\mathrm{AT}'^{(i)}\mathrm{X}_j]_\mathrm{s} \tag{4.53}$$

$$= [\mathrm{AR}'^{(i)}]_\mathrm{s}(1+\xi)^n + [\mathrm{AR}'^{(i)}]_\mathrm{s}\alpha^i\gamma L_0(1+\beta\xi)^n \tag{4.54}$$

$$= [\mathrm{AR}'^{(i)}]_\mathrm{s}\left[(1+\xi)^n + \alpha^i\gamma L_0(1+\beta\xi)^n\right] \tag{4.55}$$

$$= [\mathrm{A}](n-i)\frac{r'^{(i)}}{K_{\mathrm{s}_1}}\left[(1+\xi)^n + \alpha^i\gamma L_0(1+\beta\xi)^n\right] \tag{4.56}$$

$$= [\mathrm{A}](n-i)\frac{e'^{(i)}}{K_{\mathrm{s}_1}}\left[\frac{(1+\xi)^n + \alpha^i\gamma L_0(1+\beta\xi)^n}{(1+\xi)^n + \alpha^i L_0(1+\beta\xi)^n}\right] \tag{4.57}$$

$$= [\mathrm{A}](n-i)\sigma_1^{(i)}\left[\frac{(1+\xi)^n + \alpha^i\gamma L_0(1+\beta\xi)^n}{(1+\xi)^n + \alpha^i L_0(1+\beta\xi)^n}\right] \tag{4.58}$$

$$= [\mathrm{A}](n-i)\sigma_{1,\mathrm{app}}^{(i)} \tag{4.59}$$

where $\sigma_{1,\mathrm{app}}^{(i)} = \sigma_1^{(i)}\left[\frac{(1+\xi)^n + \alpha^i\gamma L_0(1+\beta\xi)^n}{(1+\xi)^n + \alpha^i L_0(1+\beta\xi)^n}\right]$. Similarly, the concentration of $\mathrm{E}'^{(i)}$ complexed as a product with A is expressed by

$$[\mathrm{AE}'^{(i)}]_\mathrm{p} = [\mathrm{A}](i)\pi_{1,\mathrm{app}}^{(i)} \tag{4.60}$$

where $\pi_{1,\mathrm{app}}^{(i)} = \pi_1^{(i)}\left[\frac{(1+\xi)^n + \alpha^i\gamma L_0(1+\beta\xi)^n}{(1+\xi)^n + \alpha^i L_0(1+\beta\xi)^n}\right]$.

In the absence of co-substrate and co-product, the total concentration of enzyme A is given by

$$[\mathrm{A}]_\mathrm{tot} = [\mathrm{A}] + \sum_{j=1}^n [\mathrm{AE}'^{(j-1)}]_\mathrm{s} + \sum_{j=1}^n [\mathrm{AE}'^{(j)}]_\mathrm{p} \tag{4.61}$$

$$= [\mathrm{A}]\left(1 + \sum_{j=1}^n (n-j+1)\sigma_{1,\mathrm{app}}'^{(j-1)} + \sum_{j=1}^n j\pi_{1,\mathrm{app}}'^{(j)}\right) \tag{4.62}$$

If the co-substrate and co-product, which bind independently of protein E, are also taken into account, Eq. 4.61 becomes

$$[\mathrm{A}]_\mathrm{tot} = [\mathrm{A}]\left(1 + \sum_{j=1}^n (n-j+1)\sigma_{1,\mathrm{app}}'^{(j-1)} + \sum_{j=1}^n j\pi_{1,\mathrm{app}}'^{(j)}\right)(1+\sigma_2+\pi_2) \tag{4.63}$$

The rate of the i^{th} reaction, $\mathrm{E}'^{(i-1)} + \mathrm{C}' \leftrightharpoons \mathrm{E}'^{(i)} + \mathrm{C}$, where $i \in [1, n]$, is described by

$$
\begin{aligned}
v_{\mathrm{A}i} &= k_{\mathrm{f}}\sum_{j}^{n}[\mathrm{AR}'^{(i-1)}\mathrm{X}_j\mathrm{C}'] + \alpha k_{\mathrm{f}}\sum_{j}^{n}[\mathrm{AT}'^{(i-1)}\mathrm{X}_j\mathrm{C}'] - k_{\mathrm{r}}[\mathrm{AE}'^{(i)}\mathrm{C}] \\
&= k_{\mathrm{f}}\sum_{j}^{n}[\mathrm{AR}'^{(i-1)}\mathrm{X}_j]_{\mathrm{s}}\sigma_2 + \alpha k_{\mathrm{f}}\sum_{j}^{n}[\mathrm{AT}'^{(i-1)}\mathrm{X}_j]_{\mathrm{s}}\sigma_2 - k_{\mathrm{r}}[\mathrm{AE}'^{(i)}]_{\mathrm{p}}\pi_2 \\
&= k_{\mathrm{f}}[\mathrm{AR}'^{(i-1)}]_{\mathrm{s}}(1+\xi)^n\sigma_2 + \alpha k_{\mathrm{f}}[\mathrm{AR}'^{(i-1)}]_{\mathrm{s}}\alpha^{i-1}\gamma L_0(1+\beta\xi)^n\sigma_2 - k_{\mathrm{r}}[\mathrm{AE}'^{(i)}]_{\mathrm{p}}\pi_2 \\
&= k_{\mathrm{f}}[\mathrm{AR}'^{(i-1)}]_{\mathrm{s}}\left[(1+\xi)^n + \alpha^i\gamma L_0(1+\beta\xi)^n\right]\sigma_2 - k_{\mathrm{r}}[\mathrm{AE}'^{(i)}]_{\mathrm{p}}\pi_2 \\
&= k_{\mathrm{f}}[\mathrm{A}](n-i+1)\frac{r'^{(i-1)}}{K_{\mathrm{s}_1}}\left[(1+\xi)^n + \alpha^i\gamma L_0(1+\beta\xi)^n\right]\sigma_2 - k_{\mathrm{r}}[\mathrm{A}](i)\pi_{1,\mathrm{app}}^{(i)}\pi_2 \\
&= k_{\mathrm{f}}[\mathrm{A}](n-i+1)\frac{e'^{(i-1)}}{K_{\mathrm{s}_1}}\left[\frac{(1+\xi)^n + \alpha^i\gamma L_0(1+\beta\xi)^n}{(1+\xi)^n + \alpha^{i-1}L_0(1+\beta\xi)^n}\right]\sigma_2 - k_{\mathrm{r}}[\mathrm{A}](i)\pi_{1,\mathrm{app}}^{(i)}\pi_2 \\
&= k_{\mathrm{f}}[\mathrm{A}](n-i+1)\sigma_1'^{(i-1)}\left[\frac{(1+\xi)^n + \alpha^i\gamma L_0(1+\beta\xi)^n}{(1+\xi)^n + \alpha^{i-1}\gamma L_0(1+\beta\xi)^n}\right]\sigma_2 - k_{\mathrm{r}}[\mathrm{A}](i)\pi_{1,\mathrm{app}}^{(i)}\pi_2 \\
&= k_{\mathrm{f}}[\mathrm{A}](n-i+1)\sigma_{1,\mathrm{app}}'^{(i-1)}\left[\frac{(1+\xi)^n + \alpha^i\gamma L_0(1+\beta\xi)^n}{(1+\xi)^n + \alpha^{i-1}L_0(1+\beta\xi)^n}\right]\sigma_2 - k_{\mathrm{r}}[\mathrm{A}](i)\pi_{1,\mathrm{app}}^{(i)}\pi_2 \\
&= k_{\mathrm{f,app}}^{(i)}[\mathrm{A}](n-i+1)\sigma_{1,\mathrm{app}}'^{(i-1)}\sigma_2 - k_{\mathrm{r}}[\mathrm{A}](i)\pi_{1,\mathrm{app}}^{(i)}\pi_2 \qquad (4.64)
\end{aligned}
$$

where $k_{\mathrm{f,app}}^{(i)} = k_{\mathrm{f}}\left[\frac{(1+\xi)^n + \alpha^i\gamma L_0(1+\beta\xi)^n}{(1+\xi)^n + \alpha^{i-1}L_0(1+\beta\xi)^n}\right]$. Multiplying the numerator and denominator of Eq. 4.64 with $[\mathrm{A}]_{\mathrm{tot}}$ yields

$$
\begin{aligned}
v_{\mathrm{A}i} &= \frac{k_{\mathrm{f,app}}^{(i)}[\mathrm{A}]_{\mathrm{tot}}[\mathrm{A}](n-i+1)\sigma_{1,\mathrm{app}}'^{(i-1)}\sigma_2 - k_{\mathrm{r}}[\mathrm{A}]_{\mathrm{tot}}[\mathrm{A}](i)\pi_{1,\mathrm{app}}^{(i)}\pi_2}{[\mathrm{A}]_{\mathrm{tot}}} \qquad (4.65) \\
&= \frac{k_{\mathrm{f,app}}^{(i)}[\mathrm{A}]_{\mathrm{tot}}(n-i+1)\sigma_{1,\mathrm{app}}'^{(i-1)}\sigma_2 - k_{\mathrm{r}}[\mathrm{A}]_{\mathrm{tot}}(i)\pi_{1,\mathrm{app}}^{(i)}\pi_2}{\left(1 + \sum_{j=1}^{n}(n-j+1)\sigma_{1,\mathrm{app}}'^{(j-1)} + \sum_{j=1}^{n} j\pi_{1,\mathrm{app}}'^{(j)}\right)(1+\sigma_2+\pi_2)} \qquad (4.66) \\
&= \frac{V_{\mathrm{f,app}}^{(i)}(n-i+1)\sigma_{1,\mathrm{app}}'^{(i-1)}\sigma_2 - V_{\mathrm{r}}(i)\pi_{1,\mathrm{app}}^{(i)}\pi_2}{\left(1 + \sum_{j=1}^{n}(n-j+1)\sigma_{1,\mathrm{app}}'^{(j-1)} + \sum_{j=1}^{n} j\pi_{1,\mathrm{app}}'^{(j)}\right)(1+\sigma_2+\pi_2)} \qquad (4.67) \\
& \qquad (4.68)
\end{aligned}
$$

which can also be written in terms of the equilibrium constant:

$$v_{Ai} = \frac{V_{f,app}^{(i)}(n-i+1)\sigma_{1,app}^{\prime(i-1)}\sigma_2\left(1-\dfrac{e^{\prime(i)}\cdot c^{\prime}/(e^{\prime(i-1)}\cdot c)}{\dfrac{n-i+1}{i}K_{eqA,app}^{(i)}}\right)}{\left(1+\sum_{j=1}^{n}(n-j+1)\sigma_{1,app}^{\prime(j-1)}+\sum_{j=1}^{n}j\pi_{1,app}^{\prime(j)}\right)(1+\sigma_2+\pi_2)} \tag{4.69}$$

where $V_{f,app}^{(i)} = k_{f,app}^{(i)}[A]_{tot}$, $V_r = k_r[A]_{tot}$, and $K_{eqA,app}^{(i)} = K_{eqA}\left[\dfrac{(1+\xi)^n+\alpha^i L_0(1+\beta\xi)^n}{(1+\xi)^n+\alpha^{i-1}L_0(1+\beta\xi)^n}\right]$. If it is assumed that enzyme A binds the T and R conformations of protein E with equal affinities, Eq. 4.69 simplifies to

$$v_{Ai} = \frac{V_f\phi_i(n-i+1)\sigma_1^{\prime(i-1)}\sigma_2\left(1-\dfrac{e^{\prime(i)}\cdot c^{\prime}/(e^{\prime(i-1)}\cdot c)}{\dfrac{n-i+1}{i}K_{eqA}\phi_i}\right)}{\left(1+\sum_{j=1}^{n}(n-j+1)\sigma_1^{\prime(j-1)}+\sum_{j=1}^{n}j\pi_1^{\prime(j)}\right)(1+\sigma_2+\pi_2)} \tag{4.70}$$

with $\phi_i = \left[\dfrac{(1+\xi)^n+\alpha^i L_0(1+\beta\xi)^n}{(1+\xi)^n+\alpha^{i-1}L_0(1+\beta\xi)^n}\right]$.

We will not provide a detailed derivation of the reverse reaction, but simply state that the rate of the i^{th} reverse reaction, $E^{\prime(i)} \rightleftharpoons E^{\prime(i-1)} + G$, where $i \in [1,n]$, is described by

$$v_{Bi} = \frac{V_{f,app}^{(i)} i\sigma_{app}^{\prime(i)}\left(1-\dfrac{e^{\prime(i-1)}\cdot g/e^{\prime(i)}}{\dfrac{i}{n-i+1}K_{eqB,app}^{(i)}}\right)}{\sum_{j=1}^{n}j\sigma_{app}^{\prime(j)}+(1+\pi_2)\left(1+\sum_{j=1}^{n}j\pi_{1,app}^{\prime(n-j)}\right)} \tag{4.71}$$

where $K_{eqB,app}^{(i)} = K_{eqB}\left[\dfrac{(1+\xi)^n+\alpha^{i-1}L_0(1+\beta\xi)^n}{(1+\xi)^n+\alpha^i L_0(1+\beta\xi)^n}\right]$. If it assumed that $\gamma = 1$, then Eq. 4.71 becomes

$$v_{Bi} = \frac{V_f\phi_i^{-1} i\sigma^{\prime(i)}\left(1-\dfrac{e^{\prime(i-1)}\cdot g/e^{\prime(i)}}{\dfrac{i}{n-i+1}K_{eqB}\phi_i^{-1}}\right)}{\sum_{j=1}^{n}j\sigma^{\prime(j)}+(1+\pi_2)\left(1+\sum_{j=1}^{n}j\pi_1^{\prime(n-j)}\right)} \tag{4.72}$$

with $\phi_i^{-1} = \left[\dfrac{(1+\xi)^n + \alpha^{i-1}L_0(1+\beta\xi)^n}{(1+\xi)^n + \alpha^i L_0(1+\beta\xi)^n}\right]$.

Let us briefly consider the expression for ϕ_i in more detail. So far we have considered E simply as a protein that exhibits MWC-type conformational change. E could, of course, also be an enzyme itself. Each covalent state of E could then potentially catalyse a particular reaction, and one could derive a rate equation for each state. The denominator for the rate equation of state $E'^{(i)}$ would be given by $(1+\xi)^n + \alpha^i L_0(1+\beta\xi)^n$. In general, the expression for ϕ_i is thus the ratio of the denominators of the rate equations for states $E'^{(i-1)}$ and $E'^{(i)}$, which allows expression of ϕ_i for proteins with arbitrary numbers of ligand binding sites:

$$\phi_i = \frac{i \text{ product state rate denominator}}{i \text{ substrate state rate denominator}} \tag{4.73}$$

4.4 Application to a minimal model of feedforward activation and covalent inhibition

In order to better illustrate the significance of the interaction between covalent and classic allosteric modification, we considered the minimal feedforward activation mechanism in which the regulated enzyme (enzyme 2) is also inhibited by covalent modification as shown in Fig. 4.8. Binding of modifier X pushes the T/R equilibrium towards the R conformation, whereas covalent modification pushes the equilibrium towards T.

The main pathway comprises two enzymatic reactions. Enzyme 1 catalyses the conversion of metabolite X to S according to classic reversible Michaelis-Menten kinetics:

$$v_1 = \frac{V_1\xi_1\left(1 - \dfrac{s/x}{K_{eq1}}\right)}{1 + \xi_1 + \sigma_1} \tag{4.74}$$

where $\xi_1 = \dfrac{x}{K_{1x}}$ and $\sigma_1 = \dfrac{s}{K_{1s}}$.

Enzyme 2, catalysing the conversion of S to P, is an irreversible MWC-type enzyme that has an allosteric binding site for X, which acts as an activator, and a covalent modification site, of which modification leads to inhibition. Although the MWC equation was initially developed to describe binding cooperativity in oligomeric enzymes, the behaviour we wish to explore here does not depend on cooperativity,

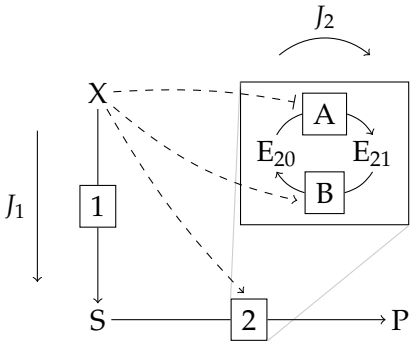

Figure 4.8: Feedforward activation mechanism in which the regulated enzyme is inhibited by covalent modification. Pathway precursor and allosteric modifier X activates enzyme 2, an MWC-type enzyme that is inhibited by covalent modification. Since covalent modification favours the T conformations and allosteric modification favours the R conformation, modifier X promotes net reversal of covalent modification by inhibiting enzyme A, which catalyses forward covalent modification, and activating enzyme B, which catalyses reverse covalent modification. The reaction network consists of two modules not connected by mass flow: the main pathway converting X to P with flux J_1, and the pathway that catalyses the interconversion between covalent states of enzyme 2 with flux J_2.

but on the transition between the T and R conformations. To simplify analysis we therefore choose $n = 1$. The rate of enzyme 2 is described by the sum of the rates catalysed by the two enzymatic states (E_{20} and E_{21}):

$$v_2 = \sum_i v_{2i} \tag{4.75}$$

$$= \sum_i \frac{c_k k_2 \cdot e_{2i} \cdot c_s \sigma_2 \cdot \alpha^i L_0 \left(\frac{1 + c_x \xi_2}{1 + \xi_2}\right) + k_2 \cdot e_{2i} \cdot \sigma_2}{(1 + c_s \sigma_2)\, \alpha^i L_0 \left(\frac{1 + c_x \xi_2}{1 + \xi_2}\right) + (1 + \sigma_2)} \tag{4.76}$$

where k_2 is the forward rate constant for the R conformation; c_k is the factor by which the rate constant for the T conformation differs from that of the R conformation so that $c_k k_2$ is the effective rate constant for the T conformation; e_{2i} is the total concentration of enzyme 2 in state i; $\sigma_2 = s/K_{r2s}$ and $c_s = K_{r2s}/K_{t2s}$; $\xi_2 = x/K_{r2x}$ and $c_x = K_{r2x}/K_{t2x}$; K_{r2s}, K_{t2s}, K_{r2x}, and K_{t2x} are the intrinsic dissociation constants with respect to S and X for the T and R conformations; α is the factor by which covalent modification alters L_0; L_0 is the allosteric constant; and $i \in [0, 1]$. We have chosen $c_x < 1$ so that modifier X prefers to bind to the R conformation, resulting in activation by virtue of $c_s < 1$ and/or $c_k < 1$. Covalent modification was chosen as inhibitory ($\alpha > 1$).

The rate equations for the forward modification reaction, catalysing the reaction $E_{20} + C' \leftrightharpoons E_{21} + C$, and for the reverse modification reaction, catalysing the reaction $E_{21} \leftrightharpoons E_{20} + G$, are of the same form as Eqs. 4.70 and 4.72, but with $n = 1$:

$$v_A = \frac{\phi \cdot k_A[A]_{tot} \cdot \sigma_{A1} \cdot \sigma_{A2} \left(1 - \frac{e_{21}c/(e_{20}c')}{\phi K_{eqA}}\right)}{(1 + \sigma_{A1} + \pi_{A1})(1 + \sigma_{A2} + \pi_{A2})} \tag{4.77}$$

and

$$v_B = \frac{\phi^{-1} k_B[B]_{tot} \cdot \sigma_B \left(1 - \frac{e_{20}g/e_{21}}{\phi^{-1}K_{eqB}}\right)}{\sigma_B + (1 + \pi_{B1})(1 + \pi_{B2})} \tag{4.78}$$

where k_A and k_B are the forward rate constants for enzymes A and B; $\sigma_{A1} = e_{20}/K_{As1}$; $\sigma_{A2} = c'/K_{As2}$; $\pi_{A1} = e_{21}/K_{Ap1}$; $\pi_{A2} = c/K_{Ap2}$; $\sigma_B = e_{21}/K_{Bs}$; $\pi_{B1} = e_{20}/K_{Bp1}$; and $\pi_{B2} = g/K_{Bp2}$. The expression for ϕ is given by the denominator of v_{21} divided by the denominator of v_{20}:

$$\phi = \frac{(1 + c_s\sigma_2)\,\alpha L_0 \left(\frac{1 + c_x\xi_2}{1 + \xi_2}\right) + (1 + \sigma_2)}{(1 + c_s\sigma_2)\,L_0 \left(\frac{1 + c_x\xi_2}{1 + \xi_2}\right) + (1 + \sigma_2)} \tag{4.79}$$

Note therefore, that all ligands of enzyme 2 are effectively also ligands of enzymes A and B. We will consider the conditions that facilitate effective regulation of the flux of this system by feedforward and covalent activation using metabolic control analysis (MCA).

Metabolic control analysis

MCA [10, 11] is a theoretical framework that quantitatively relates the responses of steady-state variables such as fluxes or variable metabolite concentrations to a perturbation in a system parameter such as the concentration of an enzyme, external metabolite, or effector. Any such systemic response is a combination of local effects (changes in the rates of individual enzymatic steps that are directly affected by the perturbation) and systemic effects (changes in steady-state fluxes or metabolite concentrations caused by these rate changes in individual enzymatic steps). Local effects are quantified by elasticity coefficients and systemic effects by control coefficients.

The elasticity coefficient is defined as

$$\varepsilon_{s_j}^{v_i} = \left.\frac{\partial \ln v_i}{\partial \ln s_j}\right|_{s_k, s_l, \ldots, p_q, p_r, \ldots} \tag{4.80}$$

where v_i is the rate of any step i in the system, s_j is any particular variable species or parameter that directly affects the step, $s_k, s_l, \ldots$ are the other variable species that directly affect the step, and $p_q, p_r, \ldots$ are the parameters of the step. Note that all variables are set to their steady-state values. Although elasticities are defined in terms of infinitesimal changes, they may be interpreted operationally as the percentage change in the rate of a step resulting from a 1% change in the value of s_j. Alternatively, the elasticity coefficient is the slope of the graph of $\ln v_i$ plotted against $\ln s_j$ at the steady-state value of s_j.

The control coefficient is defined as

$$C_{v_i}^{y} = \left.\frac{\partial \ln y}{\partial \ln v_i}\right|_{v_j, v_k, \ldots} \tag{4.81}$$

where v_i is defined as before, $v_j, v_k, \ldots$ are the rates of all other steps in the system, and y is either a flux, in which case $C_{v_i}^{y}$ is a *flux-control coefficient*, or a steady-state metabolite concentration, in which case it is a *concentration-control coefficient*. The control coefficient therefore quantifies the percentage change in a system variable (flux or steady-state concentration) that results from a 1% change in the rate of step i.

The systemic response of a flux or steady-state metabolite concentration y to a perturbation in any parameter p_j is described by the response coefficient

$$R_{p_j}^{y} = \left.\frac{\partial \ln y}{\partial \ln p_j}\right|_{p_k, p_l, \ldots} \tag{4.82}$$

where $p_k, p_l, \ldots$ are all other system parameters, and the other symbols are defined as before. The central statement of MCA is that the response coefficient of a parameter p_j that affects a single step i can be partitioned as the product of the control coefficient, quantifying the systemic effect, and the elasticity coefficient, quantifying the local effect:

$$R_{p_j}^{y} = C_{v_i}^{y} \varepsilon_{p_j}^{v_i} \tag{4.83}$$

More generally, if multiple steps are affected by a change in p_j, the response coefficient is given by:

$$R^y_{p_j} = \sum_i C^y_{v_i} \varepsilon^{v_i}_{p_j} \tag{4.84}$$

$$= \sum_i {}^iR^y_{p_j} \tag{4.85}$$

where i is an element of the set of all enzymatic steps that are directly affected by a change in p_j, and ${}^iR^y_{p_j} = C^y_{v_i}\varepsilon^{v_i}_{p_j}$ is the *partial* response coefficient, quantifying the response of y to a change in p_j through step i.

Modular control analysis

If a reaction network comprises two or more modules that are not connected by mass flow, a distinction can be made between integral or global control coefficients, describing the global control properties of the modular system, and intramodule control coefficients, describing the control properties of a given module considered in isolation [162]. The global control coefficient has the same definition (and is in fact the same measure) as the control coefficient in Eq. 4.81, but a different symbol, G, is used to distinguish it from the intramodule control coefficient:

$$G^y_{v_i} = \left.\frac{\partial \ln y}{\partial \ln v_i}\right|_{v_j, v_k, \ldots} \tag{4.86}$$

In contrast, the intramodule control coefficient is defined as

$$C^y_{v_i} = \left.\frac{\partial \ln y}{\partial \ln v_i}\right|_{v_j, v_k, \ldots, y_q, y_r, \ldots} \tag{4.87}$$

where $y_q, y_r, \ldots$ are the variables of all other modules. The integral and intramodule control coefficients have the same operational definition, i.e., it is the percentage change in a steady-state variable that results from a one percent change in the rate v_i, and differ only in scope.

Control analysis of the modular system in Fig. 4.8

The reaction network in Fig. 4.8 comprises two separate modules that are not connected by mass flow, namely, the main pathway from X through P (flux J_1), and the interconversion between states of enzyme 2 (flux J_2). All the control coefficients of this system, and thus also the response coefficients, can be expressed in terms of elasticities. In the present analysis, we are particularly interested in the flux-control

coefficients quantifying the control of flux J_1 with respect to the enzymes in the main and cyclical pathways (see Appendix B.1 for the solution of all control coefficients). For the sake of clarity and brevity, we express the integral control coefficients in terms of intramodule control coefficients where possible:

$$G^{J_1}_{v_1} = 1 - G^{J_1}_{v_2} \tag{4.88}$$

$$G^{J_1}_{v_2} = \frac{C^{J_1}_{v_2}}{1 + C^{s}_{v_2} C^{e_{20}}_{v_A} {}^{*}\varepsilon^{v_2}_{e_{20}} \left(\varepsilon^{v_B}_{s} - \varepsilon^{v_A}_{s}\right)} \tag{4.89}$$

$$G^{J_1}_{v_A} = G^{J_1}_{v_2} {}^{*}\varepsilon^{v_2}_{e_{20}} C^{e_{20}}_{v_A} \tag{4.90}$$

$$G^{J_1}_{v_B} = -G^{J_1}_{v_A} \tag{4.91}$$

where

$$C^{e_{20}}_{v_A} = \left[\left(\varepsilon^{v_B}_{e_{20}} - \varepsilon^{v_B}_{e_{21}} \cdot \frac{e_{20}}{e_{21}}\right) - \left(\varepsilon^{v_A}_{e_{20}} - \varepsilon^{v_A}_{e_{21}} \cdot \frac{e_{20}}{e_{21}}\right)\right]^{-1} \tag{4.92}$$

$$C^{J_1}_{v_1} = \frac{\varepsilon^{v_2}_{s}}{\varepsilon^{v_2}_{s} - \varepsilon^{v_1}_{s}} \tag{4.93}$$

$$C^{J_1}_{v_2} = \frac{-\varepsilon^{v_1}_{s}}{\varepsilon^{v_2}_{s} - \varepsilon^{v_1}_{s}} \tag{4.94}$$

$$C^{s}_{v_2} = \frac{-1}{\varepsilon^{v_2}_{s} - \varepsilon^{v_1}_{s}} \tag{4.95}$$

$${}^{*}\varepsilon^{v_2}_{e_{20}} = \varepsilon^{v_2}_{e_{20}} - \varepsilon^{v_2}_{e_{21}} \cdot \frac{e_{20}}{e_{21}} \tag{4.96}$$

While it may seem unusual that $\varepsilon^{v_A}_{s}$ and $\varepsilon^{v_B}_{s}$ are potentially non-zero, it should be remembered that all ligands of enzyme 2 are also indirect, but real, modifiers of enzymes A and B (see Eqs. 4.77–4.79).

Conditions for effective feedforward and covalent activation

The conditions that will permit effective activation of flux J_1 in response to an increase in concentration x are those that maximize the response coefficient $R^{J_1}_{x}$. $R^{J_1}_{x}$ can be expressed as the sum of partial response coefficients, each of which quantifies

the response of J_1 to X through one of four routes, namely, as substrate of enzyme 1, as feedforward activator of enzyme 2, as indirect inhibitor of A, and as indirect activator of B:

$$R_x^{J_1} = {}^{1}R_x^{J_1} + {}^{2}R_x^{J_1} + {}^{\mathrm{A}}R_x^{J_1} + {}^{\mathrm{B}}R_x^{J_1} \tag{4.97}$$

A partial response coefficient ${}^{i}R_p^{J_j}$ is maximized when $G_i^{J_j}$ and ε_p^i are maximized (in absolute terms). If J_j is the flux of a linear pathway, the maximal value that $G_i^{J_j}$ can achieve is unity when enzyme i is in the same module as the flux J_j or any other value, including negative values, when enzyme i is not in the same module as flux J_j.

The partial response coefficient with respect to X through enzyme 1 is given by

$$\begin{aligned} {}^{1}R_x^{J_1} &= G_{v_1}^{J_1}\varepsilon_x^{v_1} && (4.98)\\ &= \left(1 - G_{v_2}^{J_1}\right)\cdot\varepsilon_x^{v_1} && (4.99) \end{aligned}$$

and the partial response coefficient with respect to X through enzyme 2 is given by

$$\begin{aligned} {}^{2}R_x^{J_1} &= G_{v_2}^{J_1}\varepsilon_x^{v_2} && (4.100)\\ &= \frac{C_{v_2}^{J_1}}{1 + C_{v_2}^{s}C_{v_{\mathrm{A}}}^{e_{20}*}\varepsilon_{e_{20}}^{v_2}\left(\varepsilon_s^{v_{\mathrm{B}}} - \varepsilon_s^{v_{\mathrm{A}}}\right)}\cdot\varepsilon_x^{v_2} && (4.101) \end{aligned}$$

It is clear that $G_{v_1}^{J_1}$ can only be maximized at the cost of minimizing $G_{v_2}^{J_1}$, which would however also disregard any response elicited by the allosteric regulation of enzyme 2. From a regulatory perspective, this represents an uninteresting scenario. Besides, as we shall see, ${}^{1}R_x^{J_1}$ is not necessarily maximized when $G_{v_1}^{J_1}$ is maximized. We are therefore rather interested in the conditions that will maximize $G_{v_2}^{J_1}$ and $\varepsilon_x^{v_2}$. From Eq. 4.89 it is clear that the maximum value of $G_{v_2}^{J_1}$ tends to $C_{v_2}^{J_1}$ when the term $C_{v_2}^{s}C_{v_{\mathrm{A}}}^{e_{20}*}\varepsilon_{e_{20}}^{v_2}\left(\varepsilon_s^{v_{\mathrm{B}}} - \varepsilon_s^{v_{\mathrm{A}}}\right)$, which will always have a positive value, is minimized. This condition will also cause $G_{v_1}^{J_1}$ to approach its minimum, namely, $C_{v_1}^{J_1}$. Let us now, for a moment, suppose that $C_{v_2}^{s}C_{v_{\mathrm{A}}}^{e_{20}*}\varepsilon_{e_{20}}^{v_2}\left(\varepsilon_s^{v_{\mathrm{B}}} - \varepsilon_s^{v_{\mathrm{A}}}\right) = 0$, so that $G_{v_2}^{J_1} = C_{v_2}^{J_1}$ and $G_{v_1}^{J_1} = C_{v_1}^{J_1}$. It follows that $G_{v_2}^{J_1} \to 1$ and $G_{v_1}^{J_1} \to 0$ when $\left|\varepsilon_s^{v_1}\right| \gg \left|\varepsilon_s^{v_2}\right|$. This condition is achieved if enzyme 1 is near equilibrium ($\varepsilon_s^{v_1} \to -\infty$) or if enzyme 2 is saturated with its substrate ($\varepsilon_s^{v_2} = 0$). These are of course the extreme cases and combinations of both strategies will also suffice. Note, however, that when enzyme 1 is near equilibrium,

$|\varepsilon_s^{v_1}| \simeq |\varepsilon_x^{v_1}|$, so that, despite the vanishingly small value of $C_{v_1}^{J_1}$, ${}^1R_x^{J_1}$ will be approximately equal to $\varepsilon_s^{v_2}$.

As discussed by Hofmeyr *et al.* [16], saturation of enzyme 2 with its substrate has important implications for the efficiency of the feedforward loop. In particular, saturation with S will not only cause $\varepsilon_s^{v_2} \to 0$, which is desirable, but will also affect $\varepsilon_x^{v_2}$. Consider $\varepsilon_x^{v_2}$ at saturating s (see Eq. B.39 in Appendix B.2):

$$\lim_{\sigma\to\infty} \varepsilon_x^{v_2} = \frac{c_k c_s \alpha^i L_0 c_x \xi + \xi}{c_k c_s \alpha^i L_0 (1 + c_x \xi) + (1 + \xi)} - \frac{c_s \alpha^i L_0 c_x \xi + \xi}{c_s \alpha^i L_0 (1 + c_x \xi) + (1 + \xi)} \tag{4.102}$$

It is clear that if X has no catalytic effect or, put differently, that if the T and R conformations exhibit the same maximal rate (c_k=1) then $\varepsilon_x^{v_2} = 0$. However, a difference in the catalytic rates of the T and R conformation is not sufficient under all conditions to ensure a non-zero value for $\varepsilon_x^{v_2}$. In particular, if the binding affinities of the T and R conformations for S differ sufficiently $\left(\text{i.e. if } c_s \ll \frac{1}{\alpha^i L_0}\right)$, then the terms in Eq. 4.102 that contain c_s become negligible so that $\varepsilon_x^{v_2}$ again becomes zero. Our results therefore agree with those of Hofmeyr *et al.* [16], but with the added qualification that if the enzyme in question (enzyme 2 in our case) is an MWC-type enzyme saturated with substrate, then specific activation by X is not only insufficient to maximize $\varepsilon_x^{v_2}$, but will in fact let this value, and thus ${}^2R_x^{J_1}$, approach zero when it is sufficiently strong $\left(\text{i.e. if } c_s \ll \frac{1}{\alpha^i L_0}\right)$. If enzyme 2 were oligomeric, $\varepsilon_x^{v_2}$ would increase with the number of subunits, but even then a value for $\varepsilon_x^{v_2}$ above 4 would be rarely encountered.

The term $C_{v_2}^s C_{v_A}^{e_{20}} {}^*\varepsilon_{e_{20}}^{v_2} \left(\varepsilon_s^{v_B} - \varepsilon_s^{v_A}\right)$ is minimized when either or all of its factors are minimized. The value of $\left|C_{v_2}^s\right|$ is minimized by the same conditions that maximise $C_2^{J_1}$. As is evident from Eq. 4.100 it is *not* desirable to minimize either ${}^*\varepsilon_{e_{20}}^{v_2}$ or $\left|C_{v_A}^{e_{20}}\right|$, which will also minimize the absolute values of $G_{v_A}^{J_1}$ and $G_{v_B}^{J_1}$. Finally, the term $\left(\varepsilon_s^{v_B} - \varepsilon_s^{v_A}\right)$ is minimized when S saturates enzyme 2, or if S binds equally well to the T and R conformation of enzyme 2 (Appendix B.2), in which case no specific activation of enzyme 2 by X is observed. Note that in order to ensure a maximal value for $G_{v_2}^{J_1}$ if $c_s \neq 1$, then $\left|C_{v_2}^s\right|$ must have a sufficiently small value to compensate for the large value of $\left|C_{v_A}^{e_{20}} {}^*\varepsilon_{e_{20}}^{v_2}\right|$ that is necessary to maximize the response to X through covalent regulation.

The expression for ${}^A R_x^{J_1}$ is given by

$$
\begin{aligned}
{}^{A}R_x^{J_1} &= G_{v_A}^{J_1}\varepsilon_x^{v_A} \\
&= G_{v_2}^{J_1}\cdot C_{v_A}^{e_{20}}\cdot {}^{*}\varepsilon_{e_{20}}^{v_2}\cdot \varepsilon_x^{v_A}
\end{aligned}
\tag{4.103}
$$

We must therefore consider which conditions maximize the absolute values of the four factors in Eq. 4.103. We have already considered $G_{v_2}^{J_1}$ and saw that its maximum value, $C_{v_2}^{J_1}$, is increased when $\left|\varepsilon_s^{v_1}\right| \gg \left|\varepsilon_s^{v_2}\right|$. However, if this condition is met by virtue of saturating enzyme 2 with its substrate, then the effect on ${}^{*}\varepsilon_{e_{20}}^{v_2}$ and $\varepsilon_x^{v_A}$ must also be considered. At saturating S and if $c_s \ll \frac{1}{\alpha^i L_0}$ the value of ${}^{*}\varepsilon_{e_{20}}^{v_2}$ approaches zero (see Appendix B.2). This stems from the fact that all states of enzyme 2 exhibit identical kinetics when s is saturating; interconversion between these states are then of no consequence to the activity of enzyme 2. Similarly, if $c_s \ll \frac{1}{\alpha^i L_0}$ then $\varepsilon_x^{v_A} = 0$ (see Appendix B.2). This is explained by considering that, given these conditions, both forms of enzyme 2 are predominantly in the R conformation, so that an increase in X results in no significant further transition to the R form.

$\left|C_{v_A}^{e_{20}}\right|$ is maximized when its denominator $\left(\varepsilon_{e_{20}}^{v_B} - \varepsilon_{e_{21}}^{v_B}\cdot\frac{e_{20}}{e_{21}}\right) - \left(\varepsilon_{e_{20}}^{v_A} - \varepsilon_{e_{21}}^{v_A}\cdot\frac{e_{20}}{e_{21}}\right)$ is minimized in absolute terms. If the reactions catalysed by A and B are considered insensitive to their products and operate far from equilibrium, then $\varepsilon_{e_{20}}^{v_B} = 0$ and $\varepsilon_{e_{21}}^{v_A} = 0$, so that $C_{v_A}^{e_{20}}$ simplifies to (see Appendix B.2):

$$
C_{v_A}^{e_{20}} = \left[-\varepsilon_{e_{21}}^{v_B}\cdot\frac{e_{20}}{e_{21}} - \varepsilon_{e_{20}}^{v_A}\right]^{-1} \tag{4.104}
$$

$$
= \left[\left(\frac{\sigma_{B1}}{1+\sigma_{B1}} - 1\right)\cdot\frac{e_{20}}{e_{21}} + \left(\frac{\sigma_{A1}}{1+\sigma_{A1}} - 1\right)\right]^{-1} \tag{4.105}
$$

Thus we see that if both A and B are saturated with their respective substrates, i.e., if $\sigma_{B1} \to \infty$ and $\sigma_{B1} \to \infty$, then $C_{v_A}^{e_{20}} \to -\infty$. This condition is equivalent to what has been termed *zero-order ultrasensitivity* by Goldbeter & Koshland [163] and formulated in terms of MCA by Small & Fell [164]. Complete saturation is of course not necessary and will in reality not necessarily be observed because of the presence of competitive inhibitors such as the products of A and B.

The value of ${}^{A}R_x^{J_1}$ is therefore maximized if S saturates enzyme 2, but binds equally well to both the T and R conformations ($c_s = 1$). Alternatively, enzyme 1 should be near equilibrium. Interestingly, as long as X binds with different affinities to the T and R conformations, the absence of specific activation ($c_s = 1$) and catalytic

activation ($c_k = 1$) of enzyme 2 by X, will not result in a zero value for $\varepsilon_x^{v_A}$. This results from the fact that only a conformational change ($c_x \neq 1$) is required for enzyme A to be sensitive to X. For this sensitivity to be relayed to flux J_1, however, some form of activation is required, preferably catalytic activation. In addition, both A and B should exhibit reasonable substrate occupation. Since $G_{v_A}^{J_1} = -G_{v_B}^{J_1}$ and $\varepsilon_x^{v_A} = -\varepsilon_x^{v_B}$ the same conditions that maximize ${}^{A}R_x^{J_1}$ will also maximize ${}^{B}R_x^{J_1} = G_{v_B}^{J_1}\varepsilon_x^{v_B}$.

In summary then, the conditions that maximize $R_x^{J_1}$ are those that

- satisfy $\left|\varepsilon_s^{v_2}\right| \ll \left|\varepsilon_s^{v_1}\right|$
  - i.e., enzyme 1 should be near equilibrium or enzyme 2 should be saturated with substrate, with the condition that if the latter is the case, then X should be a catalytic rather than specific activator of enzyme 2
- minimize $\left(\varepsilon_s^{v_B} - \varepsilon_s^{v_A}\right)$
  - i.e., enzyme 2 should be saturated with substrate, or X must not be a specific activator of enzyme 2
- maximize ${}^{*}\varepsilon_{e_{20}}^{v_2}$
  - i.e., the different forms of enzyme 2 must not have identical kinetics. This condition is automatically met by our initial assumption that covalent modification alters L_0 by a factor of α. However, as we have seen, if X is a specific activator of enzyme 2 and if enzyme 2 is saturated with substrate, this condition is no longer necessarily met.
- maximize $\left|C_{v_A}^{e_{20}}\right|$
  - i.e., enzymes A and B must exhibit near zero-order sensitivity towards its substrate and operate far from equilibrium

We have of course chosen X and S to be catalytic effectors of enzymes A and B. This choice was, however, mandated by the fact that we chose $\alpha \neq 1$. We excluded any specific effects in the interest of simplicity and because they are not mandated by choosing $\alpha \neq 1$. We don't expect the conditions identified here to change significantly if these effects were included. We also expect similar conditions to maximize $R_x^{J_1}$ if enzyme 2 were an oligomeric enzyme.

Feedforward activation and covalent modification contribute synergistically to the flux response with respect to X

In the previous section we have stated that the contribution of X through each of four mechanisms (as initial substrate, feedforward activator, inhibitor of A, and activator of B) towards the flux is quantified by the partial response coefficients as in Eq. 4.97. If then, for instance, ${}^{2}R_x^{J_1}$ is larger than ${}^{A}R_x^{J_1}$, it can be said that X increases the flux more through the feedforward loop than by inhibiting A. Although this is certainly the case, we will here show that the contribution through the feedforward loop or the contribution through inhibition of enzymes A or B, if quantified in isolation, is an underestimation of the true contribution that is observed when both mechanisms are present. Consider the following four variations on the system in Fig. 4.8:

- FF+COV: both the feedforward loop and covalent modification are present
- FF: only the feedforward loop is present
- COV: only covalent modification is present
- NONE: neither the feedback loop nor covalent modification is present

In FF covalent modification is removed, or more precisely, its effect on the kinetics of enzyme 2 is abolished, by setting $\alpha = 1$. This has the side-effect that $\varepsilon_x^{v_A} = 0$ and $\varepsilon_x^{v_B} = 0$, so that Eq. 4.97 simplifies to

$$\begin{aligned} R_x^{J_1} &= {}^{1}R_x^{J_1} + {}^{2}R_x^{J_1} \\ &= C_{v_1}^{J_1}\varepsilon_x^{v_1} + C_{v_2}^{J_1}\varepsilon_x^{v_2} \end{aligned} \tag{4.106}$$

Note however that $\varepsilon_x^{v_2}$ is also affected since all the states of enzyme 2 now have identical kinetics, i.e., that of the unmodified state:

$$\varepsilon_x^{v_2} = \sum_i \frac{v_{2i}}{v_2}\varepsilon_x^{v_{2i}} \tag{4.107}$$

$$= \varepsilon_x^{v_{20}} \sum_i \frac{v_{2i}}{v_2} \quad \text{(since } \alpha^i = 1 \text{ for all } i\text{)} \tag{4.108}$$

$$= \varepsilon_x^{v_{20}} \tag{4.109}$$

Since covalent modification was chosen as inhibitory and allosteric modification was chosen as activatory, the value of $\varepsilon_x^{v_2}$ decreases when covalent modification is abolished.

Alternatively, in COV the feedforward loop is removed by letting K_{r2x} and K_{t2x} approach infinity or by setting $K_{\mathrm{r2x}} = K_{\mathrm{t2x}}$. This has the result that $\varepsilon_x^{v_2} = 0$, but importantly $\varepsilon_x^{v_{\mathrm{A}}}$ and $\varepsilon_x^{v_{\mathrm{B}}}$ again also become zero. Equation 4.97 then simplifies to

$$\begin{aligned} R_x^{J_1} &= {}^{1}R_x^{J_1} \\ &= C_{v_1}^{J_1}\varepsilon_x^{v_1} \end{aligned} \tag{4.110}$$

Finally, in NONE both the feedforward loop and covalent modification are removed, yielding the same expression for $R_x^{J_1}$ as COV (Eq. 4.110).

In summary, the presence of covalent modification not only increases $R_x^{J_1}$ by increasing ${}^{2}R_x^{J_1}$ (through $\varepsilon_x^{v_2}$), but also results in two additional terms (${}^{\mathrm{A}}R_x^{J_1}$ and ${}^{\mathrm{B}}R_x^{J_1}$) in the expression for $R_x^{J_1}$, leading to a further increase in flux response. However, the presence of the feedforward loop is a prerequisite for these two additional terms to be non-zero. We therefore see that the contributions of the feedforward loop and covalent modification towards the flux response with respect to X cannot be quantified in isolation; the contribution of both these mechanisms depends on whether the other is present. This finding is of consequence if one wishes to determine the relative importance of allosteric and covalent modification. By abolishing one of these mechanisms by, for instance, mutation, the response through the other is likely to be underestimated (Fig. 4.9).

4.5 Discussion

The results of the previous two chapters, namely that the kinetics of GS can be described by an MWC-type model in which both allosteric and covalent regulation elicit their effects by altering the apparent equilibrium between an inactive T and active R conformation, led us to develop a formal treatment of the interaction between allosteric and covalent regulation. Although the MWC model is the standard textbook model of GS regulation, we believe its implications have not been fully appreciated, nor has it, to our knowledge, been employed in an actual treatment of GS kinetics. In this chapter we set out to formalize the implications of interaction between allosteric and covalent modification in a manner independent of whether

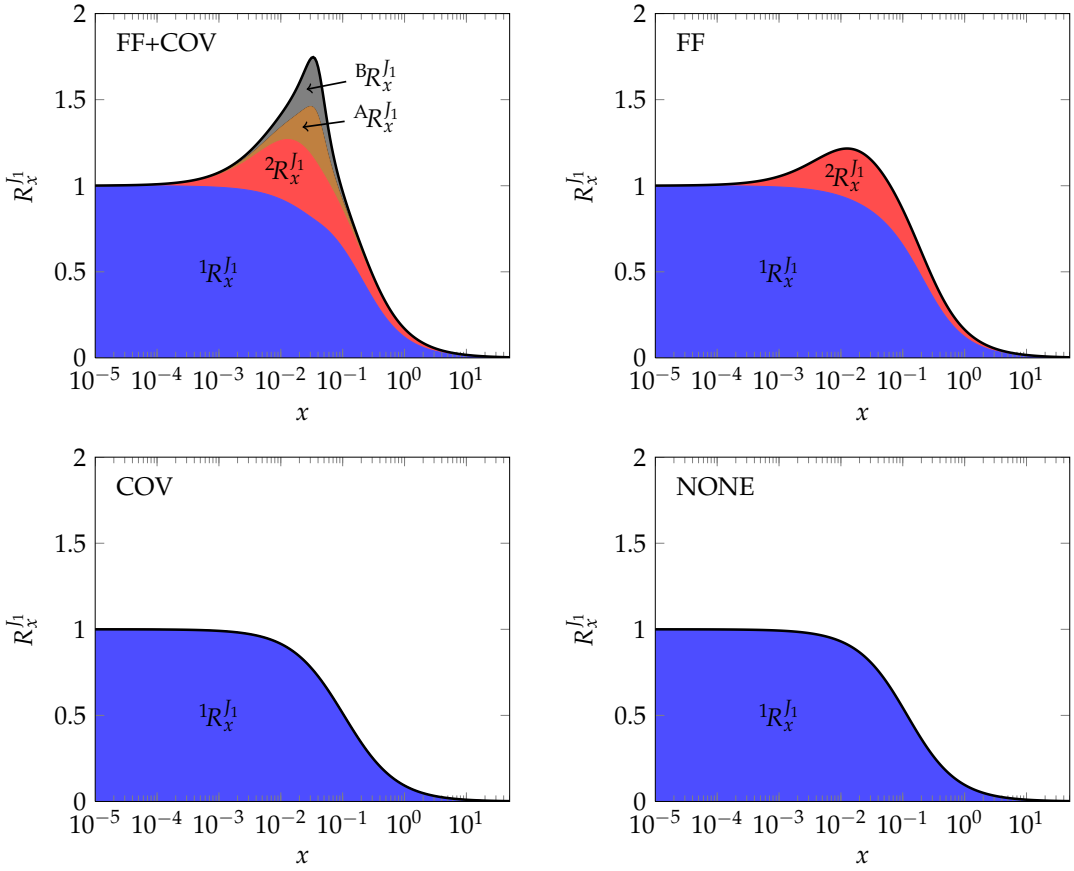

Figure 4.9: The flux response with respect to X as a function of x for the feedforward system in Fig. 4.8. The contribution of partial flux responses are stacked to add up to the overall flux response coefficient (thick black line). In FF+COV the feedforward loop and covalent modification are present. In FF or COV only the feedforward loop or covalent modification is present. In NONE neither the feedforward loop nor covalent modification is present. Covalent modification alone is not sufficient to elicit a higher flux response than what is seen when neither mechanism is present. Covalent modification does however increase $^{2}R_x^{J_1}$ (compare FF+COV and FF). The feedforward loop is necessary for any additional flux response resulting from the inhibition of A and the activation of B by X. Parameters of the system were chosen by taking the conditions that will maximize $R_x^{J_1}$, as discussed in the text, into account. Suboptimal parameters were chosen for purposes of illustration: $V_1 = 50$, $K_{1x} = 1$, $K_{1s} = 10$, $K_{eq1} = 10$, $c_k = 0$, $k_2 = 10$, $c_s = 1$, $K_{r2s} = 1$, $c_x = 0.1$, $K_{r2x} = 0.01$, $\alpha = 6$, $L_0 = 10$, $K_{eq2} = 10$, $k_F = 2$, $[A]_{tot} = 5$, $K_{As1} = 0.05$, $K_{As2} = 0.1$, $K_{Ap1} = 10$, $K_{Ap2} = 10$, $K_{eqF} = 10000$, $k_B = 2$, $[B]_{tot} = 100$, $K_{Bs1} = 0.05$, $K_{Bp1} = 10$, $K_{Bp2} = 10$, $K_{eqB} = 10000$, $x = 10$, $s = 0$, $p = 0$, $e_{20} = 1$, $e_{21} = 0$, $c' = 1$, $c = 0$, $g = 0$.

the modification results in activation or inhibition and independent of the type of covalent modification, e.g., phosphorylation. We showed that when covalent and allosteric modification act with opposing effects on an enzyme, covalent modification will inhibit the binding of allosteric modifiers, and conversely an allosteric modifier will inhibit covalent modification of the enzyme. In contrast, covalent modification will, within a certain range, enhance the binding cooperativity of an allosteric enzyme; whereas an allosteric modifier will enhance cooperativity with respect to covalent modification.

The effect of covalent modification on allosteric modification is, to a certain extent, already contained in the classic MWC equation, where it can be considered as an explicit change to the value of L_0. The effect of allosteric modification on covalent modification (over and above the apparent change to L_0), on the other hand, must be described in additional rate equations, i.e., the rate equations of forward and reverse covalent modification. We derived expressions for the modification terms that must be included in such rate equations. Two findings in this regard are of note. First, if covalent modification alters L_0, then the forward or reverse rate constants of the enzyme that catalyses the covalent modification must be multiplied by a modification term. Second, if the enzyme that catalyses the covalent modification has different affinities for the two conformations of its substrate, then its Michaelis constants must also be multiplied by modification terms. If, on the other hand, covalent modification does not alter L_0, then all modification terms, including those that modify the Michaelis constants, disappear. It has been shown in a number of cases that the ligands of an enzyme affect the $V_{\max}$ and/or Michaelis constants of kinases or phosphatases that phosphorylate and dephosphorylate the enzyme (see for instance [146, 165–168]), but to our knowledge a mechanism that formally explains this phenomenon has not been developed. We derived general rate equations containing the necessary modification terms for forward and reverse covalent modification of MWC-type enzymes.

We applied the findings to a minimal feedforward system in which the allosterically regulated enzyme is also modified covalently. We limited the allosteric effect to activation and the covalent effect to inhibition in an effort to mimic the mammalian muscle glycogen synthesis pathway. It is, however, conceivable that similar results will be obtained for feedback inhibition systems. A plausible system to study in this regard would be the feedback system in which glucose-6-phosphate (G6P) inhibits glycogen phosphorylase (GP), an enzyme activated by phosphorylation. In

agreement with the earlier findings of Hofmeyr *et al.* [16], we showed that the flux response with respect to the feedforward modifier X, as mediated through the feedforward loop, is maximized if the regulated enzyme is saturated with its immediate substrate S, but that under these conditions activation by X will only be effective if it enhances the catalytic rate, as opposed to the substrate affinity, of the regulated enzyme. In addition, however, we showed that not only is specific activation insufficient to elicit a flux response with respect to X (due to the fact that the enzyme is already saturated with its substrate), but also that it is detrimental to such a response (due to the fact that sufficiently strong specific activation causes all of the enzyme to be present in the R conformation, abolishing any further conversion to the R conformation, and thus activation, by X).

We also studied the conditions that maximize the response of the system flux to the indirect activation and inhibition of the forward and reverse covalent modification reactions by X. Since both these responses are scaled by $G_{v_2}^{J_1}$, the same conditions that maximize the flux control of enzyme 2 ($\varepsilon_s^{v_2} \rightarrow 0$) are expected to also maximize these responses. Here it is, in one respect, of little consequence whether X is a catalytic or specific activator of the regulated enzyme; instead, what is at stake is whether X brings about a significant increase of enzyme in the R conformation relative to enzyme in the T conformation. However, since in the MWC model such conformational change always goes hand in hand with differential ligand affinities, it is of consequence whether substrate binding favours the R conformation over the T conformation, i.e., whether $c_S < 1$. If the regulated enzyme is saturated with its substrate and if the substrate's preference for the R conformation is sufficiently strong, then X will not be able to bring about any further conformational change, so that the absolute values of $G_{v_A}^{J_1}$, $G_{v_B}^{J_1}$, $\varepsilon_x^{v_A}$, and $\varepsilon_x^{v_B}$ are minimized. More generally, any ligand or covalently bonded group that favours the same conformation as X to a sufficiently strong degree will minimize the flux response with respect to X. We emphasize the role of substrate S only because saturation with S is one condition that will maximize $G_{v_2}^{J_1}$.

Overall, these results indicate that in order to maximize the flux response with respect to the allosteric modifier in a feedforward activation system in which the regulated enzyme exhibits MWC kinetics and is potentially inhibited by covalent modification, it is expected that the allosteric modifier should activate the regulated enzyme by means of increasing its apparent maximal catalytic rate and not by means of increasing its affinity for its immediate substrate. In fact, the presence of specific

activation, which implies conformational change upon substrate binding, will decrease the flux response with respect to the allosteric modifier. Incidentally, these conditions are in good agreement with the GS kinetic parameters determined in the previous chapter. The optimized GS kinetic parameters indicate that the feedforward modifier G6P activates GS by increasing its maximal catalytic rate, but that in the absence of ATP the substrate UDP-glucose (UDPG) binds with equal affinity to the T and R conformations.

Covalent inhibition increases the flux response with respect to the allosteric modifier. This increase is the result of two distinct but related mechanisms. First, the apparent L_0 increases with the degree of covalent modification, which in turn increases the value of $\varepsilon_x^{v_2}$ and thus ${}^2R_x^{J_1}$, the response elicited as a result of the feedforward loop. Second, net covalent modification is inhibited by the allosteric modifier, resulting in a sharper increase in flux, i.e., a larger response coefficient, with respect to changes in x than is expected if only the feedforward loop were present. We thus see that feedforward activation and covalent inhibition increase the flux response with respect to X synergistically: covalent inhibition enhances the response elicited by the feedforward loop, and the feedforward loop is a prerequisite for the response to increase due to covalent inhibition. This situation illustrates that the response with respect to X elicited by either of these mechanisms quantified in isolation, does not reflect the response observed when both mechanisms are active.

The present treatment can be considered a combination and extension of the earlier treatments by Small & Fell [164] and Hofmeyr *et al.* [16]. Small & Fell [164] investigated the conditions that will maximize the response of steady-state variables in response to modifiers that affect the enzymes in a monocyclic covalent modification cycle. Hofmeyr *et al.* [16], on the other hand, investigated the conditions required for maximal efficiency of feedforward activation loops in which an allosteric enzyme is activated by a substrate precursor in the pathway. While Small & Fell [164] were only concerned with covalent modification and Hofmeyr *et al.* [16] were only concerned with allosteric modification, our results show that the allosteric modifiers of an enzyme must also act as modifiers of the enzymes that catalyse its covalent modification, particularly when the modified enzyme exhibits MWC-type kinetics. Apart from the addition of allosteric modification, the present treatment differs from that of Small & Fell [164] in a number of respects. First, the modification terms in the rate equations for the enzymes catalysing the interconversion of enzyme 2 are not arbitrary but are governed by the kinetics of enzyme 2. Second, all ligands of enzyme 2

are, and must be, considered effectors of the enzymes catalysing the interconversion of enzyme 2. Third, both covalent states of enzyme 2 are considered active. Fourth, by implication, all effectors have equal but opposite effects on the forward and reverse covalent modification enzymes. We show that, apart from the requirement for zero-order sensitivity, the same conditions that maximize the response of an enzyme to its activator will also maximize the flux response to these ligands through activation and inhibition of the enzymes in the covalent modification cascade.

It appears that, in the system considered here, the function of both the feedforward loop and covalent modification is to increase the response of the pathway flux to metabolite X. If this system were to be included in a larger pathway, one could consider the flux response coefficient $R_x^{J_1}$ as the elasticity of the subsystem rate with respect to changes in x. Since high elasticities generally indicate low flux control, we conclude that the regulatory mechanisms in this pathway do not function to regulate the flux through the pathway, but to maintain the concentration of metabolite X within narrow bounds. These findings have implications for the regulation of glycogen synthesis. GS is often cited as the flux-controlling enzyme of glycogen synthesis (see for instance [34, 51, 109, 127, 146, 169]). While this is almost certainly true if one considers glycogen synthesis in isolation, i.e., excluding glucose uptake and glycolysis, the results of this chapter suggest that in muscle glycogen metabolism as a whole the regulation of GS, whether by allosteric or covalent modification, functions to maintain intracellular concentrations of G6P within a narrow range and not to control the flux. Glycogen synthesis is of course much more complicated than the simple system considered here. First, in addition to activation by G6P, GS is also inhibited by ATP. Second, GS is inhibited by phosphorylation at multiple sites per subunit. Third, GS phosphorylation and the influx of glucose into muscle cells are regulated by endocrine and other stimuli. We are now in a position to construct a detailed model of glycogen metabolism and to analyse the regulatory design of this complicated metabolic system.

Chapter 5

Modelling glycogen metabolism in mammalian skeletal muscle

5.1 Introduction

Up to this point we have considered the kinetics of glycogen synthase (GS) in detail and developed a rate equation that is able to describe these kinetics as altered by allosteric and covalent modification. We considered the theoretical implications of the developed GS rate equation in a generic minimal model of feedforward activation that resembles the glycogen synthesis pathway. We are now in a position to inquire into the regulatory design of skeletal muscle glycogen metabolism using full-scale detailed kinetic models.

A model of mammalian skeletal muscle glycogen metabolism is by its very nature not expected to resemble quantitatively the skeletal glycogen metabolism of any mammal in particular. Moreover, skeletal muscle is a heterogeneous tissue that comprises fibre types that have traditionally been classified as either oxidative fast-twitch or glycolytic slow-twitch fibres [170]. Four major fibre types are now distinguished according to the fibre's speed of contraction and resistance to fatigue [170]. This classification can be further refined to many additional minor fibre types based on, amongst other factors, the isoform of myosin expressed in the fibre. By definition, these fibre types differ widely in terms of metabolism, further complicating attempts to model muscle metabolism. For the most part, the experimental data used to construct our models of glycogen metabolism were obtained from published studies using enzymes purified from rodent muscle extracts. Our model results should therefore more closely resemble non-oxidative fast-twitch muscle, the predominant

fibre type in rodent muscle. In addition to the difficulty in confining our models to a specific species and muscle fibre type, it is also subject to the usual critique levelled against the treatment of metabolic systems as well-stirred reactors in which metabolites are present at much larger concentrations than enzymes [171]. These criticisms may be even more relevant when considering the highly structured nature of muscle [171] and the fact that protein kinases and phosphatases are present at concentrations comparable to their protein substrates. In spite of these difficulties, we demonstrate (see Chapter 6) that the models presented here provide reasonable quantitative descriptions of published experimental results.

Perhaps the greatest difficulty encountered when constructing a model is its parametrization. Parameter values reported in the literature are often of poor quality. Reasons for this poor quality range from fitting parameters to linear transformations that inflate error, through erroneously treating sigmoidal kinetics as hyperbolic kinetics, to determining bi-substrate parameters at non-saturating concentrations of the co-substrate. Most important, however, is the fact that enzymes are often assayed not under the conditions prevailing in the cell but at which they operate optimally. In a more robust, but time-consuming, approach one would experimentally determine the kinetics of all model enzymes at conditions prevailing in the cell type in question [172]. Such a treatment was not within the scope of the current project. Where necessary, however, we redetermined kinetic parameters from published experimental data using non-linear regression. However, parametrized models are not the only models that are useful. The structure and regulatory features of a metabolic system on its own, informed by how one would model it, provide a framework within which experimental results can be interpreted.

In a kinetic model the time derivatives of metabolite concentrations are described in terms of reaction stoichiometry and the rates of reactions that produce or consume the metabolite in question, together constituting a system of ordinary differential equations. It is therefore necessary to obtain rate equations for all enzymatic rates, transport processes, and mass-action reactions. All enzymatic and transport rates were described with reversible rate equations of the form [173]

$$v = V_{\mathrm{f}}\,\mathcal{K}(s, p, x, \dots)\left(s - \frac{p}{K_{\mathrm{eq}}}\right) \tag{5.1}$$

where V_{f} is the maximal forward rate; $\mathcal{K}(s, p, x...)$ is a positive binding function of substrates s, products p, and modifiers x; and K_{eq} is the equilibrium constant. This form does not contain the maximal velocity of the reverse reaction (V_{r}), which is

seldom determined experimentally, and ensures thermodynamic consistency by explicitly including the K_{eq}. An exception in this regard are the rate equations of GS and glycogen phosphorylase (GP) which were modelled as irreversible reactions.

In what follows, basic knowledge of enzyme kinetics is assumed. Kinetic parameters, such as the Michaelis constant, will not be defined for each reaction. The parameter naming scheme roughly follows the format $P_{c,E,M}$, where P is any parameter further qualified by the subscript c. E and M denote the enzyme or process and metabolite or species to which the parameter pertains. $K_{i,HK,ADP}$ is then the Michaelis constant that describes inhibitory binding of ADP to hexokinase (HK). For the sake of readability, where it is clear from the context, subscripts and commas are omitted. Unless stated otherwise, identical symbols in different equations do not denote the same parameters.

Although great care was taken to include all the relevant reactions and the modifiers that affect these reactions, our main goal was to investigate the regulatory design of glycogen metabolism. As such we did not include reactions that would complicate the models unnecessarily without providing more insight in this regard.

In what follows, we first give an overview of glycogen metabolism as a basis for our choice of included reactions and their rate equations. We consider glycogen metabolism as a system that comprises several individual metabolic modules, with an emphasis on glycogen synthesis. Finally, we combine these modules in several models, of varying scope, of glycogen metabolism, and briefly discuss the software used in this process.

5.2 Glycogen metabolism

Glucose uptake and GLUT4 trafficking

Glucose is imported into muscle from the interstitial tissue by means of facilitated transport. Two transmembrane glucose transporters, glucose transporter 1 (GLUT1) and glucose transporter 4 (GLUT4), are present in muscle [174]. GLUT1, which is constitutively located in the sarcolemma [175, 176], is present at about 10 to 60% the levels of GLUT4 [174]. Under basal conditions, however, only about 5% of GLUT4 is located in the sarcolemma or in T-tubules, deep invaginations in the sarcolemma [177, 178]. It has been suggested that GLUT1 could contribute significantly to basal glucose uptake, but there is no conclusive evidence for this [174]. The majority

of GLUT4 is located in intracellular vesicles cycling between as many as 11 distinct cytosolic pools, involving GLUT4-storage vesicles, endosomes, the trans-Golgi network, and numerous protein complexes [178]. Insulin stimulation and exercise result in rapid translocation of cytosolic GLUT4 to the sarcolemma and T-tubules. Insulin stimulation increases plasma membrane GLUT4 to 40–50% of total GLUT4 [177]. Under these conditions GLUT4 accounts for the majority of glucose uptake [174]. Insulin regulates GLUT4 trafficking through the insulin-PI3K-Akt axis [179]. In this axis insulin binds to the insulin receptor resulting in the activation of insulin receptor kinase which phosphorylates insulin receptor substrate proteins. These recruit PI3-kinase (or PI3K), which converts phosphatidylinositol(4,5)P2 to phosphatidyl(3,4,5)P3 (or PIP3). PIP3 indirectly activates protein kinase B (Akt2), which in turn phosphorylates various substrates leading to the recruitment of GLUT4 to the plasma membrane. While the molecular mechanism has not been fully elucidated, it is thought that the net increase in cell surface GLUT4 is the result of increased exocytosis and not the result of decreased endocytosis [180].

In spite of the complexity of GLUT4 trafficking and the insulin-PI3K-Akt axis, we modelled insulin stimulation of exocytosis by including a hyperbolic catalytic activation term in the GLUT4 rate equation (Eq. 5.3).

In terms of glucose transport kinetics GLUT1 is probably the best-studied glucose transporter. Interest in GLUT1 kinetics arose from the observed 10-fold lower V_{max} and K_m for entry into a glucose-free cell (zero-*trans* entry) than the corresponding parameters for exit into a glucose free medium (zero-*trans* exit) [181]. Moreover, the K_m for entry is higher when determined from equilibrium exchange experiments (the glucose concentration is varied inside and outside but kept equal; labelled glucose is initially absent on the inside) than from zero-*trans* experiments or infinite-*trans* experiments (internal glucose is saturating while external glucose is varied) [182]. GLUT1 asymmetry has been challenged by observations that the asymmetry is reduced or absent when working with ghost cells (erythrocytes of which the cytosol is replaced with medium) or inside-out vesicles, suggesting that asymmetry results from interaction of cytosolic factors with the intracellular epitopes of GLUT1 [183]. It has indeed been shown that ATP inhibits GLUT1 and brings about asymmetry [184]. Others [182] have also argued that GLUT1 asymmetry is overestimated due to experimental difficulties, favouring the position that GLUT1 is intrinsically symmetric. As a further argument against GLUT1 asymmetry, it has been shown that the mobile carrier model, one of two models commonly used to describe trans-

porter kinetics [181], when adapted for asymmetry, is thermodynamically unsound [185]. This finding does, however, not completely rule out asymmetry, which can still be accounted for by a fixed site model [185]. Although GLUT1 assymetry has been observed in human erythrocytes, it has not been observed in rat and rabbit erythrocytes, nor in rat adipocytes and CHO fibroblasts [182]. In contrast, it is well-established that GLUT4 glucose transport is symmetric [186].

We modelled the transport of glucose into the muscle cell ($Glc_o \rightleftharpoons Glc_i$) by GLUT1 and GLUT4 with reversible Michaelis-Menten equations in which symmetric glucose binding was assumed. As discussed, an insulin activation term was included in the GLUT4 equation.

$$v_{GLUT1} = \frac{\frac{k_{cat}[GLUT1]}{K_{Glc}}\left([Glc_o] - \frac{[Glc_i]}{K_{eq}}\right)}{1 + \frac{[Glc_o]}{K_{Glc}} + \frac{[Glc_i]}{K_{Glc}}} \tag{5.2}$$

$$v_{GLUT4} = \frac{\frac{k_{cat}[GLUT4_{mem}]}{K_{Glc}}\left([Glc_o] - \frac{[Glc_i]}{K_{eq}}\right)}{1 + \frac{[Glc_o]}{K_{Glc}} + \frac{[Glc_i]}{K_{Glc}}} \times \frac{\frac{[Ins]}{EC50_{Ins}}}{1 + \frac{[Ins]}{EC50_{Ins}}} \tag{5.3}$$

The rate equation for total glucose transport is given by

$$v_{GLUT} = v_{GLUT1} + v_{GLUT4} \tag{5.4}$$

Since the equilibrium constant for transport of glucose across the sarcolemma is equal to one, net import of glucose by GLUT1 and GLUT4 is only possible in the presence of a glucose concentration gradient. This gradient is maintained by hexokinase which phosphorylates glucose to glucose-6-phosphate (G6P) upon entry into the cell. Two isoforms of hexokinase, hexokinase 1 (HK1) and hexokinase 2 (HK2), are present in muscle. HK2 is the predominant form in rat muscle, whereas in human muscle, based on the percentage contribution to total hexokinase activity (70–75%), HK1 is the predominant form [187]. The majority of HK1 (95%) and HK2 (72%) is recovered in a particulate fraction during extraction [187]. It has been shown that insulin stimulation leads to the translocation of HK2, but not HK1, to the particulate fraction within 30 minutes of treatment with no apparent increase in total HK2 protein [188]. Two hours after treatment, an increase in HK2 mRNA and protein is observed, with an increase in soluble fraction HK2 [189]. No increase in HK1 protein is observed. As reviewed in [190], HK1 readily associates with the

mitochondrial membrane protein, porin, possibly explaining its recovery in the particulate fraction. This association is mediated by a targeting hydrophobic region near the N-terminal of HK1 that is also present in HK2. It has been postulated that association with the mitochondrion provides 'privileged' access to ATP produced during oxidative phosphorylation. It has also been shown that the K_m for ATP is lowered and that G6P inhibition is reduced [191]. Whether these are real changes to hexokinase kinetics or simply the result of an increased apparent ATP concentration is not known.

It is thought that HK1 and HK2, both monomeric 100 kDa proteins, are the products of gene duplication and fusion of an ancestral gene coding for a 50 kDa protein [190]. This position is supported by a high degree of amino acid sequence similarity between the N-terminal and C-terminal halves, and between these halves and 50 kDa hexokinases such as hexokinase 4 (often denoted glucokinase). Only the C-terminal half of HK1 has a functional catalytic site, but the N-terminal half is still able to bind G6P and ATP [192]. In contrast, catalytic activity is retained in both the C-terminal and N-terminal halves of HK2 [193, 194]. It has also been shown that binding of glucose to the N-terminal half increases the affinity for G6P of the C-half, which is otherwise higher than that of the N-half [195]. When expressed as discrete proteins, the C-half of HK1 [192] and the C- and N-halves of HK2 [193] are inhibited by G6P. The extent to which binding of G6P to one domain inhibits the other is not clear.

In our treatment of HK kinetics we have assumed that any interaction between the C- and N-terminal domains is already contained in the apparent kinetic parameters of bi-substrate rate equations and have therefore not included any explicit interaction between these domains. Glucose phosphorylation by HK1 and HK2 ($\mathrm{Glc_i} + \mathrm{ATP} \rightleftharpoons \mathrm{G6P} + \mathrm{ADP}$) was modelled with the reversible bi-substrate Michaelis-Menten equation with random binding order. Since G6P also binds to the adenylate site and ADP also binds to the sugar site [196], additional competive inhibition terms for these ligands were included. Translocation to mitochondria and the possible accompanying change in kinetics were not considered. The identical rate equations for HK1 and HK2 are given by

$$v_{\mathrm{HK1}} = \frac{\dfrac{V_{\max}}{K_{\mathrm{Glc_i}} K_{\mathrm{ATP}}} \left([\mathrm{Glc_i}][\mathrm{ATP}] - \dfrac{[\mathrm{G6P}][\mathrm{ADP}]}{K_{\mathrm{eq}}} \right)}{\left(1 + \dfrac{[\mathrm{Glc_i}]}{K_{\mathrm{Glc_i}}} + \dfrac{[\mathrm{G6P}]}{K_{\mathrm{G6P}}} + \dfrac{[\mathrm{ADP}]}{K'_{\mathrm{ADP}}} \right) \left(1 + \dfrac{[\mathrm{ATP}]}{K_{\mathrm{ATP}}} + \dfrac{[\mathrm{ADP}]}{K_{\mathrm{ADP}}} + \dfrac{[\mathrm{G6P}]}{K'_{\mathrm{G6P}}} \right)} \tag{5.5}$$

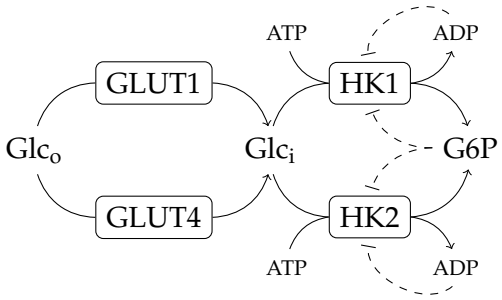

Figure 5.1: Glucose uptake pathway. External glucose is transported into the cell by GLUT1 and GLUT4 and then phosphorylated by HK1 and HK2 to produce G6P. Apart from normal product inhibition, G6P and ADP also compete with ATP and Glc_i, respectively.

and

$$v_{HK2} = \frac{\frac{V_{max}}{K_{Glc_i}K_{ATP}}\left([Glc_i][ATP] - \frac{[G6P][ADP]}{K_{eq}}\right)}{\left(1 + \frac{[Glc_i]}{K_{Glc_i}} + \frac{[G6P]}{K_{G6P}} + \frac{[ADP]}{K'_{ADP}}\right)\left(1 + \frac{[ATP]}{K_{ATP}} + \frac{[ADP]}{K_{ADP}} + \frac{[G6P]}{K'_{G6P}}\right)} \tag{5.6}$$

The overall rate of glucose phosphorylation is given by

$$v_{HK} = v_{HK1} + v_{HK2} \tag{5.7}$$

The glucose uptake module is depicted in Fig. 5.1. From here G6P is either channelled into glycogen synthesis or glycolysis. G6P can also be considered the product of glycogen degradation.

Glycogen synthesis

Phosphoglucomutase (PGLM) catalyses the reaction that converts G6P to glucose-1-phosphate (G1P), exhibiting typical reversible Michaelis-Menten kinetics [197]. The rate equation for PGLM is given by

$$v_{PGLM} = \frac{\frac{V_{max}}{K_{G6P}}\left([G6P] - \frac{[G1P]}{K_{eq}}\right)}{1 + \frac{[G6P]}{K_{G6P}} + \frac{[G1P]}{K_{G1P}}} \tag{5.8}$$

UDPG-pyrophosphorylase (UPP) converts UTP and G1P to UDP-glucose (UDPG) and pyrophosphate (PP_i). Two isoforms, the products of alternative splicing of the

same gene, are present in muscle [198]. Isoform 1, UDPG-pyrophosphorylase 1 (UPP1), exhibits hyperbolic kinetics towards all substrates, whereas isoform 2, UDPG-pyrophosphorylase 2 (UPP2), exhibits sigmoidal kinetics with respect to PP_i and possibly G1P. Only UPP1 was included in the model, as detailed kinetic parameters for UPP2 are not available. UPP1 was modelled with the reversible bi-substrate Michaelis-Menten equation with random reactant binding order:

$$v_{UPP} = \frac{\frac{V_{max}}{K_{UTP}K_{G1P}}\left([UTP][G1P] - \frac{[UDPG][PP_i]}{K_{eq}}\right)}{\left(1 + \frac{[UTP]}{K_{UTP}} + \frac{[PP_i]}{K_{PP_i}}\right)\left(1 + \frac{[UDPG]}{K_{UDPG}} + \frac{[G1P]}{K_{G1P}}\right)} \tag{5.9}$$

GS catalyses the incorporation of the glucose moiety from UDPG into an existing glycogen chain. As discussed in Chapter 2, GS is not capable of *de novo* glycogen synthesis, but instead relies on glycogenin and branching enzyme to produce glycogen primers and new branches that can be elongated by GS. The complex regulation of GS by allosteric and covalent modification is discussed in Chapter 2. A rate equation that provides a good description of GS kinetics was developed in Chapter 3. Glycogenin and branching enzyme were not included in the model. GS was modelled with Eq. 3.42, repeated here for convenience:

$$v_{GS} = \sum_{ij} \frac{k_{cat,r}[GS]_{ij} n \frac{[UDPG]}{K_{UDPG}}\left(1 + \frac{[UDPG]}{K_{UDPG}} + \frac{[ATP]}{K'_{r,ATP}}\right)^{n-1}}{\left(1 + \frac{[UDPG]}{K_{UDPG}} + \frac{[ATP]}{K'_{t,ATP}}\right)^{n} L_{0ij}\left(\frac{1 + \frac{[G6P]}{K_{t,G6P}} + \frac{[ATP]}{K_{t,ATP}}}{1 + \frac{[G6P]}{K_{r,G6P}} + \frac{[ATP]}{K_{r,ATP}}}\right)^{n} + \left(1 + \frac{[UDPG]}{K_{UDPG}} + \frac{[ATP]}{K'_{r,ATP}}\right)^{n}} \tag{5.10}$$

where i and j denote the phosphorylation states of the N-terminal and C-terminal phosphorylation clusters.

Equation 5.10 can be rewritten as (Appendix A.1):

$$v_{GS} = \frac{k_{cat,r}[GS] n \frac{[UDPG]}{K_{UDPG}}\left(1 + \frac{[UDPG]}{K_{UDPG}} + \frac{[ATP]}{K'_{r,ATP}}\right)^{n-1}}{\left(1 + \frac{[UDPG]}{K_{UDPG}} + \frac{[ATP]}{K'_{t,ATP}}\right)^{n} L_{0,app}\left(\frac{1 + \frac{[G6P]}{K_{t,G6P}} + \frac{[ATP]}{K_{t,ATP}}}{1 + \frac{[G6P]}{K_{r,G6P}} + \frac{[ATP]}{K_{r,ATP}}}\right)^{n} + \left(1 + \frac{[UDPG]}{K_{UDPG}} + \frac{[ATP]}{K'_{r,ATP}}\right)^{n}} \tag{5.11}$$

where

$$L_{0,\text{app}} = \frac{\sum_{ij} \frac{[\text{GS}]_{ij}}{\Delta_{ij}} L_{0ij}}{\sum_{ij} \frac{[\text{GS}]_{ij}}{\Delta_{ij}}} \tag{5.12}$$

$$\Delta_{ij} = \left(1 + \frac{[\text{UDPG}]}{K_{\text{UDPG}}} + \frac{[\text{ATP}]}{K'_{\text{t,ATP}}}\right)^n L_{0ij} \left(\frac{1 + \frac{[\text{G6P}]}{K_{\text{t,G6P}}} + \frac{[\text{ATP}]}{K_{\text{t,ATP}}}}{1 + \frac{[\text{G6P}]}{K_{\text{r,G6P}}} + \frac{[\text{ATP}]}{K_{\text{r,ATP}}}}\right)^n + \left(1 + \frac{[\text{UDPG}]}{K_{\text{UDPG}}} + \frac{[\text{ATP}]}{K'_{\text{r,ATP}}}\right)^n \tag{5.13}$$

Equation 5.12 can also be written as

$$L_{0,\text{app}} = \frac{\sum_{ij} t_{ij}}{\sum_{ij} r_{ij}} \tag{5.14}$$

which shows its resemblance to the original definition of L_0:

$$L_0 = \frac{t}{r} \tag{5.15}$$

where t and r are the concentrations of unliganded enzyme in the T and R conformations. Despite this similarity, in the original definition L_0 is independent of ligand concentrations, whereas $L_{0,\text{app}}$ is not.

Note that $L_{0,\text{app}}$ is a function of the concentrations of GS in its various phosphorylation states and the L_0 values for each state ij. Any change in the phosphorylation state of GS is reflected in the value of $L_{0,\text{app}}$. $L_{0,\text{app}}$ assumes its minimum value, L_{000} when GS is completely dephosphorylated, and its maximum value, L_{02a3a}, when GS is completely phosphorylated. The phosphorylation and dephosphorylation of GS may therefore be mimicked by treating $L_{0,\text{app}}$ as a parameter, designated L_0, of which the values range between L_{000} and L_{02a3a}.

In models that did not explicitly include the interconversion between the various GS phosphorylation states, we therefore used the following rate equation for GS:

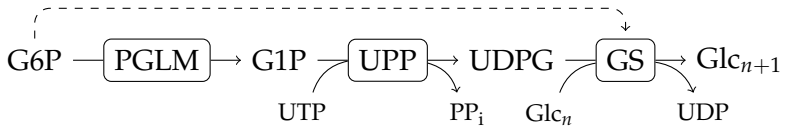

Figure 5.2: Glycogen synthesis pathway. PGLM converts G6P to G1P, which is converted to UDPG by UPP. GS incorporates the glucose moiety from UDPG into an existing glycogen chain. G6P activates GS by binding to an allosteric site.

$$v_{GS} = \frac{k_{cat,r}[GS]n\frac{[UDPG]}{K_{UDPG}}\left(1+\frac{[UDPG]}{K_{UDPG}}+\frac{[ATP]}{K'_{r,ATP}}\right)^{n-1}}{\left(1+\frac{[UDPG]}{K_{UDPG}}+\frac{[ATP]}{K'_{t,ATP}}\right)^{n} L_0\left(\frac{1+\frac{[G6P]}{K_{t,G6P}}+\frac{[ATP]}{K_{t,ATP}}}{1+\frac{[G6P]}{K_{r,G6P}}+\frac{[ATP]}{K_{r,ATP}}}\right)^{n}+\left(1+\frac{[UDPG]}{K_{UDPG}}+\frac{[ATP]}{K'_{r,ATP}}\right)^{n}} \tag{5.16}$$

The glycogen synthesis pathway is depicted in Fig. 5.2.

Glycogen degradation and glycogen phosphorylase phosphorylation

GP, a dimeric enzyme, catalyses the reaction in which the terminal glucose residue from a non-reducing end of a glycogen chain is phosphorylated and cleaved from the chain, releasing it as G1P: $\text{Glc}_{n+1} + \text{P}_\text{i} \rightleftharpoons \text{Glc}_n + \text{G1P}$ [31, 199]. Under resting conditions, GP exists primarily in an inactive form GPb which can be converted to the active form GPa by phosphorylation of Ser14 catalysed by activated phosphorylase kinase (PhK) (Fig. 5.4). Dephosphorylation of GPa is catalysed by protein phosphatase 1 (PP1). Both GP subunits undergo phosphorylation, which allows for an intermediate phosphorylation state (ab form) to exist. Apart from the covalent regulation, GP is also regulated by several modifiers at three allosteric binding sites [31, 199]. The first site, which can be considered the activation site, binds AMP and ATP which leads to activation. The AMP affinity of this site is much greater than the ATP affinity. G6P and glucose also bind to this site, but result in potent inhibition [200]. The second site, often termed the 'nucleoside site', also binds AMP and ATP, but, in contrast to the activation site, this results in inhibition [199, 201]. The AMP affinity of this site is, however, much lower than the ATP affinity, so that inhibition by AMP only occurs at supra-physiological concentrations. Finally, GP has a high-affinity non-catalytic glycogen binding site, which is believed to keep the enzyme

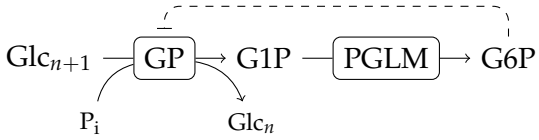

Figure 5.3: Glycogen degradation pathway. GP cleaves a terminal glucose moiety from a glycogen chain in a phosphorolysis reaction to produce G1P. G1P is in turn converted to G6P by PGLM. G6P is an allosteric inhibitor of GP. Note, however, that G6P is not included as a GP inhibitor in the model by Lambeth & Kushmerick [19].

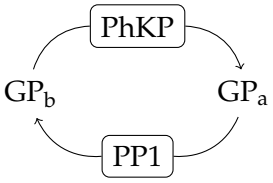

Figure 5.4: GP phosphorylation pathway. Dephosphorylated GPb is phosphorylated at Ser14 by activated PhK to produce GPa. The corresponding phosphatase reaction which converts GPa to GPb is catalysed by PP1. Co-substrates and co-products are not shown.

in tight association with glycogen between individual catalytic events [31, 199]. GP kinetics is most often described in terms of the Monod-Wyman-Changeux (MWC) model, with the prevailing hypothesis that phosphorylation and activation by allosteric modifiers stabilize an active R conformation, whereas dephosphorylation and inhibition stabilize an inactive T conformation [31, 199]. It has been suggested that a three-state MWC model provides a significantly better description of GP kinetics than the conventional two-state model [201].

We modelled GP with the same Hill-like rate equation used by Lambeth & Kushmerick [19]:

$$v_{GP} = \frac{\frac{f_{GP_a} V_{max}}{K_{i,Gly} K_{Pi}} \left([Pi][Glc_{res}] - \frac{[G1P][Glc_{res}]}{K_{eq}} \right)}{1 + \frac{Glc_{res}}{K_{Glyf}} + \frac{[Pi]}{K_{Pi}} + \frac{[Glc_{res}][Pi]}{K_{Glyf} K_{i,Pi}} + \frac{[Glc_{res}]}{K_{Glyb}} + \frac{[G1P]}{K_{G1P}} + \frac{[Glc_{res}][G1P]}{K_{Glyb} K_{i,G1P}}} + \frac{\frac{(1 - f_{GP_a}) V_{max}}{K_{i,Glyf} K_{Pi}} \left([Pi][Glc_{res}] - \frac{[G1P][Glc_{res}]}{K_{eq}} \right) \left(\frac{\frac{[AMP]^h}{\alpha K_{AMP}^h}}{1 + \frac{[AMP]^h}{\alpha K_{AMP}^h}} \right)}{1 + \frac{[Glc_{res}]}{K_{i,Glyf}} + \frac{[Pi]}{K_{i,Pi}} + \frac{[Glc_{res}]}{K_{i,Glyb}} + \frac{[G1P]}{K_{i,G1P}} + \frac{[Glc_{res}][Pi]}{K_{i,Glyf} K_{Pi}} + \frac{[Glc_{res}][G1P]}{K_{G1P} K_{i,Glyb}}} \tag{5.17}$$

As explained in the supplementary material to [202], the parameter values for the

AMP activation term in the original model of Lambeth & Kushmerick [19] are incorrect. We here use the corrected parameter values for the GPb rate equation as given in [202]. Alternatively, where indicated, we modelled GP with a three-state MWC equation of the form:

$$v_{GP} = \frac{f_{GP_a} k_{cat,r}[GP] n \frac{[Pi]}{K_{r,Pi}} \left(1 + \frac{[Pi]}{K_{r,Pi}} + \frac{[G1P]}{K_{r,G1P}}\right)^{n-1}}{\left(1 + \frac{[Pi]}{K_{r,Pi}} + \frac{[G1P]}{K_{r,G1P}}\right)^{n} + L_u \left(1 + \frac{[Pi]}{K_{u,Pi}} + \frac{[G1P]}{K_{u,G1P}}\right)^{n} \left(\frac{1 + \frac{[AMP]}{K_{u,AMP}} + \frac{[G6P]}{K_{u,G6P}}}{1 + \frac{[AMP]}{K_{r,AMP}} + \frac{[G6P]}{K_{r,G6P}}}\right)^{n} \left(\frac{1 + \frac{[ATP]}{K_{u,ATP}}}{1 + \frac{[ATP]}{K_{r,ATP}}}\right)^{n}} + \frac{(1 - f_{GP_a}) k_{cat,r}[GP] n \frac{[Pi]}{K_{r,Pi}} \left(1 + \frac{[Pi]}{K_{r,Pi}} + \frac{[G1P]}{K_{r,G1P}}\right)^{n-1}}{\left(1 + \frac{[Pi]}{K_{r,Pi}} + \frac{[G1P]}{K_{r,G1P}}\right)^{n} + L_t \left(1 + \frac{[Pi]}{K_{t,Pi}} + \frac{[G1P]}{K_{t,G1P}}\right)^{n} \left(\frac{1 + \frac{[AMP]}{K_{t,AMP}} + \frac{[G6P]}{K_{t,G6P}}}{1 + \frac{[AMP]}{K_{r,AMP}} + \frac{[G6P]}{K_{r,G6P}}}\right)^{n} \left(\frac{1 + \frac{[ATP]}{K_{t,ATP}}}{1 + \frac{[ATP]}{K_{r,ATP}}}\right)^{n}} \tag{5.18}$$

The three-state MWC model differs from the classic two-state MWC model only in that a third conformation (here indicated by U) is present in addition to the conventional T and R conformations. The U conformation may differ from the T and R conformations in catalytic capacity and ligand affinities. In Eq. 5.18 only the R conformation is catalytically active. See Appendix C.2 for the development of this equation. In addition to describing AMP activation, it also includes terms describing ATP and G6P inhibition. Note that this equation is irreversible and contains no glycogen binding terms.

GP phosphorylation is described by explicitly altering the fraction of the enzyme in the phosphorylated and dephosphorylated forms. As such, no GP kinase and phosphatase reactions were considered.

G1P produced by GP is converted to G6P by PGLM, the same enzyme that catalyses the reverse reaction in glycogen synthesis. The overall glycogen degradation pathway is depicted in Fig. 5.3.

Glycolysis

In glycolysis ATP is produced during the conversion of G6P to lactate according to the net reaction

$$\mathrm{G6P} + 2\,\mathrm{P_i} + 3\,\mathrm{ADP} \rightleftharpoons 2\,\mathrm{lactate} + 2\,\mathrm{H_2O} + 3\,\mathrm{ATP} \tag{5.19}$$

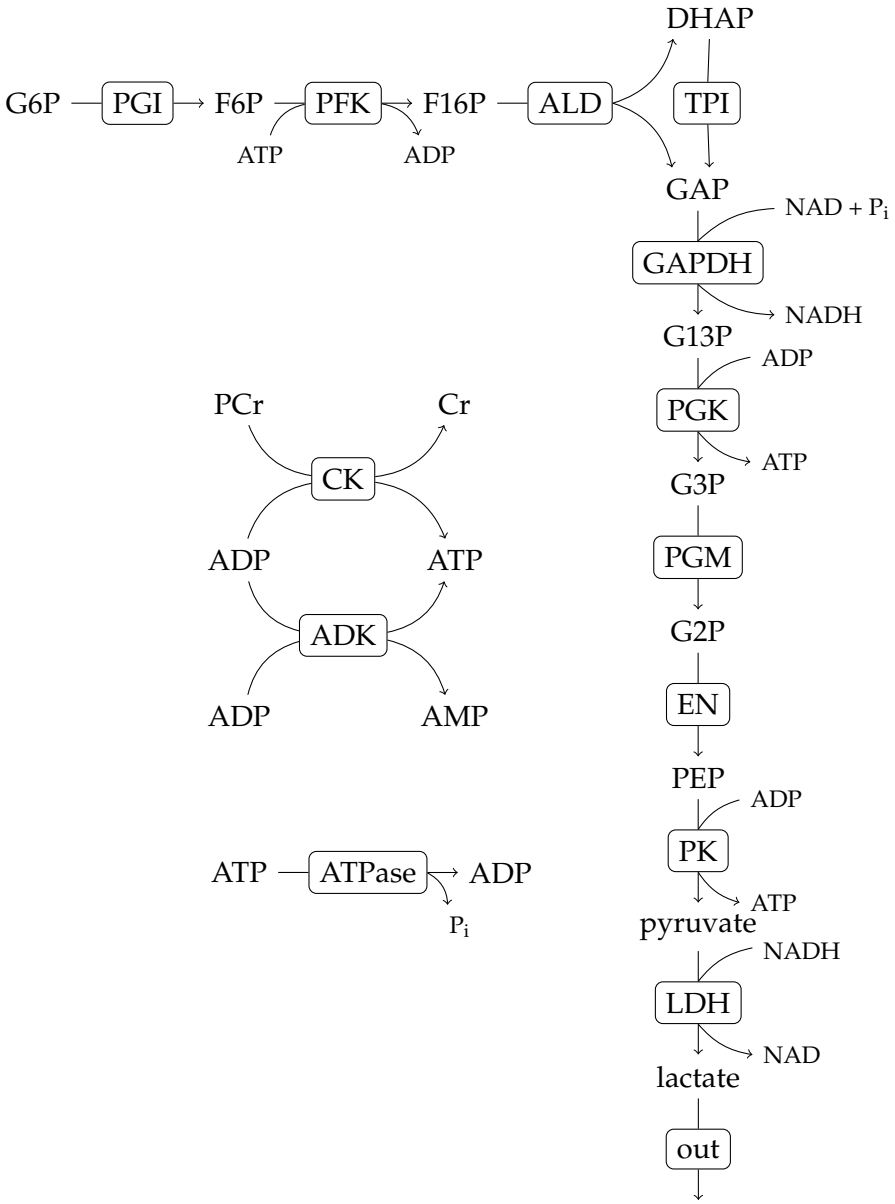

Figure 5.5: Glycolysis pathway as defined by Lambeth & Kushmerick [19]. G6P is converted to two molecules of lactate with an accompanying net production of ATP. An ATPase reaction is included as an ATP demand.

We will not here provide a detailed discussion of muscle glycolysis. We used an implementation of the model of muscle glycolysis by Lambeth & Kushmerick [19]. The glycolysis pathway, as in [19], is depicted in Fig. 5.5.

Where indicated, we used an abbreviated form of the glycolysis pathway which only includes the phosphoglucose isomerase (PGI) reaction and a quasi zero-order fructose-6-phosphate (F6P) sink reaction representing the remainder of the glycoly-

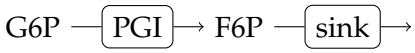

Figure 5.6: Abbreviated glycolysis pathway. Only the PGI reaction from Lambeth & Kushmerick [19] is included. The remainder of the glycolysis pathway is modelled with a quasi zero-order sink reaction.

sis pathway. The sink reaction was modelled with an irreversible Michaelis-Menten equation (Eq. 5.20).

$$v_{\text{sink}} = \frac{V_{\max}[\text{F6P}]}{[\text{F6P}] + K_{\text{F6P}}} \tag{5.20}$$

Although phosphofructokinase (PFK) is the immediate consumer of F6P, the kinetics of the sink reaction is really determined by the ATPase (or myosin) reaction, which controls the flux local to the sink block. The kinetic parameters of the sink reaction were therefore based on the values for the ATPase reaction. The abbreviated glycolysis pathway is shown in Fig. 5.6.

Cyclic AMP-dependent signalling cascade and related reactions

Upon stimulation of a membrane G-coupled receptor protein by catecholamines such as adrenaline, its α-subunit is activated and released [203]. The activated α-subunit in turn activates the enzyme adenylyl cyclase which catalyses the conversion of ATP to cyclic AMP (cAMP). Two molecules of cAMP bind each regulatory subunit of the R_2C_2 cAMP-dependent protein kinase (PKA) holoenzyme leading to the stepwise dissociation and activation of the two catalytic subunits. Several protein substrates of PKA can induce the dissociation of catalytic and regulatory subunits by competing with the regulatory subunit [139]. PKA inhibitor associates with the free catalytic subunit to inhibit it. A summary of the cAMP-dependent activation of PKA is depicted in Fig. 5.7.

The stepwise activation of PKA in response to cAMP and the sequestration of the free catalytic subunit of PKA by the PKA inhibitor protein can be considered as effectively changing the PKA concentration. Since these processes add degrees of freedom to the model parameter space, but affect only a single variable of interest, we instead modelled this variable, the concentration of PKA, as a fixed value that can be varied explicitly.

PKA phosphorylates and activates both PhK and protein phosphatase inhibitor 1 (I1). Activated I1 binds to PP1 and inhibits it. Activated PhK is dephosphorylated

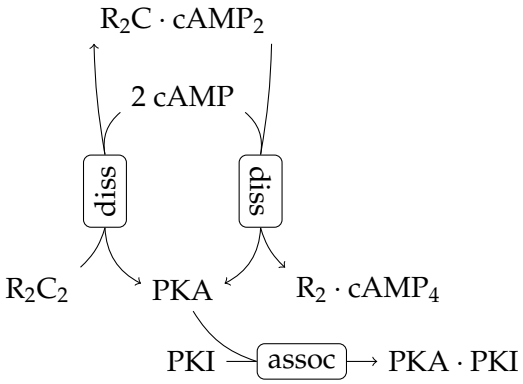

Figure 5.7: Cyclic AMP-dependent activation of PKA. The PKA holoenzyme (R_2C_2) dissociates in a stepwise manner in response to cAMP, which binds to the regulatory R subunits, to release the catalytic subunit C (here designated PKA). PKA is inhibited by the PKA inhibitor protein (PKI).

and inactivated by PP1, whereas activated I1 is dephosphorylated by protein phosphatase 2A (PP2A).

Activation and deactivation of PhK were modelled with random order bi-substrate and uni-bi Michaelis-Menten equations. As a simplifying assumption, product binding was considered negligible:

$$v_{\mathrm{PKA,PhK}} = \frac{\dfrac{k_{\mathrm{cat}}[\mathrm{C}]}{K_{\mathrm{PhK}}K_{\mathrm{ATP}}}\left([\mathrm{PhK}][\mathrm{ATP}] - \dfrac{[\mathrm{PhKP}][\mathrm{ADP}]}{K_{\mathrm{eq}}}\right)}{\left(1+\dfrac{[\mathrm{PhK}]}{K_{\mathrm{PhK}}}\right)\left(1+\dfrac{[\mathrm{ATP}]}{K_{\mathrm{ATP}}}\right)} \tag{5.21}$$

and

$$v_{\mathrm{PP1,PhKP}} = \frac{\dfrac{k_{\mathrm{cat}}[\mathrm{PP1}]}{K_{\mathrm{PhKP}}}\left([\mathrm{PhKP}] - \dfrac{[\mathrm{PhK}][\mathrm{P_i}]}{K_{\mathrm{eq}}}\right)}{\left(1+\dfrac{[\mathrm{PhKP}]}{K_{\mathrm{PhKP}}}\right)} \tag{5.22}$$

Activation and deactivation of I1 were modelled with similar equations as for PhK, but with PP2A as the phosphatase:

$$v_{\mathrm{PKA,I1}} = \frac{\dfrac{k_{\mathrm{cat}}[\mathrm{PKA}]}{K_{\mathrm{I1}}K_{\mathrm{ATP}}}\left([\mathrm{I1}][\mathrm{ATP}] - \dfrac{[\mathrm{I1P}][\mathrm{ADP}]}{K_{\mathrm{eq}}}\right)}{\left(1+\dfrac{[\mathrm{I1}]}{K_{\mathrm{I1}}}\right)\left(1+\dfrac{[\mathrm{ATP}]}{K_{\mathrm{ATP}}}\right)} \tag{5.23}$$

and

$$v_{\text{PP2A,I1P}} = \frac{\frac{k_{\text{cat}}[\text{PP1}]}{K_{\text{I1P}}}\left([\text{I1P}] - \frac{[\text{I1}][\text{P}_\text{i}]}{K_{\text{eq}}}\right)}{\left(1 + \frac{[\text{I1P}]}{K_{\text{I1P}}}\right)} \tag{5.24}$$

Inhibition of PP1 by activated I1 was modelled with mass-action kinetics:

$$v_{\text{PP1 inhibition}} = k_\text{f}[\text{PP1}][\text{I1P}] - k_\text{r}[\text{PP1}\cdot\text{I1}] \tag{5.25}$$

This treatment of cAMP-dependent signalling is loosely based on the model of Mutalik & Venkatesh [204].

Glycogen synthase phosphorylation

We have discussed the hierarchical sequential phosphorylation of GS and the kinases and phosphatases involved therein in detail in Chapter 2. We have also shown in Chapter 3 that, even if all subunits are considered equivalent and strict sequential phosphorylation is assumed, GS can theoretically exist in 1890 kinetically distinct states. One way in which the large number of phosphorylation states can be avoided, is to make the additional simplifying assumption that phosphorylation and dephosphorylation of the same site on all the subunits of the tetramer are *all-or-none*, so that if a particular site is phosphorylated, it is also simultaneously phosphorylated on the remaining three subunits. The number of GS phosphorylation states then decreases to 18. This assumption is similar to the assumption of infinitely cooperative binding in the Hill model [87], but differs in that here it is catalysis, as opposed to ligand binding, that is all-or-none. Unfortunately, several potentially interesting phenomena are partially lost when this assumption is made. First, cooperativity of phosphorylation with respect to the same site on different subunits is lost. Second, the effect of modifiers and phosphorylation of other sites on the phosphorylation of a particular site can only be described by an approximation that exaggerates inhibitory and activatory effects. To lessen the severity of these limitations we have adopted a subtle variation of this assumption.

In order to approximate the per-subunit nature of GS phosphorylation, without explicitly modelling all the possible intermediate phosphorylation states at a particular site, and the states that arise from combinations of intermediate states at different sites, we modelled subunits as independent entities each able to exist in one of

18 phosphorylation states. As would be the case for the tetramer, the conversion between the states of the monomer is catalysed by kinase and phosphatase reactions. In the rate equation for GS the enzyme was, however, modelled as a tetramer composed of subunits with identical phosphorylation states, so that the total number of tetrameric states is also 18. The 18 tetrameric states were assumed to be present in the same relative proportions as the 18 monomeric states. In its capacity as kinase and phosphatase reagent, GS was therefore treated as a monomer, but in its capacity as enzyme, it was considered a tetramer formed by the complexing of four identically modified monomers.

We have shown in Chapter 4 that kinases and phosphatases are indirectly affected by the covalent and allosteric modification of their substrates if this modification results in conformational change. These effects manifest as modification terms of either the forward or reverse maximal carrier capacity of the kinase or phosphatase. For the kinase reaction in which an n-meric enzyme with a single phosphorylation site per subunit is systematically phosphorylated in n steps, this modification term for the i^{th} step, assuming the kinase has no preference for one conformation over another ($\gamma = 1$, see Chapter 4), takes on the form

$$\phi_i = \frac{1 + \alpha^i L}{1 + \alpha^{i-1} L} \tag{5.26}$$

where $i \in [1, n]$ is the number of phosphorylated subunits before catalysis, n is the number of subunits, and α is the factor by which each additional phosphate alters the apparent equilibrium L between the conformational states of the substrate enzyme. The corresponding term for the phosphatase is simply the inverse of ϕ_i. The notion of stepwise subunit modification is strictly speaking not applicable to our simplified treatment of GS phosphorylation. However, if phosphorylation of all n sites was considered a simultaneous event, the modification term would be the product of the modification terms for the individual steps. As an approximation, we therefore included the geometric mean of the modification terms of the individual steps in the kinase and phosphatase rate equations. The geometric mean is given by

$$\begin{aligned} \phi &= \sqrt[n]{\prod_{i=1}^{n} \phi_i} \\ &= \sqrt[n]{\frac{1 + \alpha^n L}{1 + L}} \end{aligned} \tag{5.27}$$

In terms of GS phosphorylation ϕ takes on the form

$$\phi_{GS_{ij}} = \sqrt[n]{\frac{\left(1+\frac{[UDPG]}{K_{UDPG}}+\frac{[ATP]}{K'_{t,ATP}}\right)^n \alpha_{k+1}^n L_{0ij}\left(\frac{1+\frac{[G6P]}{K_{t,G6P}}+\frac{[ATP]}{K_{t,ATP}}}{1+\frac{[G6P]}{K_{r,G6P}}+\frac{[ATP]}{K_{r,ATP}}}\right)^n + \left(1+\frac{[UDPG]}{K_{UDPG}}+\frac{[ATP]}{K'_{r,ATP}}\right)^n}{\left(1+\frac{[UDPG]}{K_{UDPG}}+\frac{[ATP]}{K'_{t,ATP}}\right)^n L_{0ij}\left(\frac{1+\frac{[G6P]}{K_{t,G6P}}+\frac{[ATP]}{K_{t,ATP}}}{1+\frac{[G6P]}{K_{r,G6P}}+\frac{[ATP]}{K_{r,ATP}}}\right)^n + \left(1+\frac{[UDPG]}{K_{UDPG}}+\frac{[ATP]}{K'_{r,ATP}}\right)^n}} \tag{5.28}$$

where $k = i$ for N-terminal cluster phosphorylation and $k = j$ for C-terminal phosphorylation.

To our knowledge, a change in the forward V_{max} or K_m in response to ligands of GS has not been observed experimentally for any of the tested GS kinases. Effects on the reverse V_{max} values have not been tested due to the unfavourable equilibrium constant. The rate equation that best describes GS kinetics, however, shows that phosphorylation alters the equilibrium between the T and R conformations of GS, necessitating a change to the apparent equilibrium constant of phosphorylation. Inclusion of a modification term of the equilibrium constant of phosphorylation without an accompanying change to the forward V_{max} therefore results in an implicit change to the reverse V_{max} of the kinase reactions. We have therefore modelled the GS kinase reactions with bi-substrate Michaelis-Menten equations in which only the K_{eq} is modified by allosteric and covalent modification of GS. Product inhibition was considered negligible.

The rate equation for phosphorylation of site 2 by the catalytic subunit of PKA is given by

$$v_{PKA,GS_{0j}} = \frac{\frac{k_{cat}[PKA]}{K_{GS_{0j}}K_{ATP}}\left([GS_{0j}][ATP] - \frac{[GS_{2j}][ADP]}{\phi_{GS_{0j}}K_{eq}}\right)}{\left(1+\sum_k \frac{[GS_{0k}]}{K_{GS_{0k}}}\right)\left(1+\frac{[ATP]}{K_{ATP}}\right)} \tag{5.29}$$

for all $j \in [0, 5, 4, 3b, 3c, 3a]$ and where $k \in [0, 5, 4, 3b, 3c, 3a]$.

Phosphorylation of site 2 by PhKP and phosphorylation of site 2a by casein kinase 1 (CK1) were modelled with rate equations of the same form as that of PKA.

Since it has been demonstrated that the forward V_{max} of PP1 for the dephosphorylation of GS is affected by GS ligands [146], a modification term was included for

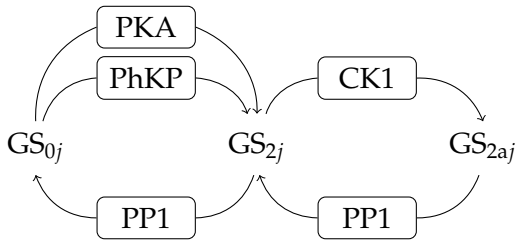

Figure 5.8: Phosphorylation of the N-terminal cluster of GS. Both PKA and activated PhK phosphorylate site 2, which allows subsequent phosphorylation of site 2a by CK1. Both sites are dephosphorylated by PP1. Phosphorylation of sites 2 and 2a is independent of C-terminal phosphorylation, of which the phosphorylation state is indicated by j. Co-substrates and co-products are not shown.

both the $V_{\max}$ and the K_{eq}, so that no modification of the reverse $V_{\max}$ is present. Dephosphorylation of the N-terminal cluster of GS was modelled with a uni-bi Michaelis-Menten equation in which product binding was considered negligible:

$$v_{\text{PP1,GS}_{ij}\to(i-1)j} = \frac{\dfrac{\phi^{-1}_{\text{GS}_{(i+1)j}} k_{\text{cat}}[\text{PP1}]}{K_{\text{GS}}}\left([\text{GS}_{ij}] - \dfrac{[\text{GS}_{(i-1)j}][\text{P}_\text{i}]}{\phi^{-1}_{\text{GS}_{(i+1)j}} K_{\text{eq}}}\right)}{\left(1 + \sum_{kl}\dfrac{[\text{GS}_{kl}]}{K_{\text{GS}}}\right)} \tag{5.30}$$

for all $i \in [2, 2\text{a}]$ and $j \in [0, 5, 4, 3\text{c}, 3\text{b}, 3\text{a}]$, and where $k \in [2, 2\text{a}]$ and $l \in [0, 5, 4, 3\text{c}, 3\text{b}, 3\text{a}]$. Phosphorylation and dephosphorylation of the N-terminal cluster of GS are depicted in Fig. 5.8.

The C-terminal phosphorylation cluster of GS is sequentially phosphorylated by casein kinase 2 (CK2) and glycogen synthase kinase 3 (GSK3) and, like the N-cluster, dephosphorylated by PP1. Phosphorylation of site 5 by CK2 was modelled with an equation of the same form as that for PKA:

$$v_{\text{CK2,GS}_{i0}} = \frac{\dfrac{k_{\text{cat}}[\text{CK2}]}{K_{\text{GS}_{i0}} K_{\text{ATP}}}\left([\text{GS}_{i0}][\text{ATP}] - \dfrac{[\text{GS}_{i5}][\text{ADP}]}{\phi_{\text{GS}_{i5}} K_{\text{eq}}}\right)}{\left(1 + \sum_{k}\dfrac{[\text{GS}_{k0}]}{K_{\text{GS}_{k0}}}\right)\left(1 + \dfrac{[\text{ATP}]}{K_{\text{ATP}}}\right)} \tag{5.31}$$

for all $i \in [0, 2, 2\text{a}]$ and where $k \in [0, 2, 2\text{a}]$. For GSK3, on the other hand, a hyperbolic insulin inhibition term was included as an abbreviation of the insulin-PI3K-Akt pathway. Stimulation of this pathway results in the phosphorylation and deactivation of GSK3. We have therefore modelled this effect as an apparent decrease in the concentration of GSK3:

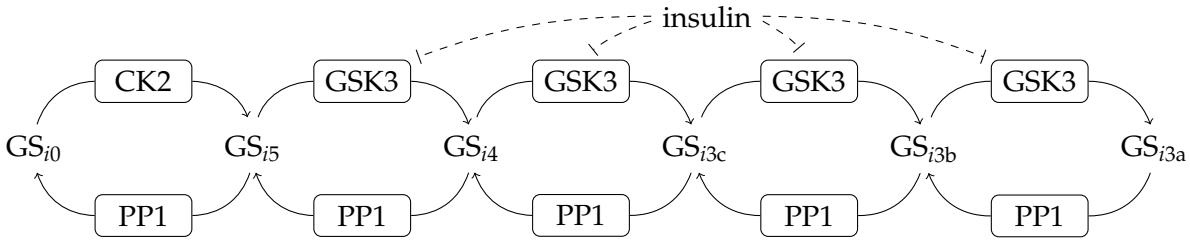

Figure 5.9: Phosphorylation of the C-terminal cluster of GS. CK2 phosphorylates site 5 and thus enables the sequential phosphorylation of the remaining site by GSK3. Dephosphorylation of all sites is catalysed by PP1. Insulin stimulation results in GSK3 inhibition. Phosphorylation of the C-terminal cluster is independent of phosphorylation at the N-terminal cluster, of which the phosphorylation state is indicated by i. Co-substrates and co-products are not shown.

$$v_{\mathrm{GSK3,GS}_{ij}} = \frac{\dfrac{k_{\mathrm{cat}}[\mathrm{GSK3}]}{K_{\mathrm{GS}_{ij}} K_{\mathrm{ATP}}} \left([\mathrm{GS}_{ij}][\mathrm{ATP}] - \dfrac{[\mathrm{GS}_{i(j+1)}][\mathrm{ADP}]}{\phi_{\mathrm{GS}_{i(j+1)}} K_{\mathrm{eq}}} \right)}{\left(1 + \sum_{kl} \dfrac{[\mathrm{GS}_{kl}]}{K_{\mathrm{GS}_{kl}}} \right) \left(1 + \dfrac{[\mathrm{ATP}]}{K_{\mathrm{ATP}}} \right)} \times \frac{1}{1 + \dfrac{[\mathrm{Ins}]}{\mathrm{EC50}_{\mathrm{Ins}}}} \tag{5.32}$$

for all $i \in [0, 2, 2\mathrm{a}]$ and $j \in [5, 4, 3\mathrm{c}, 3\mathrm{b}]$, and where $k \in [0, 2, 2\mathrm{a}]$ and $l \in [5, 4, 3\mathrm{c}, 3\mathrm{b}]$.

Dephosphorylation of the C-terminal cluster of GS was modelled with an equation of the same form as for the N-cluster:

$$v_{\mathrm{PP1:GS}_{ij} \to (i-1)j} = \frac{\dfrac{\phi^{-1}_{\mathrm{GS}_{(i+1)j}} k_{\mathrm{cat}}[\mathrm{PP1}]}{K_{\mathrm{GS}_{ij}}} \left([\mathrm{GS}_{ij}] - \dfrac{[\mathrm{GS}_{(i-1)j}][\mathrm{P_i}]}{\phi^{-1}_{\mathrm{GS}_{(i+1)j}} K_{\mathrm{eq}}} \right)}{\left(1 + \sum_{kl} \dfrac{[\mathrm{GS}_{kl}]}{K_{\mathrm{GS}}} \right)} \tag{5.33}$$

for all $i \in [0, 2, 2\mathrm{a}]$ and $j \in [5, 4, 3\mathrm{c}, 3\mathrm{b}, 3\mathrm{a}]$, and where $k \in [0, 2, 2\mathrm{a}]$ and $l \in [5, 4, 3\mathrm{c}, 3\mathrm{b}, 3\mathrm{a}]$. Phosphorylation and dephosphorylation of the C-terminal cluster of GS are depicted in Fig. 5.9.

5.3 Parametrization

Most of the earlier research on the kinetics of enzymes involved in muscle glycogen metabolism, and muscle metabolism in general, was conducted using rabbit muscle

as source. For this reason and for the sake of consistency we favoured, where available, data obtained from rabbit muscle experiments. A large number of parameters were also obtained from rat and human muscle data. For any particular enzyme, parameters reported in the same paper, by the same group, or for the same species were favoured over compiling parameters from various sources. Where rabbit muscle data were available, but a more complete set could be obtained from another species, the data from the other species were favoured. As needed, data from the same tissue, but from a different species, were preferred over data from the same species, but a different tissue, unless the same isozyme is known to be expressed in both tissues types. Preference was given to data obtained at temperatures and pH values close to the *in vivo* values (37°C and pH 7.2), but where more complete data sets were available, these were favoured. Overall, the guiding principles in choosing parameter sets were quality of experimental techniques employed in determining parameter values and per-enzyme consistency. Where unit conversion was required, 1 g wet muscle weight was taken as equivalent to 0.75 mL cell water (based on wet-to-dry weight ratio in [205]). The unit of time is minutes and the unit of concentration is mM.

Rate constants and enzyme concentrations

The maximal forward carrying capacity of an enzyme can be expressed as

$$V_{\max} = nk_{\text{cat}}[\text{E}]_{\text{tot}} \tag{5.34}$$

where n is the number of enzyme subunits; k_{cat} is the first-order rate constant; and $[\text{E}]_{\text{tot}}$ is the total holoenzyme concentration. For the most part, the right hand side expression of Eq. 5.34 was used in rate equations. Values for k_{cat}, $[\text{E}]_{\text{tot}}$ and $V_{\max}$ were either obtained directly from the literature, calculated from specific activities of crude extracts and purified enzyme, estimated from specific activities relative to known values, or combinations of these methods. The concentrations of membrane proteins, such as the glucose transporter (GLUT), was normalized to the cytosolic volume. See Appendix C.1 for detailed calculations. Rate constants, enzyme concentrations, and other parameters are listed in Tables 5.1–5.6.

Table 5.1: Kinetic parameters for glucose uptake pathway

Parameter	Value	Unit	Reference	Source
$k_{cat,GLUT1}$	72 000	min^{-1}	[207]	3T3-L1 cells (mouse)
$[GLUT1_{tot}]$	$5.5 \cdot 10^{-7}$	mM	10% of [GLUT4] [174]	human muscle
$K_{GLUT1,Glc}$	6.9	mM	[183]	human erythrocyte
$k_{cat,GLUT4}$	79 000	min^{-1}	[207]	3T3-L1 cells (mouse)
$[GLUT4_{tot}]$	$5.5 \cdot 10^{-6}$	mM	calculated from [208]	human muscle
$K_{GLUT4,Glc}$	4.6	mM	[186]	typical mammalian
$EC50_{GLUT4,Ins}$	$1.7 \cdot 10^{-7}$	mM	[209]	human muscle
$k_{cat,HK1}$	7 194	min^{-1}	Table C.1	rabbit heart
[HK1]	$6.1 \cdot 10^{-4}$	mM	calculated from [187]	human muscle
$K_{HK1,Glc}$	$4.5 \cdot 10^{-2}$	mM	[196]	rat muscle
$K_{HK1,ATP}$	0.4	mM	[196]	rat muscle
$K_{HK1,G6P}$	0.21	mM	[196]	rat muscle
$K_{HK1,ADP}$	0.62	mM	[196]	rat muscle
$K_{i,HK1,G6P}$	$2.6 \cdot 10^{-2}$	mM	[196]	rat muscle
$K_{i,HK1,ADP}$	2	mM	[196]	rat muscle
$k_{cat,HK2}$	15 065	min^{-1}	Table C.1	recombinant, human muscle
[HK2]	$9.2 \cdot 10^{-5}$	mM	calculated from [187]	human muscle
$K_{HK2,Glc}$	0.23	mM	[196]	rat muscle
$K_{HK2,ATP}$	0.78	mM	[196]	rat muscle
$K_{HK2,G6P}$	0.16	mM	[196]	rat muscle
$K_{HK2,ADP}$	2.2	mM	[196]	rat muscle
$K_{i,HK2,G6P}$	$2.1 \cdot 10^{-2}$	mM	[196]	rat muscle
$K_{i,HK2,ADP}$	5.4	mM	[196]	rat muscle

Other parameters

All Michaelis constants, dissociation constants, and half-maximal effective concentrations were obtained directly from the literature or determined by parameter optimization. Equilibrium constants (Table 5.7) were taken from the literature, estimated with the *eQuilibrator* service [36], or taken from the TECR database [206]. Equilibrium constants for protein kinase and protein phosphatase reactions were estimated by considering the reactions serine + ATP $\leftrightharpoons$ phosphoserine + ADP and phosphoserine + $H_2O \leftrightharpoons$ serine + P_i at pH 7.2 and ionic strength of 0.1 mM. A limitation of the eQuilibrator service [36] is that it only provides equilibrium constant values estimated for the standard conditions temperature of 25°C.

Metabolite and other species concentrations

In a kinetic model the steady-state concentrations of variable species are completely determined by the system parameters and, as such, it is not crucial to assign rigor-

Table 5.2: Kinetic parameters for the glycogen synthesis pathway

Parameter	Value	Unit	Reference	Source
$V_{max,PGLM}$	2 078	mM min^{-1}	[210]	rabbit muscle
$K_{PGLM,G6P}$	$5.7 \cdot 10^{-2}$	mM	[197]	rabbit muscle
$K_{PGLM,G1P}$	$1.05 \cdot 10^{-2}$	mM	[197]	rabbit muscle
$V_{max,UPP}$	200	min^{-1}	9.6% of $V_{max,PGLM}$ [211]	–
$K_{UPP,G1P}$	0.4	mM	[198]	recombinant, human muscle
$K_{UPP,UTP}$	0.92	mM	[198]	recombinant, human muscle
$K_{UPP,UDPG}$	$6.3 \cdot 10^{-2}$	mM	[198]	recombinant, human muscle
K_{UPP,PP_i}	0.38	mM	[198]	recombinant, human muscle
$K_{i,UPP,UDPG}$	$5.2 \cdot 10^{-2}$	mM	[198]	recombinant, human muscle
$K_{i,UPP,UTP}$	0.98	mM	[198]	recombinant, human muscle
n_{GS}	4	dimensionless	–	–
$k_{cat,r,GS}$	1 004	min^{-1}	Table C.1	rabbit muscle
total [GS]	$3 \cdot 10^{-3}$	mM	[212]	–
$K_{GS,UDPG}$	0.72	mM	Chapter 3	rat muscle
$K_{r,GS,G6P}$	$6.76 \cdot 10^{-2}$	mM	Chapter 3	rat muscle
$K_{t,GS,G6P}$	0.29	mM	Chapter 3	rat muscle
$K_{r,GS,ATP}$	4.94	mM	Chapter 3	rat muscle
$K_{t,GS,ATP}$	2.33	mM	Chapter 3	rat muscle
$K_{c,r,GS,ATP}$	15.92	mM	Chapter 3	rat muscle
$K_{c,t,GS,ATP}$	3.93	mM	Chapter 3	rat muscle
$L_{0,GS00}$	0.25	dimensionless	Chapter 3	–
$L_{0,GS20}$	1.23	dimensionless	Chapter 3	–
$L_{0,GS2a0}$	4.98	dimensionless	Chapter 3	–
$L_{0,GS05}$	0.25	dimensionless	Chapter 3	–
$L_{0,GS25}$	1.23	dimensionless	Chapter 3	–
$L_{0,GS2a5}$	4.98	dimensionless	Chapter 3	–
$L_{0,GS04}$	0.25	dimensionless	Chapter 3	–
$L_{0,GS24}$	1.23	dimensionless	Chapter 3	–
$L_{0,GS2a4}$	4.98	dimensionless	Chapter 3	–
$L_{0,GS03c}$	0.25	dimensionless	Chapter 3	–
$L_{0,GS23c}$	1.23	dimensionless	Chapter 3	–
$L_{0,GS2a3c}$	4.98	dimensionless	Chapter 3	–
$L_{0,GS03b}$	0.67	dimensionless	Chapter 3	–
$L_{0,GS23b}$	3.29	dimensionless	Chapter 3	–
$L_{0,GS2a3b}$	13.29	dimensionless	Chapter 3	–
$L_{0,GS03a}$	9.31	dimensionless	Chapter 3	–
$L_{0,GS23a}$	45.68	dimensionless	Chapter 3	–
$L_{0,GS2a3a}$	184.69	dimensionless	Chapter 3	–

Table 5.3: Kinetic parameters for the glycogen degradation pathway

Parameter	Value	Unit	Reference
n_{GP}	2	dimensionless	–
$V_{max,GP}$	50	mM min^{-1}	[19]
K_{r,GP,P_i}	2.08	mM	Table C.6
K_{u,GP,P_i}	4.32	mM	Table C.6
K_{t,GP,P_i}	41.53	mM	Table C.6
$K_{r,GP,G1P}$	0.67	mM	Table C.6
$K_{u,GP,G1P}$	82.02	mM	Table C.6
$K_{t,GP,G1P}$	27.92	mM	Table C.6
$K_{r,GP,AMP}$	$3.36 \cdot 10^{-3}$	mM	Table C.6
$K_{t,GP,AMP}$	0.53	mM	Table C.6
$K_{t,GP,ATP}$	3.9	mM	Table C.6
$K_{r,GP,G6P}$	7.42	mM	Table C.6
$K_{u,GP,G6P}$	0.56	mM	Table C.6
$K_{t,GP,G6P}$	0.27	mM	Table C.6
$L_{u,GP,a}$	5.93	dimensionless	Table C.6
$L_{t,GP,b}$	34 741	dimensionless	Table C.6

Table 5.4: Kinetic parameters for the abbreviated glycolysis pathway

Parameter	Value	Unit	Reference	Source
$V_{max,sink}$	$1 \cdot 10^{-2}$	mM min^{-1}	assumed	–
$K_{sink,F6P}$	$9 \cdot 10^{-3}$	mM	[213]	rabbit muscle

Table 5.5: Kinetic parameters for the cAMP signalling pathway

Parameter	Value	Unit	Reference	Source
$k_{cat,PKA,PhK}$	920	min^{-1}	Table C.3	rabbit muscle
[PKA]	$1 \cdot 10^{-5}$	mM	assumed	–
$K_{PKA,ATP}$	$2 \cdot 10^{-2}$	mM	[214]	rabbit muscle
$K_{PKA,PhK}$	$4 \cdot 10^{-4}$	mM	assumed in [204]	–
[PhK]	$2.5 \cdot 10^{-3}$	mM	[215]	rabbit muscle
[PhKP]	0	mM	–	–
$k_{cat,PKA,I1}$	84	min^{-1}	[216]	bovine heart
$K_{PKA,I1}$	$5 \cdot 10^{-3}$	mM	[216]	bovine heart
[I1]	$1.8 \cdot 10^{-3}$	mM	[217]	rabbit muscle
[I1P]	0	mM	–	–
$k_{cat,PP1,PhKP}$	110	min^{-1}	Table C.2	rabbit muscle
$K_{PP1,PhKP}$	$3.7 \cdot 10^{-3}$	mM	[218]	rabbit muscle
$k_{cat,PP2A,I1P}$	5	min^{-1}	assumed, based on [218, 219]	rabbit muscle
[PP2A]	$5 \cdot 10^{-4}$	mM	[220]	–
$K_{PP2A,I1P}$	$7 \cdot 10^{-4}$	mM	[218]	rabbit muscle
[PP1]	$6 \cdot 10^{-4}$	mM	[220]	–
[PP1 · I1P]	0	mM	–	–
$K_{d,PP1+I1P}$	$1.5 \cdot 10^{-6}$	mM	[221]	rabbit muscle

Table 5.6: Kinetic parameters for GS phosphorylation

Parameter	Value	Unit	Reference	Source
$k_{cat,PKA,GS}$	1 060	min^{-1}	Table C.3	rabbit muscle
$K_{PKA,GS}$	$3 \cdot 10^{-3}$	mM	[139]	rabbit muscle
$k_{cat,PhKP,GS}$	1 200	min^{-1}	Table C.1	rabbit muscle
$K_{PhKP,GS}$	$4.5 \cdot 10^{-3}$	mM	based on GP value [222, 223]	rabbit muscle
$K_{PhKP,ATP}$	0.5	mM	[214]	rabbit muscle
$k_{cat,CK1,GS}$	12	min^{-1}	Table C.1	rabbit muscle
[CK1]	$4.5 \cdot 10^{-4}$	mM	Table C.4	rabbit muscle
$K_{CK1,GS}$	$3 \cdot 10^{-3}$	mM	[100]	rabbit muscle
$K_{CK1,ATP}$	$1.8 \cdot 10^{-2}$	mM	[100]	rabbit muscle
$k_{cat,CK2,GS}$	70	min^{-1}	Table C.1	rabbit muscle
[CK2]	$1 \cdot 10^{-4}$	mM	Table C.4	rabbit muscle
$K_{CK2,GS}$	$1.2 \cdot 10^{-2}$	mM	[101]	rabbit muscle
$K_{CK2,ATP}$	$1 \cdot 10^{-2}$	mM	[101]	rabbit muscle
$k_{cat,GSK3,GS}$	100	min^{-1}	Table C.1	rabbit muscle
[GSK3]	$7 \cdot 10^{-5}$	mM	based on [212] and Table C.4	rabbit muscle
$K_{GSK3,GS}$	$3.6 \cdot 10^{-3}$	mM	[101]	rabbit muscle
$K_{GSK3,ATP}$	$2 \cdot 10^{-2}$	mM	[101]	rabbit muscle
$EC50_{GSK3,Ins}$	$1.7 \cdot 10^{-7}$	mM	assumed same as $EC50_{GLUT4,Ins}$	human muscle
$k_{cat,PP1,GS22a}$	115	min^{-1}	Table C.2	rabbit muscle
$k_{cat,PP1,GS43abc}$	30	min^{-1}	Table C.2	rabbit muscle
$k_{cat,PP1,GS5}$	1	min^{-1}	Table C.2	rabbit muscle
$K_{PP1,GS}$	$9.4 \cdot 10^{-3}$	mM	based on GP value [224]	rabbit muscle

Table 5.7: Equilibrium constants

Parameter	Value	Unit	Reference
$K_{eq,GLUT}$	1	dimensionless	–
$K_{eq,HK}$	2 090	dimensionless	[37]
$K_{eq,PGLM}$	$5.62 \cdot 10^{-2}$	dimensionless	[197]
$K_{eq,UPP}$	0.24	dimensionless	[225]
$K_{eq,protkin}$	70 000	dimensionless	eQuilibrator [36]
$K_{eq,protphos}$	50 000	mM	eQuilibrator [36]

Table 5.8: Metabolite and other species concentrations

Metabolite	Concentration (mM)	Reference	Source
Glc_o	5	based on [226]	human blood
Glc_i	$1 \cdot 10^{-3}$	assumed	–
G6P	0.75	[19]	–
G1P	$5.89 \cdot 10^{-2}$	[19]	–
UTP	0.13	estimated from [227]	rat muscle
PP_i	$1 \cdot 10^{-2}$	assumed	–
UDPG	$4.3 \cdot 10^{-2}$	[210]	rat muscle
$(Glc)_n$	112	[19]	–
ATP	8.2	[19]	–
ADP	$1.3 \cdot 10^{-2}$	[19]	–
P_i	4.1	[19]	–
Ins	$4 \cdot 10^{-8}$	based on [226]	human blood

ously determined initial values to these species. Realistic values for variable species are only relevant in terms of speeding up numeric analysis. Since the sums of conserved moieties are not explicitly provided in the models, but are instead inferred from the initial concentrations of species belonging to the particular moiety conservation cycle, it is important to provide accurate values for these species. In the glycogen synthesis models, moiety conservation is only observed in the signalling cascades: enzymes and their phosphorylated forms constitute moiety-conserved cycles. In the glycogenolysis model of Lambeth & Kushmerick [19], several moieties are conserved. These include the phosphate, adenylate, and creatine moieties and the NAD/NADH cycle. Additional moiety conservation cycles arise when glycogen synthesis and glycogen degradation are combined. Initial concentrations for several metabolites and other species are listed in Table 5.8.

5.4 Models

Each of the subpathways described in the previous two sections can be considered modules of glycogen metabolism. We combined these modules in various ways in several models, each describing different aspects of glycogen metabolism. In order to ensure consistency across all the models, we exploited the modular nature of glycogen metabolism and constructed each model as a combination of all the modules relevant to the model.

Each module was described using the PySCeS [228] model description language in combination with the Jinja2 templating meta-language (http://jinja.pocoo.org).

PySCeS is an open-source metabolic modelling program developed in our group. In its simplest form, a PySCeS model file is a list of reaction definitions in terms of stoichiometries and rate equations, and definitions of parameters and variables and their values. PySCeS uses this information to construct a system of ordinary differential equations, which can be solved for steady-state. The steady-state information and structural relationships in the model are then used to solve the various coefficients of metabolic control analysis. For each model a master template file was written that 1) defines the modules that should be included in the model, 2) lists the fixed species, and 3) initializes the variable species pertaining to the model. These model templates were then *rendered* to PySCeS model files with the Jinja2 template engine. Although Jinja2 was designed with web development in mind, there is no restriction on the file type that can be rendered. There are many advantages to using a template engine when dealing with multiple related models or even a single complex model:

- parameters or variables such as initial metabolite concentrations can be managed in a single file
- related module templates can *inherit* content from a parent template
- macros can be defined to perform frequently used tasks
- programming constructs such as *for*-loops and *if-else*-branches can be used
- data structures such as arrays are available
- mathematical expressions can be evaluated

Macros or functions are also built-in features of the PySCeS model description language, but native PySCeS macros offer less descriptive power and introduce overhead during model simulation. If-else-branches are also available in PySCeS but serve a different purpose, i.e., evaluation of conditions at runtime.

We will not describe the templating scheme used in detail here, but a brief illustration of how Jinja2 might be used to produce a PySCeS model file is depicted in Fig. 5.10.

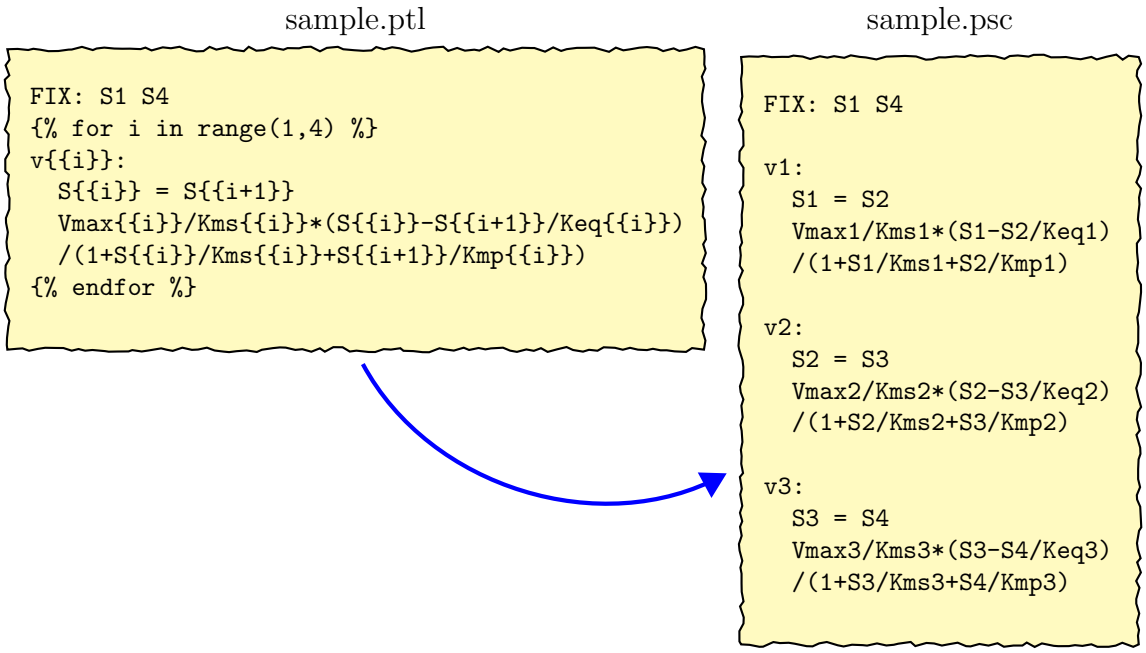

Figure 5.10: Excerpt from an example Jinja2 template file (sample.ptl) and the resulting PySCeS file (sample.psc). The example demonstrates the use of for-loops to contract repetitive snippets. All model modules were programmed as Jinja2 template files, which were combined in various ways in master templates and subsequently rendered with the Jinja2 templating engine as PySCeS model files.

GlySynth

The GlySynth model describes the synthesis of glycogen from external glucose. It comprises modules describing glucose uptake, glycogen synthesis, GLUT4 trafficking, the cAMP-dependent cascade (excluding PKA activation and inhibition), and insulin signalling. Although the concentration of GLUT4 that is present in the sarcolemma is treated as a fixed species, the activation term in the GLUT4 rate equation describes an effective increase in $[\text{GLUT4}_{\text{mem}}]$. Similarly, instead of including both the phosphorylated and dephosphorylated forms of GSK3 in the model, the inhibition of GSK3 by insulin is described as an apparent decrease in the concentration of GSK3. The fixed species are: Glc_o, ATP, ADP, UTP, PP_i, UDP, glycogen, and P_i.

GlySynthExp

This model is essentially the same as GlySynth. However, instead of including an insulin activation term in the GLUT4 rate equation, the concentration of plasma membrane GLUT4 is set explicitly (hence 'Exp'). Similarly, GS phosphorylation

and dephosphorylation as regulated by cAMP and insulin are modelled explicitly through the parameter L_0, which really is a function of the concentrations of the various GS phosphorylation states. The advantage of this model is that it allows the function of GS phosphorylation to be investigated without concern for the signalling pathways that would bring about the phosphorylation. The fixed species are: Glc_o, ATP, ADP, UTP, PP_i, UDP, and glycogen. The values for $L_0 = 5.6$ and $[GLUT4_{mem}] = 1 \times 10^{-6}$ mM were taken from the corresponding variables in GlySynth at basal insulin concentration.

LamKus

This model is an exact implementation of the mammalian muscle glycogenolysis model described by Lambeth & Kushmerick [19]. Since GP is present in only two phosphorylation states, it does not include any phosphorylation cascades, but rather describes GP phosphorylation with the parameter f_{GP_a}, the fraction of GS in the phosphorylated form. The model was implemented as a glycogen degradation module and a glycolysis module. As described later, the rate equation for GP was substituted with a MWC-type rate equation as a variation of the model.

GlyMetExp

We combined the GlySynthExp and LamKus models in an overall model of glycogen metabolism. As described later, additional rate equations and modifications were required to ensure stoichiometric consistency. The fixed species are: Glc_o, glycogen, and lactate.

In the next chapter we will use the models presented here to analyse the regulatory design of skeletal muscle glycogen metabolism.

Chapter 6

Regulatory design of glycogen metabolism

6.1 Introduction

The regulatory design of a metabolic system can be defined as the functional organization of the mechanisms that regulate it. The notion of *regulation* is, however, itself in need of definition. Traditionally, discussions of regulation in metabolism are mainly concerned with the control of flux in a system [77]. In this paradigm, enzyme modification, whether allosteric or covalent, is immediately considered a mechanism of flux control. In contrast, we here consider regulation as the concurrent control of flux and metabolite concentrations in an effort to absorb environmental perturbations. An investigation of the regulatory design of a metabolic system is, therefore, one that considers how enzyme activities are modified in coordination in order to bring about required changes in flux while maintaining metabolite concentrations within acceptable ranges. We wish to emphasize that the notion of *design*, as used here, is one that is completely void of intent and purpose.

In this chapter we analyse the models described in the previous chapter with the aim of elucidating the regulatory design of muscle glycogen metabolism. We begin with a brief review of the analytic frameworks that will be used in this regard. We proceed to discuss the function of the allosteric and covalent regulation of glycogen synthase (GS) in the glycogen synthesis pathway and consider the relative importance of allosteric and covalent regulation in fulfilling this function. We also consider the function of the modification of glycogen phosphorylase (GP) in the glycogen degradation pathway. In conclusion, we discuss the requirements of

constructing a combined model of glycogen synthesis and degradation.

6.2 Analytic frameworks

Supply-demand analysis

It is sometimes desirable to step back from the detail of a complex metabolic pathway and group reactions together in blocks linked by common intermediary metabolites [229, 230]. It has been shown that such grouped metabolic systems can be investigated with conventional metabolic control analysis (MCA). Supply-demand analysis (SDA) is a control analytic approach in which a metabolic system is divided into supply and demand blocks around a linking metabolite [15, 231]. The linking metabolite is the end product of the supply block and the initial substrate of the demand block. SDA around the linking metabolite is visually represented by plotting the *rate characteristics* of the supply and demand blocks on the same graph [231]. A rate characteristic is generated for each block as a log-log plot of the rate of the block against the concentration the linking metabolite by treating the linking metabolite as a parameter of the block. Such a rate characteristic therefore represents the variation in flux of the isolated block with regard to changes in the linking metabolite concentration. The intersection of the supply and demand rate characteristics indicates the steady-state of the supply-demand system. *Regulatory metabolites*, i.e. metabolites involved in feedback or feedforward loops, and branch point metabolites are generally good choices of linking metabolite. A general method has been proposed by which investigator bias can be removed in the process of selecting the linking metabolite [232].

As is the case for individual enzymes, each block can be assigned a flux-control and concentration-control coefficient and these can be expressed in terms of the block elasticities with respect to the linking metabolite [229, 230, 233]. Block elasticities, in turn, can be expressed in terms of the properties of the isolated blocks. In particular, since the rate of a block equals the flux through the isolated block, a block elasticity is the same as the flux-response coefficient of the particular block, considered in isolation, with respect to the linking metabolite:

$$\varepsilon_s^{v_{\text{block}_i}} = R_s^{J_i} \tag{6.1}$$

$$= \sum_j C_{v_j}^{J_i} \varepsilon_s^{v_j} \tag{6.2}$$

where i denotes the block in question; s is the linking metabolite; J_i is the flux within the isolated block (i.e. with fixed s); and j is any enzyme within block i that is sensitive to s.

Co-response analysis

In the introduction to MCA in Section 4.4, we have only considered the effect of perturbations on single steady-state variables. It is, however, instructive to consider how steady-state variables *co-respond* to perturbations. The co-response coefficient quantifies the relative change in two steady-state variables y_1 and y_2 in response to perturbation of a parameter p [234]:

$$\Omega_p^{y_1:y_2} = \frac{R_p^{y_1}}{R_p^{y_2}} = \frac{\sum_i C_{v_i}^{y_1} \varepsilon_p^{v_i}}{\sum_i C_{v_i}^{y_2} \varepsilon_p^{v_i}} \tag{6.3}$$

If only a single enzymatic step j is sensitive to p, then the expression for $\Omega_p^{y_1:y_2}$ simplifies to that of the co-control coefficient:

$$O_{v_j}^{y_1:y_2} = \frac{C_{v_j}^{y_1}}{C_{v_j}^{y_2}} \tag{6.4}$$

If y_1 is a flux and y_2 is a metabolite concentration, the co-response coefficient can be considered a quantification of metabolite homeostasis or structural stability. A large co-response coefficient indicates that metabolite y_2 changes minimally in the face of a large change in flux y_1, given the change to parameter p.

MCA (as introduced in Section 4.4), SDA, and co-response analysis will be used in our investigation of the regulatory design of glycogen metabolism.

6.3 Glycogen synthesis as a supply-demand system

The glycogen synthesis pathway can be considered a supply-demand system of glucose-6-phosphate (G6P) in which glucose uptake (glucose transporter (GLUT)

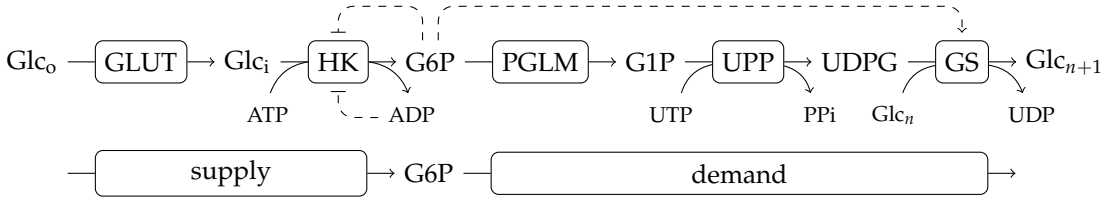

Figure 6.1: Glycogen synthesis as a supply-demand system of G6P. The glucose uptake pathway, consisting of the GLUT and HK reactions, acts as a G6P supply process, whereas the glycogen synthesis pathway, consisting of the PGLM, UPP, and GS reactions, functions as a G6P demand process. G6P is an allosteric activator of GS and a competitive inhibitor of HK with respect to ATP.

and hexokinase (HK)) functions as a supply block, and glycogen synthesis (phosphoglucomutase (PGLM), UDPG-pyrophosphorylase (UPP), and GS) as a demand block (Fig. 6.1). We chose G6P as linking metabolite because it is a feedforward activator of GS and a feedback inhibitor of HK, but also because it is the metabolite that has most often been chosen as the linking metabolite in experimental studies of GS glycogen synthesis.

The elasticity coefficients with respect to G6P for the supply and demand blocks are defined as

$$\varepsilon_{\text{G6P}}^{\text{supply}} = \frac{\partial \ln v_{\text{supply}}}{\partial \ln[\text{G6P}]} \tag{6.5}$$

and

$$\varepsilon_{\text{G6P}}^{\text{demand}} = \frac{\partial \ln v_{\text{demand}}}{\partial \ln[\text{G6P}]} \tag{6.6}$$

The flux-control coefficients of the supply and demand blocks can be expressed in terms of the supply and demand elasticities as follows:

$$C_{\text{supply}}^{J} = \frac{\varepsilon_{\text{G6P}}^{\text{demand}}}{\varepsilon_{\text{G6P}}^{\text{demand}} - \varepsilon_{\text{G6P}}^{\text{supply}}} \tag{6.7}$$

$$C_{\text{demand}}^{J} = \frac{-\varepsilon_{\text{G6P}}^{\text{supply}}}{\varepsilon_{\text{G6P}}^{\text{demand}} - \varepsilon_{\text{G6P}}^{\text{supply}}} \tag{6.8}$$

Similarly, the concentration-control coefficients are

$$C_{\text{supply}}^{\text{G6P}} = -C_{\text{demand}}^{\text{G6P}} = \frac{1}{\varepsilon_{\text{G6P}}^{\text{demand}} - \varepsilon_{\text{G6P}}^{\text{supply}}} \tag{6.9}$$

6.4 Homeostasis in response to change in external glucose concentration

The glycogen synthesis model GlySynthExp contains no signalling cascades. Instead, the effects of the various signalling cascades are contained as explicit parameters in the model. In particular, the plasma membrane glucose transporter 4 (GLUT4) concentration is set manually to a basal level and the extent of GS phosphorylation is varied explicitly by changing the value of L_0. $L_{0,\text{app}}$ is, strictly speaking, a variable, but by treating it as a parameter (designated L_0), the concentrations of GS present in the various phosphorylation states are implicitly varied, thus mimicking phosphorylation and dephosphorylation (see Eq. 5.12). Explicit control of the phosphorylation state of GS, through changes to a single parameter, makes GlySynthExp an ideal model for investigating the function of allosteric and covalent GS regulation.

Functional differentiation

A supply-demand system is said to be functionally differentiated if the absolute values of the supply and demand elasticities differ significantly, so that one block controls the flux, whereas the other block determines the magnitude of concentration-control. The degree of functional differentiation of the glycogen synthesis pathway was investigated with supply-demand rate characteristics (Fig. 6.2). Significant functional differentiation was observed between the the supply and demand blocks. In particular, $\left|\varepsilon^{\text{demand}}_{\text{G6P}}\right| \gg \left|\varepsilon^{\text{supply}}_{\text{G6P}}\right|$, so that flux control resided almost completely in the supply block ($C^{J}_{\text{supply}} = 0.999$), whereas the demand block determined the magnitude of concentration-control. The values of $\varepsilon^{\text{demand}}_{\text{G6P}}$ and $\varepsilon^{\text{GS}}_{\text{G6P}}$ were in good agreement and G6P may therefore be considered a regulatory metabolite of the demand block (see [232]).

Despite the feedback inhibition of HK by G6P, the supply block was almost completely insensitive to G6P ($\varepsilon^{\text{supply}}_{\text{G6P}} = -0.002$). This situation is explained by the very low flux-control coefficient of HK within the supply block (Fig. 6.3A). Using Eq. 6.1, the supply elasticity can be expressed as $\varepsilon^{\text{supply}}_{\text{G6P}} = C^{J_{\text{supply}}}_{\text{HK}} \varepsilon^{\text{HK}}_{\text{G6P}}$. A small $C^{J_{\text{supply}}}_{\text{HK}}$ value therefore cancels the feedback inhibition of HK by G6P which is described by $\varepsilon^{\text{HK}}_{\text{G6P}}$.

Although it is virtually uncontested that, within the supply block, GLUT controls the glucose uptake flux under basal conditions, the flux-control distribution between GLUT and HK during exercise and insulin stimulation is the topic of ongoing debate

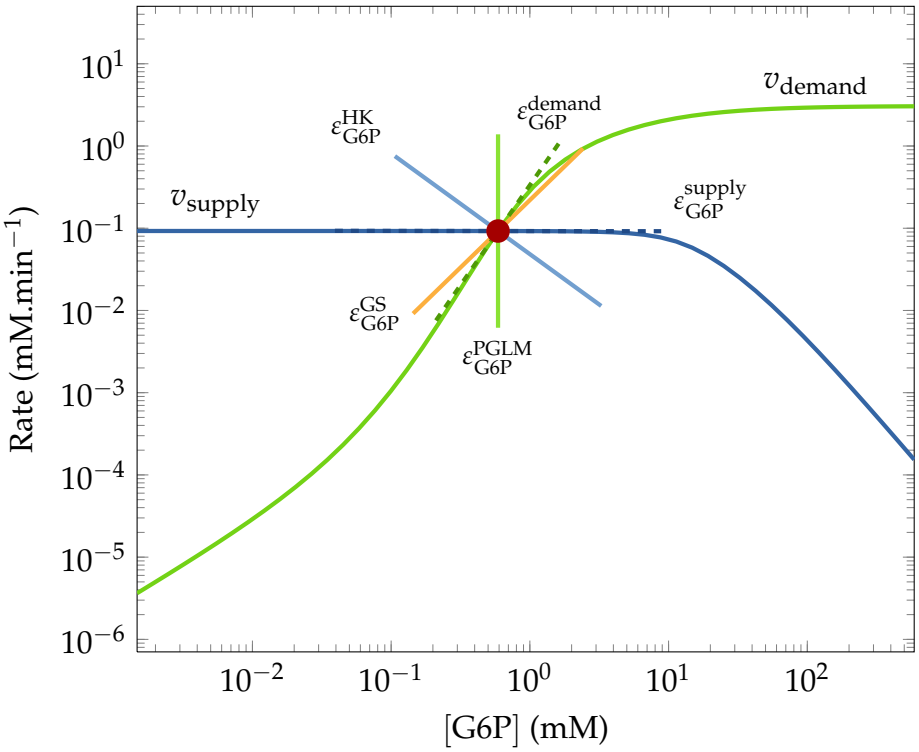

Figure 6.2: Supply-demand rate characteristics around G6P. G6P was treated as a clamped metabolite and its concentration was varied in a suitable range around its steady-state concentration. The rates of the supply and demand blocks were calculated for each G6P concentration. The intersection (red circle) of the supply and demand rates represents the steady-state of the system. The demand block is much more sensitive to G6P than the supply block (compare $\varepsilon^{\text{supply}}_{\text{G6P}}$ and $\varepsilon^{\text{demand}}_{\text{G6P}}$). This indicates that the supply block controls the flux through the system, whereas the demand block determines the magnitude of concentration control. Since GLUT controls the flux within the supply block, inhibition of HK by G6P (designated by the negative slope $\varepsilon^{\text{HK}}_{\text{G6P}}$) has little effect on the sensitivity of the supply block towards G6P. Both $\varepsilon^{\text{PGLM}}_{\text{G6P}}$ and $\varepsilon^{\text{GS}}_{\text{G6P}}$ contribute significantly towards $\varepsilon^{\text{demand}}_{\text{G6P}}$.

[235, 236]. While we concede that an increase in GLUT activity will inevitably result in the redistribution of flux control towards HK, it should be pointed out that complete flux control of glucose uptake by HK, whether achieved by activation of GLUT or inhibition of HK, can only be attained at the cost of GLUT operating near equilibrium. This point can be demonstrated visually by shifting up the v_{GLUT} curve (blue) in Fig. 6.3A such that $\varepsilon^{\text{HK}}_{\text{Glc}_i}$ approaches zero and HK thus gains almost all flux control (steady-state 2 in Fig. 6.3A). During insulin stimulation, the result of elevated glycemia, it would be disadvantageous for GLUT to operate near equilibrium, as under this condition the internal glucose concentration would rise to match the external concentration, which could be as high as 14 mM [12]. We are therefore of the

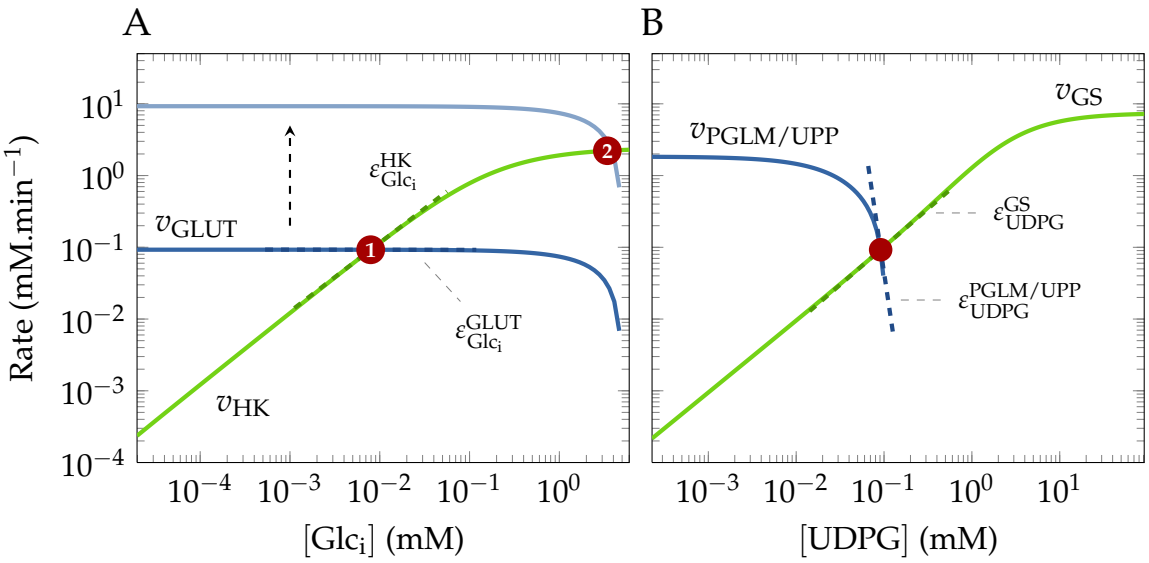

Figure 6.3: Nested supply-demand rate characteristics around Glc_i and UDPG. The concentration of G6P was clamped at its steady-state value. Red circles indicate steady-states. A) Glc_i was treated as a clamped metabolite and its concentration was varied in a suitable range around its steady-state concentration. The GLUT and HK rates were calculated for each Glc_i concentration. From the values of $\varepsilon^{GLUT}_{Glc_i}$ and $\varepsilon^{HK}_{Glc_i}$ (at steady state 1) it is clear that the HK reaction is much more sensitive to Glc_i than the GLUT reaction. The flux through the G6P supply block is thus controlled by GLUT. If the GLUT rate were activated such that HK controls the flux (at steady-state 2), the concentration of Glc_i would approach that of Glc_o. B) Rate characteristics were similarly generated around UDPG. From the values of $\varepsilon^{PGLM/UPP}_{UDPG}$ and ε^{GS}_{UDPG} it is clear that the PGLM/UPP block, which is near equilibrium, is much more sensitive to UDPG than GS. GS therefore controls the flux within the G6P demand block.

opinion that, in response to insulin stimulation, the control of glucose uptake by HK should not be expected to increase to the point where it exceeds that of GLUT.

The demand block, on the other hand, was highly sensitive to G6P. Using Eq. 6.1, the demand elasticity can be expressed as $\varepsilon^{demand}_{G6P} = C^{J_{demand}}_{PGLM}\varepsilon^{PGLM}_{G6P} + C^{J_{demand}}_{GS}\varepsilon^{GS}_{G6P}$. Since GS had the most flux control within the demand pathway ($C^{J_{demand}}_{GS} = 0.886$, Fig. 6.3B), the majority of the demand block's sensitivity to G6P can be ascribed to the feedforward activation of GS by G6P. However, since PGLM and UPP are near equilibrium, the term $C^{J_{demand}}_{PGLM}\varepsilon^{PGLM}_{G6P}$ approaches ε^{GS}_{UDPG}, which is not negligible (Fig. 6.3B, and see Section 6.9). The large flux control of GS within the demand block ($C^{J_{demand}}_{GS}$) was not the result of GS being saturated with UDP-glucose (UDPG), but rather resulted from PGLM/UPP being near equilibrium (Fig. 6.3B). Note that stating that GS controls the flux within the isolated demand block is not equivalent

to stating that GS controls the glycogen synthetic flux, which as we have seen is controlled by the supply block (GLUT in particular).

Regulation of glycogen synthase does not alter the glycogen synthetic flux

It is often stated in the literature that GS is the *rate-limiting* enzyme of glycogen synthesis; usually without any supporting citation (see for example [34, 51, 109, 127, 146, 169]). The contention that GS is the flux-controlling enzyme of glycogen synthesis is presumably based on the dated perception that cooperativity and allosterism are responsible for flux control; more so when accompanied by covalent modification. Our results, however, showed that, although GS controls the flux within the *isolated* demand block, the overall glycogen synthetic flux is controlled by glucose import. This raises questions about the function of the regulation of GS activity.

Increasing L_0 through the range of values (0.25–185) corresponding to the range of complete GS dephosphorylation to complete phosphorylation did not result in an increase in the flux, but instead increased the steady-state concentration of G6P proportionally (Fig. 6.4A). The concomitant effect on the flux and steady-state G6P concentration resulting from a change in L_0 is quantified by the co-response coefficient $\Omega_{L_0}^{J:\mathrm{G6P}}$. A small co-response indicates a small change in the flux relative to the change in steady-state G6P concentration. $\Omega_{L_0}^{J:\mathrm{G6P}}$ was virtually zero for the entire range of possible L_0 values (Fig. 6.4B). A deviation from zero, the result of HK inhibition by G6P, was only observed at very high values of L_0. This indicates that phosphorylation and dephosphorylation have no effect on the glycogen synthetic flux, but instead alter the G6P concentration. The expression for $\Omega_{L_0}^{J:\mathrm{G6P}}$ is given by

$$\Omega_{L_0}^{J:\mathrm{G6P}} = \frac{C^{J}_{\mathrm{demand}}\varepsilon^{\mathrm{demand}}_{L_0}}{C^{\mathrm{G6P}}_{\mathrm{demand}}\varepsilon^{\mathrm{demand}}_{L_0}} \tag{6.10}$$

$$= \frac{C^{J}_{\mathrm{demand}}}{C^{\mathrm{G6P}}_{\mathrm{demand}}} \tag{6.11}$$

$$= \varepsilon^{\mathrm{supply}}_{\mathrm{G6P}} \quad \text{(by Eqs. 6.8 and 6.9)} \tag{6.12}$$

The low values of $\Omega_{L_0}^{J:\mathrm{G6P}}$ are thus a direct consequence of the insensitivity of the supply block to G6P, which in turn is the result of the high flux-control coefficient of GLUT. The regulation of GS by phosphorylation does therefore not appear to function as a mechanism of flux control.

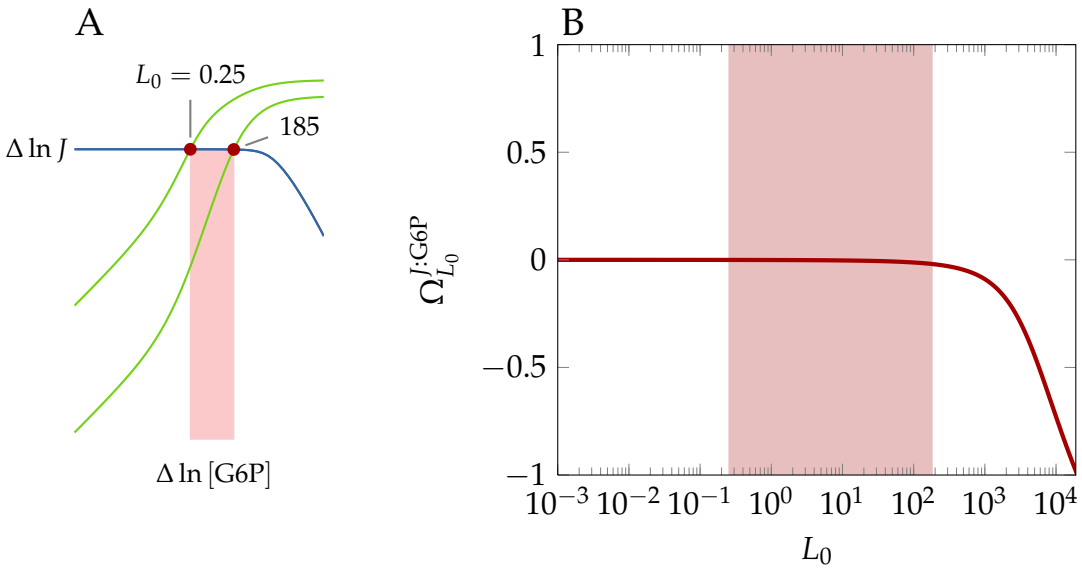

Figure 6.4: Effect of changes in L_0 on the flux and steady-state G6P concentration. A) Supply-demand rate characteristic around G6P showing the change in steady-state that results from increasing L_0 from 0.25 (corresponding to the value for completely dephosphorylated GS, Table 5.2) to 185 (corresponding to the value for completely phosphorylated GS). No change in the flux is observed, but a large change is seen in the G6P concentration. The supply and demand rates are shown in blue and green. Steady-states are shown in red. B) Dependence of $\Omega_{L_0}^{J:\mathrm{G6P}}$ on L_0. Over the entire theoretical range of values for L_0 (indicated by the shaded area), $\Omega_{L_0}^{J:\mathrm{G6P}}$ is close to zero. This indicates that a change in L_0 results in a much larger change in G6P concentration than in the flux.

Similarly, increasing the ATP concentration through a physiologically relevant range (5–8.2 mM) did not decrease the flux, but also slightly increased the G6P concentration (Fig. 6.5A). For each ATP value the ADP value was adjusted such that the sum of ATP and ADP remained constant. Within the physiological range of ATP concentrations $\Omega_{\mathrm{ATP}}^{J:\mathrm{G6P}}$, like $\Omega_{L_0}^{J:\mathrm{G6P}}$, approached zero (Fig. 6.5B). A large $\Omega_{\mathrm{ATP}}^{J:\mathrm{G6P}}$ value was observed at low ATP concentrations where ATP is limiting to and ADP inhibits HK. The expression for $\Omega_{\mathrm{ATP}}^{J:\mathrm{G6P}}$ is somewhat more complicated because ATP is an effector of both the supply and demand blocks:

$$\Omega_{\mathrm{ATP}}^{J:\mathrm{G6P}} = \frac{C_{\mathrm{supply}}^{J}\varepsilon_{\mathrm{ATP}}^{\mathrm{supply}} + C_{\mathrm{demand}}^{J}\varepsilon_{\mathrm{ATP}}^{\mathrm{demand}}}{C_{\mathrm{supply}}^{\mathrm{G6P}}\varepsilon_{\mathrm{ATP}}^{\mathrm{supply}} + C_{\mathrm{demand}}^{\mathrm{G6P}}\varepsilon_{\mathrm{ATP}}^{\mathrm{demand}}} \tag{6.13}$$

$$= \frac{\varepsilon_{\mathrm{G6P}}^{\mathrm{demand}}\varepsilon_{\mathrm{ATP}}^{\mathrm{supply}} - \varepsilon_{\mathrm{G6P}}^{\mathrm{supply}}\varepsilon_{\mathrm{ATP}}^{\mathrm{demand}}}{\varepsilon_{\mathrm{ATP}}^{\mathrm{supply}} - \varepsilon_{\mathrm{ATP}}^{\mathrm{demand}}} \quad \text{(by Eqs. 6.7, 6.8, and 6.9)} \tag{6.14}$$

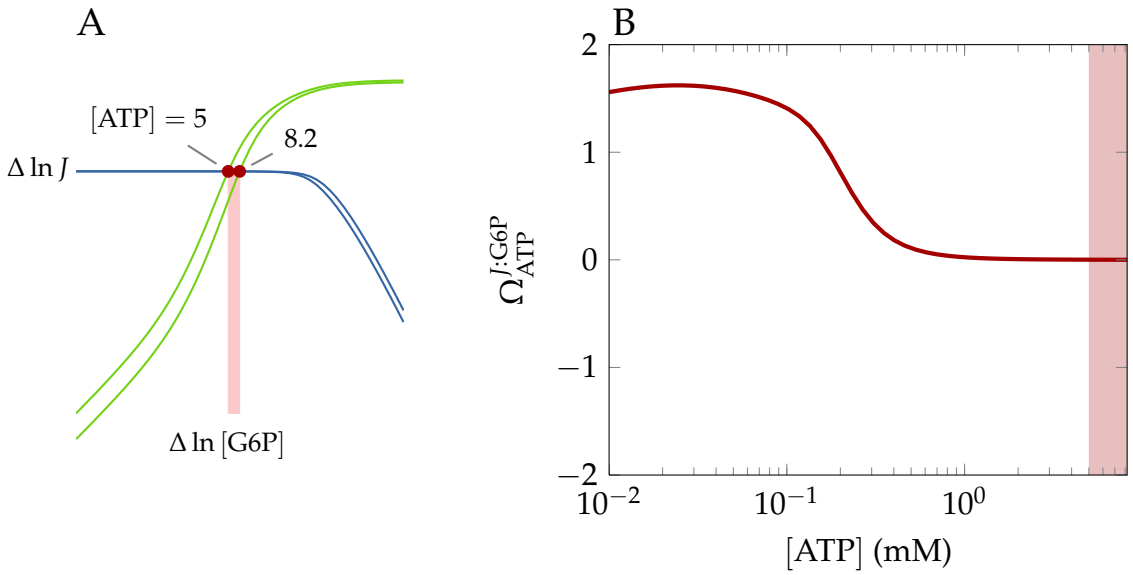

Figure 6.5: Effect of changes in ATP concentration on the flux and steady-state G6P concentration. A) Supply-demand rate characteristic around G6P showing the change in steady-state that results from increasing the ATP concentration from 5 to 8.2 mM. The increase in ATP has no effect on the flux, but leads to a small increase in G6P concentration. The supply and demand rates are shown in blue and green. Steady-states are shown in maroon. Concomitant changes in ADP were made so that the total ADP and ATP concentrations remained constant. B) Dependence of $\Omega^{J:G6P}_{ATP}$ on the ATP concentration. Over the complete range of ATP concentrations between 5 and 8.2 mM (indicated by the shaded area), $\Omega^{J:G6P}_{ATP}$ is close to zero. This indicates that a change in ATP concentration has essentially no effect on the flux, but results in a change in G6P concentration.

HK is the only enzyme in the supply block that is sensitive to ATP, but since HK does not control the glucose uptake flux, the value of $\varepsilon^{supply}_{ATP}$, like that of $\varepsilon^{supply}_{G6P}$, is close to zero. It thus follows that $\Omega^{J:G6P}_{ATP}$ has a value close to zero. Again this low value can be ascribed to the large flux control of GLUT within the demand block.

It is thus clear that regulation of the GS activity, within physiological limits, has no effect on the glycogen synthetic flux, but alters the steady-state concentration of metabolites in the pathway. This situation arises from the fact that GLUT controls the pathway flux and, by being insensitive to its immediate product, is essentially disconnected from and inelastic to the rest of the pathway. The only effective way to increase the glycogen synthetic flux is to increase the rate of glucose import.

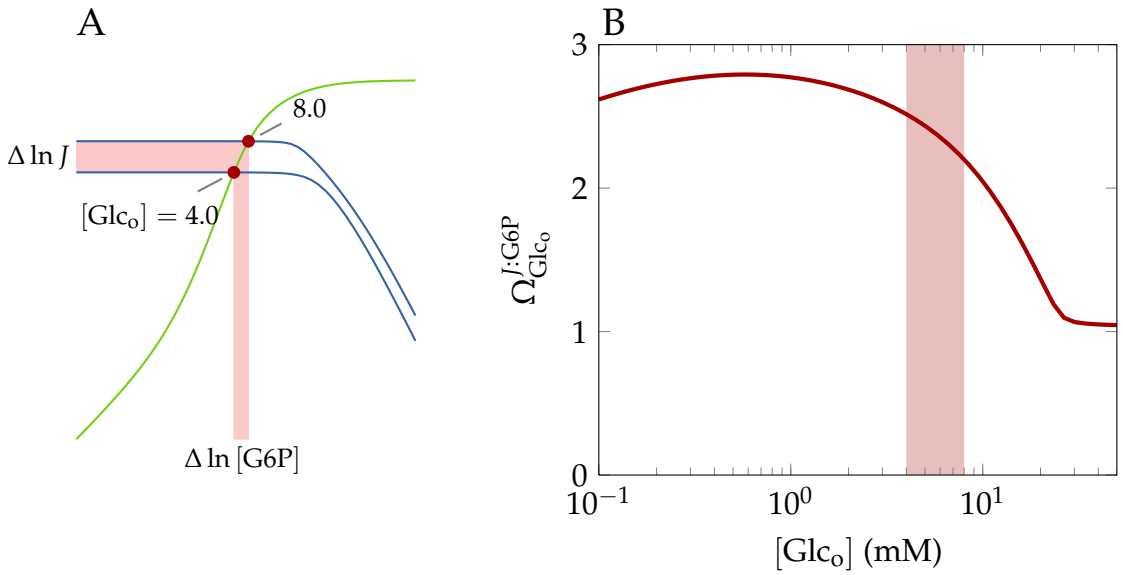

Figure 6.6: Effect of changes in external glucose concentration on the flux and steady-state G6P concentration. A) Supply-demand rate characteristic around G6P showing the change in steady-state that results from increasing the external glucose concentration from euglycemic (4.0) to hyperglycemic (8.0 mM) conditions. The increase in external glucose concentration results in a larger increase in the flux than in the steady-state G6P concentration. The supply and demand rates are shown in blue and green. Steady-states are shown in maroon. B) Dependence of $\Omega^{J:G6P}_{Glc_o}$ on the external glucose concentration. The shaded area indicates the range from euglycemic to hyperglycemic conditions.

Regulation of glycogen synthase improves glucose-6-phosphate homeostasis

The observation that L_0 and the ATP concentration are able to affect the steady-state concentration of G6P despite having no effect on the flux, suggests a role for the regulation of GS other than the regulation of flux, namely the homeostatic maintenance of metabolite concentrations. In non-diabetics, the plasma glucose concentration can be as low as 4 mM and increase, depending on diet, to about 8 mM after a meal [226]. Such an increase in the external glucose concentration leads to increased GLUT activity and thus increases the glycogen synthetic flux and also the steady-state G6P concentration. Figure 6.6A shows the increase in flux and steady-state G6P concentration resulting from an increase in external glucose from 4 to 8 mM. It is clear that the change in G6P concentration was less than the concomitant change in flux. As before, the effect of external glucose on J and the G6P concentration can be quantified with the co-response coefficient:

$$\Omega^{J:\mathrm{G6P}}_{\mathrm{Glc_o}} = \frac{C^{J}_{\mathrm{supply}}\varepsilon^{\mathrm{supply}}_{\mathrm{Glc_o}}}{C^{\mathrm{G6P}}_{\mathrm{supply}}\varepsilon^{\mathrm{supply}}_{\mathrm{Glc_o}}} \tag{6.15}$$

$$= \frac{C^{J}_{\mathrm{supply}}}{C^{\mathrm{G6P}}_{\mathrm{supply}}} \tag{6.16}$$

$$= \varepsilon^{\mathrm{demand}}_{\mathrm{G6P}} \quad \text{(by Eqs. 6.7 and 6.9)} \tag{6.17}$$

The ability of the glycogen synthesis pathway to buffer its metabolites (G6P in particular) against large increases in the system flux therefore depends on the sensitivity of the demand block to G6P. A high $\Omega^{J:\mathrm{G6P}}_{\mathrm{Glc_o}}$ value was observed at basal external glucose levels (Fig. 6.6B). As the external glucose increased, however, the system rapidly lost its ability to buffer G6P. Let us also consider how $\Omega^{J:\mathrm{G6P}}_{\mathrm{Glc_o}}$ changes with respect to L_0 and the ATP concentration. Over the range of possible L_0 values, $\Omega^{J:\mathrm{G6P}}_{\mathrm{Glc_o}}$ initially increased, but then decreased (Fig. 6.7). Over the same range, L_0 had no effect on the flux, but increased the G6P concentration. Note, however, that even though there was an optimal value of L_0 after which no further increase in $\Omega^{J:\mathrm{G6P}}_{\mathrm{Glc_o}}$ was observed, the extent of GS inhibition continues to increase with L_0 so that GS would eventually gain all flux control, resulting in a decrease in flux. At very large values of L_0 the activity of GS tends to zero. It is therefore not inhibition *per se* that increases $\Omega^{J:\mathrm{G6P}}_{\mathrm{Glc_o}}$, but rather the ability to bring about a significant further increase in the fraction of GS that is in the conformation (T) that is not favoured by G6P.

$\Omega^{J:\mathrm{G6P}}_{\mathrm{Glc_o}}$ also increased with increasing ATP (Fig. 6.7), but this increase was less pronounced than the increase induced by L_0. ATP had no effect on the flux, but slightly increased the G6P concentration. Considering these weak effects of ATP inhibition, one may wonder why ATP inhibits both glycogen synthesis and glycogen degradation. The latter case may be rationalized by considering that GP should be sensitive to the energy charge of the cell (see Section 6.10), but by the same reasoning ATP should stimulate, and not inhibit, GS. While basal muscle ATP concentrations vary between species, the ATP concentration changes very little within muscle of a particular species. We therefore speculate that ATP inhibition is not an active mechanism of GS regulation, but rather confers basal or "background" G6P sensitivity on GS. Since the ATP concentration varies little, ATP inhibition can be considered as a constant decrease in the affinity of GS for G6P. With regard to GP on the other hand, small changes in the ATP concentration are amplified as large changes in AMP

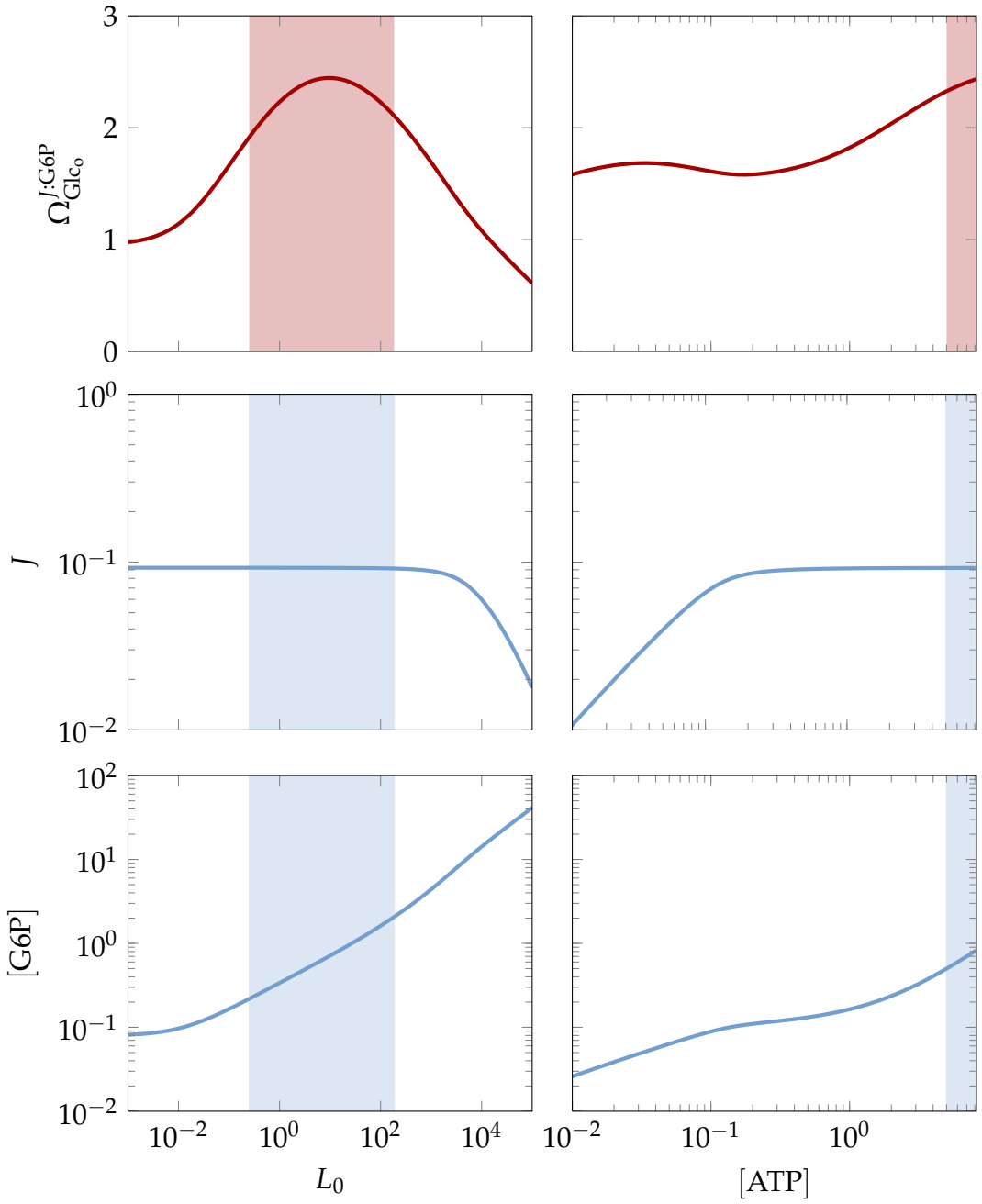

Figure 6.7: Effect of covalent and allosteric modification of GS on G6P homeostasis in response to elevated external glucose concentration. Over the physiological range of L_0 (shaded area) an increase in external glucose resulted in a larger change in flux J than in G6P. An increase in L_0 generally lead to improved G6P homeostasis (as measured by $\Omega^{J:G6P}_{Glc_o}$), but beyond a certain limit further increases in L_0 weakened homeostasis. Over the range of ATP concentrations from 5.0 to 8.2 mM (shaded area) an increase in external glucose resulted in a larger change in J than in G6P. An increase in ATP concentration led to improved G6P homeostasis (as measured by $\Omega^{J:G6P}_{Glc_o}$). The external glucose concentration was 5 mM, the ATP concentration was 8.2 mM when L_0 was varied, and L_0 was 5.6 when ATP was varied. Units are in mM and minutes.

by the enzyme adenylate kinase [77], but even in this regard it is possible that ATP inhibition simply serves to enhance the sensitivity of GP to AMP.

Using the model GlySynthExp, we have now demonstrated that allosteric and covalent regulation of GS do not function to regulate the flux through the pathway, but instead function to buffer the concentration of G6P within a narrow range in spite of the several fold increase in system flux resulting from increased external glucose. In particular, it was shown that this homeostasis of G6P results from the fact that both GS phosphorylation and high ATP concentrations increase the sensitivity of the demand block to G6P. A prolonged increase in external glucose concentration will, however, result in elevated secretion of insulin by the pancreas. Insulin secretion enhances translocation of cytosolic GLUT4 to the plasma membrane and inhibits the phosphorylation of GS. In order to consider the function of insulin stimulation in glycogen metabolism, a more sophisticated model that also describes GLUT4 trafficking and GS phosphorylation in response to insulin is required.

6.5 Degree of GS phosphorylation as a function of PKA and insulin

In the model GlySynth GS phosphorylation is not modelled as an explicit change to the parameter L_0 (as in GlySynthExp), but rather as the interconversion between GS states, each of which exhibits Monod-Wyman-Changeux (MWC) kinetics, but each with a different value for L_{0i}. However, the total ratio of unliganded GS in the T conformation to that in the R conformation can still be expressed as a function, $L_{0,\text{app}}$, of the various L_{0i} values and the concentrations of GS in each phosphorylation state. These two approaches are to a large extent equivalent, but GlySynthExp does not allow for the possibility that ligands of GS such as G6P could also affect the phosphorylation state of GS. Stimuli such as cyclic AMP (cAMP) (which increases the effective cAMP-dependent protein kinase (PKA) concentration) and insulin that affect the degree of GS phosphorylation will also affect $L_{0,\text{app}}$.

The dependence of $L_{0,\text{app}}$ on the concentrations of PKA and insulin was investigated with a parameter portrait (Fig. 6.8). As expected, the value of $L_{0,\text{app}}$ increased with the concentration of PKA, indicating an increase in the degree of GS phosphorylation. The increase in $L_{0,\text{app}}$ in response to PKA occurred in two phases, with the steepest increase near the maximal physiological concentration of PKA ($\sim 0.5\,\mu$M [237]). The effect of insulin, which inhibits the phosphorylation of GS by glycogen

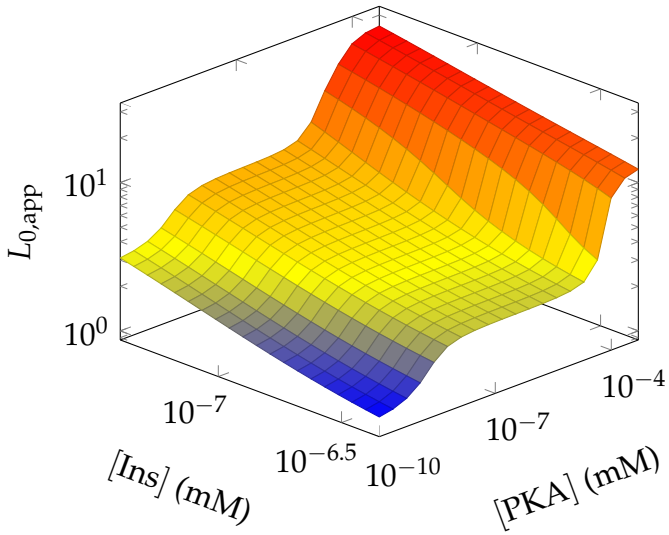

Figure 6.8: Dependence of $L_{0,\text{app}}$ on the concentration of PKA and insulin. PKA phosphorylates site 2 of GS and activates PhK which is also a site 2 kinase. In addition, PKA inhibits PP1 which dephosphorylates all GS phosphorylation sites. Insulin inhibits GSK3 and thus decreases the value of $L_{0,\text{app}}$.

synthase kinase 3 (GSK3) and thus lowers $L_{0,\text{app}}$, was most pronounced when the PKA concentration was sufficiently high (Fig. 6.8).

The increase in $L_{0,\text{app}}$ resulting from an increase in the concentration of PKA is both the consequence of increased phosphorylation at site 2 and of an increase in the phosphorylated form of protein phosphatase inhibitor 1 (I1), which in turn inhibits dephosphorylation of all GS phosphorylation sites. At basal concentrations of insulin ($\sim$ 40 pM), a rise in [PKA] initially increased the phosphate content of site 2 (due to phosphorylation by PKA and activated PhK), but phosphorylation at site 2 was not immediately followed by significant phosphorylation at site 2a (Fig. 6.9A). This result agrees with the finding by Nakielny *et al.* [109] that significant phosphorylation of site 2 *in vivo* is not accompanied by phosphorylation at site 2a, even though phosphorylation at site 2 enhances phosphorylation at site 2a *in vitro*, unless PP1 is significantly inhibited by activated I1. Based on these results, Nakielny *et al.* [109] question the significance of PKA as a GS kinase, proposing a role for PKA in the regulation of PP1 activity instead. A further increase in PKA did increase the phosphate content at site 2a, but since PKA does not phosphorylate site 2a, this increase can only be ascribed to PP1 inhibition. Phosphorylation of site 2a was accompanied by a concurrent increase in the phosphate content of all phosphorylation sites. The initial phosphorylation of site 2 and subsequent phosphorylation of the other sites

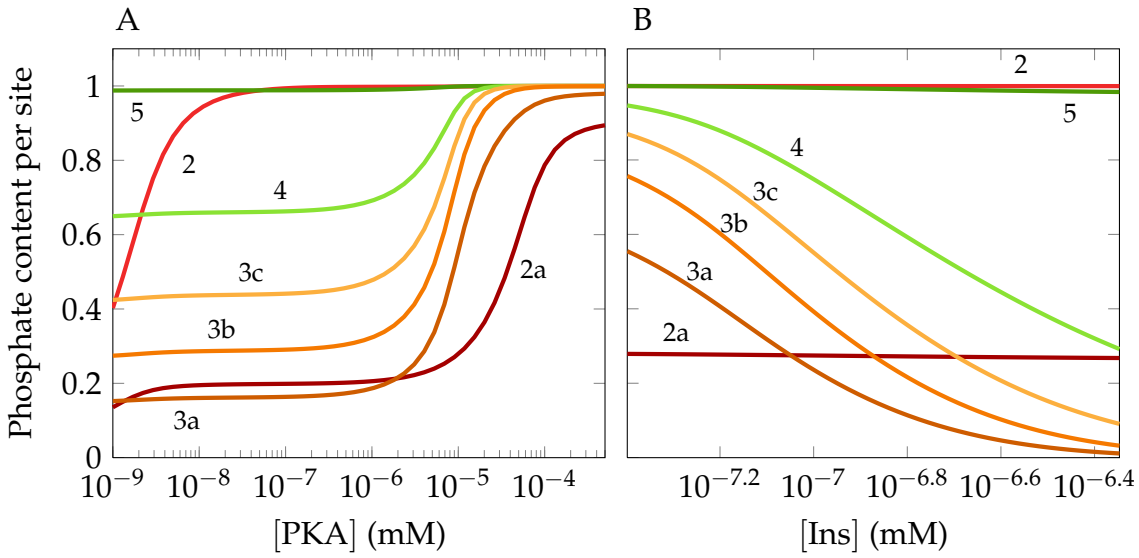

Figure 6.9: Dependence of GS phosphate content per site as a function of the PKA and insulin concentrations. A) Increasing from low concentrations of PKA, site 2 is phosphorylated by PKA and as a result of PhK activation in response to PKA. Further increasing PKA leads to the inactivation of PP1 and thus extensive phosphorylation of all GS phosphorylation sites. B) Increasing the insulin concentration has little effect on sites 2, 2a, and 5, but sites that are phosphorylated by GSK3, which is inhibited by insulin, are gradually dephosphorylated in response to insulin.

at a higher concentration of PKA explain the biphasic increase in $L_{0,\text{app}}$ in response to PKA.

At very low PKA concentrations, the phosphatase activity was sufficiently high that GS was substantially dephosphorylated at the inhibitory sites (2, 2a, 3a, 3b, see Fig. 6.9A), whereas at high PKA concentrations, GS was almost completely phosphorylated at most sites. Under these conditions, a decrease in the activity of GSK3, mimicking insulin stimulation, is not expected to activate GS markedly. In the former case GS is already activated to such an extent that insulin stimulation is without effect. In the latter case, on the other hand, PP1 is inhibited to such an extent that it cannot dephosphorylate the GSK3 sites. At a concentration of PKA that approaches the physiological maximum, however, insulin stimulation resulted in significant dephosphorylation of the sites phosphorylated by GSK3 (sites 4, 3c, 3b, and 3a; Fig. 6.9B). The phosphate content of sites 5, 2, and 2a that are not directly affected by GSK3 remained unchanged, as was also found by Parker *et al.* [238].

6.6 Homeostasis in response to change in insulin concentration

A euglycemic clamp is an experimental setup in which the external glucose concentration is kept at a constant basal concentration by infusion of glucose while the insulin concentration may be varied [239]. Here we will consider the homeostatic properties of glycogen synthesis in response to changes in kinase and insulin concentrations during a euglycemic clamp.

Using the glycogen synthesis model (GlySynthExp) in which GS phosphorylation is mimicked by an explicit change in L_0, we have already shown that an increase in L_0, up to a certain point, improves homeostasis with respect to G6P in response to changes in external glucose concentration. Using the model GlySynth, in which the complete GS phosphorylation cascade is included, we can now investigate the relationship between the degree of GS phosphorylation, as modulated by insulin and PKA, and G6P homeostasis. Since an increase in PKA leads to an increase in $L_{0,\text{app}}$, inhibition of GS as a result of PKA-induced phosphorylation is also expected to improve G6P homeostasis in response to elevated glycemia.

The effect of PKA on G6P homeostasis was investigated with parameter portraits in which $\Omega_{\text{Glc}_\text{o}}^{J:\text{G6P}}$, J, [G6P], and $L_{0,\text{app}}$ were plotted as a function of the PKA concentration (Fig. 6.10). As PKA increased, the value of $\Omega_{\text{Glc}_\text{o}}^{J:\text{G6P}}$ initially increased in two phases and then decreased. The overall variation in $\Omega_{\text{Glc}_\text{o}}^{J:\text{G6P}}$ was, however, rather modest. Even at very low concentrations of PKA more than 10% of GS was still phosphorylated at both sites 2a and 3a and about 40% was still phosphorylated at site 2 (Fig. 6.9), so that $\Omega_{\text{Glc}_\text{o}}^{J:\text{G6P}}$ was maintained at the high value of 2. No change in the flux J was observed, but G6P and $L_{0,\text{app}}$ increased in two phases, corresponding to the phosphorylation of site 2 and the inactivation of PP1.

The relationship between PKA and $\Omega_{\text{Glc}_\text{o}}^{J:\text{G6P}}$ differed from the ideal relationship that was found between L_0 and $\Omega_{\text{Glc}_\text{o}}^{J:\text{G6P}}$ (Fig. 6.7) in the GlySynthExp model. This difference is the result of at least two factors. First, in GlySynth, $L_{0,\text{app}}$ is a non-linear function of [PKA]. Second, the concentration of G6P, which changes with the degree of GS phosphorylation, can influence the degree of GS phosphorylation, which was not allowed in GlySynthExp. In order to elucidate the relationship between PKA and $\Omega_{\text{Glc}_\text{o}}^{J:\text{G6P}}$, we also considered to component values that constitute $\Omega_{\text{Glc}_\text{o}}^{J:\text{G6P}}$. We have shown that $\Omega_{\text{Glc}_\text{o}}^{J:\text{G6P}} = \varepsilon_{\text{G6P}}^{\text{demand}}$ (Eq. 6.17). As will be discussed in Section 6.9, $\varepsilon_{\text{G6P}}^{\text{demand}}$ is the sum of the partial flux-response coefficients of the isolated demand block with

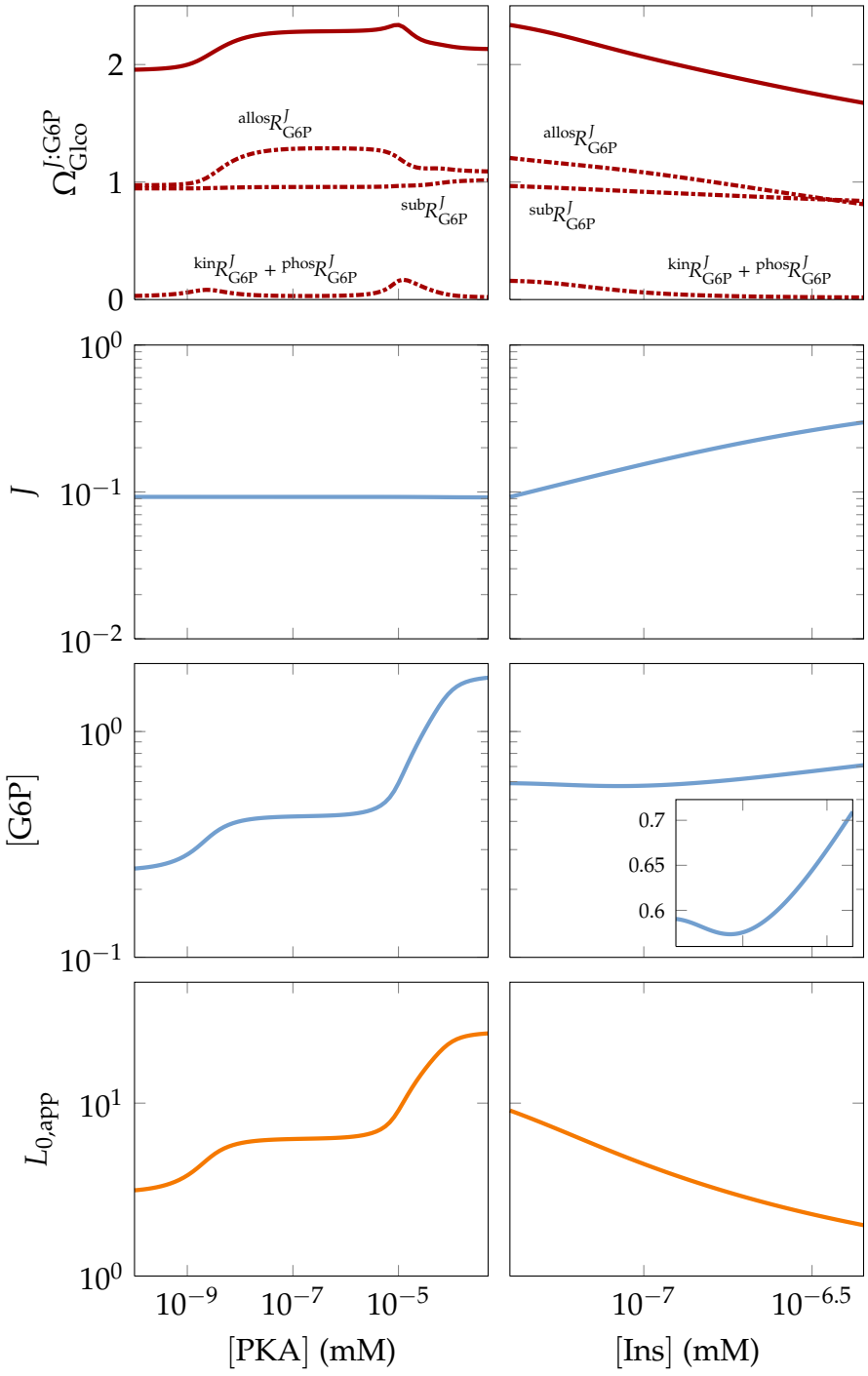

Figure 6.10: Dependence of $\Omega_{Glc_o}^{J:G6P}$, J, G6P, and $L_{0,app}$ on PKA and insulin. PKA initially increased and then decreased $\Omega_{Glc_o}^{J:G6P}$. PKA had no effect on the flux, J, but increased the concentration of G6P and $L_{0,app}$ in two phases. Insulin steadily lowered $\Omega_{Glc_o}^{J:G6P}$ with a small change in G6P and $L_{0,app}$. Insulin increased J. The insulin concentration was 40 pM when PKA was varied, and [PKA] was 1×10^{-5} mM when insulin was varied. Units are in mM and minutes.

respect to G6P:

$$\varepsilon^{\text{demand}}_{\text{G6P}} = {}^{\text{sub}}R^{J_{\text{demand}}}_{\text{G6P}} + {}^{\text{allos}}R^{J_{\text{demand}}}_{\text{G6P}} + {}^{\text{kin}}R^{J_{\text{demand}}}_{\text{G6P}} + {}^{\text{phos}}R^{J_{\text{demand}}}_{\text{G6P}} \tag{6.18}$$

These partial response coefficients were therefore also plotted as a function of [PKA] (Fig. 6.10). ${}^{\text{sub}}R^{J_{\text{demand}}}_{\text{G6P}}$, describing the function of G6P as a substrate of the demand block, remained near unity over the entire range of PKA concentrations. ${}^{\text{sub}}R^{J_{\text{demand}}}_{\text{G6P}}$, describing the function of G6P as activator of the demand block, initially increased with PKA, but decreased again at higher PKA concentrations. The sum of ${}^{\text{kin}}R^{J_{\text{demand}}}_{\text{G6P}}$ and ${}^{\text{phos}}R^{J_{\text{demand}}}_{\text{G6P}}$, describing the function of G6P as GS kinase inhibitor and GS phosphatase activator, peaked at the PKA concentrations where the largest changes in G6P and $L_{0,\text{app}}$ were observed.

In order to facilitate comparison to Fig. 6.7, the results in Fig. 6.10 were also plotted against the variable $L_{0,\text{app}}$ (Fig. 6.11). As was found with respect to L_0 in the appropriate range in Fig. 6.7, there was an almost linear relationship between G6P and $L_{0,\text{app}}$, but the flux, J, did not vary with $L_{0,\text{app}}$.

An increase in insulin, on the other hand, led to a steady decrease in $\Omega^{J:\text{G6P}}_{\text{Glc}_\text{o}}$ (Fig. 6.10), indicating that it weakens G6P homeostasis with respect to changes in the external glucose concentration. Although this decrease is ultimately the result of GS dephosphorylation ($L_{0,\text{app}}$ decreased as as insulin increased), it is explained by a decrease in the sensitivity of the demand block to G6P in its capacity as PGLM substrate, allosteric GS activator, GS kinase inhibitor, and GS phosphatase activator, as measured by the decreases in the partial response coefficients ${}^{\text{sub}}R^{J_{\text{demand}}}_{\text{G6P}}$, ${}^{\text{allos}}R^{J_{\text{demand}}}_{\text{G6P}}$, ${}^{\text{kin}}R^{J_{\text{demand}}}_{\text{G6P}}$, and ${}^{\text{phos}}R^{J_{\text{demand}}}_{\text{G6P}}$. The flux J increased with insulin over the entire range, but G6P initially decreased and then increased again at higher insulin concentrations (Fig. 6.10). The overall change in G6P in response to insulin was, however, very small compared to that in response to PKA.

These results indicate that GS phosphorylation, brought about by an increase in the concentration of PKA, functions to improve G6P homeostasis in response to changes in the external glucose concentration. Insulin, on the other hand, weakens this homeostasis. However, the modest increase in G6P, in spite of the large change in J, that resulted from insulin stimulation, suggests that insulin brings about G6P homeostasis by means of a different mechanism in which the supply and demand blocks are coordinately activated [13]. It is therefore instructive to also consider the value of $\Omega^{J:\text{G6P}}_{\text{Ins}}$, which quantifies the co-response of the flux and the steady-state G6P concentration to a change in insulin concentration. $\Omega^{J:\text{G6P}}_{\text{Ins}}$ is expressed as

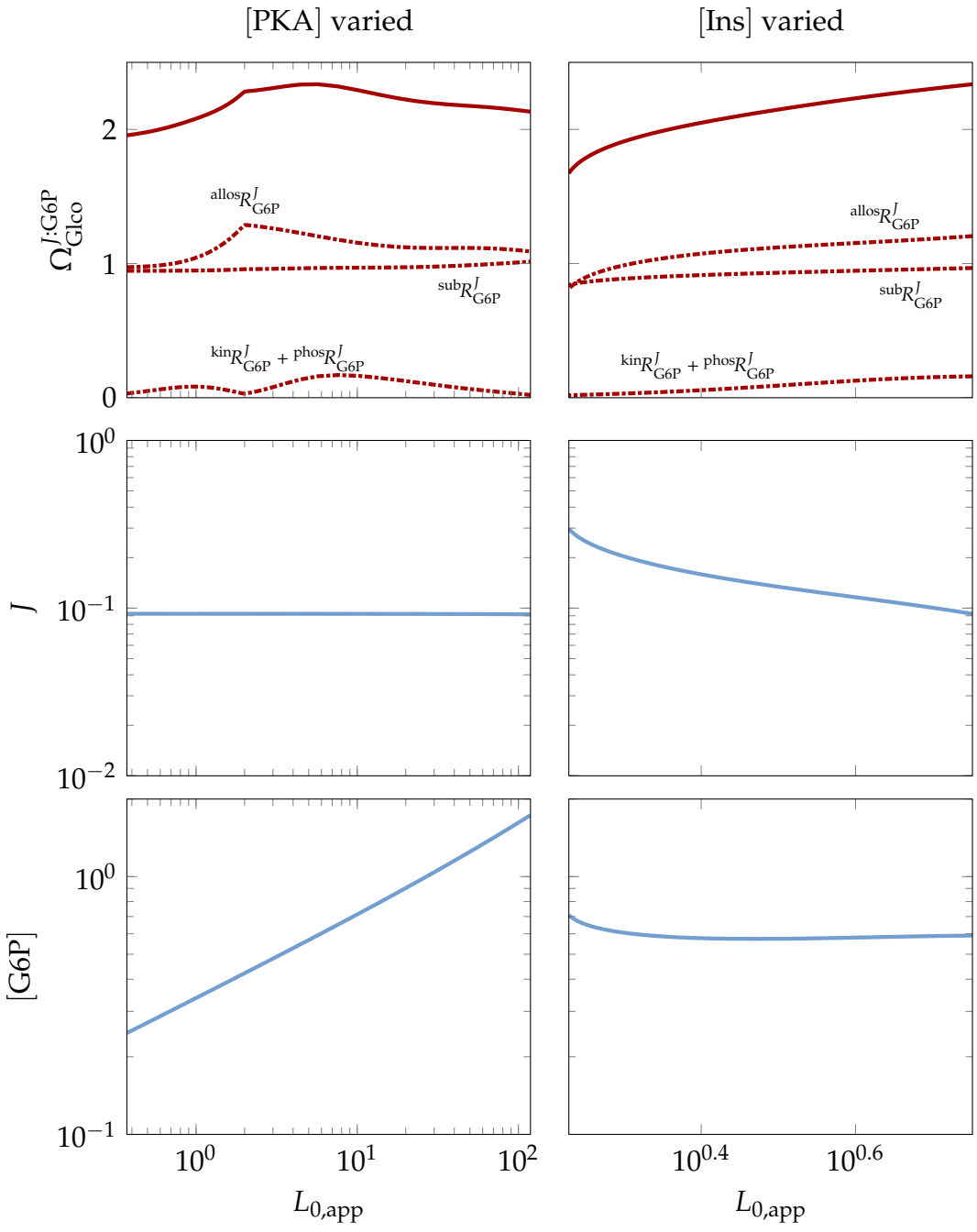

Figure 6.11: Correlation of $\Omega^{J:G6P}_{Glc_o}$, J, and G6P with $L_{0,app}$ in response to changes in PKA and insulin. The data in Fig. 6.10 were replotted against $L_{0,app}$. Conditions were as in Fig. 6.10

.

$$\Omega_{\text{Ins}}^{J:\text{G6P}} = \frac{C_{\text{supply}}^{J}\varepsilon_{\text{Ins}}^{\text{supply}} + C_{\text{demand}}^{J}\varepsilon_{\text{Ins}}^{\text{demand}}}{C_{\text{supply}}^{\text{G6P}}\varepsilon_{\text{Ins}}^{\text{supply}} + C_{\text{demand}}^{\text{G6P}}\varepsilon_{\text{Ins}}^{\text{demand}}} \tag{6.19}$$

$$= \frac{\varepsilon_{\text{G6P}}^{\text{demand}}\varepsilon_{\text{Ins}}^{\text{supply}} - \varepsilon_{\text{G6P}}^{\text{supply}}\varepsilon_{\text{Ins}}^{\text{demand}}}{\varepsilon_{\text{Ins}}^{\text{supply}} - \varepsilon_{\text{Ins}}^{\text{demand}}} \quad \text{(by Eqs. 6.7, 6.8, and 6.9)} \tag{6.20}$$

$$= \frac{\Omega_{\text{Glc}_\text{o}}^{J:\text{G6P}}\varepsilon_{\text{Ins}}^{\text{supply}} - \varepsilon_{\text{G6P}}^{\text{supply}}\varepsilon_{\text{Ins}}^{\text{demand}}}{\varepsilon_{\text{Ins}}^{\text{supply}} - \varepsilon_{\text{Ins}}^{\text{demand}}} \quad \text{(by Eq. 6.17)} \tag{6.21}$$

$$\simeq \frac{\Omega_{\text{Glc}_\text{o}}^{J:\text{G6P}}\varepsilon_{\text{Ins}}^{\text{supply}}}{\varepsilon_{\text{Ins}}^{\text{supply}} - \varepsilon_{\text{Ins}}^{\text{demand}}} \quad (\text{since } \varepsilon_{\text{G6P}}^{\text{supply}} \simeq 0) \tag{6.22}$$

The absolute value of $\Omega_{\text{Ins}}^{J:\text{G6P}}$ was much larger than unity for the entire range of insulin concentrations (Fig. 6.12A). When $\varepsilon_{\text{Ins}}^{\text{supply}} = \varepsilon_{\text{Ins}}^{\text{demand}}$, then $\Omega_{\text{Ins}}^{J:\text{G6P}}$ tends to infinity and perfect homeostasis in response to a change in insulin is observed regardless of the value of $\Omega_{\text{Glc}_\text{o}}^{J:\text{G6P}}$. If, however, $\varepsilon_{\text{Ins}}^{\text{supply}}$ and $\varepsilon_{\text{Ins}}^{\text{demand}}$ differ significantly, the contribution of $\Omega_{\text{Glc}_\text{o}}^{J:\text{G6P}}$ to the value of $\Omega_{\text{Ins}}^{J:\text{G6P}}$ is potentially substantial. As insulin increased, both $\varepsilon_{\text{Ins}}^{\text{supply}}$ and $\varepsilon_{\text{Ins}}^{\text{demand}}$ increased (Fig. 6.12B), but, as we have seen, $\varepsilon_{\text{G6P}}^{\text{demand}}$ decreased. $\varepsilon_{\text{G6P}}^{\text{supply}}$ remained close to zero over the entire range of insulin concentrations. Initially, the demand block was activated to a lesser extent than the supply block, but proceeded to match and then surpass activation of the supply block, before returning again to a lower insulin sensitivity. Increasing insulin from basal to stimulated levels (indicated by shaded area in Fig. 6.12) therefore had the effect that G6P initially decreased but then increased again (inset in Fig. 6.10).

Whether $\varepsilon_{\text{Ins}}^{\text{demand}}$ does indeed exceed $\varepsilon_{\text{Ins}}^{\text{supply}}$ depends on, amongst other factors, the concentration of PKA. At a lower PKA concentration, the activity of PP1 would be higher and thus GS would already be in a more active state so that the demand block is less sensitive to insulin. There is, however, experimental evidence that a transition from a regime during which G6P decreases to a regime during which G6P increases occurs as insulin is increased during a euglycemic clamp [240, 241], which supports our results that in the physiological range of insulin concentrations $\varepsilon_{\text{Ins}}^{\text{demand}}$ initially exceeded $\varepsilon_{\text{Ins}}^{\text{supply}}$. The transition from a basal insulin concentration to hyperinsulinemic conditions resulted in a large change in the glycogen synthetic flux with very little change in the concentration of G6P (Fig. 6.13). Note, however, that if the insulin concentration is increased even further, G6P will also increase significantly.

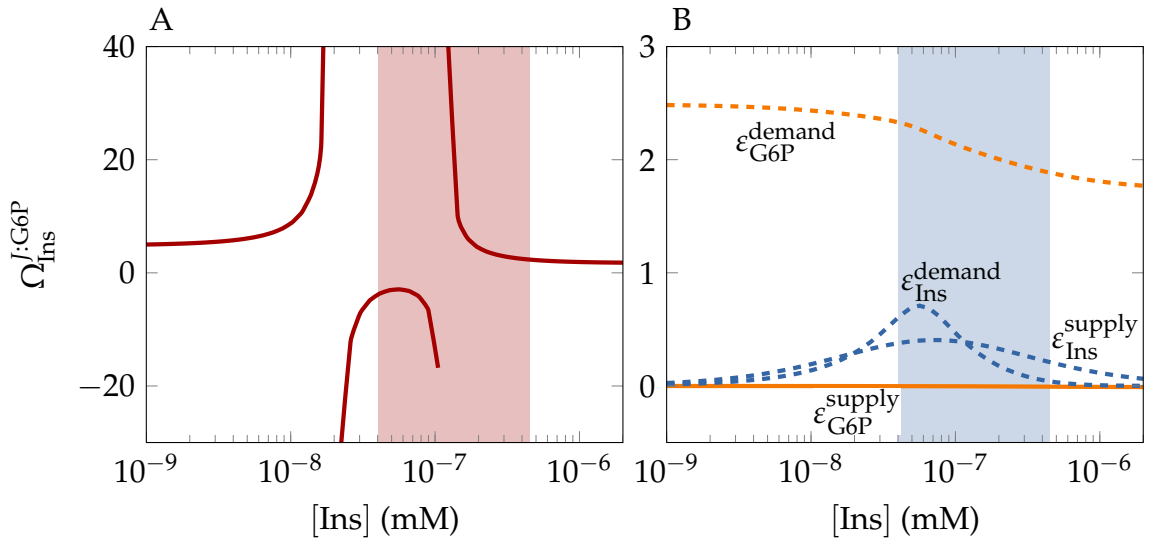

Figure 6.12: Homeostasis of G6P in response to insulin stimulation. Physiological normoinsulinemic and hyperinsulinemic concentrations are indicated with vertical lines. A) Dependence of $\Omega_{\text{Ins}}^{J:\text{G6P}}$ on insulin concentration. The absolute value of $\Omega_{\text{Ins}}^{J:\text{G6P}}$ is larger than unity over the entire range of insulin concentrations. This indicates that insulin stimulation results in a much larger change in flux than in G6P concentration. B) Dependence of $\varepsilon_{\text{G6P}}^{\text{supply}}$, $\varepsilon_{\text{G6P}}^{\text{demand}}$, $\varepsilon_{\text{Ins}}^{\text{supply}}$, and $\varepsilon_{\text{Ins}}^{\text{demand}}$ on insulin concentration.

Beyond the point where glucose uptake is sensitive to insulin, no further increase in flux or G6P concentration will occur.

Overall, these results suggest that covalent modification functions to improve the homeostasis of G6P in response to changes in external glucose concentration by virtue of increasing $\varepsilon_{\text{G6P}}^{\text{demand}}$. In addition, however, covalent modification (or more precisely, the reversal of covalent modification) also facilitates G6P homeostasis in response to changes in the insulin concentration by virtue of an increase in $\varepsilon_{\text{Ins}}^{\text{demand}}$ in addition to the increase in $\varepsilon_{\text{Ins}}^{\text{supply}}$ brought about by sequestration of GLUT4 to the plasma membrane.

The present analysis is similar to that of Schafer *et al.* [13], in which experimentally determined coefficients were employed to determine the proportional activation of the supply and demand blocks by insulin. Schafer *et al.* [13] calculated the ratio $\varepsilon_{\text{Ins}}^{\text{demand}}/\varepsilon_{\text{Ins}}^{\text{supply}}$ (their proportional activation term π_X^{AB}) according to the expression

$$\frac{\varepsilon_{\text{Ins}}^{\text{demand}}}{\varepsilon_{\text{Ins}}^{\text{supply}}} = \frac{1 - \varepsilon_{\text{G6P}}^{\text{demand}} \Omega_{\text{Ins}}^{\text{G6P}:J}}{1 - \varepsilon_{\text{G6P}}^{\text{supply}} \Omega_{\text{Ins}}^{\text{G6P}:J}} \tag{6.23}$$

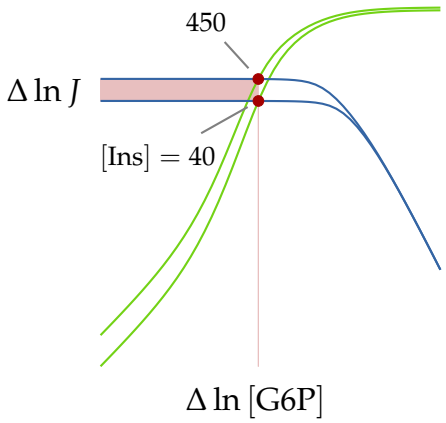

Figure 6.13: Supply-demand rate characteristic around G6P showing the change in steady-state that results from increasing the insulin concentration from basal (40 pM) to hyperglycemic (450 pM) conditions. The increase in insulin results in a much larger increase in the flux ($\Delta \ln J$) than in the steady-state G6P concentration ($\Delta \ln[\text{G6P}]$). The supply and demand rates are shown in blue and green. Steady-states are shown in maroon.

where $\Omega_{\text{Ins}}^{\text{G6P:}J}$ is the reciprocal of $\Omega_{\text{Ins}}^{J:\text{G6P}}$. They used values for $\varepsilon_{\text{G6P}}^{\text{supply}}$ and $\varepsilon_{\text{G6P}}^{\text{demand}}$ that were determined by Chase *et al.* [12] during a hyperinsulinemic clamp. Since the glycolytic flux is considered negligible in the treatment of Schafer *et al.* [13], they chose the value of $\varepsilon_{\text{G6P}}^{\text{supply}}$ that was determined at the lowest glycolytic flux by Chase *et al.* [12]. The values reported by Chase *et al.* [12] for this elasticity in the text (-0.185) and Table 3 (-0.015), however, differ markedly. Unless the other values in Table 3 are also to be considered erroneous, it appears that -0.015 is the correct value. Schafer *et al.* [13], however, used the value -0.185.

The plasma insulin concentrations during the hyperinsulinemic clamp were in the order of 216–308 mU.mL^{-1} [12], or 1–2 μM (1 U = 5.995 nmol), which is four orders of magnitude higher than physiological hyperinsulinemia ($\sim$ 450 pM [226]). Under these conditions glucose uptake and glycogen synthesis were completely insensitive to insulin in our model (not shown). Other rat studies [240, 241] using insulin infusion rates and durations comparable to those of Chase *et al.* [12] report nanomolar plasma insulin concentrations, leading us to suspect that the micromolar values reported by Chase *et al.* [12] are a misprint.

Schafer *et al.* [13] obtained values for $\Omega_{\text{Ins}}^{\text{G6P:}J}$ from the slopes of the graphs of $\ln[\text{G6P}]$ against $\ln J$ for rats fasted 6 hours and 24 hours using experimental results from Rossetti & Hu [241]. In these experiments the insulin concentration was varied in the range 250–2700 pM. Schafer *et al.* [13] found $\Omega_{\text{Ins}}^{\text{G6P:}J}$ to be small (0.15–0.28)

Table 6.1: Comparison of control analytic coefficients compiled or calculated by Schafer *et al.* [13] from experimental data to our model values. Symbols used in [13] are given in parentheses. The experimental values were determined at various insulin concentrations, but mostly under hyperinsulinemic conditions. The model values were calculated at an insulin concentration of 450 pM, a typical physiological hyperinsulinemic concentration.

Coefficient	Schafer *et al.* [13]	Model value
$\varepsilon^{\text{demand}}_{\text{G6P}}$ (*in vivo* ε^{B}_{M})	1.9	1.89
$\Omega^{\text{G6P:}J}_{\text{Ins}}$ (τ)	0.15–0.28	0.43
$\varepsilon^{\text{demand}}_{\text{Ins}}/\varepsilon^{\text{supply}}_{\text{G6P}}$ (π^{AB}_{X})	0.44–0.7	0.19

and, within accuracy, independent of the insulin concentration. Our results, however, show that while the absolute value of $\Omega^{\text{G6P:}J}_{\text{Ins}}$ is indeed small (< 1) over the entire range of insulin concentrations, $\Omega^{\text{G6P:}J}_{\text{Ins}}$ can also be negative (for insulin concentrations in which activation of glycogen synthesis exceeds activation of glucose uptake) and zero (at the points where glycogen synthesis and glucose uptake are stimulated in equal proportions). This discrepancy is of little consequence to the conclusions drawn by Schafer *et al.* [13] regarding the function of covalent modification in G6P homeostasis, but demonstrates that, although both glucose uptake and glycogen synthesis are activated by insulin, the proportion to which they are activated is not independent of the insulin concentration.

Values of 0.7 (6 hour fasted rats) and 0.44 (24 hour fasted rats) were determined for the ratio $\varepsilon^{\text{demand}}_{\text{Ins}}/\varepsilon^{\text{supply}}_{\text{Ins}}$, indicating that glucose uptake is stimulated to a greater extent than glycogen synthesis during hyperinsulinemic conditions [13]. Our results agree with this finding, but predicts that the converse will be true at basal insulin concentrations. This prediction is supported by the observation that the concentration of G6P initially decreases and then increases with insulin stimulation [240, 241]. Overall, our findings are in good agreement with those of Schafer *et al.* [13]. A comparison of our and their results is shown in Table 6.1. Our values were calculated under typical physiological hyperinsulinemic conditions (450 pM).

6.7 Effect of glycolysis on the flux control of glycogen synthesis

Up to now we have assumed that the glycolytic flux is negligible under conditions of glycogen synthesis. In recognition that this is not always a reasonable assumption,

Chase *et al.* [12] determined the control properties of glycogen synthesis experimentally at various glycolytic fluxes during a hyperinsulinemic clamp. They treated glycogen synthesis as a supply-demand system of G6P in which glucose uptake (gu) produces G6P and glycogen synthesis (gs) consumes G6P, but with glycolysis (glycol) as an additional demand process (Fig. 6.14). They determined ε^{gu}_{G6P} and ε^{gs}_{G6P} by modulating the plasma glucose concentration during a hyperinsulinemic clamp using the expressions

$$\varepsilon^{gu}_{G6P} = \frac{\dfrac{J_{gu_H} - J_{gu_E}}{J_{gu_E}} - \dfrac{[Glc_o]_H - [Glc_o]_E}{[Glc_o]_E}}{\dfrac{[G6P]_H - [G6P]_E}{[G6P]_E}} \tag{6.24}$$

and

$$\varepsilon^{gs}_{G6P} = \frac{\dfrac{J_{gs_H} - J_{gs_E}}{J_{gs_E}}}{\dfrac{[G6P]_H - [G6P]_E}{[G6P]_E}} \tag{6.25}$$

where J denotes the flux, E indicates euglycemic (5.5 mM) conditions, and H indicates hyperglycemic (13.9 mM) conditions. ε^{gs}_{G6P} and $\varepsilon^{glycol}_{G6P}$ were assumed to remain unchanged with increased J_{glycol}. The value of $\varepsilon^{glycol}_{G6P}$ was taken as zero.

Chase *et al.* [12] proceeded to calculate the glycogen synthetic flux-control coefficients according to the equations

$$C^{J_{gs}}_{gu} = \frac{1}{1 - \dfrac{\varepsilon^{gu}_{G6P} - (J_{glycol}/J_{gu})\varepsilon^{glycol}_{G6P}}{\varepsilon^{gs}_{G6P}} - J_{glycol}/J_{gu}} \tag{6.26}$$

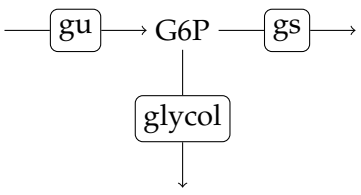

Figure 6.14: Glycogen synthesis and glycolysis as a supply-demand system of G6P. Glucose uptake (gu) produces G6P, whereas glycogen synthesis (gs) and glycolysis (glycol) consume G6P.

$$C^{J_{gs}}_{gs} = -C^{J_{gs}}_{gu}\frac{\varepsilon^{gu}_{G6P} - (J_{glycol}/J_{gu})\varepsilon^{glycol}_{G6P}}{\varepsilon^{gs}_{G6P}} \tag{6.27}$$

$$C^{J_{gs}}_{glycol} = -C^{J_{gs}}_{gu}(J_{glycol}/J_{gu}) \tag{6.28}$$

We reproduced the values in [12] using the model GlySynth with an additional abbreviated glycolysis branch and by setting all fixed concentrations to the values in [12]. The glycolysis branch included the phosphoglucose isomerase (PGI) reaction, catalysing the conversion of G6P to fructose-6-phosphate (F6P), and an irreversible sink reaction representing the remainder of the glycolysis pathway. The kinetics of the sink reaction was chosen according to that of the ATPase reaction, because ATPase controls the glycolytic flux [19]. The elasticity of glycolysis with respect to G6P can be expressed in terms of the elasticities of individual enzymes as follows:

$$\begin{aligned}
\varepsilon^{glycol}_{G6P} &= C^{J_{glycol}}_{PGI}\varepsilon^{PGI}_{G6P} && (6.29)\\
&= \frac{\varepsilon^{sink}_{F6P}}{\varepsilon^{sink}_{F6P} - \varepsilon^{PGI}_{F6P}}\varepsilon^{PGI}_{G6P} && (6.30)\\
&= \varepsilon^{sink}_{F6P} \quad (\text{since } \left|\varepsilon^{PGI}_{F6P}\right| \gg \left|\varepsilon^{sink}_{F6P}\right| \text{ and } \left|\varepsilon^{PGI}_{F6P}\right| \simeq \left|\varepsilon^{PGI}_{G6P}\right|) && (6.31)\\
&\simeq 0 \quad (\text{ATPase is insensitive to its immediate substrate ATP}) && (6.32)
\end{aligned}$$

While PGI is near equilibrium and $C^{J_{glycol}}_{PGI}$ is thus virtually zero, the value of ε^{PGI}_{G6P} is very large and approximately equal to the absolute value of ε^{PGI}_{F6P}, so that $\varepsilon^{glycol}_{G6P}$ does not approach zero. Instead, $\varepsilon^{glycol}_{G6P}$ approaches ε^{sink}_{F6P}, which incidentally approaches zero by virtue of being saturated with its substrate. We see then that although the sink reaction is insensitive to G6P, it governs the sensitivity of the glycolysis block to G6P. In a more realistic treatment of glycolysis, more enzymes would be present and the expression for $C^{J_{glycol}}_{PGI}$ would be more complicated. The large elasticities of PGI would, however, still cancel and $\varepsilon^{ATPase}_{ATP}$ would be a factor of the numerator, resulting in a small $\varepsilon^{glycol}_{G6P}$ value.

We calculated all the relevant elasticities and control coefficients for a range of glycolysis to glucose uptake flux ratios using PySCeS. To obtain the range of flux ratios reported by Chase *et al.* [12], we varied $V_{max,sink}$, the maximal forward rate of the sink reaction, over a suitable range (Fig. 6.15). The calculated elasticities and control coefficients are shown in Fig. 6.16 with the experimentally determined values

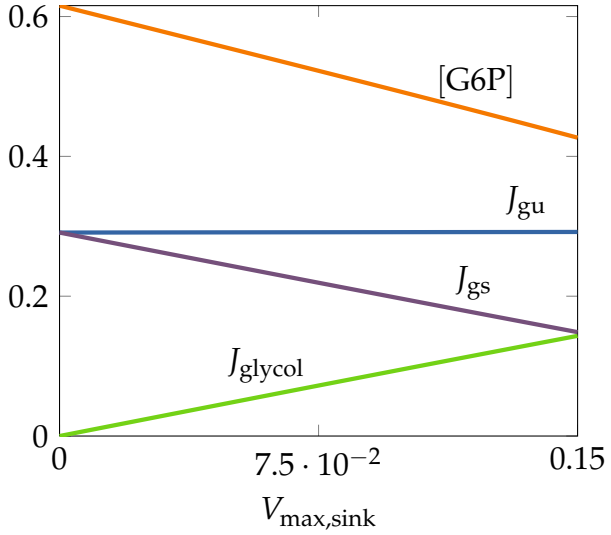

Figure 6.15: Dependence of glucose uptake, glycogen synthesis, glycolysis, and G6P on the maximal rate of the glycolytic sink reaction. Fluxes are given in mM.min^{-1} and the G6P concentration is given in mM.

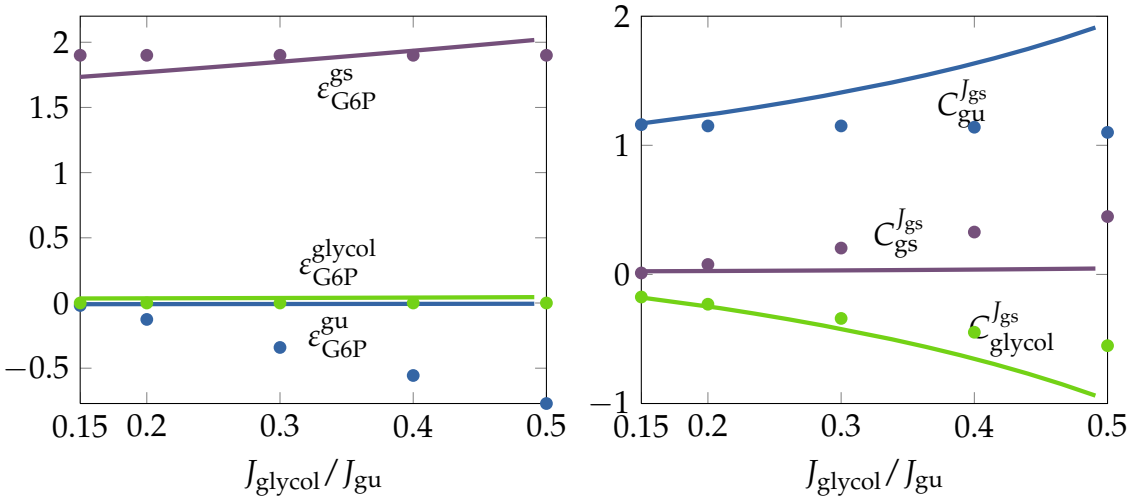

Figure 6.16: Influence of the glycolytic rate on elasticities with respect to G6P and glycogen synthetic flux control. Dots represent experimental values from [12]. Lines represent values calculated from our model.

from [12]. Note that we used the model value for $\varepsilon^{glycol}_{G6P}$ and did not follow Chase *et al.* [12] in explicitly setting this value to zero.

The model results are generally in good agreement with the experimental results. In particular, the model results show that Chase *et al.* [12] were justified in assuming constant values for ε^{gs}_{G6P} and $\varepsilon^{glycol}_{G6P}$ over the range of flux ratios. Both the model

and the experimental results also show that glucose uptake has the largest glycogen synthetic flux control over the entire range of flux ratios. The agreement is, however, not perfect and a few discrepancies warrant discussion. First, Chase *et al.* [12] found that the absolute value of ε^{gu}_{G6P} increased with the glycolytic rate, while we found that ε^{gu}_{G6P} remained close to zero for the entire range. Since HK is the only reaction in the glucose uptake block that is sensitive to G6P, an increase in $\left|\varepsilon^{gu}_{G6P}\right|$ indicates gain of glucose uptake flux control by the HK reaction. This, in turn, can only result from inhibition of HK by G6P, and we must conclude that the results of Chase *et al.* [12] indicate that G6P increases as the glycolytic flux increases. While this result seems contradictory, it must be recalled that glycolysis rarely increases without a concomitant increase in glycogenolysis, which will replenish G6P. Our model, which does not include glycogenolysis, however, predicts a decrease in G6P as the glycolytic flux increases (Fig. 6.15).

It should also be noted that the coefficients in [12] were calculated from large changes in G6P and J_{gu} resulting from an increase in the external glucose concentration from euglycemia to hyperglycemia. While this method should provide reasonable approximations of the coefficients determined from infinitesimal changes, it is not without pitfalls. At basal insulin concentrations, GLUT controls the glucose uptake flux. Increasing the insulin concentration, however, gradually shifts flux control to HK. Additionally increasing the external glucose concentration further shifts flux control to HK. In the process, the glucose uptake flux becomes increasingly sensitive to G6P. Even if the majority of flux control is still held by GLUT under hyperinsulinemic hyperglycemic conditions, the glucose uptake flux at hyperglycemia (J_{gu_H}) would be inhibited more than the glucose uptake flux at euglycemia (J_{gu_E}), so that $(J_{gu_H} - J_{gu_E})/J_{gu_E}$ is an underestimation of the fractional change in J_{gu}. This has the consequence that the $([Glc_o]_H - [Glc_o]_E)/[Glc_o]_E$ term dominates the numerator of Eq. 6.24 and the overall absolute value of ε^{gu}_{G6P} is larger.

We must point out that while Chase *et al.* [12] calculated ε^{gu}_{G6P} for various values of the ratio J_{glycol}/J_{gu}, it is not immediately clear to us how this calculation was performed, since Eq. 6.24 does not contain this ratio. We do not contest that ε^{gu}_{G6P} should vary with this ratio (our own estimates of this value do indeed vary, albeit slightly), but we contend that the dependence can only be obtained by experimentally changing the flux of glycolysis and determining the value at each flux. Chase *et al.* [12], however, do not report physically altering or measuring the glycolytic flux.

In conclusion, our results and those of Chase *et al.* [12] suggest that, if glycolysis

decreases G6P, it should be expected that the control of the glycogen synthetic flux by glucose uptake and glycolysis should increase with the glycolytic flux, whereas, if glycolysis increases G6P, glycogen synthesis increasingly controls its own flux as the glycolytic flux increases.

6.8 Relative importance of allosteric and covalent modification in glycogen synthesis

Insulin can stimulate glycogen synthesis in the absence of GS dephosphorylation

In order to assess the relative importance of covalent and allosteric modification of GS in response to insulin stimulation, Bouskila *et al.* [17] studied knock-in mice in which the genes of the α and β isoforms of GSK3 were replaced with mutant forms that cannot be phosphorylated. Since insulin stimulation inhibits wildtype GSK3 by phosphorylation, GSK3 is constitutively active in the mutant mice. It was found that insulin stimulation increased GS activity in the wildtype mice, but failed to bring about dephosphorylation and thus activation of GS in the mutant mice (Fig. 6.17). Insulin stimulation did, however, increase the glycogen synthesis rate to the same extent in the wildtype and mutant mice and also increased the concentration of G6P (Fig. 6.17). Bouskila *et al.* [17] interpreted these results as evidence that allosteric regulation (through G6P-stimulation) and not covalent regulation (through inactivation of GSK3) is the dominant mechanism by which insulin stimulates glycogen synthesis.

We sought to reproduce the results of Bouskila *et al.* [17] with the model GlySynth and found a good qualitative agreement between the experimental and model results (Fig. 6.17). To mimic the insensitivity of GSK3 to insulin in the mutant mice, we removed the insulin inhibition term from all GSK3 rate equations. Bouskila *et al.* [17] did not report the basal or insulin-stimulated blood insulin concentrations. We therefore used the values (86 and 430 pM) reported in a similar study by the same group [18]. In both the experimental and model results insulin increased the intrinsic activity of GS in the wildtype mice, but not in the mutant mice. Despite the failure to decrease the degree of GS phosphorylation, however, an increase in the glycogen synthetic flux comparable to what was observed in the wildtype mice, was also observed in the mutant mice in both the experimental and model results. Finally, the

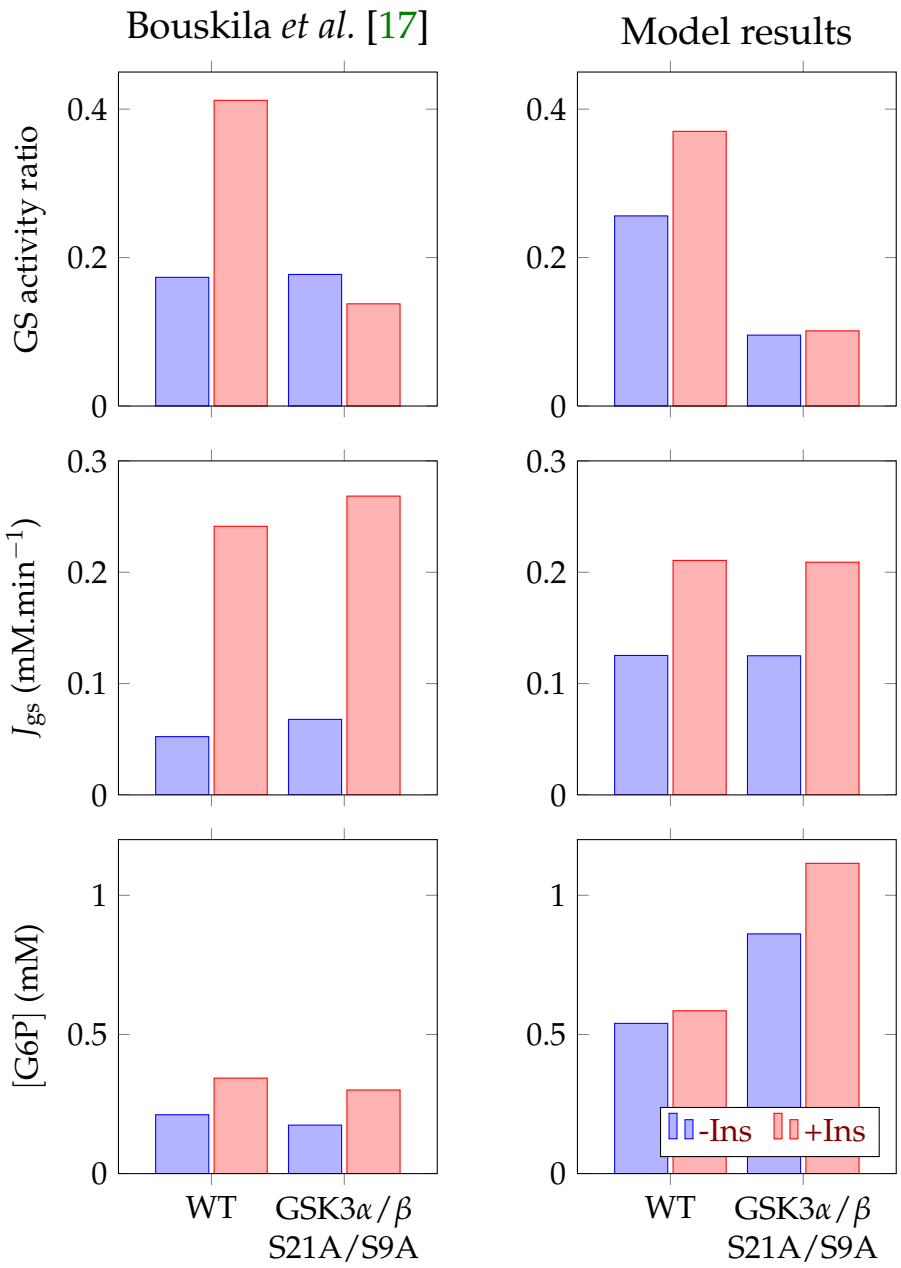

Figure 6.17: Reproduction of experimental data obtained by Bouskila *et al.* [17] from wild-type (WT) mice and knock-in (GSK3α/β/S21A/S9A) mice in which GSK3 is insensitive to insulin. The basal (-Ins) and stimulated (+Ins) insulin concentrations were not reported by Bouskila *et al.* [17]; we therefore used the values from Bouskila *et al.* [18] instead: 86 and 430 pM. The mutation was mimicked in the model by removing the insulin inhibition terms from the rate equations of all GSK3-catalysed reactions. The GS activity ratio is the ratio of GS activity in the absence and presence of G6P as defined in [17]. The values from [17] were converted to units of minutes and mM. One gram of wet muscle was considered equivalent to 0.75 mL cell water, and one gram of dry muscle was considered equivalent to 3 mL cell water.

experimental and model results show that insulin stimulation leads to an increase in the G6P concentration in both the wildtype and mutant mice.

While our results are generally in good agreement with those of Bouskila *et al.* [17], our interpretation of these results differs in a few respects. We have previously shown (see Sections 6.4 and 6.6) that, since GS does not control the glycogen synthetic flux, neither allosteric nor covalent regulation of GS is expected to alter the glycogen synthetic flux. It is therefore not surprising that the glycogen synthetic flux is stimulated to the same extent in the wildtype and mutant mice in response to insulin. Whether GS is dephosphorylated (as in the wildtype mice) or remains phosphorylated (as in the mutant mice), the increase in glycogen synthetic flux in response to insulin is the result of increased glucose uptake (resulting from an increase in plasma membrane GLUT4) and not the result of increased GS activity. Instead, the increased GS activity in wildtype mice—resulting from increased G6P and dephosphorylation—allows the glycogen synthetic flux to match the flux of glucose uptake at a lower G6P concentration. In agreement with this position, our model shows a larger increase in G6P concentration in the mutant mice over basal than in the wildtype mice, indicating disturbed G6P homeostasis. The same result was not observed by Bouskila *et al.* [17]. It is, however, possible that other pathways compensate for the increase in G6P *in vivo* in the mutant mice. Bouskila *et al.* [17] also reported a higher insulin-stimulated increase in G6P in the wildtype mice than our model suggests. The small increase in G6P predicted by our model results from the coordinated activation of glucose uptake and glycogen synthesis, but, as we have discussed before, also depends on cAMP, which effectively regulates the concentration of PKA. In conclusion, we suggest that these results indicate that the regulation of GS activity does not alter the glycogen synthetic flux and that they should not be interpreted as evidence that dephosphorylation of GSK3 in response to insulin stimulation is less important than allosteric activation.

Insulin fails to restore the glycogen synthetic flux in mice with G6P-desensitized GS

To corroborate their earlier findings, Bouskila *et al.* [18] also studied knock-in mice in which the gene for GS was replaced by a mutant gene (denoted R285A) of which the product GS is insensitive to G6P, but which still exhibits normal activity in the absence of G6P. We reproduced the results of Bouskila *et al.* [18] with a model in which

all G6P binding terms in the GS rate equation were removed. The -G6P/+G6P activity ratio or fractional velocity is often used as an indication of GS phosphorylation state or intrinsic activity. These measures are, however, not applicable to the present study, since a value of unity results for G6P-insensitive GS regardless of phosphorylation state. Bouskila *et al.* [18] therefore only report the -G6P activity.

Bouskila *et al.* [18] found that, while the mutant GS was insensitive to G6P, insulin stimulation was able to increase the -G6P activity to similar levels in both wildtype and mutant mice (Fig. 6.18). Our model results likewise showed that the intrinsic activity of GS was similar in the wildtype and mutant mice and that insulin stimulation activated GS in the mutant mice to the same extent that it activated GS in the wildtype mice. In further agreement with Bouskila *et al.* [18], we also found that in double knock-in mice—in which GS is insensitive to G6P and GSK3 is constitutively active—insulin still resulted in an increase in glycogen synthesis. Although in our model results this increase was very small, and possibly insignificant, we discuss a possible mechanism behind this phenomenon in Section 6.9.

Bouskila *et al.* [18] reported a significantly higher basal and insulin-stimulated G6P concentration in mutant mice compared to wildtype mice (Fig. 6.18). While we also found an increase in mutant G6P concentration, the wildtype G6P concentrations and the fold increase of the mutant over wildtype G6P concentrations were much larger than what was found by Bouskila *et al.* [18]. This result is possibly explained by the fact that our model does not include pathways such as glycolysis into which excess G6P could be channelled to compensate for the mutation, a position supported by the observation that a 2.5-fold increase in the glycolytic flux was observed in mutant mice relative to wildtype mice [18]. A side-effect of the high G6P concentrations in our model of the mutant mice was that the glucose uptake flux was significantly inhibited as a result of HK inhibition by G6P. Bouskila *et al.* [18] did not observe a decrease in glucose uptake in the mutant mice, but concede that their direct measurement of glucose uptake, as estimated by 2-deoxyglucose uptake, would not reveal HK inhibition, because 2-deoxyglucose-6-phosphate does not inhibit HK. A decrease in glycogen synthetic flux without a decrease in glucose uptake flux is, however, also explained by an increase in glycolysis.

Bouskila *et al.* [18] interpreted these results, namely that insulin fails to restore glycogen synthesis in mutants to wildtype levels, as further evidence that insulin increases the glycogen synthetic flux not by dephosphorylating GS, but by the allosteric activation of GS by G6P. Despite the good agreement between the results of

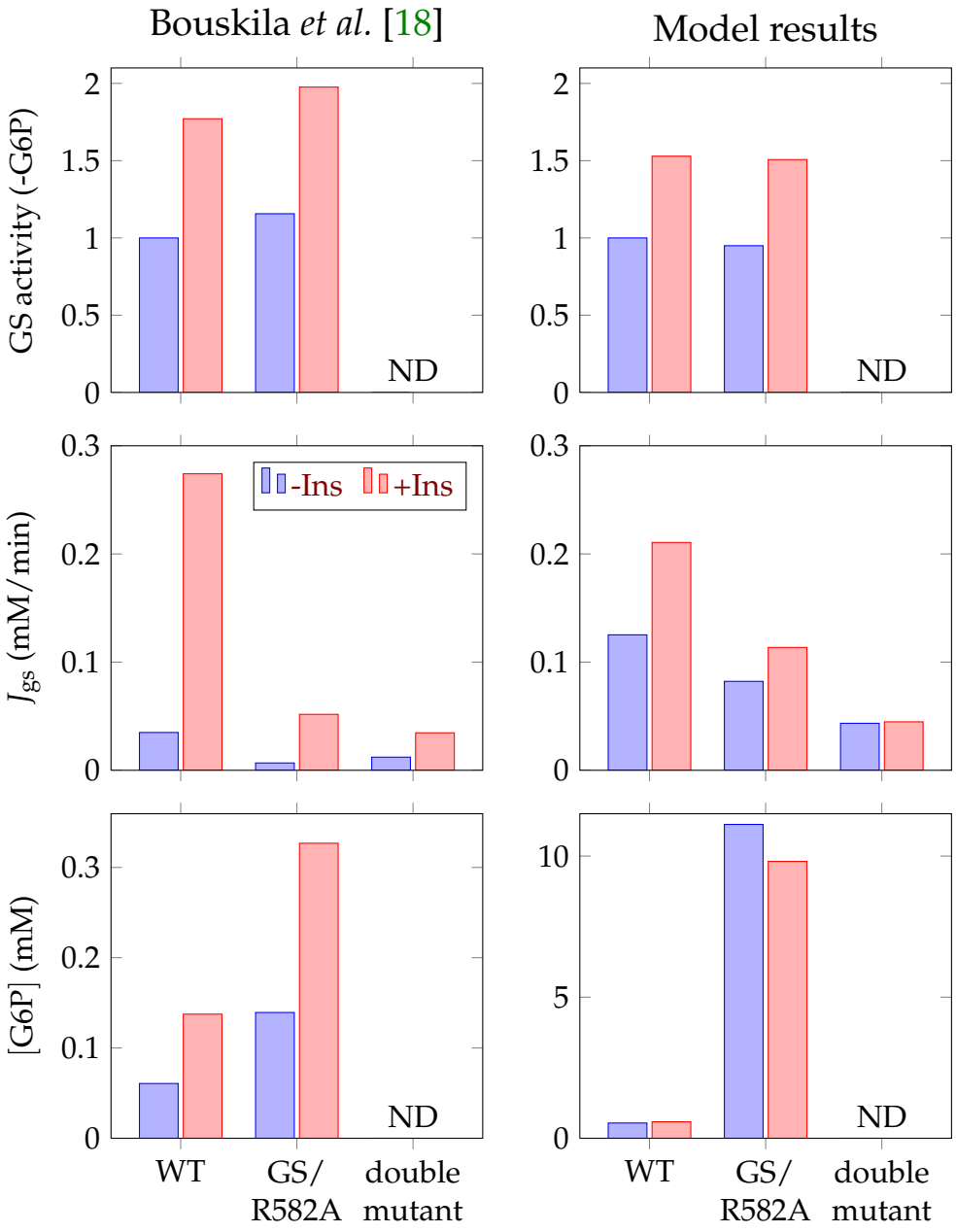

Figure 6.18: Reproduction of experimental data obtained by Bouskila *et al.* [18] from wild-type (WT) mice and knock-in (GS/R582A) mice in which GS is insensitive to G6P. The basal (-Ins) and stimulated (+Ins) insulin concentrations were 86 and 430 pM. The R582A mutation was mimicked in the model by removing the G6P binding terms from the GS rate equation. A double mutant, with both the GS/R582A and GSK3α/β/S21A/S9A mutations, was also considered. The -G6P GS activities were normalized to the wildtype basal values. Note the different scales of the graphs showing experimental and model G6P concentrations. The values from [18] were converted to units of minutes and mM. One gram of wet muscle was considered equivalent to 0.75 mL cell water. ND, not determined.

Bouskila *et al.* [18] and those reported here, our interpretation of these results differs. It is intriguing that, judged by the GS activity in the absence of G6P, insulin stimulated the dephosphorylation of GS to the same extent in wildtype and mutant animals, but that this dephosphorylation was not sufficient to activate GS in the mutant mice. This indicates that the activation arising from the dephosphorylation of GS sites that are GSK3 substrates in response to insulin is not sufficient to overcome the inhibition brought about by phosphorylation at other sites and by allosteric inhibition. On the other hand, inhibition by phosphorylation and ATP can be overcome by the allosteric activator G6P. This is, however, not evidence that, in response to insulin, activation by G6P is stronger than activation by dephosphorylation of GS, but instead indicates that the allosteric activation of GS by G6P, whether at basal or insulin-stimulated concentrations, is critically important to the normal functioning of glycogen synthesis. If the light bulb is removed, darkness should not be blamed on the switch.

Change in the fraction of glycogen synthase in the R conformation in response to insulin and external glucose

The extent to which a change in the GS activity results in a change in the pathway flux is quantified by the flux control coefficient C^J_{GS}. Changes to the activity of GS—whether by allosteric or covalent modification—will only have a significant effect on the glycogen synthetic flux if C^J_{GS} has a large value. Consequently, the question of whether insulin stimulates glycogen synthesis mostly through allosteric or mostly through covalent activation of GS is only relevant if GS has significant control over the glycogen synthetic flux. If, as we have argued earlier, the function of GS regulation, whether allosteric or covalent, is not the control of flux, but the homeostatic maintenance of metabolite concentrations in the face of large fluctuations in the glucose uptake flux, then the answer to the question of whether allosteric or covalent regulation contributes the most to the glycogen synthetic flux in response to insulin can only be that neither mechanism contributes to a change in the flux.

The relative importance of allosteric and covalent GS modification in response to insulin can also be assessed by only considering the local activity change of GS without considering the global effect, such as a change in flux or metabolite concentration, brought about by a local change in the GS activity. We thus pose the question whether an increase—in addition to what is already observed at basal insulin

concentrations—in the allosteric activation of GS as a result of the insulin-stimulated increase in G6P contributes more towards GS activation than the dephosphorylation of GS that occurs during the transition from basal to insulin-stimulated conditions. This question differs from that of Bouskila *et al.* [18] in that it is not concerned with the glycogen synthetic flux at all, but rather with the intrinsic activity state of GS. Another difference is that it emphasizes that the change in GS activity must be considered relative to the basal activity in wildtype mice. While this question is difficult to address experimentally, it is readily investigated with an appropriate mathematical model.

Since we have found that the activity of GS in a particular phosphorylation state is best described by an MWC-type rate equation in which only the R conformation is catalytically active, the fraction of GS that is present in the R conformation provides a measure of the intrinsic activity of the enzyme. Another aspect of the rate equation is that both allosteric and covalent modification manifest as an apparent alteration to the equilibrium between unliganded enzyme in the T and R conformations. This alteration is implicit in the case of allosteric modification, but involves an explicit change to L_0 in the case of covalent modification, i.e., a different L_0 value is assigned to each phosphorylation state of GS. The fraction of GS in a particular phosphorylation state i that is present in the R conformation in the absence of ligands is given by

$$\overline{R_{0i}} = \frac{R_{0i}}{R_{0i} + T_{0i}} \tag{6.33}$$

$$= \frac{1}{1 + L_{0i}} \tag{6.34}$$

The definition of $\overline{R_{0i}}$ is very similar to that of the GS activity ratio which is expressed as $I/(I + D)$, where I and D represent the G6P-independent and G6P-dependent activity of GS. Indeed, we showed in Chapter 3 that the activity ratio is an approximation of $\overline{R_0}$. The overall fraction of GS in the R conformation, considering all phosphorylation states, is then given by

$$\overline{R_0} = \sum_i \frac{[\text{GS}]_i}{[\text{GS}]_{\text{tot}}} \overline{R_{0i}} \tag{6.35}$$

The value of $\overline{R_0}$ is independent of any allosteric modification and only reflects the activity state as altered by covalent modification. As phosphorylation is inhibitory, $\overline{R_0}$ increases in response to insulin stimulation which leads to the dephosphorylation

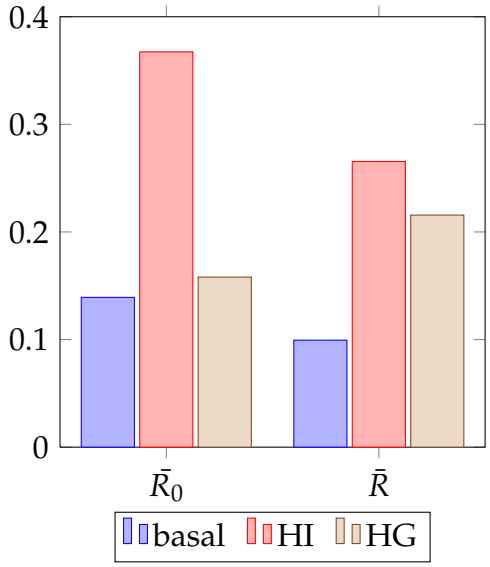

Figure 6.19: Fraction of unliganded ($\overline{R_0}$) and liganded ($\overline{R}$) GS in the R conformation under basal, hyperinsulinemic (HI) and hyperglycemic (GI) conditions. A change in $\overline{R_0}$ reflects a change in covalent modification state, whereas a change in $\overline{R}$ reflects a change in both covalent and allosteric modification state. The fold change in $\overline{R_0}$ and $\overline{R}$ in response to insulin is approximately equal, whereas only $\overline{R}$ changes appreciably in response to elevated external glucose.

of GS. If the effect of ligands on the fraction of GS in the R conformation is also considered, Eq. 6.33 is transformed to

$$\overline{R_i} = \frac{1}{1 + L_{0i}\dfrac{\left(1 + \dfrac{[\text{UDPG}]}{K_{\text{UDPG}}} + \dfrac{[\text{ATP}]}{K'_{\text{t,ATP}}}\right)^n \left(1 + \dfrac{[\text{G6P}]}{K_{\text{t,G6P}}} + \dfrac{[\text{ATP}]}{K_{\text{t,ATP}}}\right)^n}{\left(1 + \dfrac{[\text{UDPG}]}{K_{\text{UDPG}}} + \dfrac{[\text{ATP}]}{K'_{\text{r,ATP}}}\right)^n \left(1 + \dfrac{[\text{G6P}]}{K_{\text{r,G6P}}} + \dfrac{[\text{ATP}]}{K_{\text{r,ATP}}}\right)^n}} \tag{6.36}$$

Similarly, Eq. 6.35 is transformed to

$$\overline{R} = \sum_i \frac{[\text{GS}]_i}{[\text{GS}]_{\text{tot}}} \overline{R_i} \tag{6.37}$$

Ligands that prefer to bind to the R conformation (activators) will increase $\overline{R}$, whereas ligands that prefer to bind to the T conformation (inhibitors) will decrease $\overline{R}$.

We calculated $\overline{R_0}$ and $\overline{R}$ at basal (40 pM) and hyperinsulinemic (450 pM) conditions (Fig. 6.19). $\overline{R_0}$ increased 2.64-fold from 0.14 to 0.37, whereas $\overline{R}$ increased 2.67-fold from 0.1 to 0.27. Since $\overline{R}$, which accounts for both allosteric and covalent modi-

fication, increases only very slightly more than $\overline{R_0}$, which only accounts for covalent modification, we may conclude that the major part of the resulting activation of GS in response to insulin is due to the dephosphorylation of GS and not to allosteric activation by G6P. We also calculated $\overline{R_0}$ and $\overline{R}$ at euglycemic (5.5 mM) and hyperglycemic (13 mM) conditions (Fig. 6.19). $\overline{R_0}$ increased 1.14-fold from 0.14 to 0.16, whereas $\overline{R}$ increased 2.17-fold from 0.1 to 0.22. This indicates that, in response to an increase in the external glucose concentration, GS activation results mostly from activation by G6P and not from dephosphorylation of the enzyme. These results are in agreement with experimental results showing that insulin [242], but not external glucose [243, 244], increases the GS fractional velocity.

While we were able to reproduce the results of Bouskila *et al.* [17, 18] reasonably well, we argue that those results cannot be interpreted as evidence that, in response to insulin stimulation, allosteric modification "trumps" [245] covalent modification. To the contrary, our analysis indicates that insulin-dependent dephosphorylation of GS accounts for the major part of GS activation in response to insulin.

Using $\overline{R_0}$ and $\overline{R}$ to quantify the relative contributions of allosteric and covalent modification to GS activation is, however, not without its shortcomings. If most of the unliganded GS is already present in the R conformation, then the effect of ligands that also favour the R conformation is less than what would be observed if most of the unliganded GS was in the T conformation. Our values for $\overline{R_0}$ were, however, well below 0.5 and the importance of allosteric modification would only be marginally underestimated. Another shortcoming is that while a change in $\overline{R_0}$ reflects a change in the covalent state of GS, it is also true that G6P can alter the phosphorylation state of GS by virtue of PP1 activation. This is evident in the change in $\overline{R_0}$ that results from an increase in external glucose. This insulin-independent change in $\overline{R_0}$ is, however, much smaller than the change in $\overline{R}$ and we therefore do not expect it to significantly affect the change in $\overline{R_0}$ resulting from an increase in insulin.

These results agree well with our earlier findings that the value of $\Omega^{J:\mathrm{G6P}}_{\mathrm{Glc_o}}$ is completely determined by the value of $\varepsilon^{\mathrm{demand}}_{\mathrm{G6P}}$, whereas $\Omega^{J:\mathrm{G6P}}_{\mathrm{Ins}}$ is only influenced by $\varepsilon^{\mathrm{demand}}_{\mathrm{G6P}}$ when the absolute values of $\varepsilon^{\mathrm{supply}}_{\mathrm{Ins}}$ and $\varepsilon^{\mathrm{demand}}_{\mathrm{Ins}}$ differ significantly. That is, activation of the demand block (glycogen synthesis) by G6P is essential for the homeostatic maintenance of G6P in response to the increased flux resulting from elevated external glucose. In response to insulin, on the other hand, the mechanism by which G6P is maintained in a narrow range involves the coordinate activation of glucose uptake and glycogen synthesis. The situation is, however, more

complex, because G6P is also able to stimulate net dephosphorylation of GS in an insulin-independent mechanism. The result is that $\varepsilon_{G6P}^{demand}$ is not a pure indication of allosteric activation, and $\varepsilon_{Ins}^{demand}$ is not a pure indication of covalent activation.

The relative importance of allosteric and covalent modification can also be investigated with MCA. In this framework, the effect of insulin on $\overline{R}$ can be quantified with the response coefficient $R_{Ins}^{\overline{R}}$, which is expressed as

$$R_{Ins}^{\overline{R}} = C_{GLUT}^{\overline{R}} \varepsilon_{Ins}^{GLUT} + \sum_i C_{GSK3_i}^{\overline{R}} \varepsilon_{Ins}^{GSK3_i} \tag{6.38}$$

where i denotes a particular GSK3-catalysed reaction. $C_{GLUT}^{\overline{R}}$ and $C_{GSK3_i}^{\overline{R}}$ can be expressed in terms of conventional concentration-control coefficients and hence also in terms of elasticities. One would then proceed to separate all the terms that describe allosteric modification from those that describe covalent modification, provided that this distinction can be clearly made, in order to quantify the contributions of these two mechanisms toward a change in $\overline{R}$. The resulting expression is, however, so complicated that we will not attempt this analysis here. $R_{Glc_o}^{\overline{R}}$ could similarly be employed to investigate the relative contributions of allosteric and covalent modification to a change in $\overline{R}$ in response to an increase in external glucose concentration.

6.9 The mechanisms by which glucose-6-phosphate stimulates glycogen synthesis

In Section 6.4 we saw that $\varepsilon_{G6P}^{demand}$, the elasticity of the glycogen synthesis block to G6P, is an important determinant of the extent to which the concentration of G6P is maintained in a narrow range in the face of large increases in the flux resulting from elevated external glucose concentrations. In Chapter 2 we reviewed five mechanisms by which G6P stimulates glycogen synthesis. Four of these mechanisms were included in our model of glycogen synthesis (GlySynth):

- G6P is a precursor of UDPG and can thus be considered the substrate of the demand (glycogen synthesis) block
- G6P is an allosteric activator of GS
- G6P is a substrate-specific inhibitor of GS kinases
- G6P is a substrate-specific activator of GS phosphatases

In this section we consider the contribution of each of these mechanisms towards the value of $\varepsilon^{\text{demand}}_{\text{G6P}}$.

Since $\varepsilon^{\text{demand}}_{\text{G6P}}$ is a block elasticity it can be expressed in terms of the elasticities of individual enzymes in the block with respect to G6P, each scaled by the flux-control coefficient of the particular enzyme within the block. Stated otherwise, $\varepsilon^{\text{demand}}_{\text{G6P}}$ is the flux-response coefficient of the isolated block with respect to G6P:

$$\varepsilon^{\text{demand}}_{\text{G6P}} = R^{J_{\text{demand}}}_{\text{G6P}} \tag{6.39}$$

$$= C^{J_{\text{demand}}}_{\text{PGLM}} \varepsilon^{\text{PGLM}}_{\text{G6P}} + C^{J_{\text{demand}}}_{\text{GS}} \varepsilon^{\text{GS}}_{\text{G6P}} + \sum_i C^{J_{\text{demand}}}_{\text{kin}_i} \varepsilon^{\text{kin}_i}_{\text{G6P}} + \sum_j C^{J_{\text{demand}}}_{\text{phos}_j} \varepsilon^{\text{phos}_j}_{\text{G6P}} \tag{6.40}$$

where kin_i is any GS kinase reaction and phos_j is any GS phosphatase reaction. If we define these partial response coefficients:

$${}^{\text{sub}}R^{J_{\text{demand}}}_{\text{G6P}} = C^{J_{\text{demand}}}_{\text{PGLM}} \varepsilon^{\text{PGLM}}_{\text{G6P}} \tag{6.41}$$

$${}^{\text{allos}}R^{J_{\text{demand}}}_{\text{G6P}} = C^{J_{\text{demand}}}_{\text{GS}} \varepsilon^{\text{GS}}_{\text{G6P}} \tag{6.42}$$

$${}^{\text{kin}}R^{J_{\text{demand}}}_{\text{G6P}} = \sum_i C^{J_{\text{demand}}}_{\text{kin}_i} \varepsilon^{\text{kin}_i}_{\text{G6P}} \tag{6.43}$$

$${}^{\text{phos}}R^{J_{\text{demand}}}_{\text{G6P}} = \sum_j C^{J_{\text{demand}}}_{\text{phos}_j} \varepsilon^{\text{phos}_j}_{\text{G6P}} \tag{6.44}$$

then Eq. 6.39 can be rewritten as

$$\varepsilon^{\text{demand}}_{\text{G6P}} = {}^{\text{sub}}R^{J_{\text{demand}}}_{\text{G6P}} + {}^{\text{allos}}R^{J_{\text{demand}}}_{\text{G6P}} + {}^{\text{kin}}R^{J_{\text{demand}}}_{\text{G6P}} + {}^{\text{phos}}R^{J_{\text{demand}}}_{\text{G6P}} \tag{6.45}$$

The contribution of each of the four terms in Eq. 6.45 as a function of G6P concentration is shown in Fig. 6.20.

Contribution of G6P as substrate precursor

The contribution of G6P as substrate precursor of GS to the value of $\varepsilon^{\text{demand}}_{\text{G6P}}$ is quantified by ${}^{\text{sub}}R^{J_{\text{demand}}}_{\text{G6P}}$. In order to express ${}^{\text{sub}}R^{J_{\text{demand}}}_{\text{G6P}}$ completely in terms of elasticities of the demand block, it is necessary to find an expression for $C^{J_{\text{demand}}}_{\text{PGLM}}$. In addition to the glycogen synthesis pathway, the demand block also contains the pathway describing the interconversion between all the GS phosphorylation states. If no intermediates

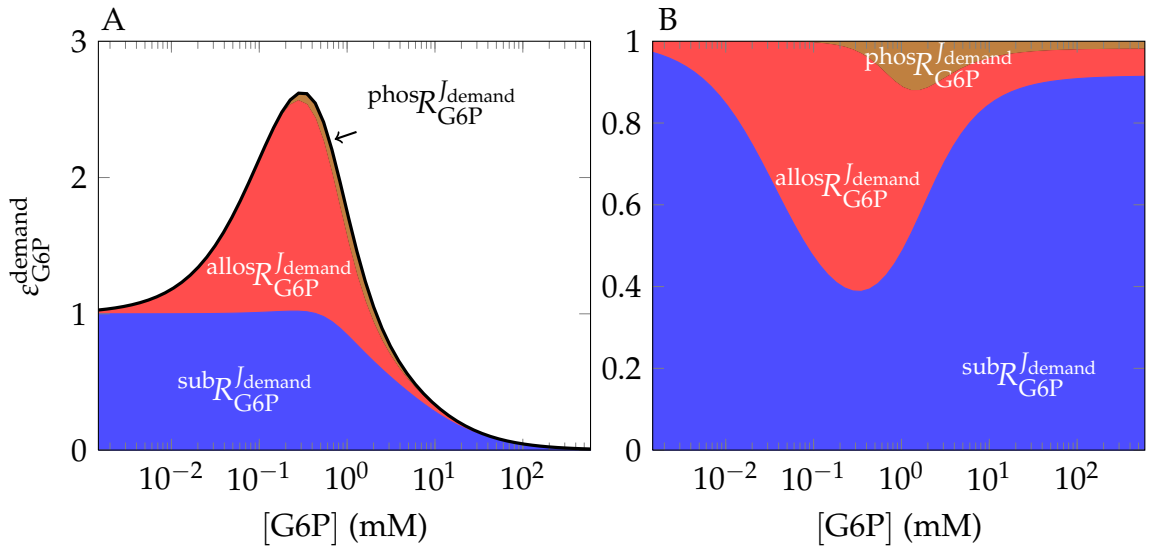

Figure 6.20: The relative contributions of four mechanisms by which G6P activates glycogen synthesis. The values of $^{\text{sub}}R^{J_{\text{demand}}}_{\text{G6P}}$, $^{\text{allos}}R^{J_{\text{demand}}}_{\text{G6P}}$, $^{\text{kin}}R^{J_{\text{demand}}}_{\text{G6P}}$, and $^{\text{phos}}R^{J_{\text{demand}}}_{\text{G6P}}$ were calculated for a range of G6P values by considering the glycogen synthesis pathway, together with the GS phosphorylation module, in isolation from the rest of the system. In all cases $^{\text{kin}}R^{J_{\text{demand}}}_{\text{G6P}}$ was negligible. A) $\varepsilon^{\text{demand}}_{\text{G6P}}$ (black line) as the sum of the (stacked) partial response coefficients. B) Fractional contribution of the partial response coefficients to $\varepsilon^{\text{demand}}_{\text{G6P}}$.

in the glycogen synthesis pathway affect the rates of the kinases and phosphatases that catalyse the interconversion of GS, then $C^{J_{\text{demand}}}_{\text{PGLM}}$ could be expressed in terms of elasticities by considering the glycogen synthesis pathway in isolation from the interconversion pathway:

$$C^{J_{\text{demand}}}_{\text{PGLM}} = \frac{\varepsilon^{\text{UPP}}_{\text{G1P}}\varepsilon^{\text{GS}}_{\text{UDPG}}}{\varepsilon^{\text{PGLM}}_{\text{G1P}}\varepsilon^{\text{UPP}}_{\text{UDPG}} - \varepsilon^{\text{PGLM}}_{\text{G1P}}\varepsilon^{\text{GS}}_{\text{UDPG}} + \varepsilon^{\text{UPP}}_{\text{G1P}}\varepsilon^{\text{GS}}_{\text{UDPG}}} \tag{6.46}$$

In reality UDPG affects both the kinase and phosphatase reactions by virtue of being a GS ligand. Although UDPG binds with equal affinities to both the T and R conformations of GS, and should therefore not result in a conformational change that would affect the kinase and phosphatase reactions, competition for the catalytic binding site by ATP offsets the balance so that binding of UDPG does result in a slight conformational change. While Eq. 6.46 then only provides an approximation of the real value of $C^{J_{\text{demand}}}_{\text{PGLM}}$, we will nevertheless use this expression in what follows. The expression of $^{\text{sub}}R^{J_{\text{demand}}}_{\text{G6P}}$ in terms of elasticities is then given by

$$^{\text{sub}}R_{\text{G6P}}^{J_{\text{demand}}} \simeq \frac{\varepsilon_{\text{G1P}}^{\text{UPP}}\varepsilon_{\text{UDPG}}^{\text{GS}}}{\varepsilon_{\text{G1P}}^{\text{PGLM}}\varepsilon_{\text{UDPG}}^{\text{UPP}} - \varepsilon_{\text{G1P}}^{\text{PGLM}}\varepsilon_{\text{UDPG}}^{\text{GS}} + \varepsilon_{\text{G1P}}^{\text{UPP}}\varepsilon_{\text{UDPG}}^{\text{GS}}} \cdot \varepsilon_{\text{G6P}}^{\text{PGLM}} \tag{6.47}$$

Since both PGLM and UPP are near equilibrium, it follows that $\left|\varepsilon_{\text{G6P}}^{\text{PGLM}}\right| \simeq \left|\varepsilon_{\text{G1P}}^{\text{PGLM}}\right|$, $\left|\varepsilon_{\text{G1P}}^{\text{UPP}}\right| \simeq \left|\varepsilon_{\text{UDPG}}^{\text{UPP}}\right|$, and that the value of $\varepsilon_{\text{UDPG}}^{\text{GS}}$ is much smaller than $\varepsilon_{\text{G6P}}^{\text{PGLM}}$ and $\varepsilon_{\text{G1P}}^{\text{UPP}}$ in absolute terms. Equation 6.47 then simplifies to

$$^{\text{sub}}R_{\text{G6P}}^{J_{\text{demand}}} \simeq \varepsilon_{\text{UDPG}}^{\text{GS}} \tag{6.48}$$

The high activities of PGLM and UPP essentially keep the concentrations of G6P and UDPG in a fixed ratio, so that a small percentage change in G6P results in an equal percentage change in UDPG. The relative effect of G6P as substrate precursor of GS is therefore identical to that of the real GS substrate. At low G6P concentrations $^{\text{sub}}R_{\text{G6P}}^{J_{\text{demand}}}$ is the sole contributor to $\varepsilon_{\text{G6P}}^{\text{demand}}$ and has a value close to unity (Fig. 6.20A). As G6P further increases, the UDPG concentration enters the range in which slight UDPG binding cooperativity is observed, so that $^{\text{sub}}R_{\text{G6P}}^{J_{\text{demand}}}$ increases to just above 1. Finally, at very high G6P concentrations, the UDPG concentration becomes saturating to GS with the result that $^{\text{sub}}R_{\text{G6P}}^{J_{\text{demand}}}$ approaches zero. Note that if we modelled GS as a reversible reaction, $^{\text{sub}}R_{\text{G6P}}^{J_{\text{demand}}}$ would approach infinity, not unity, at very low G6P concentrations where the GS reaction is near equilibrium.

Contribution of G6P as allosteric activator

The contribution of G6P as allosteric activator of GS to the value of $\varepsilon_{\text{G6P}}^{\text{demand}}$ is quantified by $^{\text{allos}}R_{\text{G6P}}^{J_{\text{demand}}} = C_{\text{GS}}^{J_{\text{demand}}}\varepsilon_{\text{G6P}}^{\text{GS}}$. Following the same reasoning as above, the value of $C_{\text{GS}}^{J_{\text{demand}}}$ can be approximated by considering glycogen synthesis as a pathway that is isolated from the GS interconversion pathway. The expression for $C_{\text{GS}}^{J_{\text{demand}}}$ then reads

$$C_{\text{GS}}^{J_{\text{demand}}} = \frac{\varepsilon_{\text{G1P}}^{\text{PGLM}}\varepsilon_{\text{UDPG}}^{\text{UPP}}}{\varepsilon_{\text{G1P}}^{\text{PGLM}}\varepsilon_{\text{UDPG}}^{\text{UPP}} - \varepsilon_{\text{G1P}}^{\text{PGLM}}\varepsilon_{\text{UDPG}}^{\text{GS}} + \varepsilon_{\text{G1P}}^{\text{UPP}}\varepsilon_{\text{UDPG}}^{\text{GS}}} \tag{6.49}$$

Considering that PGLM and UPP operate near equilibrium, Eq. 6.49 simplifies to

$$C_{\text{GS}}^{J_{\text{demand}}} \simeq 1 \tag{6.50}$$

and Eq. 6.42 simplifies to

$$^{\text{allos}}R_{\text{G6P}}^{J_{\text{demand}}} \simeq \varepsilon_{\text{G6P}}^{\text{GS}} \tag{6.51}$$

The condition $C_{GS}^{J_{demand}} \simeq 1$ could also be achieved if GS were saturated with its substrate UDPG, i.e., if $\varepsilon_{UDPG}^{GS} \simeq 0$ held. If this were the case, one would expect G6P to activate GS by increasing the maximal rate of catalysis and not the affinity of UDPG, as discussed by Hofmeyr *et al.* [16] and in Chapter 4. However, since UDPG is not saturating in our model, no such restriction is placed on the mechanism by which G6P activates GS. Indeed, the rate equation that we have found to provide the best description of GS kinetics mandates that G6P activates GS both by increasing the rate constant (by favouring the catalytically active conformation) and by increasing the affinity for UDPG (by favouring the conformation in which ATP competition with UDPG is the weakest).

ε_{G6P}^{GS} itself can be expressed as a sum of weighted elasticities: the elasticity of each phosphorylation state of GS to G6P contributes to ε_{G6P}^{GS} in proportion to the fraction that catalysis by the particular phosphorylation state contributes toward the overall GS rate (Appendix A.2):

$$\varepsilon_{G6P}^{GS} = \sum_i \frac{v_{GSi}}{v_{GS}} \varepsilon_{G6P}^{GS_i} \tag{6.52}$$

where

$$\varepsilon_{G6P}^{GS_i} = \frac{n\left(1+\frac{[UDPG]}{K_{UDPG}}+\frac{[ATP]}{K'_{t,ATP}}\right)^n L_{0i}\left(\frac{1+\frac{[G6P]}{K_{t,G6P}}+\frac{[ATP]}{K_{t,ATP}}}{1+\frac{[G6P]}{K_{r,G6P}}+\frac{[ATP]}{K_{r,ATP}}}\right)^n\left[\frac{\frac{[G6P]}{K_{r,G6P}}}{1+\frac{[G6P]}{K_{r,G6P}}+\frac{[ATP]}{K_{r,ATP}}}-\frac{\frac{[G6P]}{K_{t,G6P}}}{1+\frac{[G6P]}{K_{t,G6P}}+\frac{[ATP]}{K_{t,ATP}}}\right]}{\left(1+\frac{[UDPG]}{K_{UDPG}}+\frac{[ATP]}{K'_{t,ATP}}\right)^n L_{0i}\left(\frac{1+\frac{[G6P]}{K_{t,G6P}}+\frac{[ATP]}{K_{t,ATP}}}{1+\frac{[G6P]}{K_{r,G6P}}+\frac{[ATP]}{K_{r,ATP}}}\right)^n+\left(1+\frac{[UDPG]}{K_{UDPG}}+\frac{[ATP]}{K'_{r,ATP}}\right)^n} \tag{6.53}$$

The theoretical maximum value of $\varepsilon_{G6P}^{GS_i}$ is $n = 4$, which is achieved if the enzyme is present only in the T conformation ($L_{0i} \to \infty$) and if G6P is saturating ($K_{r,G6P} \ll [G6P]$), but does not bind to the T conformation ($K_{t,G6P} \to \infty$). These conditions are not met for any of the GS phosphorylation states and therefore $\varepsilon_{G6P}^{GS_i}$ and thus ε_{G6P}^{GS} are smaller than 4 for all i.

Rubin & Changeux [161] have shown that the slope of the graph of fractional saturation against ligand concentration is maximized when $L = \sqrt{K_t^n / K_r^n}$. Since the effects of ligand binding and covalent modification both manifest as changes in L_{app} (which is proportional to $L_{0,app}$ but takes ligand concentrations into account), it is instructive to consider the value of L_{app} that will result in a maximum $\varepsilon_{G6P}^{GS_i}$ value. The present situation, however, differs from the one considered by Rubin & Changeux

[161] in that we are interested in the relationship between v_{GS}, which is proportional to the fractional saturation of GS with UDPG (as opposed to G6P) and G6P. Nevertheless, from the fitted values of $K_{t,G6P}$ and $K_{r,G6P}$ the value of L_{app} that maximizes ε^{GS}_{G6P} is calculated as 18.4. ATP inhibits GS both by preferentially binding to the T conformation and by competing with G6P for the allosteric site. Since competition of ATP with G6P results in an apparent change to $K_{t,G6P}$ and $K_{r,G6P}$, the value of L_{app} that results in a maximal value of ε^{GS}_{G6P} depends on the ATP concentration. Other ligands will also alter the optimal L_{app} value.

The values of L_{0i} range between 0.25 for the dephosphorylated enzyme and 185 for the completely phosphorylated enzyme. While phosphorylation will continue to inhibit GS beyond L_{app} values of about 18.4, depending on the concentrations of GS ligands, this inhibition will not be accompanied by a further increase in ε^{GS}_{G6P}. In fact, a steady decrease in ε^{GS}_{G6P} is expected. Similarly, inhibition by ATP will increase ε^{GS}_{G6P} only as long as L_{app} remains below 18.4. In summary then, the value of ε^{GS}_{G6P} is the result of the cooperative binding of G6P to GS, the degree of which is enhanced by ATP and phosphorylation, but only up to a point.

At very low concentrations G6P is not able to activate GS and ${}^{allos}R^{J_{demand}}_{G6P}$ does not contribute to $\varepsilon^{demand}_{G6P}$ (Fig. 6.20). As G6P increases to within the range between $K_{r,G6P}$ and $K_{t,G6P}$, ${}^{allos}R^{J_{demand}}_{G6P}$ increases and passes through its maximal value. Further increases in G6P cause GS to become saturated with G6P, so that ${}^{allos}R^{J_{demand}}_{G6P}$ decreases asymptotically to zero again.

Contribution of G6P as kinase inhibitor and phosphatase activator

The contribution of G6P as GS kinase inhibitor and GS phosphatase activator to the value of $\varepsilon^{demand}_{G6P}$ is quantified by ${}^{kin}R^{J_{demand}}_{G6P}$ and ${}^{phos}R^{J_{demand}}_{G6P}$. While it is possible to express these two partial elasticities in terms of elasticities of individual enzymes in the demand block, the resulting expressions are too complicated to be workable. It is, however, reasonable to assume that the same conditions identified for the simpler system considered in Chapter 4 will also maximize ${}^{kin}R^{J_{demand}}_{G6P}$ and ${}^{phos}R^{J_{demand}}_{G6P}$. These conditions, as applied to GS modification, are

1. GS must control the flux within the isolated glycogen synthesis pathway
2. UDPG must bind equally well to the T and R conformations of GS
3. the various phosphorylation states of GS must exhibit different kinetics

4. the GS kinases and phosphatase must exhibit zero-order sensitivity to GS as substrate

We have already seen that the first condition is satisfied by virtue of PGLM and UPP operating near equilibrium. The second condition is not met, because although UDPG binds equally well to the T and R conformations in the absence of ATP, competition with ATP at the catalytic site alters the apparent affinity of GS for UDPG to such an extent that, in the presence of ATP, UDPG binds preferentially to the R conformation. It must, however, be recalled that we fitted the kinetic parameters for GS to experimental data that were obtained under conditions (low pH) were ATP inhibition is very pronounced [39, 67]. At any rate, judging by the mild UDPG cooperativity observed, the violation of the second condition is not significant.

While not all the GS phosphorylation states exhibit the same kinetics, the kinetics of some states are not altered by phosphorylation. Conversion between GS states with identical kinetics will not contribute to ${}^{\text{kin}}R^{J_{\text{demand}}}_{\text{G6P}}$ and ${}^{\text{phos}}R^{J_{\text{demand}}}_{\text{G6P}}$. The third condition is thus only partially satisfied.

Finally, for a number of reasons, the fourth condition is also not met. The Michaelis constants for the phosphatase and kinase reactions are rather high (in the order of the concentrations of the various GS states) and thus neither the kinase nor the phosphatase reactions are near saturation. For the phosphatase reactions, the high Michaelis constants are possibly explained by the fact that glycogen is generally omitted in assays. Since both GS and PP1 are in association with glycogen *in vivo* which results in an apparent increase in GS concentration, the kinetics determined in the absence of glycogen would overestimate the Michaelis constant. Moreover, GS in phosphorylation states that do not affect the kinetics of the enzyme compete with GS in states that do, which further increases the apparent Michaelis constants. More extensive kinetic data are required to assess whether this condition is met *in vivo*.

Although most of the conditions that would maximize ${}^{\text{kin}}R^{J_{\text{demand}}}_{\text{G6P}}$ and ${}^{\text{phos}}R^{J_{\text{demand}}}_{\text{G6P}}$ are not satisfied, ${}^{\text{phos}}R^{J_{\text{demand}}}_{\text{G6P}}$ still contributes to the value of $\varepsilon^{\text{demand}}_{\text{G6P}}$, albeit to an extent well below the theoretical maximum of infinity. The relationship between ${}^{\text{phos}}R^{J_{\text{demand}}}_{\text{G6P}}$ and G6P follow a similar profile as that of the relationship between ${}^{\text{allos}}R^{J_{\text{demand}}}_{\text{G6P}}$ and G6P: initially the values are very small but then peak between $K_{\text{r,G6P}}$ and $K_{\text{t,G6P}}$, only to decrease to zero again (Fig. 6.20). Note, however, that the peaks of ${}^{\text{kin}}R^{J_{\text{demand}}}_{\text{G6P}}$, if present, and ${}^{\text{phos}}R^{J_{\text{demand}}}_{\text{G6P}}$ will generally not coincide with each other or with the peak of ${}^{\text{allos}}R^{J_{\text{demand}}}_{\text{G6P}}$. Also note that the contribution of ${}^{\text{kin}}R^{J_{\text{demand}}}_{\text{G6P}}$ to $\varepsilon^{\text{demand}}_{\text{G6P}}$ is negligible.

This results from the fact that we only included modification terms that alter the K_{eq} (and the reverse V_{max} by implication) of kinase reactions. Since the kinase reactions are practically irreversible, the modification terms have almost no effect on the kinase reaction rates. While it is reasonable to expect that G6P also affects the forward V_{max} values of GS kinases *in vivo*, we found no direct evidence from the limited data available in the literature that would suggest that modification terms that alter the forward V_{max} must also be included in kinase reactions. We are, however, to our knowledge, the first to propose a theory that would suggest that such modification terms should be looked for in the first place.

Since PKA and insulin affect $L_{0,app}$, it is expected that the values of ${}^{allos}R^{J_{demand}}_{G6P}$, ${}^{kin}R^{J_{demand}}_{G6P}$, and ${}^{phos}R^{J_{demand}}_{G6P}$ will be influenced by PKA and insulin. Here we will consider the relationships between PKA and insulin, and ${}^{phos}R^{J_{demand}}_{G6P}$. Over a physiologically relevant range of PKA concentrations (as would be observed in response to adrenergic stimulation and the subsequent increase in cellular cAMP), two peak areas are observed for ${}^{phos}R^{J_{demand}}_{G6P}$ (Fig. 6.21A). The first (at a lower [PKA]) corresponds to the phosphorylation of site 2 by PKA (compare Fig. 6.9), whereas the second corresponds to the phosphorylation of the remaining GS phosphorylation sites resulting from inhibition of PP1 by PKA. The value of ${}^{phos}R^{J_{demand}}_{G6P}$ decreases as the insulin concentration increases (Fig. 6.21B), because GS is already substantially dephosphorylated under these conditions and further stimulation of net dephosphorylation does not significantly alter the rate of the GS reaction.

Discussion

Chase *et al.* [12] determined the value of ε^{GS}_{G6P} *in vivo* and *in vitro* experimentally under hyperinsulinemic conditions and found a large discrepancy between these values (1.9 and 0.79). In reality, however, the *in vivo* and *in vitro* values of Chase *et al.* [12] correspond to our $\varepsilon^{demand}_{G6P}$ and ε^{GS}_{G6P}. Since the value of ε^{GS}_{UDPG} is about 1, Schafer *et al.* [13] were correct in suggesting that the discrepancy can be resolved by also considering the contribution of G6P as substrate precursor of GS. The remaining difference (about 0.1) is probably not significant within error. However, here we have shown that the contribution of ${}^{phos}R^{J_{demand}}_{G6P}$ to $\varepsilon^{demand}_{G6P}$ is indeed in the order of 0.1 and could therefore explain this remaining discrepancy. The significant contribution of ${}^{sub}R^{J_{demand}}_{G6P}$ to $\varepsilon^{demand}_{G6P}$ could also explain why Bouskila *et al.* [18] observed an increase in the glycogen synthetic flux in response to insulin in the double knock-in mice in which GS is insensitive to G6P and GSK3 is insensitive to insulin, a possibility also

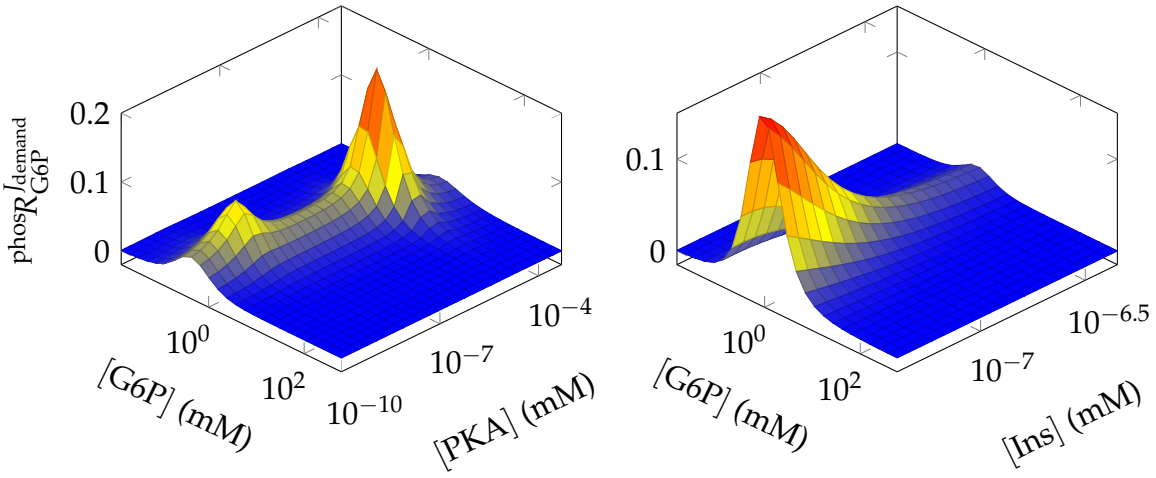

Figure 6.21: Dependence of ${}^{\text{phos}}R^{J_{\text{demand}}}_{\text{G6P}}$ on the PKA and insulin concentrations. Two peak areas, corresponding to the phosphorylation of site 2 and the inhibition of PP1 (which results in the phosphorylation of all sites) are observed when PKA is varied. ${}^{\text{phos}}R^{J_{\text{demand}}}_{\text{G6P}}$ decreases as insulin increases from a basal to hyperinsulinemic concentration.

considered by them.

The relevance (or even presence) of ${}^{\text{kin}}R^{J_{\text{demand}}}_{\text{G6P}}$ and ${}^{\text{phos}}R^{J_{\text{demand}}}_{\text{G6P}}$ *in vivo* is not established. While modification of GS kinases and phosphatases by G6P is an established phenomenon *in vitro*, to our knowledge, we are the first to provide quantification of these effects in a detailed model. In Chapter 4 we have shown from first principles, given that GS is a MWC-type equation, that the inclusion of these effects is necessary to satisfy thermodynamic constraints. The theory developed in Chapter 4 is supported by a wealth of experimental data. Unfortunately, the experimental data were obtained from experiments *in vitro*, are mostly qualitative, and in many cases the exact phosphorylation state of the enzyme used in assays is unknown. We have only included terms that modify the forward V_{max} for kinase and phosphatase reactions where it has been shown experimentally that G6P influences the V_{max}. In all other cases we have only included these terms for the K_{eq} to satisfy the thermodynamic constraints. Due to the large K_{eq} values of kinase and phosphatase reactions, terms that modify the K_{eq} are practically without effect on the activity of the kinases and phosphatases. While the effects quantified by ${}^{\text{kin}}R^{J_{\text{demand}}}_{\text{G6P}}$ and ${}^{\text{phos}}R^{J_{\text{demand}}}_{\text{G6P}}$ have not been observed *in vivo*, it would be surprising, given the theoretical considerations and *in vitro* data, if these effects are not present *in vivo*.

As we have seen, the values of ${}^{\text{kin}}R^{J_{\text{demand}}}_{\text{G6P}}$ and ${}^{\text{phos}}R^{J_{\text{demand}}}_{\text{G6P}}$ are small in comparison

to ${}^{\text{sub}}R^{J_{\text{demand}}}_{\text{G6P}}$ and ${}^{\text{allos}}R^{J_{\text{demand}}}_{\text{G6P}}$. The question then arises as to what function kinase inhibition and phosphatase activation by G6P fulfil that is not already fulfilled by allosteric activation of GS. We have already discussed the possibility that ${}^{\text{kin}}R^{J_{\text{demand}}}_{\text{G6P}}$ and ${}^{\text{phos}}R^{J_{\text{demand}}}_{\text{G6P}}$ are underestimated in our model, but even if this is the case the value of $\varepsilon^{\text{demand}}_{\text{G6P}}$ determined by Chase *et al.* [12] indicates that the underestimation cannot be very large. A very large $\varepsilon^{\text{demand}}_{\text{G6P}}$ value would result in switch-like behaviour in response to G6P. While switch-like behaviour is desirable in many systems, the possibility must be considered that glycogen synthesis could have evolved to repress this behaviour. This possibility must be considered with regard to the sites phosphorylated by casein kinase 2 (CK2) and GSK3 in particular. GS states that are phosphorylated to various extents at this cluster will all serve as PP1 substrates, but only the dephosphorylation of sites 3a and 3b would be enhanced by G6P. The other sites in this cluster will serve as competitive inhibitors in the dephosphorylation of sites 3a and 3b and their presence will therefore diminish the value of ${}^{\text{phos}}R^{J_{\text{demand}}}_{\text{G6P}}$. Similarly, GS that is not phosphorylated at sites 4 and 3c will diminish the inhibition by G6P of phosphorylation at sites 3b and 3a by GSK3. It appears therefore that multisite phosphorylation could act as a mechanism that minimizes ${}^{\text{kin}}R^{J_{\text{demand}}}_{\text{G6P}}$ and ${}^{\text{phos}}R^{J_{\text{demand}}}_{\text{G6P}}$. More substantive conclusions can, however, only be drawn when more detailed experimental data are available.

6.10 Energy charge homeostasis in response to ATP demand

Up to this point we have only considered the regulation of glycogen synthesis. In many respects the regulation of glycogen synthesis and glycogen degradation is reciprocal: G6P activates GS, but inhibits GP; phosphorylation generally inhibits GS, but activates GP. Since we have established that the regulation of glycogen synthesis involves the maintenance of G6P homeostasis in response to elevated external glucose and insulin—and not the control of the glycogen synthetic flux—it is of interest to also consider the function of the regulation of glycogen degradation. For this purpose we employed an implementation of the mathematical model (LamKus) of mammalian skeletal muscle glycogenolysis by Lambeth & Kushmerick [19]. Since it was first published, this model has been extended to also take into account the effect of pH on kinetic parameters and reaction equilibria [202]. We will, however, only be

concerned with the original model.

With regard to the rate equation and kinetics for GP, Lambeth & Kushmerick [19] chose to only include activation of the dephosphorylated enzyme by AMP, but omitted inhibition by ATP and G6P. Considering the possibility that the modifiers omitted by Lambeth & Kushmerick [19] could play important roles in the regulation of glycogen degradation, we developed an alternative GP rate equation that includes these modifiers. In developing this rate equation, we followed the same basic strategy as Walcott & Lehman [201], but with the important difference that G6P inhibition was included and that, similar to our treatment of GS, the kinetics of both phosphorylation states of GP were simultaneously fitted to experimental data. See Appendix C.2 for more details. The developed rate equation is a MWC-type equation in which phosphorylation alters the equilibria between the T, R, and U conformations. Only the R conformation is catalytically active. We substituted the GP rate equation in the model of Lambeth & Kushmerick [19] with this equation (GP MWC). We also considered a form of the equation that excludes G6P inhibition for purposes of comparison (GP G6P-insensitive).

The presence of a feedback inhibition loop in which G6P inhibits GP leaves little doubt that G6P could be considered, as in glycogen synthesis, to be a regulatory metabolite of glycogen degradation. Unfortunately, glycogen degradation cannot be treated as a simple supply-demand system of G6P, because G6P is involved in a phosphate moiety-conserved cycle, which prevents the system from being divided into functionally differentiated blocks unambiguously. At any rate, it is much more likely that the regulation of glycogen degradation is primarily concerned with the maintenance of the cellular energy charge than with the homeostasis of G6P.

Energy charge, ψ, is a secondary system variable and has been defined by Atkinson [246] as:

$$\psi = \frac{2[\text{ATP}] + [\text{ADP}]}{2([\text{ATP}] + [\text{ADP}] + [\text{AMP}])} \tag{6.54}$$

In what follows we will be mainly concerned with the energy charge and ignore most glycolytic intermediates.

In order to assess the impact on the steady-state of replacing the rate equation of GP, we compared the steady-states of the adapted models to the original model of Lambeth & Kushmerick [19] (Fig. 6.22). No change in any of the fluxes was observed. The differences between metabolite concentrations were, for the most part, very small and in all cases the values from the adapted and original models were

within the same order of magnitude. The absence of any difference in flux values is already an indication that alteration to the kinetics of GP, whether in the form of a different rate equation or in the form of allosteric and covalent modification, has little effect on the glycogen degradation flux.

We also considered the effects of varying the parameters k_{ATPase}, the first-order rate constant of the ATPase reaction, and f_{GP_a}, the fraction of GP that is present in the phosphorylated form, on the ATPase flux, J_{ATPase}, and on the energy charge (Fig. 6.23). As expected, since the ATPase reaction has almost complete control of the ATPase flux ($C^{J_{\text{ATPase}}}_{\text{ATPase}} = 0.99$) [19], J_{ATPase} increased linearly with k_{ATPase} in all three the models considered. On the other hand, increasing f_{GP_a} from 0.001 to 1 had virtually no effect on the ATPase flux (or any other flux in the system, not shown) in any of the models.

From the graphs on the right in Fig. 6.23, it is clear that an increased ATPase flux resulted in a decrease in energy charge. This decrease could, however, be reversed by an increase in the fraction of GP that is present in the active conformation. Overall these results indicate that the regulation of GP by phosphorylation does not function to regulate the flux of glycogen degradation, but instead enables the system to match the demand for ATP in such a way that the energy charge of the cell is maintained within a narrow range.

The extent to which the energy charge is buffered in the face of large changes in the demand for ATP is described by the co-response coefficient

$$\Omega^{J_{\text{ATPase}}:\psi}_{k_{\text{ATPase}}} = \frac{C^{J_{\text{ATPase}}}_{\text{ATPase}} \varepsilon^{\text{ATPase}}_{k_{\text{ATPase}}}}{C^{\psi}_{\text{ATPase}} \varepsilon^{\text{ATPase}}_{k_{\text{ATPase}}}} \tag{6.55}$$

$$= \frac{C^{J_{\text{ATPase}}}_{\text{ATPase}}}{C^{\psi}_{\text{ATPase}}} \tag{6.56}$$

The value of $C^{J_{\text{ATPase}}}_{\text{ATPase}}$ is readily obtainable by standard MCA methodology. Since ψ is really a function of steady-state variables, C^{ψ}_{ATPase} can be expressed in terms of conventional concentration-control coefficients. An expression for the control coefficient of ψ with respect to an arbitrary enzymatic step v is derived as follows. Taking the natural logarithm on the right and left hand sides of Eq. 6.54 yields

$$\ln \psi = \ln(2[\text{ATP}] + [\text{ADP}]) - \ln(2[\text{ATP}] + 2[\text{ADP}] + 2[\text{AMP}]) \tag{6.57}$$

From the definition of C^{ψ}_{v} we have

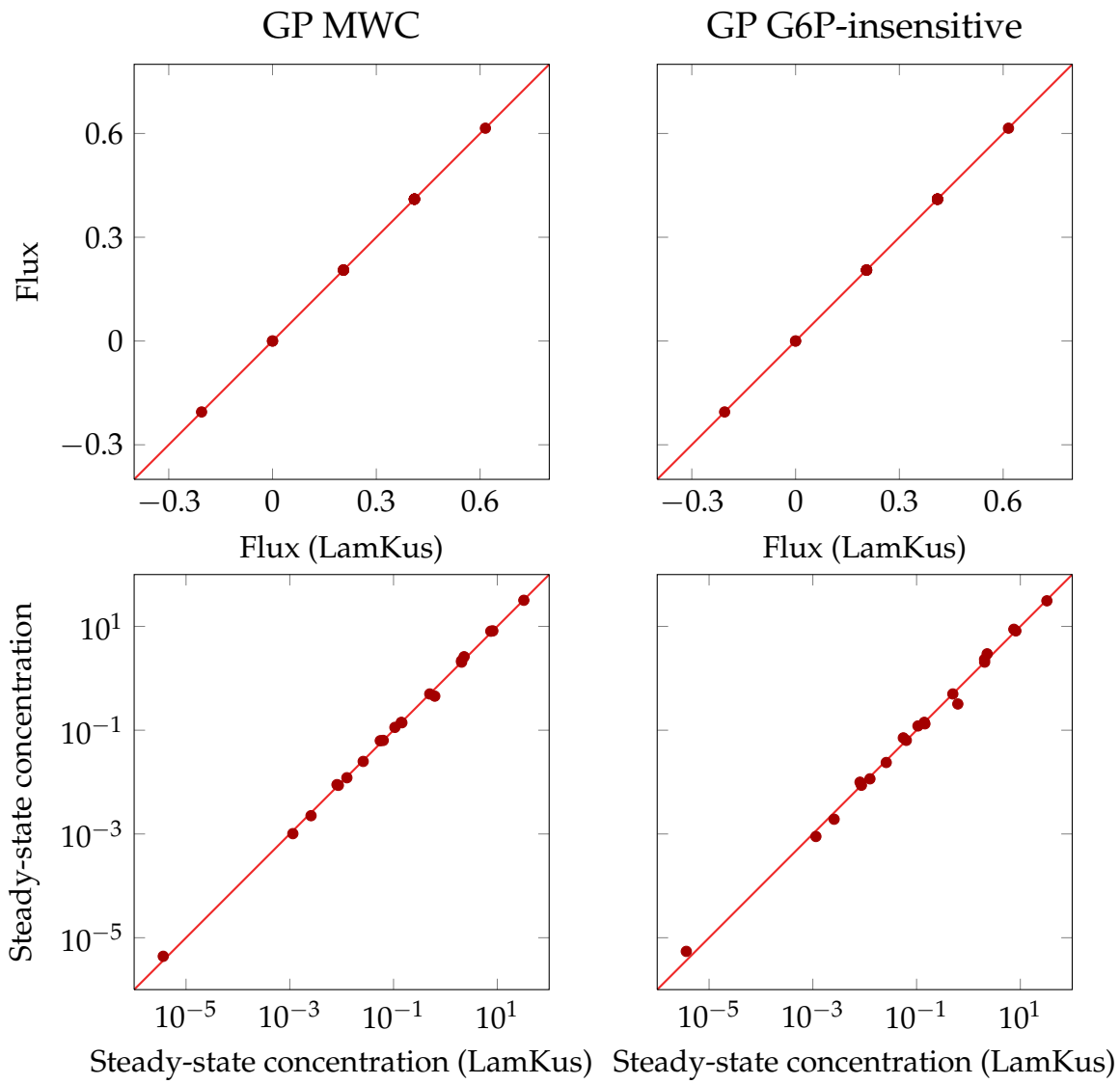

Figure 6.22: Correlation of fluxes and steady-state concentrations of the original (LamKus) and adapted Lambeth & Kushmerick [19] models. The model designated 'GP MWC' is identical to the original model with the exception that the rate equation for GP was replaced by a MWC-type equation that describes ATP and G6P inhibition in addition to AMP activation. The model designated 'GP G6P-insensitive' is identical to GP MWC with the exception that G6P inhibition was omitted from the rate equation. Note that all fluxes were integer multiples of the flux through GP. Red lines represent the function $y = x$.

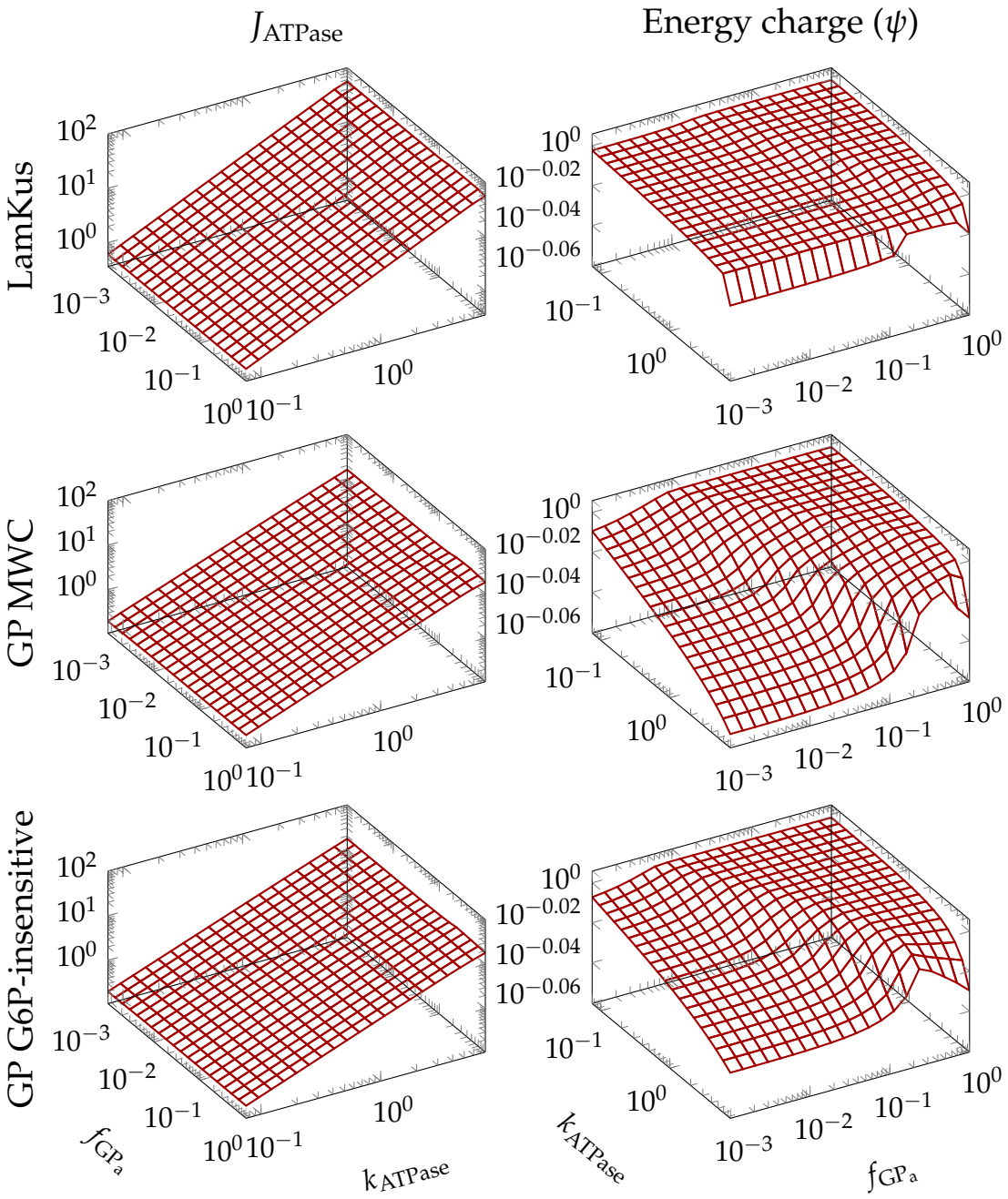

Figure 6.23: ATPase flux (J_{ATPase}) and energy charge (ψ) as functions of GP fractional phosphorylation ($f_{\mathrm{GP_a}}$) and ATP demand (k_{ATPase}). LamKus, the original model by Lambeth & Kushmerick [19]; GP MWC, the original model with a replaced GP rate equation that describes ATP and G6P inhibition in addition to AMP activation; GP G6P-insensitive, the same as GP MWC but without any G6P binding terms in the GP rate equation.

$$C_v^{\psi} = \frac{\partial \ln \psi}{\partial \ln v} \tag{6.58}$$

$$= \frac{\partial}{\partial \ln v}\Big[\ln(2[\mathrm{ATP}]+[\mathrm{ADP}]) - \ln(2[\mathrm{ATP}]+2[\mathrm{ADP}]+2[\mathrm{AMP}])\Big] \tag{6.59}$$

$$= \frac{\dfrac{2[\mathrm{ATP}]\dfrac{\partial \ln[\mathrm{ATP}]}{\partial \ln v} + [\mathrm{ADP}]\dfrac{\partial \ln[\mathrm{ADP}]}{\partial \ln v}}{2[\mathrm{ATP}]+[\mathrm{ADP}]}}{\quad - \dfrac{2[\mathrm{ATP}]\dfrac{\partial \ln[\mathrm{ATP}]}{\partial \ln v} + 2[\mathrm{ADP}]\dfrac{\partial \ln[\mathrm{ADP}]}{\partial \ln v} + 2[\mathrm{AMP}]\dfrac{\partial \ln[\mathrm{AMP}]}{\partial \ln v}}{2[\mathrm{ATP}]+2[\mathrm{ADP}]+2[\mathrm{AMP}]}} \tag{6.60}$$

$$= \frac{\dfrac{2[\mathrm{ATP}]C_v^{\mathrm{ATP}} + [\mathrm{ADP}]C_v^{\mathrm{ADP}}}{2[\mathrm{ATP}]+[\mathrm{ADP}]}}{\quad - \dfrac{[\mathrm{ATP}]C_v^{\mathrm{ATP}} + [\mathrm{ADP}]C_v^{\mathrm{ADP}} + [\mathrm{AMP}]C_v^{\mathrm{AMP}}}{[\mathrm{ATP}]+[\mathrm{ADP}]+[\mathrm{AMP}]}} \tag{6.61}$$

Finally, we substitute v for v_{ATPase} to obtain an expression for $C^{\psi}_{\mathrm{ATPase}}$.

We calculated $\Omega^{J_{\mathrm{ATPase}}:\psi}_{k_{\mathrm{ATPase}}}$ for a range of k_{ATPase} and $f_{\mathrm{GP_a}}$ values (Fig. 6.24). In all cases the absolute value of $\Omega^{J_{\mathrm{ATPase}}:\psi}_{k_{\mathrm{ATPase}}}$ was well above unity. This indicates that a change in ATPase activity results in a much larger change in the ATPase flux than in the energy charge. In other words, the energy charge is homeostatically buffered despite changing energy demands. The best homeostasis of energy charge was observed when there was a low ATP demand and the majority of GP was present in the dephosphorylated state. Note that $\Omega^{J_{\mathrm{ATPase}}:\psi}_{k_{\mathrm{ATPase}}}$ is negative, since the energy charge decreases with ATP demand.

Although, we varied k_{ATPase} and $f_{\mathrm{GP_a}}$ independently, these parameters are subject to coordinated regulation *in vivo*. During muscle contraction, calcium ions stimulate both PhK (which activates GP and thus increases $f_{\mathrm{GP_a}}$) and myosin (modelled as an increase in k_{ATPase}). The situation is therefore very similar to the coordinated activation of glucose uptake and glycogen synthesis by insulin, and, in analogy, we speculate that the coordinated regulation of ATPase and GP functions to increase the flux in response to ATP demand, by increasing k_{ATPase}, while maintaining the energy charge within a narrow range, by increasing $f_{\mathrm{GP_a}}$.

It has been found in numerous experiments *in vitro* that, in addition to allosteric modification, the ligands of GP also promote its covalent modification. It is well-established that AMP inhibits PP1 in the reaction with phosphorylated GP as substrate [167, 247, 248]. The effect of ATP is less clear, because our results suggests

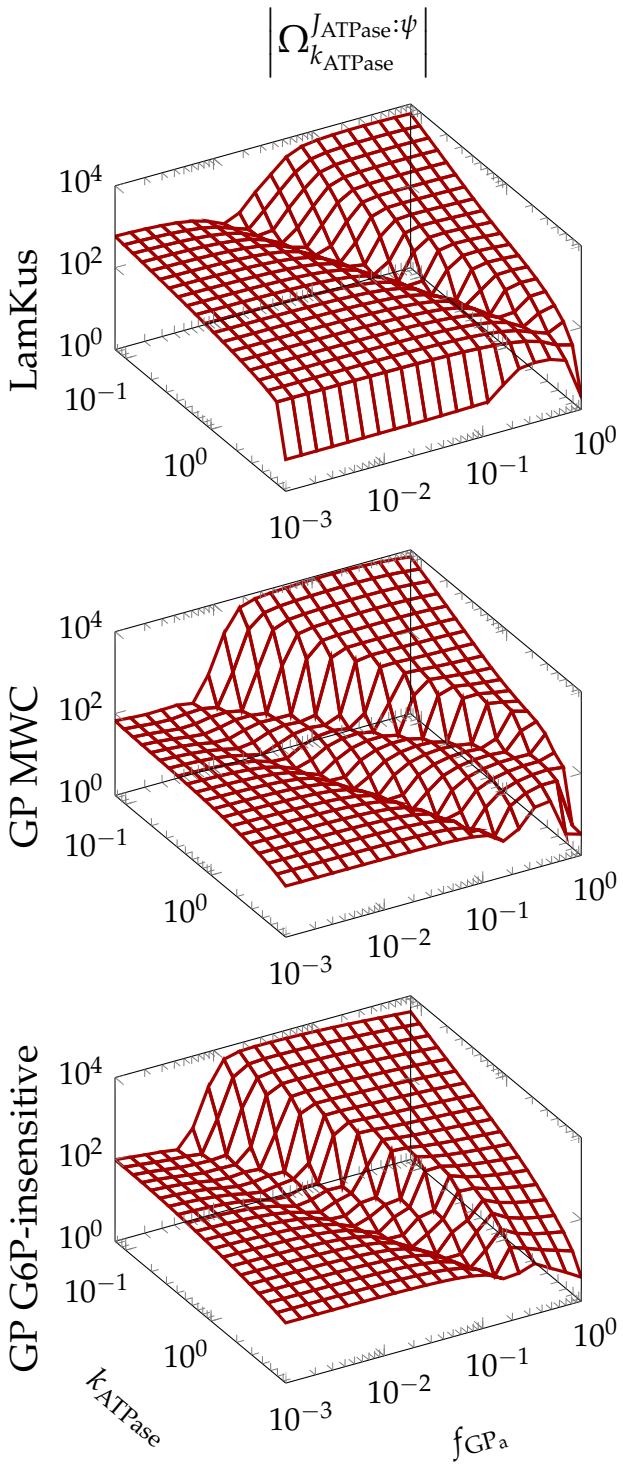

Figure 6.24: Co-response of ATPase flux (J_{ATPase}) and energy charge (ψ) to ATP demand (k_{ATPase}) as a function of GP fractional phosphorylation ($f_{\mathrm{GP_a}}$) and ATP demand. LamKus, the original model by Lambeth & Kushmerick [19]; GP MWC, the original model with a replaced GP rate equation that describes ATP and G6P inhibition in addition to AMP activation; GP G6P-insensitive, the same as GP MWC but without any G6P binding terms in the GP rate equation.

that, in addition to being a PhK substrate, it should also be a non-competitive inhibitor with GP as substrate. G6P, on the other hand, inhibits PhK and activates PP1 [166, 168, 222, 249]. These experimental results are in agreement with our finding that ligands of MWC-enzymes of which covalent modification results in a change in the equilibrium between conformations of the enzyme will affect the rates of covalent modification (see Section 4.3). While the effects of GP ligands on its covalent modification have not been studied in detail, it seems reasonable to speculate that a decrease in energy charge (decrease in ATP, increase in AMP) will of its own—independent of GP activation by calcium or cAMP—stimulate net phosphorylation of GP and thus act as a mechanism that increases the energy charge.

Any differences between the results obtained from the original model of Lambeth & Kushmerick [19] and the models with the adapted GP rate equations seem to be primarily quantitative and not qualitative. The differences are most apparent when energy charge is shown as a function of k_{ATPase} and f_{GP_a} (Fig. 6.24). In the models with MWC-type GP rate equations, the restoration of energy charge by f_{GP_a} was more pronounced than in the original model, but it should be noted that the decrease in energy charge in the original model in response to increases ATP demand was also much less pronounced. It is unlikely that ATP inhibition and G6P inhibition in the 'GP MWC' and 'GP G6P-insensitive' models are the primary factors contributing to these quantitative differences, because the ATP concentration changes very little and there is only a slight difference between the graphs of the 'GP MWC' and 'GP G6P-insensitive' models. The differences are most likely due to inherent differences between the Hill and MWC models. In particular, the degree of binding cooperativity is constant in the Hill model, but variable in the MWC model. The role of the feedback loop in which G6P inhibits GP is unclear from the present results.

Several other mechanisms in glycogenolysis probably play more significant roles in the homeostasis of energy charge. These mechanisms include the amplification of the sensitivity to changes in the ATP/ADP ratio by adenylate kinase perceived as a large change in AMP [77], the supplementation of ATP from phosphocreatine by creatine kinase, and the regulation of phosphofructokinase by AMP and ATP. Our emphasis on the covalent modification of GP results only from the fact that GP is often considered the rate-limiting enzyme of glycogenolysis (see for example [250–252]), with the implication that its covalent regulation should function to regulate the glycogenolytic flux. Here we have demonstrated instead that the covalent regulation

of GP is involved in the homeostasis of energy charge.

6.11 Combining glycogen synthesis and degradation

The natural next step is to combine the models of glycogen synthesis and glycogen degradation in an overall model of glycogen metabolism. In order to build such an overall model, several problems need to be addressed. First, it is necessary to formulate a description of glycogen concentration that accounts for the fact that not all glucose residues in the glycogen molecule are accessible to enzymes such as GS and GP. Second, additional enzymatic steps must be included to ensure that the system's stoichiometry is consistent.

Glycogen concentration

Glycogen is usually quantified as either the total residual glucose concentration or as the non-reducing end concentration. The former is readily determined experimentally, but it is the latter that is relevant in terms of enzymatic catalysis. Here we will show that the structural properties of the glycogen molecule allow one to approximate the non-reducing end concentration in terms of the glycogenin concentration and the total residual glucose concentration. As discussed earlier, glycogen synthesis is initiated by the enzyme glycogenin, which remains covalently bound to the glycogen molecule. Glycogen is synthesized by the linear elongation of glucose chains by means of $\alpha(1 \rightarrow 4)$ glycosidic bonds and by the introduction of branches initiated by means of $\alpha(1 \rightarrow 6)$ glycosidic bonds. Glycogen chains are on average 13 residues long, and each chain branches twice on average.

If, as a simplification, it is assumed that all glycogen chains have the same length and degree of branching, the total number of chains C_T and the total number of glucose residues G_T per glycogen molecule can be expressed as follows [2]:

$$C_T = \frac{1 - C_A r}{1 - r} \tag{6.62}$$

and

$$G_T = C_T g_c \tag{6.63}$$

where C_A is the number of chains in the outermost tier of branching, $r = 2$ is the degree of branching, and $g_c = 13$ is the number of glucose residues per glycogen chain. Substituting Eq. 6.62 into Eq. 6.63 yields

$$G_T = \frac{1 - C_A r}{1 - r} g_c \tag{6.64}$$

which can be rewritten with C_A on the left hand side:

$$C_A = \frac{G_T(r-1) + g_c}{g_c r} \tag{6.65}$$

The number of outermost chains for n molecules of glycogen is then given by

$$C_A = \sum_i^n C_{Ai} \tag{6.66}$$

$$= \sum_i^n \frac{G_{Ti}(r-1) + g_c}{g_c r} \tag{6.67}$$

$$= \frac{\sum_i^n G_{Ti}(r-1) + n g_c}{g_c r} \tag{6.68}$$

$$= \frac{G_T(r-1) + n g_c}{g_c r} \tag{6.69}$$

where the index i denotes a particular glycogen molecule. The amounts in Eq. 6.69 are readily transformed to concentrations to yield

$$[\text{NRE}] = \frac{[\text{Glc}_{\text{res}}](r-1) + [\text{GN}] g_c}{g_c r} \tag{6.70}$$

$$= \frac{[\text{Glc}_{\text{res}}] + 13[\text{GN}]}{26} \tag{6.71}$$

where [NRE] is the total non-reducing end concentration, $[\text{Glc}_{\text{res}}]$ is the total residual glucose concentration, and [GN] is the concentration of glycogenin. Note that the number of glycogen molecules, n, is equal to the number of glycogenin molecules.

The reaction stoichiometries for GS and GP would then be given by

$$\text{UDPG} \rightleftharpoons \text{UDP} + \text{Glc}_{\text{res}} \tag{6.72}$$

$$\text{P}_\text{i} + \text{Glc}_{\text{res}} \rightleftharpoons \text{G1P} \tag{6.73}$$

so that the model differential equations describe the change in residual glucose, but only the non-reducing end concentration is used within rate equations. Glycogen is thus effectively treated as a pool of glucose of which only a fraction, which can be calculated with knowledge of the structure of glycogen, can take part in enzymatic reactions.

This treatment is, however, not without shortcomings. First, not all non-reducing ends function as both substrates and products for GS and GP. The present treatment does not allow substrate non-reducing ends to be distinguished from product non-reducing ends. But, for sufficiently large glycogen molecules, substrate and product non-reducing ends overlap to such an extent that all non-reducing ends may be considered both substrates and products. Neglecting the difference between substrate and product non-reducing ends, however, results in further problems. It has the implication that GS is only sensitive to the ratio of UDPG and UDP, and that GP is only sensitive to the ratio of glucose-1-phosphate (G1P) and phosphate. Glycogen synthesis is therefore completely decoupled from glycogen degradation and glycogen will either accumulate or be depleted; no steady-state can be reached. This is of course not only a modelling problem but is potentially also a problem for the cell itself. It is therefore to be expected that glycogen sensitivity is conferred on GS and GP by mechanisms other than glycogen simply functioning as a reagent. Indeed, it is well-established that glycogen content regulates GS activity in a phosphorylation-dependent manner [138, 253]. A role in this regard has been suggested for AMP-activated protein kinase (AMPK) [254], a GS kinase that is able to sense glycogen branch points. Whether a similar mechanism also facilitates the sensitivity of GP to glycogen remains to be seen.

Second, Eq. 6.70 predicts a non-zero non-reducing end concentration in the absence of residual glucose. With regard to glycogen synthesis, this anomaly is indeed required to facilitate *de novo* glycogen synthesis. It does, however, allow glycogen degradation to continue even in the absence of residual glucose and thus could result in a negative residual glucose concentration. Third, it enforces no upper limit on the size of glycogen granules, whereas in reality steric constraints limit granules to 12 tiers (levels of branching). Finally, the roles of branching enzyme, debranching enzyme, and, to a certain extent, glycogenin are ignored. Until it becomes possible to address these problems, the issue of glycogen concentration can be side-stepped by treating the non-reducing end concentration as a clamped value in the model. The irony of this solution is of course that such a model of glycogen metabolism does not

actually describe the metabolism of glycogen.

Stoichiometric considerations

In the models of glycogen synthesis so far considered ATP and ADP are treated as clamped species. In a single cycle from external glucose to elongated glycogen, 3 phosphate moieties enter the system as a molecule of ATP, of which 2 leave again as an ADP. Three phosphate moieties also enter as UTP, whereas two leave as PP_i and another two as UDP. There is thus no gain or loss of phosphate moieties in the system:

$$\underset{\text{ATP}}{3} \quad \underset{\text{ADP}}{-2} \quad \underset{\text{UTP}}{+3} \quad \underset{\text{PP}_i}{-2} \quad \underset{\text{UDP}}{-2} \quad = 0 \tag{6.74}$$

When the glycogen synthesis model is combined with the model of glycogenolysis, ATP and ADP, however, become variable species. The conservation of phosphate moieties is then given by:

$$\underset{\text{UTP}}{3} \quad \underset{\text{PP}_i}{-2} \quad \underset{\text{UDP}}{-2} \quad = -1 \tag{6.75}$$

which reveals that the phosphate moiety drains from the system. Treating also PP_i as a variable species and adding an inorganic diphosphatase (PPase) reaction that breaks PP_i down to two molecules of P_i yields

$$\underset{\text{UTP}}{3} \quad \underset{\text{UDP}}{-2} \quad = 1 \tag{6.76}$$

so that now the phosphate moiety accumulates in the system. It is therefore also necessary to treat UTP and UDP as variable species and to add a reaction that converts UDP back to UTP at the cost of ATP.

A combined model of glycogen synthesis and glycogen degradation

Keeping the above considerations in mind, we proceeded to construct a model (GlyMetExp) of glycogen metabolism by combining the model GlySynthExp with the model of glycogenolysis by Lambeth & Kushmerick [19]. We treated glycogen as a fixed metabolite. In addition to the reactions already present in these models we also

Table 6.2: Kinetic parameters for PPase and NDPK

Parameter	Value	Unit	Reference	Source
$V_{max,PPase}$	30	mM min^{-1}	Table C.4	rabbit muscle
$K_{PPase:PPi}$	$5.1 \cdot 10^{-3}$	mM	[255]	rabbit muscle
$K_{PPase:ATP}$	0.3	mM	[255]	rabbit muscle
$K_{PPase:Pi}$	1	mM	based on value from [113]	–
$K_{eq,PPase}$	2,460	mM	TECR database [206]	–
$V_{max,NDPK}$	440	mM min^{-1}	Table C.4	bovine heart
$K_{NDPK,UDP}$	$7 \cdot 10^{-2}$	mM	based on value with ADP as substrate [256]	rat liver
$K_{NDPK,ATP}$	0.5	mM	[256]	rat liver
$K_{NDPK,UTP}$	0.7	mM	assumed	–
$K_{NDPK,ADP}$	0.14	mM	[256]	rat liver
$K_{eq,NDPK}$	1	–	eQuilibrator [36]	–

added the PPase and nucleoside diphosphokinase (NDPK) reactions. PPase catalyses the reaction $PP_i \leftrightharpoons 2P_i$. We modelled the reaction with a uni-bi Michaelis-Menten rate equation containing an additional ATP inhibition term:

$$v_{PPase} = \frac{\frac{V_{max}}{K_{PP_i}}\left([PP_i] - \frac{[P_i]^2}{K_{eq}}\right)}{\frac{[PP_i]}{K_{PP_i}} + \frac{[ATP]}{K_{ATP}} + \left(1 + \frac{[P_i]}{K_{P_i}}\right)^2} \tag{6.77}$$

NDPK catalyses, amongst others, the reaction UDP + ATP $\leftrightharpoons$ UTP + ADP. We modelled this reaction with a random-order bi-bi Michaelis-Menten equation:

$$v_{NDPK} = \frac{\frac{V_{max}}{K_{UDP}K_{ATP}}\left([UDP][ATP] - \frac{[UTP][ADP]}{K_{eq}}\right)}{\left(1 + \frac{[UDP]}{K_{UDP}} + \frac{[UTP]}{K_{UTP}}\right)\left(1 + \frac{[ATP]}{K_{ATP}} + \frac{[ADP]}{K_{ADP}}\right)} \tag{6.78}$$

The kinetic parameter values for the PPase and NDPK reactions are listed in Table 6.2.

Steady-state analysis of the model, however, revealed that, even under resting conditions, the glycolytic flux ($J_{PGI} = 2.43 \times 10^{-1}$ mM min^{-1}) was almost three times larger than the glucose uptake flux ($J_{GLUT} = 9.06 \times 10^{-2}$ mM min^{-1}). Accordingly, GS had a large flux-control coefficient for the glycogen synthetic flux ($C_{GS}^{J_{GS}} = 0.89$). If glycogen were not treated as a fixed species, this high glycolytic flux would result in complete glycogen depletion. The glycolytic flux could be reduced by decreasing the first-order rate constant of the ATPase reaction (a parameter that was assigned an arbitrary value by Lambeth & Kushmerick [19]), but with the side-effect that the

concentration of G6P decreased to values where its activatory effect on GS was no longer able to overcome inhibition by ATP and phosphorylation. Decreasing the rate constant for lactate export very slightly increased G6P again, but at the cost of lactate accumulation. We also replaced the mass-action rate equations for the lactate export and ATPase reactions with irreversible Michaelis-Menten equations so as not to force unit elasticities on these reactions. These modifications did not improve the situation.

While it is possible that appropriate parameter adjustments will yield a model that is in qualitative agreement with *in vivo* glycogen metabolism, the merit of such an approach is questionable unless great care it taken to only use parameter values that fall within experimentally determined ranges. Since construction of a detailed model of glycogen degradation is not within the scope of the present research, we did not pursue this avenue further. Future attempts will have to ensure that the same modelling approach and philosophy is followed in constructing the glycogen synthesis and degradation modules.

Chapter 7

Discussion

7.1 Glycogen metabolism as a molecular economy

The inner workings of the cell have been described in terms of a molecular economy of supply and demand [15, 257]. In this analogy between human economies and cellular processes, biosynthesis can be compared to a factory in which a certain product is manufactured for consumption by the public. A typical cellular example of such a factory is the biosynthesis of amino acids for consumption by the process of protein synthesis. Just as uncontrolled manufacturing without regard for consumer demand results in overrun or shortage in human economies, usually with financial loss, so any cellular biosynthetic process that is not controlled by the demand for its product would be detrimental to the proper functioning of the cell.

If biosynthesis is a factory, muscle glycogen metabolism is a warehouse or, perhaps more appropriately, a granary. One may view glycogen metabolism as a supply-demand system of glycogen in which glycogen synthesis and degradation are the supply and demand processes. However, while glycogen is consumed during exercise, it is not primarily exercise that immediately drives glycogen synthesis. Nor is it feeding that drives exercise. It is therefore more instructive to view glycogen synthesis and degradation as processes that can themselves be divided into supply and demand systems. In keeping with our analogy, the process in which glycogen is synthesized is comparable to the storage of harvested animal feed in the granary. It is clear that the rate at which feed is stored should be determined by the harvest and that there really is no immediate *demand*, so to speak, by the granary for feed. In glycogen synthesis one therefore expects glucose uptake to control the flux of glycogen synthesis. Glycogen degradation, on the other hand, can be compared to

feeding farm animals from the granary. Here it is clear that the rate at which feed is removed from the granary should be determined by the dietary requirements of the animals and not by the supply of feed in the granary. With regard to glycogen degradation, one would therefore expect the rate of glycogenolysis to be controlled by the demand for energy and not by the supply of glycogen.

We see then that glycogen synthesis should be expected to be a supply-driven process, whereas glycogen degradation should be expected to be a demand-driven. While it is reasonable to expect that the demand process controls the flux in a biosynthetic pathway, it may well be that the supply controls the flux in other pathways. In both glycogen synthesis and degradation it is interesting to note that allosteric and covalent regulation does not affect the activities of the flux controlling processes. We may then ask why the activities of enzymes that do not affect the flux are regulated.

7.2 Regulation of glycogen metabolism

Using detailed mathematical models of glycogen synthesis, we have shown first that the basal levels of glycogen synthase (GS) phosphorylation and ATP inhibition in conjunction with the feedforward activation of GS by glucose-6-phosphate (G6P) impart G6P sensitivity on the demand block that greatly surpasses that of the supply block (Section 6.4). We have also shown that this high G6P sensitivity of the demand block allows it to match any increases in the flux of the supply block, which would typically result from elevated glycemia, with only minimal increases in G6P. This suggests that the allosteric and covalent regulation of GS functions to maintain G6P homeostasis despite large increases in the blood glucose concentration after meals. Note that changes in the external glucose concentration do not lead to changes in the GS degree of phosphorylation. The basal phosphorylation state of GS is therefore sufficient to ensure G6P homeostasis.

With regard to insulin stimulation, on the other hand, we have shown that GS phosphorylation is not involved in increasing the sensitivity of the demand block to G6P (Section 6.6). On the contrary, insulin stimulation results in the dephosphorylation of GS and therefore weakens G6P homeostasis with respect to increases in external glucose. Insulin stimulation achieves G6P homeostasis via an entirely different mechanism, namely, the coordinated activation of glucose uptake and glycogen synthesis. These results do not only agree with but also elaborate on the findings of Schafer *et al.* [13] in that a wide range of insulin concentrations is considered.

Using the existing model of glycogenolysis by Lambeth & Kushmerick [19], we have also shown that the covalent regulation of glycogen phosphorylase (GP) is not involved in flux control, but rather functions to maintain the energy charge of the cell within narrow limits despite large changes in the cell's energy demand (Section 6.10). While we have not explicitly considered the function of allosteric regulation of GP, GP phosphorylation affects the apparent affinities of GP for its various allosteric modifiers, so that we may assume similar functions for allosteric and covalent regulation of GP. Note that we do not claim that energy charge homeostasis is the sole function of the regulation of GP, or even that GP regulation is the most important cellular mechanism that enhances energy charge homeostasis. The function of GP regulation is, however, certainly not the flux control of glycogenolysis.

While it appears that the function of GS regulation is the homeostasis of G6P and the function of GP regulation is the homeostasis of energy charge, the function of the regulation of enzyme activities is by no means limited to homeostatic maintenance. Flux-controlling enzymes are often regulated, so that changes in the activity of these enzymes will result in changes to the flux. Indeed, in the coordinated regulation of glucose uptake and glycogen synthesis by insulin stimulation, the activities of both the flux-controlling enzyme, glucose transporter 4 (GLUT4), and the "regulated" enzyme GS, are simultaneously increased. It may be that such coordinated regulation is far more common than is currently recognized and may even be a requirement for effective flux regulation [258]. We have argued that coordinated regulation is also at work in glycogen degradation during exercise. Here too the flux-controlling enzyme, ATPase, as well as the "regulated" enzyme, GP, are activated in response to calcium.

7.3 Relative importance of allosteric and covalent modification of glycogen synthase

The presence of both allosteric and covalent regulation in glycogen metabolism has led to questions regarding the relative importance of these mechanisms. Hofmeyr & Cornish-Bowden [15] have pointed out that a mechanism's "regulatory performance should always be measured in terms of a specified function." In judging the relative importance of allosteric and covalent modification, one must therefore first identify its function and also ascertain that both mechanisms indeed have the same function. We have argued that in glycogen synthesis both allosteric and covalent regulation

function to maintain the homeostasis of G6P. There is, however, some indication that these mechanisms do not perform this function in response to the same stimuli. We have shown that the increase in intrinsic GS activity in response to elevated glycemia, measured as the fraction of enzyme in the active R conformation, is almost entirely the result of allosteric activation by G6P. On the other hand, the increase in intrinsic GS activity in response to elevated insulin is almost entirely the result of net dephosphorylation of GS. In a certain sense then, the question of whether allosteric or covalent modification is the most important mechanism of G6P homeostasis becomes irrelevant.

The question of whether allosteric or covalent modification is most important may also be posed in a different way: which mechanism contributes most to the basal activity state of GS? It is well-established that sufficiently high concentrations of G6P are able to completely reverse inhibition of GS by phosphorylation. In agreement with this, Bouskila *et al.* [18] have found that insulin is unable to restore the basal activity of GS that has been desensitized to G6P. In other words, dephosphorylation of the GS sites that are phosphorylated by glycogen synthase kinase 3 (GSK3) does not overcome the inhibition of GS caused by phosphorylation at the remaining sites and the additional inhibition by ATP. Bouskila *et al.* [18] have interpreted these results as evidence that allosteric, and not covalent, regulation of GS is the most important mechanism by which insulin stimulates GS activity. We agree that G6P activation is an essential component of the basal GS activity, but argue that the results of Bouskila *et al.* [18] give no indication of the relative contributions of allosteric and covalent activation beyond the basal state.

7.4 Qualitative equivalence of allosteric and covalent regulation

Covalent enzyme modification is often considered to be fundamentally different from allosteric modification. The various covalent forms of enzymes such as GS and GP are often studied separately. This probably results from the fact that, while terms for allosteric modification can be incorporated into initial velocity equations, the same cannot be done for covalent modification. Instead, separate rate equations are required for each covalent form of an enzyme. In a very real sense covalent modification is, however, also a form of allosteric modification in that the covalent bond is usually formed at a site other than the catalytic site. Despite this agreement, the

model of cooperativity and allosterism identified as providing the best description of allosteric modification for a particular enzyme is often disregarded when covalent modification is considered. A *carte blanche* is given to covalent modification to alter any kinetic parameter without consideration for an underlying kinetic model or mechanism by which such alteration is explained.

We have conducted a comprehensive review of GS kinetics and regulation and concluded that the interaction between the allosteric and covalent modification of GS behaves in a qualitatively identical manner to what is expected for the interaction between two classic heterotropic Monod-Wyman-Changeux (MWC)-type effectors (Chapter 2). This led us to propose a unified view of allosteric and covalent regulation of GS in which only the equilibrium between between the T and R conformation may be altered. In this unified view there is no need to determine the full set of kinetic parameters for the rate equations of all phosphorylation states of GS. The only requirement is that L_0, the T/R equilibrium, should be determined for each phosphorylation state. However, for many states L_0 can be estimated from the values of "component" states. This model allowed us to develop which is to our knowledge the first kinetic treatment of GS that is able to account for both allosteric and covalent regulation (Chapter 3). The same model, but with an additional conformation, was also used to obtain a rate equation for GP that describes its allosteric modification by all the major effectors as well as its covalent modification.

To be sure, we are not advocating the position that covalent modification will be qualitatively identical to allosteric modification for all enzymes. Nor do we argue that covalent modification can always be described as bringing about a conformational change. As but one example, phosphorylation of isocitrate dehydrogenase does not involve any conformational change, but instead prevents substrate binding by obstructing the catalytic site [259]. This type of covalent modification cannot be described with the MWC model. With regard to GS there are many phosphorylation sites that do not affect the enzyme's activity. These sites can, however, be accounted for in the MWC model by simply considering phosphorylation at each of these sites as multiplying L_0 with a factor of one.

Since activation of GS by G6P and inhibition of GS by phosphorylation stabilize opposing conformations of the enzyme, they also reverse each other's effect on the activity of GS. This reversal is not only the result of conformational change, but also results because phosphorylation promotes a state in which G6P associates less readily with GS and G6P promotes a state that is more readily dephosphorylated.

Phosphorylation favours the T conformation, which is inactive, but also decreases the affinity of GS for G6P and may even cause G6P to dissociate. G6P, on the other hand, favours the R conformation, countering the effect of phosphorylation. Because phosphate is covalently bound, however, G6P is not able to directly cause the phosphate group to dissociate from GS. G6P nevertheless promotes net dephosphorylation of GS by kinase inhibition and phosphatase activation. Such interaction between allosteric and covalent regulation has been observed experimentally for GS (see for example [139, 146]) and GP (see for example [260]). An explanation in terms of an underlying mechanism has to our knowledge not been proposed before.

Covalent modification of an enzyme is itself catalysed by enzymes. Activation or inhibition of these covalent interconversion enzymes by allosteric modifiers of the substrate enzyme should therefore manifest as apparent changes to their kinetic parameters. From thermodynamic considerations, we have shown that apparent changes in both the rate constants and Michaelis constants can result from such allosteric modification (Section 4.3). Changes in the rate constant result entirely from the fact that covalent modification alters the T/R equilibrium of the substrate enzyme. The factor by which rate constants are modified is therefore determined by the kinetics of the substrate protein and not by the kinetics of the covalent interconversion enzymes. Changes in the Michaelis constants, on the other hand, are specific to the interconversion enzymes and are not governed by the substrate enzyme's kinetics. The substrate and product Michaelis constants are modified by the same factor. If covalent modification does not alter the T/R equilibrium of the substrate enzyme, then changes are observed in neither the rate constants nor the Michaelis constants. Note that these effects on the kinetics of the interconversion enzymes are independent of their kinetic mechanism. Indeed, it may be that the interconversion enzymes are themselves MWC-type enzymes.

The regulation of muscle glycogen synthesis therefore involves a feedforward activation loop in which G6P activates GS, but also a complex phosphorylation cascade in which all GS ligands are also indirect ligands of the interconversion enzymes. Hofmeyr *et al.* [16] considered the conditions that would allow feedforward loops to function optimally. Small & Fell [164], on the other hand, considered the conditions that would allow covalent modification cascades to elicit an optimal response in response to external effectors. The situation in glycogen metabolism differs from these analyses in that the feedforward activator is also the effector that regulates the covalent modification of GS. We analysed the conditions that would maximize the flux

response to an allosteric modifier in a minimal feedforward system in which the allosteric enzyme is also regulated by a monocyclic cascade (Section 4.4). Broadly speaking, our results indicated that one would expect the feedforward activation of the regulated enzyme to be dominated by a catalytic and not a specific component, and that the enzymes catalysing the covalent modification of the regulated enzyme should be saturated with their protein substrates.

Is glucose-6-phosphate really a specific activator?

The GS rate equation and parameters that we identified as providing the best description of experimental data incidentally show that G6P is a catalytic activator of GS. There is, however, also a slight specific component which results from the competition of ATP with the UDP-glucose (UDPG) substrate. Since, however, GS is not saturated with its substrate and because the enzyme that precedes it operates close to equilibrium, the strict requirement for catalytic activation may be relaxed. The strong catalytic component predicted by our results and the absence of specific activation in the absence of ATP is, however, at variance with the standard view of GS kinetics which holds that phosphorylation decreases the UDPG affinity, whereas G6P increases it. This discrepancy could be explained by considering that the experimental data that we used for GS parameter optimization were determined at a lower pH (6.6) than what is usually used (7.8). High pH values suppress ATP inhibition in GS assays [67]. Piras *et al.* [39, 67] found significant differences in GS kinetics when comparing data obtained at low and high pH values. Another possible explanation is that GS kinetic parameters are routinely determined from linear transformations of initial velocity data even though GS is a cooperative enzyme. Walcott & Lehman [201] have shown that this practice, when applied to GP kinetics, portrays ATP as a competitive inhibitor with respect to AMP, whereas non-linear regression, which allows for fitting sigmoidal curves, suggests that ATP is also a non-competitive inhibitor and that the non-competitive component is in fact the dominant component. Similar artefacts are to be expected for GS kinetics when cast in a Michaelis-Menten mould.

7.5 Modelling glycogen metabolism

The model of glycogen synthesis, GlySynth, in which the interconversion between GS phosphorylation states is described with the appropriate kinase and phosphatase reactions, as well as the combined model of glycogen metabolism that incorporates the existing model by Lambeth & Kushmerick [19], contains a substantial number of parameters that were obtained from the literature. Considering the accumulation of experimental error in the determined kinetic parameters, this large number of parameters poses a threat to the validity of the models. We have nevertheless shown that in many respects the models' predicted behaviour is qualitatively in agreement with experimentally observed behaviour. It should be noted that the GlySynth model consists of two modules that are not connected by mass flow: the main pathway and the GS interconversion pathway. While the interconversion pathway is sensitive to G6P and UDPG from the main pathway, the main pathway is only sensitive to the concentrations of GS in its various states as determined by the interconversion pathway. In effect, therefore, the only "parameter" of the main pathway that is determined by the interconversion pathway is the equilibrium between the T and R conformations of GS. Any error in the interconversion pathway is therefore propagated to the main pathway as an error in a single parameter, unless one is specifically interested in the concentrations of GS in its various states.

Existing models of muscle metabolism that include glycogen synthesis are for the most part based on the model by Cabrera *et al.* [261]. This model has been extended to incorporate many additional aspects of muscle metabolism, such as insulin signalling and compartmentation. Some of the more recent extensions are those by Dash *et al.* [262] and Li *et al.* [263]. While this model includes a GS reaction, its focus is not on glycogen metabolism. It treats the GS reaction as the combined reactions of GS and UDPG-pyrophosphorylase (UPP). The GS reaction is modelled with a hyperbolic Michaelis-Menten type rate equation that does not include the G6P feed-forward activation loop. No description of GS phosphorylation is present, although insulin stimulation terms have been incorporated in some versions. The model also treats glycogen as a pool of glucose in which all residues, as opposed to only non-reducing residues, are visible to enzymes.

We have demonstrated the usefulness of the models that we have constructed in shedding light on the regulatory design of muscle glycogen metabolism. It is essential to understand the regulation of muscle glycogen metabolism by endocrine

and other signals in order to fully comprehend the pathology of insulin resistance and diabetes mellitus type 2. Insulin resistance is, however, a whole-body syndrome involving the systemic malfunctioning of insulin-dependent metabolism in various tissues. There is thus a need to integrate models of insulin-dependent metabolism from various tissues. Such models have been constructed [264, 265], but are mostly phenomenological, contain only abbreviated descriptions of glycogen metabolism, or only include glucose uptake.

While we appreciate the merits of phenomenological modelling, we argue that great care must be taken to ensure that important regulatory features of a pathway are not obscured by disregard for the underlying mechanisms. In many cases mechanism does matter. It may be of little consequence, for instance, whether a bi-bi reaction is modelled with a ping-pong or random order rate equation [266], but it has been demonstrated that the seemingly inconsequential difference between catalytic and specific activation can have important implications for the effectiveness of regulatory mechanisms such as feedback and feedforward loops [16]. An uninformed modelling choice could lead to the inclusion of such regulatory mechanisms that turn out to perform no function at all. Incidentally, careful consideration of the mechanism of GS cooperativity was instrumental both in understanding the regulatory design of glycogen synthesis and in the identification of novel regulatory aspects. Nevertheless, even very detailed mechanistic models are of little use if they are parametrized with parameter sets of poor quality. There is a pressing need for high-quality muscle enzyme kinetic data. It is essential that research in muscle metabolism does not neglect enzyme kinetics in favour of semi-quantitative studies. Much can be learned from a good model in less time than from experimentation.

7.6 Future research

Many aspects of muscle glycogen metabolism remain unaddressed by the present research. In future research the model of glycogen synthesis can be extended to also describe the phosphorylation of GS by AMP-activated protein kinase (AMPK), an enzyme that is able to sense the glycogen concentration as well as the energy charge in the cell [252]. We have also disregarded the targeting of protein phosphatase 1 (PP1) to various subcellular pools and the role of phosphorylation in this regard [1, 31]. Additionally, it would be of interest to construct a combined model of glycogen synthesis and degradation in which glycogen itself is a variable species.

It would also be instructive to validate the unified view of allosteric and covalent GS regulation experimentally. Finally, kinetic parameters for the interconversion between GS phosphorylation states and for the main pathway should be determined under conditions that would prevail *in vivo*.

Appendix A

Miscellaneous derivations

A.1 Expression of the sum of MWC-type rate equations as a single term

Consider the irreversible two-state MWC rate equation:

$$v = e\frac{nk_{\text{cat,r}}\left(1+\sigma_r\right)^{n-1} + nk_{\text{cat,t}}\left(1+\sigma_t\right)^{n-1}L_0}{\left(1+\sigma_r\right)^{n} + \left(1+\sigma_t\right)^{n}L_0} \tag{A.1}$$

Let

$$\text{num}_r = nk_{\text{cat,r}}\left(1+\sigma_r\right)^{n-1} \tag{A.2}$$

$$\text{num}_t = nk_{\text{cat,t}}\left(1+\sigma_t\right)^{n-1}L_0 \tag{A.3}$$

$$\text{den}_r = \left(1+\sigma_r\right)^{n} \tag{A.4}$$

$$\text{den}_t = \left(1+\sigma_t\right)^{n}L_0 \tag{A.5}$$

then

$$v = e\frac{\text{num}_r + \text{num}_t L_0}{\text{den}_r + \text{den}_t L_0} \tag{A.6}$$

With appropriate definitions, any two-state MWC rate equation, including reversible forms, can be written in this form. Consider now the sum of rates $v = \sum_i v_i$,

where each rate v_i is of the form of Eq. A.6, but in which only the parameter L_0 depends on i (each enzyme concentration e_i is a variable):

$$v = \sum_i e_i \frac{\text{num}_r + \text{num}_t L_{0i}}{\text{den}_r + \text{den}_t L_{0i}} \tag{A.7}$$

Multiplication of the numerator and denominator with $\sum_i e_i$ yields

$$v = \frac{\left(\sum_i e_i\right)\left(\sum_i e_i \dfrac{\text{num}_r + \text{num}_t L_{0i}}{\text{den}_r + \text{den}_t L_{0i}}\right)}{\sum_i e_i} \tag{A.8}$$

Further multiplying each sum term in the denominator with $\dfrac{\text{den}_r + \text{den}_t L_{0i}}{\text{den}_r + \text{den}_t L_{0i}}$ gives

$$v = \frac{\left(\sum_i e_i\right)\left(\sum_i e_i \dfrac{\text{num}_r + \text{num}_t L_{0i}}{\text{den}_r + \text{den}_t L_{0i}}\right)}{\sum_i e_i \dfrac{\text{den}_r + \text{den}_t L_{0i}}{\text{den}_r + \text{den}_t L_{0i}}} \tag{A.9}$$

The fractions in the numerator and denominator can be separated so that

$$v = \frac{\left(\sum_i e_i\right)\sum_i \left(e_i \dfrac{\text{num}_r}{\text{den}_r + \text{den}_t L_{0i}} + e_i \dfrac{\text{num}_t L_{0i}}{\text{den}_r + \text{den}_t L_{0i}}\right)}{\sum_i \left(e_i \dfrac{\text{den}_r}{\text{den}_r + \text{den}_t L_{0i}} + e_i \dfrac{\text{den}_t L_{0i}}{\text{den}_r + \text{den}_t L_{0i}}\right)} \tag{A.10}$$

$$= \frac{\left(\sum_i e_i\right)\left(\sum_i e_i \dfrac{\text{num}_r}{\text{den}_r + \text{den}_t L_{0i}} + \sum_i e_i \dfrac{\text{num}_t L_{0i}}{\text{den}_r + \text{den}_t L_{0i}}\right)}{\sum_i e_i \dfrac{\text{den}_r}{\text{den}_r + \text{den}_t L_{0i}} + \sum_i e_i \dfrac{\text{den}_t L_{0i}}{\text{den}_r + \text{den}_t L_{0i}}} \tag{A.11}$$

Extracting terms that are independent on i from the sums yields

$$v = \frac{\left(\sum_i e_i\right)\left(\text{num}_r \sum_i e_i \dfrac{1}{\text{den}_r + \text{den}_t L_{0i}} + \text{num}_t \sum_i e_i \dfrac{L_{0i}}{\text{den}_r + \text{den}_t L_{0i}}\right)}{\text{den}_r \sum_i e_i \dfrac{1}{\text{den}_r + \text{den}_t L_{0i}} + \text{den}_t \sum_i e_i \dfrac{L_{0i}}{\text{den}_r + \text{den}_t L_{0i}}} \tag{A.12}$$

Finally, division of the numerator and denominator by $\sum_i e_i \dfrac{1}{\text{den}_r + \text{den}_t L_{0i}}$ gives

$$v = \frac{(\sum_i e_i)\left(\text{num}_r + \text{num}_t \dfrac{\sum_i e_i \dfrac{L_{0i}}{\text{den}_r + \text{den}_t L_{0i}}}{\sum_i e_i \dfrac{1}{\text{den}_r + \text{den}_t L_{0i}}}\right)}{\text{den}_r + \text{den}_t \dfrac{\sum_i e_i \dfrac{L_{0i}}{\text{den}_r + \text{den}_t L_{0i}}}{\sum_i e_i \dfrac{1}{\text{den}_r + \text{den}_t L_{0i}}}} \tag{A.13}$$

If we then define

$$L_{0,\text{app}} = \frac{\sum_i e_i \dfrac{L_{0i}}{\text{den}_r + \text{den}_t L_{0i}}}{\sum_i e_i \dfrac{1}{\text{den}_r + \text{den}_t L_{0i}}} \tag{A.14}$$

and

$$e = \sum_i e_i \tag{A.15}$$

Eq. A.13 is rewritten as

$$v = e \frac{\text{num}_r + \text{num}_t L_{0,\text{app}}}{\text{den}_r + \text{den}_t L_{0,\text{app}}} \tag{A.16}$$

Note also that, since $e_i = r(\text{den}_r + \text{den}_t L_{0i})$ and $t_i = L_{0i} r_i$, it follows that

$$L_{0,\text{app}} = \frac{\sum_i t_i}{\sum_i r_i} \tag{A.17}$$

A.2 Expression of the overall elasticity of a sum of rates in terms of elasticities of individual rates

Let v be the sum of rates catalysed by isoforms or different covalent states of a particular enzyme:

$$v = \sum_i v_i \tag{A.18}$$

The elasticity of the rate v towards an arbitrary ligand X is then given by

$$\begin{aligned}
\varepsilon_x^v &= \frac{\partial \ln v}{\partial \ln x} && \text{(A.19)}\\
&= \frac{x}{v} \cdot \frac{\partial v}{\partial x} && \text{(A.20)}\\
&= \frac{x}{v} \cdot \frac{\partial}{\partial x}\left[\sum_i v_i\right] && \text{(A.21)}\\
&= \frac{x}{v} \cdot \sum_i \frac{\partial v_i}{\partial x} && \text{(A.22)}\\
&= \frac{x}{v} \cdot \sum_i \frac{v_i}{x} \cdot \frac{\partial \ln v_i}{\partial \ln x} && \text{(A.23)}\\
&= \sum_i \frac{v_i}{v} \cdot \frac{\partial \ln v_i}{\partial \ln x} && \text{(A.24)}\\
&= \sum_i \frac{v_i}{v} \cdot \varepsilon_x^{v_i} && \text{(A.25)}
\end{aligned}$$

Appendix B

Control analysis of two-module system in which allosteric and covalent modification interact

B.1 Control analysis

The control matrix **C** of a system with arbitrary complexity can be expressed in terms of the matrix formulation

$$\mathbf{C} = \mathbf{E}^{-1} \tag{B.1}$$

where **C** is the matrix of control-coefficients with respect to independent fluxes and species, and **E** is a matrix containing structural properties and elasticities. Hofmeyr & Westerhoff [162] have shown that, if a system comprises modules that are not connected by mass flow, Eq. B.1 becomes

$$\mathbf{G} = \mathbf{E}^{-1} \tag{B.2}$$

The use of G-notation indicates that the control matrix contains global or integral control coefficients. The internal structure of **G** is the same as that of **C**, but for a system of two modules the rows and columns of **G** and **E** can be rearranged to allow the following partitioning:

$$\begin{bmatrix} \mathbf{G}_1^1 & \mathbf{G}_2^1 \\ \mathbf{G}_1^2 & \mathbf{G}_2^2 \end{bmatrix} = \begin{bmatrix} \mathbf{E}_1^1 & \mathbf{E}_2^1 \\ \mathbf{E}_1^2 & \mathbf{E}_2^2 \end{bmatrix}^{-1} \tag{B.3}$$

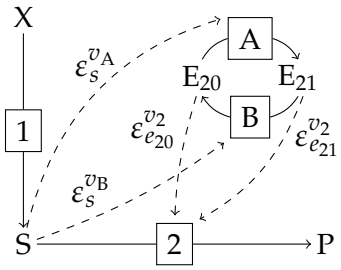

Figure B.1: Feedforward activation mechanism in which the regulated enzyme is inhibited by covalent modification. Pathway precursor and allosteric modifier X activates enzyme 2, an MWC-type enzyme that is inhibited by covalent modification. Since covalent modification favours the T conformations and allosteric modification favours the R conformation, modifier X promotes net reversal of covalent modification by inhibiting enzyme A, which catalyses forward covalent modification, and activating enzyme B, which catalyses reverse covalent modification. Enzymes A and B are also influenced by substrate S, if S binds with different affinities to the T and R conformations of enzyme 2. The reaction network consists of two modules not connected by mass flow: the main pathway converting X to P with flux J_1, and the pathway that catalyses the interconversion between covalent states of enzyme 2 with flux J_A. Internal elasticities are indicated with dashed arrows.

where $\mathbf{G}_j^i$ is the control matrix of the variables in modules i with respect to the steps in module j; and

$$\mathbf{E}_j^i = \begin{cases} \begin{bmatrix} \mathcal{K}_i & -\boldsymbol{\varepsilon}_i^i \mathcal{L}_i \end{bmatrix} & \text{if } i = j \\ \begin{bmatrix} \mathbf{0} & -\boldsymbol{\varepsilon}_j^i \mathcal{L}_j \end{bmatrix} & \text{if } i \neq j \end{cases} \tag{B.4}$$

where $\mathcal{K}_i$ and $\mathcal{L}_i$ are the scaled kernel and link matrices obtained from the reduced stoichiometric matrix.

Let us now apply this treatment to the system in Fig. B.1. Let L be the linear pathway from X to P, and C the cyclical pathway from E_{20} to E_{21}.

In module L either J_1 or J_2 can be chosen as the independent flux. We choose J_1, so that

$$\begin{bmatrix} J_1 \\ J_2 \end{bmatrix} = \begin{bmatrix} 1 \\ 1 \end{bmatrix} \begin{bmatrix} J_1 \end{bmatrix} \tag{B.5}$$

The kernel matrix for module L is then given by

$$\mathbf{K}_L = \begin{bmatrix} 1 \\ 1 \end{bmatrix} \tag{B.6}$$

and since no branching is present, $\mathcal{K}_L = \mathbf{K}_L$. As there is no moiety conservation in module L, it also follows that $\mathcal{L}_L = \mathbf{L}_L = [1]$, where $\mathbf{L}$ is the link matrix. Finally the elasticity matrix for module L is given by

$$\boldsymbol{\varepsilon}_L^L = \begin{bmatrix} \varepsilon_s^{v_1} \\ \varepsilon_s^{v_2} \end{bmatrix} \tag{B.7}$$

We choose J_A as the independent flux in module C. As for module L, $\mathcal{K}_C = \mathbf{K}_C = [1 \quad 1]^T$. Since E_{20} and E_{21} constitute a moiety-conserved cycle, $\frac{de_{20}}{dt} = -\frac{de_{21}}{dt}$, so that

$$\begin{bmatrix} \frac{de_{20}}{dt} \\ \frac{de_{21}}{dt} \end{bmatrix} = \begin{bmatrix} 1 \\ -1 \end{bmatrix} \begin{bmatrix} \frac{de_{20}}{dt} \end{bmatrix} \tag{B.8}$$

The link matrix for module C is then $\mathbf{L}_C = [1 \quad -1]^T$, and the scaled link matrix is the matrix product

$$\mathcal{L}_C = \begin{bmatrix} \frac{1}{e_{20}} & \\ & \frac{1}{e_{21}} \end{bmatrix} \mathbf{L}_C \begin{bmatrix} e_{20} \end{bmatrix} = \begin{bmatrix} 1 \\ \frac{-e_{20}}{e_{21}} \end{bmatrix} \tag{B.9}$$

Finally the elasticity matrix for module C is given by

$$\boldsymbol{\varepsilon}_C^C = \begin{bmatrix} \varepsilon_{e_{20}}^{v_A} & \varepsilon_{e_{21}}^{v_A} \\ \varepsilon_{e_{20}}^{v_B} & \varepsilon_{e_{21}}^{v_B} \end{bmatrix} \tag{B.10}$$

Similarly

$$\boldsymbol{\varepsilon}_C^L = \begin{bmatrix} \varepsilon_{e_{20}}^{v_1} & \varepsilon_{e_{21}}^{v_1} \\ \varepsilon_{e_{20}}^{v_2} & \varepsilon_{e_{21}}^{v_2} \end{bmatrix} = \begin{bmatrix} 0 & 0 \\ \varepsilon_{e_{20}}^{v_2} & \varepsilon_{e_{21}}^{v_2} \end{bmatrix} \tag{B.11}$$

and

$$\boldsymbol{\varepsilon}_L^C = \begin{bmatrix} \varepsilon_s^{v_A} \\ \varepsilon_s^{v_B} \end{bmatrix} \tag{B.12}$$

Note that $\varepsilon_{e_{20}}^{v_1}$ and $\varepsilon_{e_{21}}^{v_1}$ are zero, as the intermediates in module C only affect enzyme 2 in module L. Also, since S is a ligand of enzyme 2, it potentially affects the interconversion between covalent forms of enzyme 2, so that $\varepsilon_s^{v_A}$ and $\varepsilon_s^{v_B}$ are potentially non-zero.

The expressions for the partitioned $\mathbf{E}$ matrices are then

$$\mathbf{E}_L^L = \begin{bmatrix} \mathcal{K}_L & -\boldsymbol{\varepsilon}_L^L \mathcal{L}_L \end{bmatrix} \tag{B.13}$$

$$\mathbf{E}_C^L = \begin{bmatrix} \mathbf{0} & -\boldsymbol{\varepsilon}_C^L \mathcal{L}_C \end{bmatrix} \tag{B.14}$$

$$\mathbf{E}_L^C = \begin{bmatrix} \mathbf{0} & -\boldsymbol{\varepsilon}_L^C \mathcal{L}_L \end{bmatrix} \tag{B.15}$$

and

$$\mathbf{E}_C^C = \begin{bmatrix} \mathcal{K}_C & -\boldsymbol{\varepsilon}_C^C \mathcal{L}_C \end{bmatrix} \tag{B.16}$$

The control matrix $\mathbf{G}$ is then

$$\begin{bmatrix} G_{v_1}^{J_1} & G_{v_2}^{J_1} & G_{v_A}^{J_1} & G_{v_B}^{J_1} \\ G_{v_1}^{s} & G_{v_2}^{s} & G_{v_A}^{s} & G_{v_B}^{s} \\ G_{v_1}^{J_A} & G_{v_2}^{J_A} & G_{v_A}^{J_A} & G_{v_B}^{J_A} \\ G_{v_1}^{e_{20}} & G_{v_2}^{e_{20}} & G_{v_A}^{e_{20}} & G_{v_B}^{e_{20}} \end{bmatrix} = \begin{bmatrix} \mathcal{K}_L & -\boldsymbol{\varepsilon}_L^L \mathcal{L}_L & \mathbf{0} & -\boldsymbol{\varepsilon}_C^L \mathcal{L}_C \\ \mathbf{0} & -\boldsymbol{\varepsilon}_L^C \mathcal{L}_L & \mathcal{K}_C & -\boldsymbol{\varepsilon}_C^C \mathcal{L}_C \end{bmatrix}^{-1} \tag{B.17}$$

$$= \begin{bmatrix} 1 & -\varepsilon_s^{v_1} & 0 & 0 \\ 1 & -\varepsilon_s^{v_2} & 0 & -{}^*\varepsilon_{e_{20}}^{v_2} \\ 0 & -\varepsilon_s^{v_A} & 1 & -{}^*\varepsilon_{e_{20}}^{v_A} \\ 0 & -\varepsilon_s^{v_B} & 1 & -{}^*\varepsilon_{e_{20}}^{v_B} \end{bmatrix}^{-1} \tag{B.18}$$

$$= \begin{bmatrix} \varepsilon_s^{v_2}({}^*\varepsilon_{e_{20}}^{v_B} - {}^*\varepsilon_{e_{20}}^{v_A}) - {}^*\varepsilon_{e_{20}}^{v_2}(\varepsilon_s^{v_B} - \varepsilon_s^{v_A}) & -\varepsilon_s^{v_1}({}^*\varepsilon_{e_{20}}^{v_B} - {}^*\varepsilon_{e_{20}}^{v_A}) & -\varepsilon_s^{v_1}{}^*\varepsilon_{e_{20}}^{v_2} & \varepsilon_s^{v_1}{}^*\varepsilon_{e_{20}}^{v_2} \\ {}^*\varepsilon_{e_{20}}^{v_B} - {}^*\varepsilon_{e_{20}}^{v_A} & {}^*\varepsilon_{e_{20}}^{v_A} - {}^*\varepsilon_{e_{20}}^{v_B} & -{}^*\varepsilon_{e_{20}}^{v_2} & {}^*\varepsilon_{e_{20}}^{v_2} \\ {}^*\varepsilon_{e_{20}}^{v_B}\varepsilon_s^{v_A} - {}^*\varepsilon_{e_{20}}^{v_A}\varepsilon_s^{v_B} & {}^*\varepsilon_{e_{20}}^{v_A}\varepsilon_s^{v_B} - {}^*\varepsilon_{e_{20}}^{v_B}\varepsilon_s^{v_A} & {}^*\varepsilon_{e_{20}}^{v_B}(\varepsilon_s^{v_2} - \varepsilon_s^{v_1}) - {}^*\varepsilon_{e_{20}}^{v_2}\varepsilon_s^{v_B} & {}^*\varepsilon_{e_{20}}^{v_2}\varepsilon_s^{v_A} - {}^*\varepsilon_{e_{20}}^{v_A}(\varepsilon_s^{v_2} - \varepsilon_s^{v_1}) \\ \varepsilon_s^{v_A} - \varepsilon_s^{v_B} & \varepsilon_s^{v_B} - \varepsilon_s^{v_A} & \varepsilon_s^{v_2} - \varepsilon_s^{v_1} & \varepsilon_s^{v_1} - \varepsilon_s^{v_2} \end{bmatrix} \frac{1}{(\varepsilon_s^{v_2} - \varepsilon_s^{v_1})({}^*\varepsilon_{e_{20}}^{v_B} - {}^*\varepsilon_{e_{20}}^{v_A}) - {}^*\varepsilon_{e_{20}}^{v_2}(\varepsilon_s^{v_B} - \varepsilon_s^{v_A})} \tag{B.19}$$

where ${}^*\varepsilon_{e_{20}}^{v_2} = \varepsilon_{e_{20}}^{v_2} - \varepsilon_{e_{21}}^{v_2}\frac{e_{20}}{e_{21}}$, ${}^*\varepsilon_{e_{20}}^{v_A} = \varepsilon_{e_{20}}^{v_A} - \varepsilon_{e_{21}}^{v_A}\frac{e_{20}}{e_{21}}$, and ${}^*\varepsilon_{e_{20}}^{v_B} = \varepsilon_{e_{20}}^{v_B} - \varepsilon_{e_{21}}^{v_B}\frac{e_{20}}{e_{21}}$ are "effective" elasticities [230].

We can also solve for the control matrices of the two modules independently, yielding intramodule control coefficients:

$$\begin{bmatrix} C_{v_1}^{J_1} & C_{v_2}^{J_1} \\ C_{v_1}^{s} & C_{v_2}^{s} \end{bmatrix} = \begin{bmatrix} \mathcal{K}_L & -\boldsymbol{\varepsilon}_L^L \mathcal{L}_L \end{bmatrix}^{-1} \tag{B.20}$$

$$= \begin{bmatrix} \dfrac{\varepsilon_s^{v_2}}{\varepsilon_s^{v_2} - \varepsilon_s^{v_1}} & \dfrac{-\varepsilon_s^{v_1}}{\varepsilon_s^{v_2} - \varepsilon_s^{v_1}} \\ \dfrac{1}{\varepsilon_s^{v_2} - \varepsilon_s^{v_1}} & \dfrac{-1}{\varepsilon_s^{v_2} - \varepsilon_s^{v_1}} \end{bmatrix} \tag{B.21}$$

and

$$\begin{bmatrix} C^{J_A}_{v_A} & C^{J_A}_{v_B} \\ C^{e_{20}}_{v_A} & C^{e_{20}}_{v_B} \end{bmatrix} = \begin{bmatrix} \mathcal{K}_C & -\boldsymbol{\varepsilon}^C_C \mathcal{L}_C \end{bmatrix}^{-1} \tag{B.22}$$

$$= \begin{bmatrix} \frac{{}^*\varepsilon^{v_B}_{e_{20}}}{{}^*\varepsilon^{v_B}_{e_{20}} - {}^*\varepsilon^{v_A}_{e_{20}}} & \frac{-{}^*\varepsilon^{v_A}_{e_{20}}}{{}^*\varepsilon^{v_B}_{e_{20}} - {}^*\varepsilon^{v_A}_{e_{20}}} \\ \frac{1}{{}^*\varepsilon^{v_B}_{e_{20}} - {}^*\varepsilon^{v_A}_{e_{20}}} & \frac{-1}{{}^*\varepsilon^{v_B}_{e_{20}} - {}^*\varepsilon^{v_A}_{e_{20}}} \end{bmatrix} \tag{B.23}$$

B.2 Elasticity expressions

The elasticity expressions derived in this section all pertain to the reactions in Fig. B.1.

Elasticities with respect to S

The elasticity of v_1 with respect to S is given by

$$\varepsilon^{v_1}_s = \frac{-\frac{s/x}{K_{eq1}}}{1 - \frac{s/x}{K_{eq1}}} - \frac{\sigma_1}{1 + \xi_1 + \sigma_1} \tag{B.24}$$

where $\xi_1 = \frac{x}{K_{1x}}$ and $\sigma_1 = \frac{s}{K_{1s}}$. The absolute value of $\varepsilon^{v_1}_s$ increases from zero to unity as s increases from zero to saturation and then suddenly increases to infinity as equilibrium is approached. $\left|\varepsilon^{v_1}_s\right|$ therefore has a maximum value near equilibrium.

The elasticity of v_2 with respect to S is given by

$$\varepsilon^{v_2}_s = \sum_i \frac{v_{2i}}{v_2} \varepsilon^{v_{2i}}_s \tag{B.25}$$

where

$$\varepsilon^{v_{2i}}_s = 1 - \frac{c_s \sigma_2 \alpha^i L(1 + c_x \xi_2) + \sigma_2(1 + \xi_2)}{(1 + c_s \sigma_2)\alpha^i L(1 + c_x \xi_2) + (1 + \sigma_2)(1 + \xi_2)} \tag{B.26}$$

where c_k is the factor by which the rate constant for the T conformation differs from that of the R conformation; $\sigma_2 = s/K_{r2s}$ and $c_s = K_{r2s}/K_{t2s}$; $\xi_2 = x/K_{r2x}$ and $c_x = K_{r2x}/K_{t2x}$; K_{r2s}, K_{t2s}, K_{r2x}, and K_{t2x} are the intrinsic dissociation constants with respect to S and X for the T and R conformations; α is the factor by which covalent

modification alters L; L is the allosteric constant; and $i \in [0,1]$. $|\varepsilon_s^{v_{2i}}| \to 0$ in the limit $\sigma_2 \to \infty$:

$$\lim_{\sigma_2 \to \infty} \varepsilon_s^{v_{2i}} = 1 - \frac{c_s \alpha^i L(1 + c_x \xi_2) + (1 + \xi_2)}{c_s \alpha^i L(1 + c_x \xi_2) + (1 + \xi_2)} \tag{B.27}$$

$$= 0 \tag{B.28}$$

The expressions for $\varepsilon_s^{v_A}$ and $\varepsilon_s^{v_A}$ are given by

$$\varepsilon_s^{v_A} = \left[\frac{\phi'_{num}}{\phi_{num}} - \frac{\phi'_{den}}{\phi_{den}}\right] \left(1 - \frac{\frac{e_{21} c/(e_{20} c')}{\phi K_{eqA}}}{1 - \frac{e_{21} c/(e_{20} c')}{\phi K_{eqA}}}\right) \tag{B.29}$$

and

$$\varepsilon_s^{v_B} = \left[\frac{\phi'_{den}}{\phi_{den}} - \frac{\phi'_{num}}{\phi_{num}}\right] \left(1 - \frac{\frac{e_{20} g/e_{21}}{\phi^{-1} K_{eqB}}}{1 - \frac{e_{20} g/e_{21}}{\phi^{-1} K_{eqB}}}\right) \tag{B.30}$$

where

$$\phi'_{num} = c_s \sigma_2 \alpha L(1 + c_x \xi_2) + \sigma_2(1 + \xi_2) \tag{B.31}$$

$$\phi_{num} = (1 + c_s \sigma_2)(1 + c_x \xi_2)\alpha L + (1 + \sigma_2)(1 + \xi_2) \tag{B.32}$$

$$\phi'_{den} = c_s \sigma_2 (1 + c_x \xi_2) L + \sigma_2 (1 + \xi_2) \tag{B.33}$$

$$\phi_{den} = (1 + c_s \sigma_2)(1 + c_x \xi_2) L + (1 + \sigma_2)(1 + \xi_2) \tag{B.34}$$

If reactions A and B operate far from equilibrium

$$\varepsilon_s^{v_B} + \varepsilon_s^{v_A} = \left[\frac{\phi'_{den}}{\phi_{den}} - \frac{\phi'_{num}}{\phi_{num}}\right] + \left[\frac{\phi'_{num}}{\phi_{num}} - \frac{\phi'_{den}}{\phi_{den}}\right] = 0 \tag{B.35}$$

If enzyme 2 is saturated with S, or if $c_s = 1$, then $\varepsilon_s^{v_A} = \varepsilon_s^{v_B} = 0$.

Elasticities with respect to X

The elasticity of v_1 with respect to X is given by

$$\varepsilon_x^{v_1} = \frac{1}{1 - \dfrac{x/s}{K_{\text{eq1}}}} - \frac{\xi_1}{1 + \xi_1 + \sigma_1} \tag{B.36}$$

The elasticity of v_2 with respect to X is given by

$$\varepsilon_x^{v_2} = \sum_i \frac{v_{2i}}{v_2} \varepsilon_x^{v_{2i}} \tag{B.37}$$

where

$$\varepsilon_x^{v_{2i}} = \frac{c_k c_s \alpha^i L c_x \xi_2 + \xi_2}{c_k c_s \alpha^i L (1 + c_x \xi_2) + (1 + \xi_2)} - \frac{(1 + c_s \sigma_2) \alpha^i L c_x \xi_2 + (1 + \sigma_2) \xi_2}{(1 + c_s \sigma_2) \alpha^i L (1 + c_x \xi_2) + (1 + \sigma_2)(1 + \xi_2)} \tag{B.38}$$

When enzyme 2 is saturated with S, $\varepsilon_x^{v_{2i}}$ is given by

$$\lim_{\sigma_2 \to \infty} \varepsilon_x^{v_{2i}} = \frac{c_k c_s \alpha^i L c_x \xi_2 + \xi_2}{c_k c_s \alpha^i L (1 + c_x \xi_2) + (1 + \xi_2)} - \frac{c_s \alpha^i L c_x \xi_2 + \xi_2}{c_s \alpha^i L (1 + c_x \xi_2) + (1 + \xi_2)} \tag{B.39}$$

which if $c_k = 1$ or if $c_s \ll \frac{1}{\alpha^i L}$ equals zero.

The elasticities of v_A and v_B with respect to X are given by

$$\varepsilon_x^{v_A} = \left[\frac{\phi'_{\text{num}}}{\phi_{\text{num}}} - \frac{\phi'_{\text{den}}}{\phi_{\text{den}}} \right] \left(1 - \frac{\dfrac{e_{21} c / (e_{20} c')}{\phi K_{\text{eqA}}}}{1 - \dfrac{e_{21} c / (e_{20} c')}{\phi K_{\text{eqA}}}} \right) \tag{B.40}$$

and

$$\varepsilon_x^{v_B} = \left[\frac{\phi'_{\text{den}}}{\phi_{\text{den}}} - \frac{\phi'_{\text{num}}}{\phi_{\text{num}}} \right] \left(1 - \frac{\dfrac{e_{20} g / e_{21}}{\phi^{-1} K_{\text{eqB}}}}{1 - \dfrac{e_{20} g / e_{21}}{\phi^{-1} K_{\text{eqB}}}} \right) \tag{B.41}$$

where

$$\phi'_{\text{num}} = (1 + c_s \sigma_2) c_x \xi_2 \alpha^i L + (1 + \sigma_2) \xi_2 \tag{B.42}$$

$$\phi_{\text{num}} = (1 + c_s\sigma_2)(1 + c_x\xi_2)\alpha^i L + (1 + \sigma_2)(1 + \xi_2) \tag{B.43}$$

$$\phi'_{\text{den}} = (1 + c_s\sigma_2)c_x\xi_2 L + (1 + \sigma_2)\xi_2 \tag{B.44}$$

$$\phi_{\text{den}} = (1 + c_s\sigma_2)(1 + c_x\xi_2)L + (1 + \sigma_2)(1 + \xi_2) \tag{B.45}$$

If enzyme 2 is saturated with S, then $\left[\frac{\phi'_{\text{num}}}{\phi_{\text{num}}} - \frac{\phi'_{\text{den}}}{\phi_{\text{den}}}\right] = \left[\frac{\phi'_{\text{num}}}{\phi_{\text{num}}} - \frac{\phi'_{\text{den}}}{\phi_{\text{den}}}\right] = 0$, so that $\varepsilon_x^{v_A} = \varepsilon_x^{v_B} = 0$. If enzymes A and B operate far from equilibrium, then $\varepsilon_x^{v_A} = -\varepsilon_x^{v_B}$.

Elasticities with respect to e_2

The expression for $\varepsilon_{e_{20}}^{v_2}$ is given by

$$\varepsilon_{e_{20}}^{v_2} = \frac{v_{20}}{v_2}\varepsilon_{e_{20}}^{v_{20}} + \frac{v_{21}}{v_2}\varepsilon_{e_{20}}^{v_{21}} \tag{B.46}$$

$$= \frac{v_{20}}{v_2} \quad (\text{since } \varepsilon_{e_{20}}^{v_{20}} = 1, \text{ and } \varepsilon_{e_{20}}^{v_{21}} = 0) \tag{B.47}$$

Similarly, $\varepsilon_{e_{21}}^{v_2} = \frac{v_{21}}{v_2}$. It follows that

$$\varepsilon_{e_{20}}^{v_2} - \varepsilon_{e_{21}}^{v_2} \cdot \frac{e_{20}}{e_{21}} = \frac{v_{20} - v_{21} \cdot \frac{e_{20}}{e_{21}}}{v_2} \tag{B.48}$$

$$= \frac{\dfrac{c_k k_2 e_{20} c_s \sigma_2 L\left(\dfrac{1 + c_x\xi_2}{1 + \xi_2}\right) + k_2 e_{20}\sigma_2}{(1 + c_s\sigma_2)\, L\left(\dfrac{1 + c_x\xi_2}{1 + \xi_2}\right) + (1 + \sigma_2)} - \dfrac{c_k k_2 e_{20} c_s \sigma_2 \alpha^i L\left(\dfrac{1 + c_x\xi_2}{1 + \xi_2}\right) + k_2 e_{20}\sigma_2}{(1 + c_s\sigma_2)\, \alpha^i L\left(\dfrac{1 + c_x\xi_2}{1 + \xi_2}\right) + (1 + \sigma_2)}}{v_2} \tag{B.49}$$

or if S saturates enzyme 2:

$$\varepsilon_{e_{20}}^{v_2} - \varepsilon_{e_{21}}^{v_2} \cdot \frac{e_{20}}{e_{21}} = \frac{\dfrac{c_k k_2 e_{20} c_s L\left(\dfrac{1 + c_x\xi_2}{1 + \xi_2}\right) + k_2 e_{20}}{c_s L\left(\dfrac{1 + c_x\xi_2}{1 + \xi_2}\right) + 1} - \dfrac{c_k k_2 e_{20} c_s \alpha L\left(\dfrac{1 + c_x\xi_2}{1 + \xi_2}\right) + k_2 e_{20}}{c_s \alpha L\left(\dfrac{1 + c_x\xi_2}{1 + \xi_2}\right) + 1}}{v_2} \tag{B.50}$$

$$= 0 \quad (\text{if } c_s \ll \frac{1}{\alpha L}) \tag{B.51}$$

The expression for $\varepsilon_{e_{20}}^{v_A}$ is given by

$$\varepsilon_{e_{20}}^{v_A} = \frac{1}{1-\dfrac{e_{21}c/(e_{20}c')}{\phi K_{eqA}}} - \frac{\sigma_{A1}}{1+\sigma_{A1}+\pi_{A1}} \tag{B.52}$$

$$= 1 - \frac{\sigma_{A1}}{1+\sigma_{A1}} \quad \text{(assuming } \pi_{A1} \to 0 \text{ and } K_{eqA} \to \infty\text{)} \tag{B.53}$$

Similarly, $\varepsilon_{e_{21}}^{v_B}$ is given by

$$\varepsilon_{e_{21}}^{v_B} = 1 - \frac{\sigma_{B1}}{1+\sigma_{B1}} \tag{B.54}$$

The expression for $\varepsilon_{e_{21}}^{v_A}$ is given by

$$\varepsilon_{e_{21}}^{v_A} = \frac{-\dfrac{e_{21}c/(e_{20}c')}{\phi K_{eqA}}}{1-\dfrac{e_{21}c/(e_{20}c')}{\phi K_{eqA}}} - \frac{\pi_{A1}}{1+\sigma_{A1}+\pi_{A1}} \tag{B.55}$$

$$= 0 \quad \text{(assuming } \pi_{A1} \to 0 \text{ and } K_{eqA} \to \infty\text{)} \tag{B.56}$$

Similarly, $\varepsilon_{e_{20}}^{v_B}$ is given by

$$\varepsilon_{e_{20}}^{v_B} = 0 \tag{B.57}$$

Appendix C

Model parametrization

C.1 Calculation of rate constants, enzyme concentrations, and maximal velocities

Calculation of k_{cat} and V_{max} from specific activity

If the mass of total protein per volume is known, V_{max} can be calculated directly from the specific activity (usually product formation per time per mass protein) of crude cell extracts according to the equation [210]:

$$V_{max} = \text{crude specific activity} \times \text{protein per cell volume} \tag{C.1}$$

From the V_{max}, if the subunit composition is known, either k_{cat} or $[E]_{tot}$ can be calculated if the other is known. If the holoenzyme molecular mass is known, nk_{cat} can be calculated from the specific activity of cell extracts purified to homogeneity according to the equation

$$nk_{cat} = \text{purified specific activity} \times \text{holoenzyme molecular mass} \tag{C.2}$$

Alternatively

$$k_{cat} = \text{purified specific activity} \times \text{subunit molecular mass} \tag{C.3}$$

Multimeric enzymes that exhibit no cooperativity may be treated as monomeric enzymes ($n = 1$), so that the calculated k_{cat} is really an apparent value.

Table C.1: Rate constants calculated from specific activities of purified enzymes. Molecular masses were obtained from the UniProt database [267], or from the given reference. See text for calculation details.

Enzyme	Specific activity (mol/g/min)	n	Holoenzyme molecular mass (g/mol)	k_{cat} (min^{-1})	Substrate	Ref.	Source
CK1	$3.1 \cdot 10^{-4}$	1	37 567	11.65	casein	[268]	rabbit muscle
CK2	$4.91 \cdot 10^{-4}$	1	140 116	68.8	GS	[214]	rabbit muscle
GS	$1.2 \cdot 10^{-2}$	4	334 580	1 004.58	UDPG	[41]	rabbit muscle
GSK3	$2.2 \cdot 10^{-3}$	1	46 744	102.84	GS	[269]	rabbit muscle
HK1	$7.02 \cdot 10^{-2}$	1	102 486	7 194.52	Glc	[270]	rabbit heart
HK2	0.15	1	102 486	15 065.44	Glc	[193]	human, recombinant
PhKP	$3.8 \cdot 10^{-3}$	1	318 000	1 208.4	GS	[271]	rabbit muscle

Table C.2: Rate constants for dephosphorylation of various PP1 substrates. The activities of PP1 with various substrates relative to the activity with PhKP as substrate are converted to activities relative to the activity with GPa as substrate. Values for k_{cat} for each substrate can then be calculated from $k_{cat,PP1,GPa}$. The value of $k_{cat,PP1,GPa}$ is 30 mM/min [272].

PP1 substrate	Relative PhKP dephosphorylation activity [273]	Relative GPa dephosphorylation activity	k_{cat}
PhKP	1	3.7	111.11
GPa	0.27	1	–
GS22a	1.03	3.81	114.44
GS43abc	0.28	1.04	31.11
GS5	$1 \cdot 10^{-2}$	$3.7 \cdot 10^{-2}$	1.11

Table C.3: Rate constants for phosphorylation of various PKA substrates. The activities of PKA with various substrates relative to the activity with PhK as substrate are converted to activities relative to the activity with histone as substrate. Values for k_{cat} for each substrate can then be calculated from $k_{cat,PKA,histone}$. The value of $k_{cat,PKA,histone}$ is 291 mM/min [237].

PKA substrate	Relative PhK phosphorylation activity [57] 1	2	Relative histone phosphorylation activity 1	2	Average relative activity	k_{cat}
histone	0.18	0.16	1	1	1	–
PhK	1	1	2.98	3.32	3.15	917.76
GS	1.12	1.18	3.34	3.93	3.63	1 057.63

Table C.4: Maximal velocities calculated from specific activities of crude enzyme extracts. The total protein per cell volume for mammalian muscle was taken as 260 mg/mL (based on rat muscle value) [210]. See text for calculation details.

Enzyme	Specific activity (μmol/min/mg)	V_{max} (mM/min)	$[E]_{tot}$ (mM)	Substrate	Ref.	Source
CK1	$2 \cdot 10^{-5}$	0.0052	$4.47 \cdot 10^{-4}$	casein	[268]	rabbit muscle
CK2	$2.7 \cdot 10^{-5}$	0.00702	$1.02 \cdot 10^{-4}$	GS	[214]	rabbit muscle
GSK3	$3 \cdot 10^{-5}$	0.0078	$7.58 \cdot 10^{-5}$	GS	[269]	rabbit muscle
PPase	0.11	27.3	–	PP_i	[255]	rabbit muscle
NDPK	1.7	442	–	–	[256]	bovine heart

Table C.5: Experimental data used during parameter optimization

Phosphorylation state	Reaction direction	Ligand dependence	Reference
GPa	forward	P_i vs. AMP	[274]
GPa	reverse	glucose-1-phosphate (G1P) vs. G6P	[275]
GPb	forward	P_i vs. ATP	[276]
GPb	reverse	G1P vs. G6P	[277]
GPb	reverse	AMP vs. G6P	[277]

C.2 Glycogen phosphorylase rate equation and parameter optimization

A rate equation for GP was recently proposed by Walcott & Lehman [201]. Their equation, however, only describes the kinetics of the dephosphorylated enzyme, GPb. They also did not consider inhibition of GP by G6P. Since we are interested in a rate equation for both GP phosphorylation states that is also able to describe inhibition by G6P, a new rate equation was developed.

Experimental data

As far as possible we used only experimental data that were obtained under the same conditions and preferably in the same lab. Data points were obtained by digitizing graphs from the PDF versions of published articles. The data sources are listed in Table C.5.

Algorithm and software

The parameter optimization was carried out using a combination of Python programming language modules: NumPy and SciPy for numeric procedures, and LMfit-py, a wrapper around the SciPy implementation of the Levenberg-Marquardt algorithm with added support for constraints. IPython was used as an interactive shell for Python. IPython's built-in support for parallel computing was used to speed up optimizations. To increase the likelihood of finding a global minimum, the optimization was repeated 1000 times with random initial parameter values for each iteration.

Rate equation and feature selection

Guided by the observation that GP ligands also influence the rate of the kinase and phosphatase that catalyse the covalent modification of GP, we chose an MWC-type rate equation similar to that of Walcott & Lehman [201], but in which phosphorylation and dephosphorylation are considered to only affect the equilibria between the various GP conformations. Like Walcott & Lehman [201] we used a MWC equation with three conformations (R, T, and U) of which only the R conformation is catalytically active.

The GP literature suggests that AMP, ATP, and G6P all bind to the activation site, but that G6P is inhibitory and that ATP, although activatory, binds with a weak affinity to this site. AMP and ATP also both bind to the nucleoside site, where they result in inhibition, but AMP binds only with a weak affinity and is not a physiological inhibitor of GP. We could not obtain a rich enough data set from the literature that would allow parameters that describe the binding of ATP to the activation site and the binding of AMP to the inhibition site to be optimized. These features were thus omitted from the onset. In addition, glycogen was considered saturating and was thus also omitted. The number of subunits were taken as two. Separate V_{max} values were fitted for data from different source and for the reverse and forward reactions.

The initial rate equation, which was further simplified during a process of feature selection, is given by

$$v_{GP} = \sum_i \frac{V_{max,r} n \frac{[Pi]}{K_{r,Pi}} \left(1 + \frac{[Pi]}{K_{r,Pi}} + \frac{[G1P]}{K_{r,G1P}}\right)^{n-1} \left(1 + \frac{[AMP]}{K_{r,AMP}} + \frac{[G6P]}{K_{r,G6P}}\right)^{n} \left(1 + \frac{[ATP]}{K_{r,ATP}}\right)^{n}}{\left(1 + \frac{[Pi]}{K_{r,Pi}} + \frac{[G1P]}{K_{r,G1P}}\right)^{n} \left(1 + \frac{[AMP]}{K_{r,AMP}} + \frac{[G6P]}{K_{r,G6P}}\right)^{n} \left(1 + \frac{[ATP]}{K_{r,ATP}}\right)^{n}} + L_{t,i} \left(1 + \frac{[Pi]}{K_{t,Pi}} + \frac{[G1P]}{K_{t,G1P}}\right)^{n} \left(1 + \frac{[AMP]}{K_{t,AMP}} + \frac{[G6P]}{K_{t,G6P}}\right)^{n} \left(1 + \frac{[ATP]}{K_{t,ATP}}\right)^{n} + L_{u,i} \left(1 + \frac{[Pi]}{K_{u,Pi}} + \frac{[G1P]}{K_{u,G1P}}\right)^{n} \left(1 + \frac{[AMP]}{K_{u,AMP}} + \frac{[G6P]}{K_{u,G6P}}\right)^{n} \left(1 + \frac{[ATP]}{K_{u,ATP}}\right)^{n}} \tag{C.4}$$

A preliminary optimization revealed that the T conformation was negligible for GPa and that the U conformation was negligible for GPb. We therefore set $L_{t,a} = 0$ and $L_{u,b} = 0$. So that Eq. C.4 simplifies to

$$v_{GP} = \frac{k_{cat,r}[GP]_a n \frac{[Pi]}{K_{r,Pi}} \left(1 + \frac{[Pi]}{K_{r,Pi}} + \frac{[G1P]}{K_{r,G1P}}\right)^{n-1}}{\left(1 + \frac{[Pi]}{K_{r,Pi}} + \frac{[G1P]}{K_{r,G1P}}\right)^{n} + L_u \left(1 + \frac{[Pi]}{K_{u,Pi}} + \frac{[G1P]}{K_{u,G1P}}\right)^{n} \left(\frac{1 + \frac{[AMP]}{K_{u,AMP}} + \frac{[G6P]}{K_{u,G6P}}}{1 + \frac{[AMP]}{K_{r,AMP}} + \frac{[G6P]}{K_{r,G6P}}}\right)^{n} \left(\frac{1 + \frac{[ATP]}{K_{u,ATP}}}{1 + \frac{[ATP]}{K_{r,ATP}}}\right)^{n}} + \frac{k_{cat,r}[GP]_b n \frac{[Pi]}{K_{r,Pi}} \left(1 + \frac{[Pi]}{K_{r,Pi}} + \frac{[G1P]}{K_{r,G1P}}\right)^{n-1}}{\left(1 + \frac{[Pi]}{K_{r,Pi}} + \frac{[G1P]}{K_{r,G1P}}\right)^{n} + L_t \left(1 + \frac{[Pi]}{K_{t,Pi}} + \frac{[G1P]}{K_{t,G1P}}\right)^{n} \left(\frac{1 + \frac{[AMP]}{K_{t,AMP}} + \frac{[G6P]}{K_{t,G6P}}}{1 + \frac{[AMP]}{K_{r,AMP}} + \frac{[G6P]}{K_{r,G6P}}}\right)^{n} \left(\frac{1 + \frac{[ATP]}{K_{t,ATP}}}{1 + \frac{[ATP]}{K_{r,ATP}}}\right)^{n}} \tag{C.5}$$

However, since, none of our data sets contained ATP binding data for GPa, binding of ATP to the U conformation had to be considered negligible, so that

$$v_{GP} = \frac{k_{cat,r}[GP]_a n \frac{[Pi]}{K_{r,Pi}} \left(1 + \frac{[Pi]}{K_{r,Pi}} + \frac{[G1P]}{K_{r,G1P}}\right)^{n-1}}{\left(1 + \frac{[Pi]}{K_{r,Pi}} + \frac{[G1P]}{K_{r,G1P}}\right)^{n} + L_u \left(1 + \frac{[Pi]}{K_{u,Pi}} + \frac{[G1P]}{K_{u,G1P}}\right)^{n} \left(\frac{1 + \frac{[AMP]}{K_{u,AMP}} + \frac{[G6P]}{K_{u,G6P}}}{1 + \frac{[AMP]}{K_{r,AMP}} + \frac{[G6P]}{K_{r,G6P}}}\right)^{n} \left(\frac{1}{1 + \frac{[ATP]}{K_{r,ATP}}}\right)^{n}} + \frac{k_{cat,r}[GP]_b n \frac{[Pi]}{K_{r,Pi}} \left(1 + \frac{[Pi]}{K_{r,Pi}} + \frac{[G1P]}{K_{r,G1P}}\right)^{n-1}}{\left(1 + \frac{[Pi]}{K_{r,Pi}} + \frac{[G1P]}{K_{r,G1P}}\right)^{n} + L_t \left(1 + \frac{[Pi]}{K_{t,Pi}} + \frac{[G1P]}{K_{t,G1P}}\right)^{n} \left(\frac{1 + \frac{[AMP]}{K_{t,AMP}} + \frac{[G6P]}{K_{t,G6P}}}{1 + \frac{[AMP]}{K_{r,AMP}} + \frac{[G6P]}{K_{r,G6P}}}\right)^{n} \left(\frac{1 + \frac{[ATP]}{K_{t,ATP}}}{1 + \frac{[ATP]}{K_{r,ATP}}}\right)^{n}} \tag{C.6}$$

Table C.6: Optimized parameters for the best-fit equation (Eq. C.7).

Parameter	Value	Error	Unit
R^2	0.9991	–	–
$\bar{R}^2$	0.999	–	–
$V_{\text{max,a,reverse}}$	31.446	0.917	μmol.min^{-1}mg^{-1}
$V_{\text{max,a,forward}}$	257.71	1.348	U.mg^{-1}
$V_{\text{max,b,reverse,AMP}}$	26.778	0.592	μmol.min^{-1}mg^{-1}
$V_{\text{max,b,reverse,G1P}}$	38.181	1.005	μmol.min^{-1}mg^{-1}
$K_{\text{r,GP:G6P}}$	7.4174	2.73	mM
$K_{\text{u,GP:G6P}}$	0.5551	0.12	mM
$K_{\text{t,GP:G6P}}$	0.2685	$4.853 \cdot 10^{-2}$	mM
$K_{\text{r,GP:AMP}}$	$3.3581 \cdot 10^{-3}$	$3.958 \cdot 10^{-3}$	mM
$K_{\text{t,GP:AMP}}$	0.525	0.283	mM
$K_{\text{t,GP:ATP}}$	3.8991	22.627	mM
$K_{\text{r,GP:G1P}}$	0.6671	$8.345 \cdot 10^{-2}$	mM
$K_{\text{u,GP:G1P}}$	82.016	53.359	mM
$K_{\text{t,GP:G1P}}$	27.923	9.316	mM
$K_{\text{r,GP:Pi}}$	2.0821	$4.402 \cdot 10^{-2}$	mM
$K_{\text{u,GP,Pi}}$	4.3177	0.177	mM
$K_{\text{t,GP,Pi}}$	41.532	547.57	mM
$L_{\text{u,GP,a}}$	5.9348	0.405	dimensionless
$L_{\text{t,GP,a}}$	0	0	dimensionless
$L_{\text{u,GP,b}}$	0	0	dimensionless
$L_{\text{t,GP,b}}$	34,741	72,931	dimensionless

We further found that neither $K_{\text{u,AMP}}$ nor $K_{\text{r,ATP}}$ affected the goodness of fit whatsoever. Equation C.6 thus simplifies to

$$v_{\text{GP}} = \frac{k_{\text{cat,r}}[\text{GP}]_a n \frac{[\text{Pi}]}{K_{\text{r,Pi}}} \left(1 + \frac{[\text{Pi}]}{K_{\text{r,Pi}}} + \frac{[\text{G1P}]}{K_{\text{r,G1P}}}\right)^{n-1}}{\left(1 + \frac{[\text{Pi}]}{K_{\text{r,Pi}}} + \frac{[\text{G1P}]}{K_{\text{r,G1P}}}\right)^{n} + L_{\text{u}} \left(1 + \frac{[\text{Pi}]}{K_{\text{u,Pi}}} + \frac{[\text{G1P}]}{K_{\text{u,G1P}}}\right)^{n} \left(\frac{1 + \frac{[\text{G6P}]}{K_{\text{u,G6P}}}}{1 + \frac{[\text{AMP}]}{K_{\text{r,AMP}}} + \frac{[\text{G6P}]}{K_{\text{r,G6P}}}}\right)^{n}} + \frac{k_{\text{cat,r}}[\text{GP}]_b n \frac{[\text{Pi}]}{K_{\text{r,Pi}}} \left(1 + \frac{[\text{Pi}]}{K_{\text{r,Pi}}} + \frac{[\text{G1P}]}{K_{\text{r,G1P}}}\right)^{n-1}}{\left(1 + \frac{[\text{Pi}]}{K_{\text{r,Pi}}} + \frac{[\text{G1P}]}{K_{\text{r,G1P}}}\right)^{n} + L_{\text{t}} \left(1 + \frac{[\text{Pi}]}{K_{\text{t,Pi}}} + \frac{[\text{G1P}]}{K_{\text{t,G1P}}}\right)^{n} \left(\frac{1 + \frac{[\text{AMP}]}{K_{\text{t,AMP}}} + \frac{[\text{G6P}]}{K_{\text{t,G6P}}}}{1 + \frac{[\text{AMP}]}{K_{\text{r,AMP}}} + \frac{[\text{G6P}]}{K_{\text{r,G6P}}}}\right)^{n} \left(1 + \frac{[\text{ATP}]}{K_{\text{t,ATP}}}\right)^{n}} \tag{C.7}$$

The parameters that provided the best fit (Fig. C.1) to Eq. C.7 are listed in Table C.6.

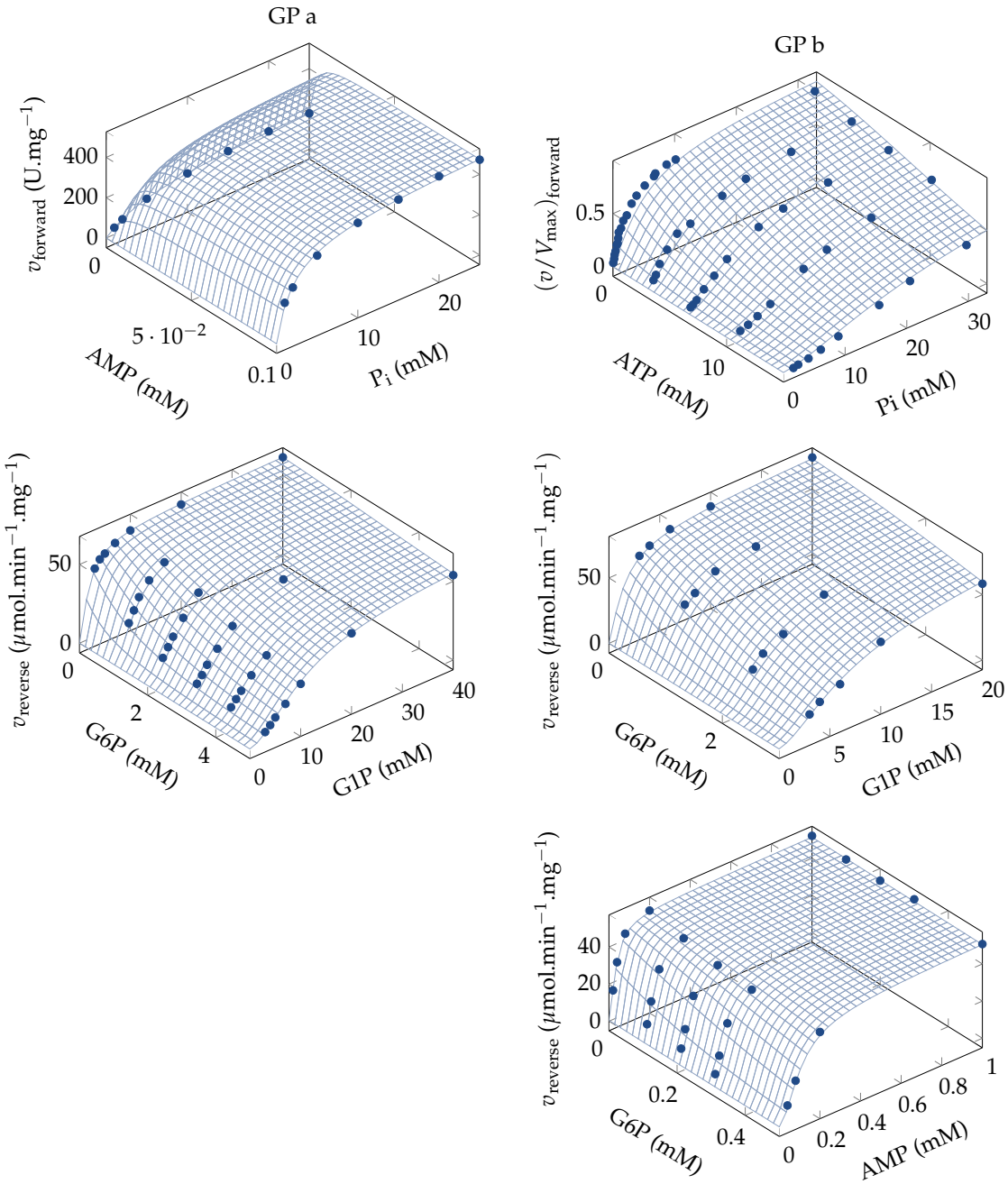

Figure C.1: Comparison of experimental data points to the rates calculated from the best-fit equation (Eq. C.7).

Bibliography

[1] Roach PJ, DePaoli-Roach AA, Hurley TD & Tagliabracci VS (2012) Glycogen and its metabolism: some new developments and old themes. *Biochem J* **441**, 763–787.

[2] Meléndez-Hevia E, Waddell TG & Shelton ED (1993) Optimization of molecular design in the evolution of metabolism: the glycogen molecule. *Biochem J* **295**, 477–483.

[3] DeFronzo RA, Gunnarsson R, Björkman O, Olsson M & Wahren J (1985) Effects of insulin on peripheral and splanchnic glucose metabolism in noninsulin-dependent (type II) diabetes mellitus. *J Clin Invest* **76**, 149–155.

[4] Shulman GI, Rothman DL, Jue T, Stein P, DeFronzo RA & Shulman RG (1990) Quantitation of muscle glycogen synthesis in normal subjects and subjects with non-insulin-dependent diabetes by 13C nuclear magnetic resonance spectroscopy. *N Engl J Med* **322**, 223–228.

[5] Jensen J & Lai YC (2009) Regulation of muscle glycogen synthase phosphorylation and kinetic properties by insulin, exercise, adrenaline and role in insulin resistance. *Arch Physiol Biochem* **115**, 13–21.

[6] DeFronzo RA & Tripathy D (2009) Skeletal muscle insulin resistance is the primary defect in type 2 diabetes. *Diabetes Care* **32**, S157–S163.

[7] Jensen J, Jebens E, Brennesvik EO, Ruzzin J, Soos MA, Engebretsen EML, O'Rahilly S & Whitehead JP (2006) Muscle glycogen inharmoniously regulates glycogen synthase activity, glucose uptake, and proximal insulin signaling. *Am J Physiol Endocrinol Metab* **290**, E154–E162.

[8] Shulman RG, Bloch G & Rothman DL (1995) In vivo regulation of muscle glycogen synthase and the control of glycogen synthesis. *Proc Natl Acad Sci USA* **92**, 8535–8542.

[9] Shulman RG & Rothman DL (1996) Enzymatic phosphorylation of muscle glycogen synthase: a mechanism for maintenance of metabolic homeostasis. *Proc Natl Acad Sci USA* **93**, 7491–7495.

[10] Kacser H & Burns JA (1973) The control of flux. *Sym Soc Exp Biol* **27**, 65–104.

[11] Heinrich R & Rapoport TA (1974) A linear steady-state treatment of enzymatic chains. General properties, control and effector strength. *Eur J Biochem* **42**, 89–95.

[12] Chase JR, Rothman DL & Shulman RG (2001) Flux control in the rat gastrocnemius glycogen synthesis pathway by in vivo 13C/31P NMR spectroscopy. *Am J Physiol Endocrinol Metab* **280**, 598–607.

[13] Schafer JRA, Fell DA, Rothman D & Shulman RG (2004) Protein phosphorylation can regulate metabolite concentrations rather than control flux: the example of glycogen synthase. *Proc Natl Acad Sci USA* **101**, 1485–1490.

[14] Jucker BM, Barucci N & Shulman GI (1999) Metabolic control analysis of insulin-stimulated glucose disposal in rat skeletal muscle. *Am J Physiol Endocrinol Metab* **277**, E505–E512.

[15] Hofmeyr JHS & Cornish-Bowden A (2000) Regulating the cellular economy of supply and demand. *FEBS Lett* **476**, 47–51.

[16] Hofmeyr JHS, Rohwer JM & Snoep JL (2006) Conditions for effective allosteric feedforward and feedback in metabolic pathways. *IEE Proc-Syst Biol* **153**, 327–331.

[17] Bouskila M, Hirshman MF, Jensen J, Goodyear LJ & Sakamoto K (2008) Insulin promotes glycogen synthesis in the absence of GSK3 phosphorylation in skeletal muscle. *Am J Physiol Endocrinol Metab* **294**, E28–E35.

[18] Bouskila M, Hunter RW, Ibrahim AFM, Delattre L, Peggie M, van Diepen JA, Voshol PJ, Jensen J & Sakamoto K (2010) Allosteric regulation of glycogen synthase controls glycogen synthesis in muscle. *Cell Metab* **12**, 456–466.

[19] Lambeth MJ & Kushmerick MJ (2002) A computational model for glycogenolysis in skeletal muscle. *Ann Biomed Eng* **30**, 808–827.

[20] Palm DC, Rohwer JM & Hofmeyr JHS (2013) Regulation of glycogen synthase from mammalian skeletal muscle - a unifying view of allosteric and covalent regulation. *FEBS J* **280**, 2–27.

[21] Leloir LF & Cardini CE (1957) Biosynthesis of glycogen from uridine diphosphate glucose. *J Am Chem Soc* **79**, 6340–6341.

[22] Leloir LF, Olavarria JM, Goldemberg SH & Carminatti H (1959) Biosynthesis of glycogen from uridine diphosphate glucose. *Arch Biochem Biophys* **81**, 508–520.

[23] Hauk R & Brown DH (1959) Preparation and properties of uridinediphosphoglucose-glycogen transferase from rabbit muscle. *Biochim Biophys Acta* **33**, 556–559.

[24] Salsas E & Larner J (1975) Kinetic studies on muscle glycogen synthase. *J Biol Chem* **250**, 3471–3475.

[25] Smythe C, Caudwell FB, Ferguson M & Cohen P (1988) Isolation and structural analysis of a peptide containing the novel tyrosyl-glucose linkage in glycogenin. *EMBO J* **7**, 2681–2686.

[26] Cao Y, Mahrenholz AM, DePaoli-Roach AA & Roach PJ (1993) Characterization of rabbit skeletal muscle glycogenin. Tyrosine 194 is essential for function. *J Biol Chem* **268**, 14687–14693.

[27] Pitcher J, Smythe C & Cohen P (1988) Glycogenin is the priming glucosyltransferase required for the initiation of glycogen biogenesis in rabbit skeletal muscle. *Eur J Biochem* **176**, 391–395.

[28] Lin A, Mu J, Yang J & Roach PJ (1999) Self-glucosylation of glycogenin, the initiator of glycogen biosynthesis, involves an inter-subunit reaction. *Arch Biochem Biophys* **363**, 163–170.

[29] Lomako J, Lomako WM & Whelan WJ (2004) Glycogenin: the primer for mammalian and yeast glycogen synthesis. *Biochim Biophys Acta* **1673**, 45–55.

[30] Smythe C, Watt P & Cohen P (1990) Further studies on the role of glycogenin in glycogen biosynthesis. *Eur J Biochem* **189**, 199–204.

[31] Roach PJ (2002) Glycogen and its metabolism. *Curr Mol Med* **2**, 101–120.

[32] Kornfeld R & Brown DH (1962) Preparation and properties of uridine diphosphate glucose-glycogen transglucosylase. *J Biol Chem* **237**, 1772–1777.

[33] Goldberg RN, Bell D, Tewari YB & McLaughlin MA (1991) Thermodynamics of hydrolysis of oligosaccharides. *Biophys Chem* **40**, 69–76.

[34] Gold AM (1980) Kinetic mechanism of rabbit muscle glycogen synthase I. *Biochemistry* **19**, 3766–3772.

[35] Jankowski MD, Henry CS, Broadbelt LJ & Hatzimanikatis V (2008) Group contribution method for thermodynamic analysis of complex metabolic networks. *Biophys J* **95**, 1487–1499.

[36] Flamholz A, Noor E, Bar-Even A & Milo R (2012) eQuilibrator–the biochemical thermodynamics calculator. *Nucleic Acids Res* **40**, D770–D775.

[37] Kashiwaya Y, Sato K, Tsuchiya N, Thomas S, Fell DA, Veech RL & Passonneau JV (1994) Control of glucose utilization in working perfused rat heart. *J Biol Chem* **269**, 25502–25514.

[38] Fox J, Kawaguchi K, Greenberg E & Preiss J (1976) Biosynthesis of bacterial glycogen. Purification and properties of the Escherichia coli B ADPglucose:1,4-alpha-D-glucan 4-alpha-glucosyltransferase. *Biochemistry* **15**, 849–857.

[39] Piras R, Rothman LB & Cabib E (1967) Metabolite regulation of the I and D form of rat muscle glycogen synthetase. *Biochem Biophys Res Commun* **28**, 54–58.

[40] Plesner L, Plesner IW & Esmann V (1974) Kinetic mechanism of glycogen synthase D from human polymorphonuclear leukocytes. *J Biol Chem* **249**, 1119–1125.

[41] Brown NE & Larner J (1971) Molecular characteristics of the totally dependent and independent forms of glycogen synthase of rabbit skeletal muscle. I. Preparation and characteristics of the totally glucose 6-phosphate dependent form. *Biochim Biophys Acta* **242**, 69–80.

[42] Sølling H (1979) Studies on the allosteric properties of glycogen synthase I. *Eur J Biochem* **94**, 231–242.

[43] Sølling H & Esmann V (1977) The hysteretic properties of glycogen synthase I. *Eur J Biochem* **81**, 129–139.

[44] Krivokobyl'skaia II & Solov'eva GA (1984) [Formation of the glycogen synthase I-glycogen complex]. *Biokhimiia* **49**, 1819–1827.

[45] Salsas E & Larner J (1975) Action pattern of muscle glycogen synthase. *Mol Cell Biochem* **7**, 195–199.

[46] Parodi AJ, Mordoh J, Krisman CR & Leloir LF (1970) Action patterns of phosphorylase and glycogen synthetase on glycogen. *Eur J Biochem* **16**, 499–507.

[47] Baskaran S, Chikwana VM, Contreras CJ, Davis KD, Wilson WA, DePaoli-Roach AA, Roach PJ & Hurley TD (2011) Multiple glycogen-binding sites in eukaryotic glycogen synthase are required for high catalytic efficiency toward glycogen. *J Biol Chem* **286**, 33999–34006.

[48] Bourne Y & Henrissat B (2001) Glycoside hydrolases and glycosyltransferases: families and functional modules. *Curr Opin Struct Biol* **11**, 593–600.

[49] Buschiazzo A, Ugalde JE, Guerin ME, Shepard W, Ugalde RA & Alzari PM (2004) Crystal structure of glycogen synthase: homologous enzymes catalyze glycogen synthesis and degradation. *EMBO J* **23**, 3196–3205.

[50] Sheng F, Jia X, Yep A, Preiss J & Geiger JH (2009) The crystal structures of the open and catalytically competent closed conformation of Escherichia coli glycogen synthase. *J Biol Chem* **284**, 17796–17807.

[51] Baskaran S, Roach PJ, DePaoli-Roach AA & Hurley TD (2010) Structural basis for glucose-6-phosphate activation of glycogen synthase. *Proc Natl Acad Sci USA* **107**, 17563–17568.

[52] Horcajada C, Guinovart JJ, Fita I & Ferrer JC (2006) Crystal structure of an archaeal glycogen synthase: insights into oligomerization and substrate binding of eukaryotic glycogen synthases. *J Biol Chem* **281**, 2923–2931.

[53] Baskaran S (2010) *Structure and Regulation of Yeast Glycogen Synthase*. Ph.D. thesis, Indiana University.

[54] Takeda Y, Brewer HB & Larner J (1975) Structural studies on rabbit muscle glycogen synthase. I. Subunit composition. *J Biol Chem* **250**, 8943–8950.

[55] Staneloni RJ & Piras R (1971) Reversible aggregation of muscle glycogen synthetase by metabolites. *Biochem Biophys Res Commun* **42**, 237–244.

[56] Brown JH, Thompson B & Mayer SE (1977) Conversion of skeletal muscle glycogen synthase to multiple glucose 6-phosphate dependent forms by cyclic adenosine monophosphate dependent and independent protein kinases. *Biochemistry* **16**, 5501–5508.

[57] Soderling TR, Hickenbottom JP, Reimann EM, Hunkeler FL, Walsh DA & Krebs EG (1970) Inactivation of glycogen synthetase and activation of phosphorylase kinase by muscle adenosine 3', 5'-monophosphate-dependent protein kinases. *J Biol Chem* **245**, 6317–6328.

[58] Issa HA & Mendicino J (1973) Role of enzyme-enzyme interactions in the regulation of glycolysis and gluconeogenesis. Properties of glycogen synthetase isolated from swine kidney. *J Biol Chem* **248**, 685–696.

[59] Nimmo HG, Proud CG & Cohen P (1976) The purification and properties of rabbit skeletal muscle glycogen synthase. *Eur J Biochem* **68**, 21–30.

[60] Soderling TR (1976) Regulation of glycogen synthetase. Effects of trypsin on the structure, activity, and phosphorylation of the skeletal muscle enzyme. *J Biol Chem* **251**, 4359–4364.

[61] Sølling H & Esmann V (1977) Purification and properties of glycogen synthase I from human leukocytes. *Eur J Biochem* **81**, 119–128.

[62] Smith CH & Larner J (1972) Differential aggregation of the totally converted D and I forms of rabbit muscle glycogen synthase. *Biochim Biophys Acta* **264**, 224–228.

[63] Pederson BA, Cheng C, Wilson WA & Roach PJ (2000) Regulation of glycogen synthase. Identification of residues involved in regulation by the allosteric ligand glucose-6-P and by phosphorylation. *J Biol Chem* **275**, 27753–62771.

[64] Hanashiro I & Roach PJ (2002) Mutations of muscle glycogen synthase that disable activation by glucose 6-phosphate. *Arch Biochem Biophys* **397**, 286–292.

[65] Pruitt KD, Tatusova T, Brown GR & Maglott DR (2012) NCBI Reference Sequences (RefSeq): current status, new features and genome annotation policy. *Nucleic Acids Res* **40**, D130–D135.

[66] Rao ST & Rossmann MG (1973) Comparison of super-secondary structures in proteins. *J Mol Biol* **76**, 241–256.

[67] Piras R, Rothman LB & Cabib E (1968) Regulation of muscle glycogen synthetase by metabolites. Differential effects on the I and D forms. *Biochemistry* **7**, 56–66.

[68] Barash V, Schramm H & Gutman A (1973) Adipose tissue glycogen synthetase. I. Kinetic properties. *J Biol Chem* **248**, 3733–3738.

[69] Nakai C & Thomas JA (1975) Effects of magnesium on the kinetic properties of bovine heart glycogen synthase D. *J Biol Chem* **250**, 4081–4086.

[70] Passonneau JV, Schwartz JP & Rottenberg DA (1975) The partial purification and properties of pig brain glycogen synthase. *J Biol Chem* **250**, 2287–2292.

[71] Rosell-Perez M, Villar-Palasi C & Larner J (1962) Studies on UDPG-glycogen transglucosylase. I. Preparation and differentiation of two activities of UDPG-glycogen transglucosylase from rat skeletal muscle. *Biochemistry* **1**, 763–768.

[72] Roach PJ, Takeda Y & Larner J (1976) Rabbit skeletal muscle glycogen synthase. I. Relationship between phosphorylation state and kinetic properties. *J Biol Chem* **251**, 1913–1919.

[73] Roach PJ, Rosell-Perez M & Larner J (1977) Muscle glycogen synthase in vivo state: Effects of insulin administration on the chemical and kinetic properties of the purified enzyme. *FEBS Lett* **80**, 95–98.

[74] Roach PJ & Larner J (1977) Covalent phosphorylation in the regulation of glycogen synthase activity. *Mol Cell Biochem* **15**, 179–200.

[75] Steiner DF, Younger L & King J (1965) Purification and properties of uridine diphosphate glucose-glycogen glucosyltransferase from rat liver. *Biochemistry* **4**, 740–751.

[76] Díaz A, Martínez-Pons C, Fita I, Ferrer JC & Guinovart JJ (2011) Processivity and subcellular localization of glycogen synthase depend on a non-catalytic high affinity glycogen-binding site. *J Biol Chem* **286**, 18505–18514.

[77] Cornish-Bowden A (2004) *Fundamentals of Enzyme Kinetics*. 3rd edn., Portland Press, London.

[78] Rosell-Perez M & Larner J (1964) Studies on UDPG: alpha-1, 4-glucan alpha-4-glucosyltransferase. VI. Specificity and structural requirements for the activator of the D form of the dog muscle enzyme. *Biochemistry* **3**, 773–778.

[79] Roach PJ & Larner J (1976) Rabbit skeletal muscle glycogen synthase. II. Enzyme phosphorylation state and effector concentrations as interacting control parameters. *J Biol Chem* **251**, 1920–1925.

[80] Goldemberg SH (1962) Specificity of uridine diphosphate glucose-glycogen glucosyltransferase. *Biochim Biophys Acta* **56**, 357–359.

[81] Passonneau JV, Brunner EA, Molstad C & Passonneau R (1971) The effects of altered endocrine states and of ether anaesthesia on mouse brain. *J Neurochem* **18**, 2317–2328.

[82] Plesner L, Plesner IW & Esmann V (1976) Purification and steady state kinetic mechanism of glycogen synthase-D from human polymorpho-nuclear leukocytes. *Mol Cell Biochem* **12**, 45–61.

[83] Manchester KL (1980) Determination of magnesium and potassium binding constants to phosphoenolpyruvate, 2- and 3-phosphoglycerate and a number of other anions. *Biochim Biophys Acta* **630**, 225–231.

[84] O'Sullivan WJ & Perrin DD (1964) The stability constants of metal-adenine nucleotide complexes. *Biochemistry* **3**, 18–26.

[85] Poulter L, Ang SG, Gibson BW, Williams DH, Holmes CFB, Caudwell FB, Pitcher J & Cohen P (1988) Analysis of the in vivo phosphorylation state of rabbit skeletal muscle glycogen synthase by fast-atom-bombardment mass spectrometry. *Eur J Biochem* **175**, 497–510.

[86] Roach PJ (1990) Control of glycogen synthase by hierarchal protein phosphorylation. *FASEB J* **4**, 2961–2968.

[87] Hofmeyr JHS & Cornish-Bowden A (1997) The reversible Hill equation: how to incorporate cooperative enzymes into metabolic models. *Comput Appl Biosci* **13**, 377–385.

[88] Westermark PO, Hellgren-Kotaleski J & Lansner A (2004) Derivation of a reversible Hill equation with modifiers affecting catalytic properties. *WSEAS Trans Biol Med* **1**, 91–98.

[89] Villar-Palasi C & Larner J (1960) Insulin-mediated effect on the activity of UDPG-glycogen transglucosylase of muscle. *Biochim Biophys Acta* **39**, 171–173.

[90] Guinovart JJ, Salavert A, Massagué J, Ciudad CJ, Salsas E & Itarte E (1979) Glycogen synthase: a new activity ratio assay expressing a high sensitivity to the phosphorylation state. *FEBS Lett* **106**, 284–288.

[91] Roach PJ (1991) Multisite and hierarchal protein phosphorylation. *J Biol Chem* **266**, 14139–14142.

[92] Skurat AV & Dietrich AD (2004) Phosphorylation of Ser640 in muscle glycogen synthase by DYRK family protein kinases. *J Biol Chem* **279**, 2490–2498.

[93] Wilson WA, Skurat AV, Probst B, DePaoli-Roach A, Roach PJ & Rutter J (2005) Control of mammalian glycogen synthase by PAS kinase. *Proc Natl Acad Sci USA* **102**, 16596–16601.

[94] Kuma Y, Campbell DG & Cuenda A (2004) Identification of glycogen synthase as a new substrate for stress-activated protein kinase 2b/p38beta. *Biochem J* **379**, 133–139.

[95] Chan KF, Hurst MO & Graves DJ (1982) Phosphorylase kinase specificity. A comparative study with cAMP-dependent protein kinase on synthetic peptides and peptide analogs of glycogen synthase and phosphorylase. *J Biol Chem* **257**, 3655–3659.

[96] Rylatt DB, Embi N & Cohen P (1979) Glycogen synthase kinase-2 from rabbit skeletal muscle is activated by the calcium-dependent regulator protein. *FEBS Lett* **98**, 76–80.

[97] Soderling TR, Sheorain V & Ericsson L (1979) Phosphorylation of glycogen synthase by phosphorylase kinase: stoichiometry, specificity and site of phosphorylation. *FEBS Lett* **106**, 181–184.

[98] Woodgett JR, Tonks NK & Cohen P (1982) Identification of a calmodulin-dependent glycogen synthase kinase in rabbit skeletal muscle, distinct from phosphorylase kinase. *FEBS Lett* **148**, 5–11.

[99] Carling D & Hardie DG (1989) The substrate and sequence specificity of the AMP-activated protein kinase. Phosphorylation of glycogen synthase and phosphorylase kinase. *Biochim Biophys Acta* **1012**, 81–86.

[100] Kuret J, Woodgett JR & Cohen P (1985) Multisite phosphorylation of glycogen synthase from rabbit skeletal muscle. Identification of the sites phosphorylated by casein kinase-I. *Eur J Biochem* **151**, 39–48.

[101] Cohen P, Yellowlees D, Aitken A, Donella-Deana A, Hemmings BA & Parker PJ (1982) Separation and characterisation of glycogen synthase kinase 3, glycogen synthase kinase 4 and glycogen synthase kinase 5 from rabbit skeletal muscle. *Eur J Biochem* **124**, 21–35.

[102] Fiol CJ, Mahrenholz AM, Wang Y, Roeske RW & Roach PJ (1987) Formation of protein kinase recognition sites by covalent modification of the substrate. Molecular mechanism for the synergistic action of casein kinase II and glycogen synthase kinase 3. *J Biol Chem* **262**, 14042–14048.

[103] Rylatt DB, Aitken A, Bilham T, Condon GD, Embi N & Cohen P (1980) Glycogen synthase from rabbit skeletal muscle. Amino acid sequence at the sites phosphorylated by glycogen synthase kinase-3, and extension of the N-terminal sequence containing the site phosphorylated by phosphorylase kinase. *Eur J Biochem* **107**, 529–537.

[104] Parker PJ, Aitken A, Bilham T, Embi N & Cohen P (1981) Amino acid sequence of a region in rabbit skeletal muscle glycogen synthase phosphorylated by cyclic AMP-dependent protein kinase. *FEBS Lett* **123**, 332–336.

[105] Woodgett JR, Davison MT & Cohen P (1983) The calmodulin-dependent glycogen synthase kinase from rabbit skeletal muscle. Purification, subunit structure and substrate specificity. *Eur J Biochem* **136**, 481–487.

[106] Flotow H & Roach PJ (1989) Synergistic phosphorylation of rabbit muscle glycogen synthase by cyclic AMP-dependent protein kinase and casein kinase I. Implications for hormonal regulation of glycogen synthase. *J Biol Chem* **264**, 9126–9128.

[107] Zhang W, DePaoli-Roach AA & Roach PJ (1993) Mechanisms of multisite phosphorylation and inactivation of rabbit muscle glycogen synthase. *Arch Biochem Biophys* **304**, 219–225.

[108] Picton C, Woodgett J, Hemmings B & Cohen P (1982) Multisite phosphorylation of glycogen synthase from rabbit skeletal muscle. Phosphorylation of site

5 by glycogen synthase kinase-5 (casein kinase-II) is a prerequisite for phosphorylation of sites 3 by glycogen synthase kinase-3. *FEBS Lett* **150**, 191–196.

[109] Nakielny S, Campbell DG & Cohen P (1991) The molecular mechanism by which adrenalin inhibits glycogen synthesis. *Eur J Biochem* **199**, 713–722.

[110] Salazar C & Höfer T (2003) Allosteric regulation of the transcription factor NFAT1 by multiple phosphorylation sites: a mathematical analysis. *J Mol Biol* **327**, 31–45.

[111] Fiol CJ, Wang A, Roeske RW & Roach PJ (1990) Ordered multisite protein phosphorylation. Analysis of glycogen synthase kinase 3 action using model peptide substrates. *J Biol Chem* **265**, 6061–6065.

[112] Friedman DL & Larner J (1963) Studies on UDPG-α-glucan transglucosylase. III. Interconversion of two forms of muscle UDPG-α-glucan transglucosylase by a phosphorylation-dephosphorylation reaction sequence. *Biochemistry* **2**, 669–675.

[113] Stalmans W & Hers HG (1973) Glycogen synthesis from UDPG. In *The Enzymes* (Boyer PD, ed.), vol. IX, 3rd edn., pp. 310–357, Academic Press, New York and London.

[114] Skurat AV, Wang Y & Roach PJ (1994) Rabbit skeletal muscle glycogen synthase expressed in COS cells. Identification of regulatory phosphorylation sites. *J Biol Chem* **269**, 25534–25542.

[115] Skurat AV & Roach PJ (1995) Phosphorylation of sites 3a and 3b (Ser640 and Ser644) in the control of rabbit muscle glycogen synthase. *J Biol Chem* **270**, 12491–12497.

[116] Rosell-Perez M & Larner J (1964) Studies on UDPG-alpha-glucan transglucosylase. IV. Purification and characterization of two forms from rabbit skeletal muscle. *Biochemistry* **3**, 75–81.

[117] Rosell-Perez M & Larner J (1964) Studies on UDPG-alpha-glucan transglycolysase. V. Two forms of the enzyme in dog skeletal muscle and their interconversion. *Biochemistry* **3**, 81–88.

[118] Brown DF, Hegazy M & Reimann EM (1986) Kinetic properties of glycogen synthase from skeletal muscle after phosphorylation by glycogen synthase kinase 4. *Biochem Biophys Res Commun* **134**, 1129–1135.

[119] Nimmo HG, Proud CG & Cohen P (1976) The phosphorylation of rabbit skeletal muscle glycogen synthase by glycogen synthase kinase-2 and adenosine-3′:5′-monophosphate-dependent protein kinase. *Eur J Biochem* **68**, 31–44.

[120] Wang Y & Roach PJ (1993) Inactivation of rabbit muscle glycogen synthase by glycogen synthase kinase-3. Dominant role of the phosphorylation of Ser-640 (site-3a). *J Biol Chem* **268**, 23876–23880.

[121] Hardy TA & Roach PJ (1993) Control of yeast glycogen synthase-2 by COOH-terminal phosphorylation. *J Biol Chem* **268**, 23799–23805.

[122] Skurat AV, Dietrich AD & Roach PJ (2000) Glycogen synthase sensitivity to insulin and glucose-6-phosphate is mediated by both NH2- and COOH-terminal phosphorylation sites. *Diabetes* **49**, 1096–1100.

[123] Graham TE, Yuan Z, Hill AK & Wilson RJ (2010) The regulation of muscle glycogen: the granule and its proteins. *Acta Physiol* **199**, 489–498.

[124] Prats C, Gómez-Cabello A & Hansen AV (2011) Intracellular compartmentalization of skeletal muscle glycogen metabolism and insulin signalling. *Exp Physiol* **96**, 385–390.

[125] Prats C, Cadefau JA, Cussó R, Qvortrup K, Nielsen JN, Wojtaszewski JFP, Hardie DG, Stewart G, Hansen BF & Ploug T (2005) Phosphorylation-dependent translocation of glycogen synthase to a novel structure during glycogen resynthesis. *J Biol Chem* **280**, 23165–23172.

[126] Prats C, Helge JW, Nordby P, Qvortrup K, Ploug T, Dela F & Wojtaszewski JFP (2009) Dual regulation of muscle glycogen synthase during exercise by activation and compartmentalization. *J Biol Chem* **284**, 15692–15700.

[127] Brady MJ, Kartha PM, Aysola AA & Saltiel AR (1999) The role of glucose metabolites in the activation and translocation of glycogen synthase by insulin in 3T3-L1 adipocytes. *Biochemistry* **274**, 27497–27504.

[128] Litherland GJ, Morris NJ, Walker M & Yeaman SJ (2007) Role of glycogen content in insulin resistance in human muscle cells. *J Cell Physiol* **211**, 344–352.

[129] Ortmeyer HK, Adall Y, Marciani KR, Katsiaras A, Ryan AS, Bodkin NL & Hansen BC (2005) Skeletal muscle glycogen synthase subcellular localization: effects of insulin and PPAR-alpha agonist (K-111) administration in rhesus monkeys. *Am J Physiol Regul Integr Comp Physiol* **288**, R1509–R1517.

[130] Cid E, Cifuentes D, Baqué S, Ferrer JC & Guinovart JJ (2005) Determinants of the nucleocytoplasmic shuttling of muscle glycogen synthase. *FEBS J* **272**, 3197–3213.

[131] Nielsen JN, Derave W, Kristiansen S, Ralston E, Ploug T & Richter EA (2001) Glycogen synthase localization and activity in rat skeletal muscle is strongly dependent on glycogen content. *J Physiol* **531**, 757–769.

[132] Cohen P (2000) The regulation of protein function by multisite phosphorylation–a 25 year update. *Trends Biochem Sci* **25**, 596–601.

[133] Salazar C & Höfer T (2009) Multisite protein phosphorylation–from molecular mechanisms to kinetic models. *FEBS J* **276**, 3177–3198.

[134] Gunawardena J (2005) Multisite protein phosphorylation makes a good threshold but can be a poor switch. *Proc Natl Acad Sci USA* **102**, 14617–14622.

[135] Frame S & Cohen P (2001) GSK3 takes centre stage more than 20 years after its discovery. *Biochem J* **359**, 1–16.

[136] Algranati ID & Cabib E (1962) Uridine diphosphate glucosyltransferase D-glucose-glycogen glycosyltransferase from yeast. *J Biol Chem* **237**, 1007–1013.

[137] Rosell-Perez M & Larner J (1962) Studies on UDPG-glycogen transglucosylase. II. Species variation of glucose-6-phosphate sensitivity of UDPG-glycogen transglucosylase. *Biochemistry* **1**, 769–772.

[138] Lai YC, Stuenaes JT, Kuo CH & Jensen J (2007) Glycogen content and contraction regulate glycogen synthase phosphorylation and affinity for UDP-glucose in rat skeletal muscles. *Am J Physiol Endocrinol Metab* **293**, 1622–1629.

[139] Villar-Palasi C (1994) Inhibition by glucose 6-phosphate of cyclic AMP-dependent protein kinase phosphorylation of glycogen synthase. *Biochim Biophys Acta* **1207**, 88–92.

[140] Taylor SS (1989) cAMP-dependent protein kinase. *J Biol Chem* **264**, 8443–8446.

[141] Huang D, Wilson WA & Roach PJ (1997) Glucose-6-P control of glycogen synthase phosphorylation in yeast. *J Biol Chem* **272**, 22495–22501.

[142] Traut RR & Lipmann F (1963) Activation of glycogen synthetase by glucose 6-phosphate. *J Biol Chem* **238**, 1213–1221.

[143] Kato K & Bishop JS (1972) Glycogen synthetase-D phosphatase. I. Some new properties of the partially purified enzyme from rabbit skeletal muscle. *J Biol Chem* **247**, 7420–7429.

[144] Thomas JA & Nakai C (1973) Control of glycogen synthase phosphatase from rat heart. The role of substrate. *J Biol Chem* **248**, 2208–2213.

[145] Okubo M, Bogardus C, Lillioja S & Mott DM (1988) Glucose-6-phosphate stimulation of human muscle glycogen synthase phosphatase. *Metabolism* **37**, 1171–1176.

[146] Villar-Palasi C (1991) Substrate specific activation by glucose 6-phosphate of the dephosphorylation of muscle glycogen synthase. *Biochim Biophys Acta* **1095**, 261–267.

[147] Villar-Palasi C & Guinovart JJ (1997) The role of glucose 6-phosphate in the control of glycogen synthase. *FASEB J* **11**, 544–558.

[148] Fernández-Novell JM, Ariño J, Vilaró S & Guinovart JJ (1992) Glucose induces the translocation and the aggregation of glycogen synthase in rat hepatocytes. *Biochem J* **281**, 443–448.

[149] Fernández-Novell JM, Bellido D, Vilaró S & Guinovart JJ (1997) Glucose induces the translocation of glycogen synthase to the cell cortex in rat hepatocytes. *Biochem J* **321**, 227–231.

[150] Westermark PO & Lansner A (2003) A model of phosphofructokinase and glycolytic oscillations in the pancreatic beta-cell. *Biophys J* **85**, 126–139.

[151] Embi N, Rylatt DB & Cohen P (1980) Glycogen synthase kinase-3 from rabbit skeletal muscle. Separation from cyclic-AMP-dependent protein kinase and phosphorylase kinase. *Eur J Biochem* **107**, 519–527.

[152] Gilboe DP & Nuttall FQ (1972) The role of ATP and glucose 6-phosphate in the regulation of glycogen synthetase D phosphatase. *Biochem Biophys Res Commun* **48**, 898–906.

[153] Nakai C & Thomas JA (1974) Properties of a phosphoprotein phosphatase from bovine heart with activity on glycogen synthase, phosphorylase, and histone. *J Biol Chem* **249**, 6459–6467.

[154] Wang P & Bantle G (1974) The combined effect of glycogen and ATP on the D to I conversion of glycogen synthetase. *Biochem Biophys Res Commun* **57**, 148–153.

[155] Koshland DE, Némethy G & Filmer D (1966) Comparison of experimental binding data and theoretical models in proteins containing subunits. *Biochemistry* **5**, 365–385.

[156] Monod J, Wyman J & Changeux JP (1965) On the nature of allosteric transitions: A plausible model. *J Mol Biol* **12**, 88–118.

[157] Popova SV & Sel'kov EE (1975) Generalization of the model by Monod, Wyman and Changeux for the case of reversible monosubstrate reaction S = P. *FEBS Lett* **53**, 269–273.

[158] Marquardt DW (1963) An algorithm for least-squares estimation of nonlinear parameters. *J Soc Ind Appl Math* **11**, 431–441.

[159] Vaz AIF & Vicente LN (2007) A particle swarm pattern search method for bound constrained global optimization. *Journal of Global Optimization* **39**, 197–219.

[160] Pérez F & Granger BE (2007) IPython: a system for interactive scientific computing. *Comput Sci Eng* **9**, 21–29.

[161] Rubin MM & Changeux JP (1966) On the nature of allosteric transitions: implications of non-exclusive ligand binding. *J Mol Biol* **21**, 265–274.

[162] Hofmeyr JHS & Westerhoff HV (2001) Building the cellular puzzle: control in multi-level reaction networks. *J Theor Biol* **208**, 261–285.

[163] Goldbeter A & Koshland DE (1981) An amplified sensitivity arising from covalent modification in biological systems. *Proc Natl Acad Sci USA* **78**, 6840–6844.

[164] Small JR & Fell DA (1990) Covalent modification and metabolic control analysis. Modification to the theorems and their application to metabolic systems containing covalently modifiable enzymes. *Eur J Biochem* **191**, 405–411.

[165] Killilea SD, Brandt H, Lee EYC & Whelan WJ (1976) Evidence for the coordinate control of activity of liver glycogen synthase and phosphorylase by a single protein phosphatase. *J Biol Chem* **251**, 2363–2368.

[166] Detwiler TC, Gratecos D & Fischer EH (1977) Rabbit muscle phosphorylase phosphatase. 2. Kinetic properties and behavior in glycogen particles. *Biochemistry* **16**, 4818–4823.

[167] Martensen TM, Brotherton JE & Graves DJ (1973) Kinetic studies of the inhibition of muscle phosphorylase phosphatase. *J Biol Chem* **248**, 8323–8328.

[168] Tu JI & Graves DJ (1973) Inhibition of the phosphorylase kinase catalyzed reaction by glucose-6-P. *Biochem Biophys Res Commun* **53**, 59–65.

[169] Echigoya Y, Okabe H, Itou T, Endo H & Sakai T (2011) Molecular characterization of glycogen synthase 1 and its tissue expression profile with type II hexokinase and muscle-type phosphofructokinase in horses. *Mol Biol Rep* **38**, 461–469.

[170] Schiaffino S & Reggiani C (2011) Fiber types in mammalian skeletal muscles. *Physiological reviews* **91**, 1447–1531.

[171] Suarez RK (2003) Shaken and stirred: muscle structure and metabolism. *J Exp Biol* **206**, 2021–2029.

[172] van Eunen K, Bouwman J, Daran-Lapujade P, Postmus J, Canelas AB, Mensonides FIC, Orij R, Tuzun I, van den Brink J, Smits GJ, van Gulik WM, Brul S, Heijnen JJ, de Winde JH, de Mattos MJT, Kettner C, Nielsen J, Westerhoff HV & Bakker BM (2010) Measuring enzyme activities under standardized in vivo-like conditions for systems biology. *FEBS J* **277**, 749–760.

[173] Rohwer JM & Hofmeyr JHS (2010) Kinetic and thermodynamic aspects of enzyme control and regulation. *J Phys Chem B* **114**, 16280–16289.

[174] Kraegen EW, Sowden JA, Halstead MB, Clark PW, Rodnick KJ, Chisholm DJ & Jamest DE (1993) Glucose transporters and in vivo glucose uptake in skeletal

and cardiac muscle: fasting, insulin stimulation and immunoisolation studies of GLUT1 and GLUT4. *Biochem J* **295**, 287–293.

[175] Wang W, Hansen PA, Marshall BA, Holloszy JO & Mueckler M (1996) Insulin unmasks a COOH-terminal Glut4 epitope and increases glucose transport across T-tubules in skeletal muscle. *J Cell Biol* **135**, 415–430.

[176] Mueckler M (2001) Insulin resistance and the disruption of Glut4 trafficking in skeletal muscle. *J Clin Invest* **107**, 1211–1213.

[177] Fazakerley D & Coster A (2010) Muscling in on GLUT4 kinetics. *Commun Integr Biol* **3**, 260–262.

[178] Bryant NJ, Govers R & James DE (2002) Regulated transport of the glucose transporter GLUT4. *Nat Rev Mol Cell Biol* **3**, 267–277.

[179] Rowland AF, Fazakerley DJ & James DE (2011) Mapping insulin/GLUT4 circuitry. *Traffic* **12**, 672–681.

[180] Foley K, Boguslavsky S & Klip A (2011) Endocytosis, recycling, and regulated exocytosis of glucose transporter 4. *Biochemistry* **50**, 3048–3061.

[181] Carruthers A, DeZutter J, Ganguly A & Devaskar SU (2009) Will the original glucose transporter isoform please stand up! *Am J Physiol Endocrinol Metab* **297**, E836–E848.

[182] Cloherty EK, Heard KS & Carruthers A (1996) Human erythrocyte sugar transport is incompatible with available carrier models. *Biochemistry* **35**, 10411–10421.

[183] Carruthers A & Melchior DL (1983) Asymmetric or symmetric? Cytosolic modulation of human erythrocyte hexose transfer. *Biochim Biophys Acta* **728**, 254–266.

[184] Levine KB, Cloherty EK, Hamill S & Carruthers A (2002) Molecular determinants of sugar transport regulation by ATP. *Biochemistry* **41**, 12629–12638.

[185] Naftalin RJ (2008) Alternating carrier models of asymmetric glucose transport violate the energy conservation laws. *Biophys J* **95**, 4300–4314.

[186] Gould GW & Holman GD (1993) The glucose transporter family: structure, function and tissue-specific expression. *Biochem J* **295**, 329–341.

[187] Ritov VB & Kelley DE (2001) Hexokinase isozyme distribution in human skeletal muscle. *Diabetes* **50**, 1253–1262.

[188] Vogt C, Yki-Jarvinen H, Iozzo P, Pipek R, Pendergrass M, Koval J, Ardehali H, Printz R, Granner D, DeFronzo R & Mandarino L (1998) Effects of insulin on subcellular localization of hexokinase II in human skeletal muscle in vivo. *J Clin Endocrinol Metab* **83**, 230–234.

[189] Vogt C, Ardehali H, Iozzo P, Yki-Järvinen H, Koval J, Maezono K, Pendergrass M, Printz R, Granner D, DeFronzo R & Mandarino L (2000) Regulation of hexokinase II expression in human skeletal muscle in vivo. *Metabolism* **49**, 814–818.

[190] Wilson JE (2003) Isozymes of mammalian hexokinase: structure, subcellular localization and metabolic function. *J Exp Biol* **206**, 2049–2057.

[191] Southworth R, Davey KAB, Warley A & Garlick PB (2007) A reevaluation of the roles of hexokinase I and II in the heart. *Am J Physiol Heart Circ Physiol* **292**, H378–H386.

[192] Arora KK, Filburns CR & Pederseng PL (1993) Structure/function relationships in hexokinase. Site-directed mutational analyses and characterization of overexpressed fragments implicate different functions for the N- and C-terminal halves of the enzyme. *J Biol Chem* **268**, 18259–18266.

[193] Ardehali H, Yano Y, Printz RL, Koch S, Whitesell RR, May JM & Granner DK (1996) Functional organization of mammalian hexokinase II. Retention of catalytic and regulatory functions in both the NH2- and COOH-terminal halves. *J Biol Chem* **271**, 1849–1852.

[194] Tsai HJ & Wilson JE (1996) Functional organization of mammalian hexokinases: both N- and C-terminal halves of the rat type II isozyme possess catalytic sites. *Arch Biochem Biophys* **329**, 17–23.

[195] Ardehali H, Printz RL, Whitesell RR, May JM & Granner DK (1999) Functional interaction between the N- and C-terminal halves of human hexokinase II. *J Biol Chem* **274**, 15986–15989.

[196] Grossbard L & Schimke RT (1966) Multiple hexokinases of rat tissues. Purification and comparison of soluble forms. *J Biol Chem* **241**, 3546–3560.

[197] Gao H & Leary JA (2004) Kinetic measurements of phosphoglucomutase by direct analysis of glucose-1-phosphate and glucose-6-phosphate using ion/molecule reactions and Fourier transform ion cyclotron resonance mass spectrometry. *Anal Biochem* **329**, 269–275.

[198] Duggleby RG, Chao YC, Huang JG, Peng HL & Chang HY (1996) Sequence differences between human muscle and liver cDNAs for UDPglucose pyrophosphorylase and kinetic properties of the recombinant enzymes expressed in Escherichia coli. *Eur J Biochem* **235**, 173–179.

[199] Johnson LN (1992) Glycogen phosphorylase: Control by phosphorylation and allosteric effectors. *FASEB J* **6**, 2274–2282.

[200] Johnson LN, Snape P, Martin JL, Acharya KR, Barford D & Oikonomakos NG (1993) Crystallographic binding studies on the allosteric inhibitor glucose-6-phosphate to T state glycogen phosphorylase b. *J Mol Biol* **232**, 253–267.

[201] Walcott S & Lehman SL (2007) Enzyme kinetics of muscle glycogen phosphorylase b. *Biochemistry* **46**, 11957–11968.

[202] Vinnakota K, Kemp ML & Kushmerick MJ (2006) Dynamics of muscle glycogenolysis modeled with pH time course computation and pH-dependent reaction equilibria and enzyme kinetics. *Biophys J* **91**, 1264–1287.

[203] Meinkoth JL, Alberts AS, Went W, Fantozzi D, Taylor SS, Hagiwara M, Montminy M & Feramisco JR (1993) Signal transduction through the cAMP-dependent protein kinase. *Mol Cell Biochem* **127-128**, 179–186.

[204] Mutalik VK & Venkatesh KV (2005) Quantification of the glycogen cascade system: the ultrasensitive responses of liver glycogen synthase and muscle phosphorylase are due to distinctive regulatory designs. *Theor Biol Med Model* **2**, 19.

[205] Harmer AR, McKenna MJ, Sutton JR, Snow RJ, Ruell PA, Booth J, Thompson MW, Mackay NA, Stathis CG, Crameri RM, Carey MF & Eager DM (2000) Skeletal muscle metabolic and ionic adaptations during intense exercise following sprint training in humans. *J Appl Physiol* **89**, 1793–803.

[206] Goldberg RN, Tewari YB & Bhat TN (2004) Thermodynamics of enzyme-catalyzed reactions–a database for quantitative biochemistry. *Bioinformatics* **20**, 2874–2877.

[207] Palfreyman PW, Clark AE, Denton RM & Holman GD (1992) Kinetic resolution of the separate GLUT1 and GLUT4 glucose transport activities in 3T3-L1 cells. *Biochem J* **284**, 275–281.

[208] Ryder JW, Yang J, Galuska D, Rincón J, Björnholm M, Krook A, Lund S, Pedersen O, Wallberg-Henriksson H, Zierath JR & Holman GD (2000) Use of a novel impermeable biotinylated photolabeling reagent to assess insulin- and hypoxia-stimulated cell surface GLUT4 content in skeletal muscle from type 2 diabetic patients. *Diabetes* **49**, 647–654.

[209] Stagsted J, Hansen T, Roth RA, Goldstein A & Olsson L (1993) Correlation between insulin receptor occupancy and tyrosine kinase activity at low insulin concentrations and effect of major histocompatibility comples class I-derived peptide. *J Pharmacol Exp Ther* **267**, 997–1001.

[210] Albe KR, Butler MH & Wright BE (1990) Cellular concentrations of enzymes and their substrates. *J Theor Biol* **143**, 163–195.

[211] Villar-Palasi C & Larner J (1960) Levels of activity of the enzymes of the glycogen cycle in rat tissues. *Arch Biochem Biophys* **86**, 270–273.

[212] Cohen P & Goldstone T (1983) Protein phosphorylation and the control of glycogen metabolism in skeletal muscle. *Philos Trans R Soc Lond, B, Biol Sci* **302**, 13–25.

[213] Amitani I, Sakamoto T & Ando T (2001) Link between the enzymatic kinetics and mechanical behavior in an actomyosin motor. *Biophys J* **80**, 379–397.

[214] Huang KP, Itarte E, Singh TJ & Akatsuka A (1982) Phosphorylation of glycogen synthase by cyclic AMP-independent casein kinase-2 from rabbit skeletal muscle. *J Biol Chem* **257**, 3236–3242.

[215] Embi N, Rylatt DB & Cohen P (1979) Glycogen synthase kinase-2 and phosphorylase kinase are the same enzyme. *Eur J Biochem* **100**, 339–347.

[216] Hemmings HC, Nairn AC & Greengard P (1984) DARPP-32, a dopamine- and adenosine 3':5'-monophosphate- regulated neuronal phosphoprotein. II. Comparison of the kinetics of phosphorylation of DARPP-32 and phosphatase inhibitor 1. *J Biol Chem* **259**, 14491–14497.

[217] Foulkes JG & Cohen P (1980) The regulation of glycogen metabolism. Purification and properties of protein phosphatase inhibitor-2 from rabbit skeletal muscle. *Eur J Biochem* **105**, 195–203.

[218] Nimmo GA & Cohen P (1978) The regulation of glycogen metabolism. Phosphorylation of inhibitor-1 from rabbit skeletal muscle, and its interaction with protein phosphatase-III and -II. *Eur J Biochem* **87**, 353–365.

[219] Ingebritsen TS, Stewart AA & Cohen P (1983) The protein phosphatases involved in cellular regulation. 6. Measurement of type-1 and type-2 protein phosphatases in extracts of mammalian tissues; an assessment of their physiological roles. *Eur J Biochem* **132**, 297–307.

[220] Shacter E, Chock PB & Stadtman ER (1984) Energy consumption in a cyclic phosphorylation/dephosphorylation cascade. *J Biol Chem* **259**, 12260–12264.

[221] Foulkes JG, Strada SJ, Henderson PJF & Cohen P (1983) A Kinetic Analysis of the Effects of Inhibitor-1 and Inhibitor-2 on the Activity of Protein Phosphatase-1. *Eur J Biochem* **132**, 309–313.

[222] Krebs EG, Love DS, Bratvold GE, Trayser KA, Meyer WL & Fischer EH (1964) Purification and properties of rabbit skeletal muscle phosphorylase b kinase. *Biochemistry* **3**, 1022–1033.

[223] Wang ZX, Cheng Q & Killilea SD (1995) A continuous spectrophotometric assay for phosphorylase kinase. *Anal Biochem* **230**, 55–61.

[224] Meinke MH & Edstrom RD (1991) Muscle glycogenolysis. Regulation of the cyclic interconversion of phosphorylase a and phosphorylase b. *J Biol Chem* **266**, 2259–2266.

[225] Bergamini C, Signorini M, Ferrari C & Dallocchio F (1983) Non-Michaelian kinetics of rabbit muscle uridine diphosphoglucose pyrophosphorylase. *Arch Biochem Biophys* **227**, 397–405.

[226] Daly ME, Vale C, Walker M, Littlefield A, Alberti KG & Mathers JC (1998) Acute effects on insulin sensitivity and diurnal metabolic profiles of a high-sucrose compared with a high-starch diet. *Am J Clin Nutr* **67**, 1186–1196.

[227] Keppler D, Rudiger J & Decker K (1970) Enzymatic determination of uracil nucleotides in tissues. *Anal Biochem* **38**, 105–114.

[228] Olivier BG, Rohwer JM & Hofmeyr JHS (2005) Modelling cellular systems with PySCeS. *Bioinformatics* **21**, 560–561.

[229] Kacser H (1983) The control of enzyme systems in vivo: elasticity analysis of the steady state. *Biochem Soc Trans* **11**, 35–40.

[230] Fell DA & Sauro HM (1985) Metabolic control and its analysis. Additional relationships between elasticities and control coefficients. *Eur J Biochem* **561**, 555–561.

[231] Hofmeyr JHS & Rohwer JM (2011) Supply-demand analysis: a framework for exploring the regulatory design of metabolism. *Methods Enzymol* **500**, 533–554.

[232] Rohwer JM & Hofmeyr JHS (2008) Identifying and characterising regulatory metabolites with generalised supply-demand analysis. *J Theor Biol* **252**, 546–554.

[233] Schuster S, Kahn D & Westerhoff HV (1993) Modular analysis of the control of complex metabolic pathways. *Biophys Chem* **48**, 1–17.

[234] Hofmeyr JHS & Cornish-Bowden A (1996) Co-response analysis: a new experimental strategy for metabolic control analysis. *J Theor Biol* **182**, 371–380.

[235] Wasserman DH & Fueger PT (2006) Point-Counterpoint: Glucose phosphorylation is/is not a significant barrier to muscle glucose uptake by the working muscle. *J Appl Physiol* **101**, 1803–1805.

[236] Ploug T & Vinten J (2006) Counterpoint: Glucose phosphorylation is not a significant barrier to glucose uptake by the working muscle. *J Appl Physiol* **101**, 1805–1806.

[237] Beavo JA, Bechtel PJ & G KE (1974) Activation of protein kinase by physiological concentrations of cyclic AMP. *Proc Natl Acad Sci USA* **71**, 3580–3583.

[238] Parker PJ, Caudwell FB & Cohen P (1983) Glycogen synthase from rabbit skeletal muscle; effect of insulin on the state of phosphorylation of the seven phosphoserine residues in vivo. *Eur J Biochem* **130**, 227–234.

[239] DeFronzo RA, Tobin JD & Andres R (1979) Glucose clamp technique: a method for quantifying insulin secretion and resistance. *Am J Physiol Endocrinol Metab* **237**, E214–E223.

[240] Rossetti L & Giaccari A (1990) Relative contribution of glycogen synthesis and glycolysis to insulin-mediated glucose uptake. A dose-response euglycemic clamp study in normal and diabetic rats. *J Clin Invest* **85**, 1785–1792.

[241] Rossetti L & Hu M (1993) Skeletal muscle glycogenolysis is more sensitive to insulin than is glucose transport/phosphorylation. Relation to the insulin-mediated inhibition of hepatic glucose production. *J Clin Invest* **92**, 2963–2974.

[242] Farrace S & Rossetti L (1992) Hyperglycemia markedly enhances skeletal muscle glycogen synthase activity in diabetic, but not in normal conscious rats. *Diabetes* **41**, 1453–1463.

[243] Kruszynska YT, Home PD & Alberti KGMM (1986) In vivo regulation of liver and skeletal muscle glycogen synthase activity by glucose and insulin. *Diabetes* **35**, 662–667.

[244] Mandarino LJ, Consoli A, Jain A & Kelley DE (1993) Differential regulation of intracellular glucose metabolism by glucose and insulin in human muscle. *Am J Physiol Endocrinol Metab* **265**, E898–E905.

[245] Brady MJ (2010) Allosteric trumps covalent in the control of glycogen synthesis. *Cell Metab* **12**, 428–430.

[246] Atkinson DE (1968) The energy charge of the adenylate pool as a regulatory parameter. Interaction with feedback modifiers. *Biochemistry* **7**, 4030–4034.

[247] Bailey JM & Whelan WJ (1972) The roles of glucose and AMP in regulating the conversion of phosphorylase a into phosphorylase b. *Biochem Biophys Res Commun* **46**, 191–197.

[248] Wang ZX (1999) Influence of substrates on in vitro dephosphorylation of glycogen phosphorylase a by protein phosphatase-1. *Biochem J* **341**, 545–554.

[249] Holmes PA & Mansour TE (1968) Glucose as regulator of glycogen phosphorylase in rat diaphragm. II. Effect of glucose and related compounds on phosphorylase phosphatase. *Biochim Biophys Acta* **156**, 275–284.

[250] Young AA, Mott DM, Stone K & Cooper GJS (1991) Amylin activates glycogen phosphorylase in the isolated soleus of the rat. *FEBS Lett* **281**, 149–151.

[251] Baqué S, Guinovart JJ & Gómez-Foix AM (1996) Overexpression of muscle glycogen phosphorylase in cultured human muscle fibers causes increased glucose consumption and nonoxidative disposal. *J Biol Chem* **271**, 2594–2598.

[252] McBride A & Hardie DG (2009) AMP-activated protein kinase–a sensor of glycogen as well as AMP and ATP? *Acta Physiol* **196**, 99–113.

[253] Danforth WH (1965) Glycogen synthase activity in skeletal muscle: Interconversion of two forms and control of glycogen synthesis. *J Biol Chem* **240**, 588–593.

[254] McBride A, Ghilagaber S, Nikolaev A & Hardie DG (2009) The glycogen-binding domain on the AMPK beta subunit allows the kinase to act as a glycogen sensor. *Cell Metab* **9**, 23–34.

[255] Morita JI & Yasui T (1978) Purification and some properties of a neutral muscle pyrophosphatase. *Journal of Biochemistry* **83**, 719–726.

[256] Colomb MG, Chéruy A & Vignais PV (1972) Nucleoside diphosphokinase from beef heart cytosol. I. Physical and kinetic properties. *Biochemistry* **11**, 3370–3378.

[257] Cascante M & Martí E (1997) Organization and regulation of the metabolic factory. In *New beer in an old bottle: Edward Buchner and the growth of biochemical knowledge* (Cornish-Bowden A, ed.), 1897, pp. 199–214, Universitat de València, Valencia.

[258] Fell DA & Thomas S (1995) Physiological control of metabolic flux: the requirement for multisite modulation. *Biochem J* **311**, 35–39.

[259] Hurleys JH, Deans AM, Thorsness PE, Koshland DE & Stroud RM (1990) Regulation of isocitrate dehydrogenase by phosphorylation involves no long-range conformational change in the free enzyme. *J Biol Chem* **265**, 3599–3602.

[260] Villar-Palasi C (1994) On the mechanism of inactivation of muscle glycogen phosphorylase by insulin. *Biochim Biophys Acta* **1224**, 384–388.

[261] Cabrera ME, Saidel GM & Kalhan SC (1998) Role of O2 in regulation of lactate dynamics during hypoxia: mathematical model and analysis. *Ann Biomed Eng* **26**, 1–27.

[262] Dash RK, Dibella JA & Cabrera ME (2007) A computational model of skeletal muscle metabolism linking cellular adaptations induced by altered loading states to metabolic responses during exercise. *Biomed Eng Online* **6**, 14.

[263] Li Y, Solomon TPJ, Haus JM, Saidel GM, Cabrera ME & Kirwan JP (2010) Computational model of cellular metabolic dynamics: effect of insulin on glucose disposal in human skeletal muscle. *Am J Physiol Endocrinol Metab* **298**, E1198–E1209.

[264] Liu W, Hsin C & Tang F (2009) A molecular mathematical model of glucose mobilization and uptake. *Math Biosci* **221**, 121–129.

[265] Xu K, Morgan KT, Todd Gehris A, Elston TC & Gomez SM (2011) A whole-body model for glycogen regulation reveals a critical role for substrate cycling in maintaining blood glucose homeostasis. *PLoS Comput Biol* **7**, e1002272.

[266] Rohwer JM, Hanekom AJ, Crous C, Snoep JL & Hofmeyr JHS (2006) Evaluation of a simplified generic bi-substrate rate equation for computational systems biology. *IEE Proc-Syst Biol* **153**, 338–341.

[267] Apweiler R, Bairoch A, Wu CH, Barker WC, Boeckmann B, Ferro S, Gasteiger E, Huang H, Lopez R, Magrane M, Martin MJ, Natale DA, O'Donovan C, Redaschi N & Yeh LSL (2004) UniProt: the Universal Protein knowledgebase. *Nucleic Acids Res* **32**, D115–D119.

[268] Itarte E & Huang KP (1979) Purification and properties of cyclic AMP-independent glycogen synthase kinase 1 from rabbit skeletal muscle. *J Biol Chem* **254**, 4052–4057.

[269] Woodgett JR & Cohen P (1984) Multisite phosphorylation of glycogen synthase. Molecular basis for the substrate specificity of glycogen synthase kinase-3 and casein kinase-II (glycogen synthase kinase-5). *Biochim Biophys Acta* **788**, 339–347.

[270] Illg D & Pette D (1979) Turnover rates of hexokinase I, phosphofructokinase, pyruvate kinase and creatine kinase in slow-twitch soleus muscle and heart of the rabbit. *Eur J Biochem* **97**, 267–273.

[271] Soderling TR, Srivastava AK, Bass MA & Khatra BS (1979) Phosphorylation and inactivation of glycogen synthase by phosphorylase kinase. *Proc Natl Acad Sci USA* **76**, 2536–2540.

[272] Gratecos D, Detwiler TC, Hurd S & Fischer EH (1977) Rabbit muscle phosphorylase phosphatase. 1. Purification and chemical properties. *Biochemistry* **16**, 4812–4817.

[273] Ingebritsen TS & Cohen P (1983) The protein phosphatases involved in cellular regulation. 1. Classification and substrate specificities. *Eur J Biochem* **132**, 255–261.

[274] Rush JWE & Spriet LL (2001) Skeletal muscle glycogen phosphorylase akinetics: effects of adenine nucleotides and caffeine. *J Appl Physiol* **91**, 2071–2078.

[275] Melpidou AE & Oikonomakos NG (1983) Effect of glucose-6-P on the catalytic and structural properties of glycogen phosphorylase a. *FEBS Lett* **154**, 105–110.

[276] Madsen NB & Shechosky S (1967) Allosteric properties of phosphorylase b. II. Comparison with a kinetic model. *J Biol Chem* **242**, 3301–3307.

[277] Oikonomakos NG, Zographos SE, Johnson LN, Papageorgiou AC & Acharya KR (1995) The binding of 2-deoxy-D-glucose 6-phosphate to glycogen phosphorylase b: kinetic and crystallographic studies. *J Mol Biol* **254**, 900–917.